The role of bis-calix[4]arenes in the synthesis of multi-component polymetallic clusters

Marco Coletta

Submitted for the degree of Doctor of Philosophy

Heriot-Watt University

School of Engineering and Physical Sciences

December 2016

Abstract

The work presented in this thesis encompasses the synthesis of novel *p-tert*-butylcalix[4]arene-based ligands with the overall aim of exploring and understanding their coordination chemistry. The ligands described have been obtained *via* substitution and functionalisation of *p-tert*-butylcalix[4]arene at one methylene bridge position, the mechanism of which is discussed in detail herein. Once isolated, these ligands were reacted with a selection of transition (TM), lanthanide metals (Ln) and 3*d*-4*f* metal ion mixtures in order to systematically study the formation of polymetallic clusters and their prevailing magnetic properties. This also provided the opportunity to gain insight into ligand influence over the associated coordination chemistry, all of which was possible through the growth and *X*-ray diffraction study of single crystals in each case.

Chapter 1 contains an overview of calix[*n*]arene synthesis (and related derivatives), with a particular emphasis on calix[4]arene, its conformational properties, and synthetic modifications at the upper-, lower-rim and methylene bridge positions. Discussion then moves to a qualitative description of single-molecule magnets and molecular refrigerants, highlighting some of the seminal achievements in the area. The final section of Chapter 1 discusses the coordination properties of calix[4]arene, including the formation of metal clusters that represent the foundation of the work presented in Chapters 2 – 5.

Chapter 2 presents the synthesis of 2,2'-biscalix[4]arene prior to discussion of the use of this ligand in reactions with TM / Ln ion mixtures, the results of which were the isolation of a series of 2,2'-biscalix[4]arene-supported 3*d*/4*f* metal clusters. This was carried out with a particular focus on stoichiometric control over cluster synthesis, which subsequently afforded novel cluster topologies that are closely related to species already obtained from previous research within the group.

Chapter 3 covers exploratory cluster formation that was carried out using 2,2'-biscalix[4]arene in the presence of complementary and competitive co-ligands. The co-ligands employed were carefully chosen based on their known metal ion binding properties, resulting in dramatic changes to the topologies of the prevailing polymetallic clusters, the structures of which are described in detail.

Chapter 4 describes a modified synthetic procedure that facilitated the isolation of a family of flexible alkyl chain tethered biscalix[4]arenes. These ligands were then used in exploratory cluster formation and afforded a series of known cluster topologies when the length of the alkyl tether permitted this. Structural discussion highlights these similarities and draws comparison with the TBC[4]-supported clusters presented in Chapter 1.

Chapter 5 focuses on exploratory coordination chemistry that was carried out with rigidly tethered biscalix[4]arenes. The chapter begins with a brief description of the synthesis of these ligands before moving on to discussion of the new polymetallic clusters isolated, highlighting important structural analogies and differences with the architectures described in Chapters 1 and 4.

Chapter 6 presents a summary of the work included in this thesis, as well as an outlook of future work to be undertaken in this area.

I would like to dedicate this work to my family.

ACKNOWLEDGEMENTS

I would like to thank my supervisor, Dr Scott J. Dalgarno, for giving me the opportunity of studying in such an interesting area of research. His guidance, encouragement and inspiration have been invaluable and thanks to his constant supervision and help, I have been able to learn more than I hoped. It has been an honour and a pleasure to be part of the Supramolecular Chemistry Group.

I am very grateful to Dr Ruaraidh D. McIntosh for the precious hints and tips that helped me throughout my PhD years. He has always been happy to answer any doubt, question and curiosity with useful advice and suggestions.

Many thanks go to Dr Ross McLellan, whose knowledge has been of great help during the first six months of my PhD. I like to think that what I have learned from him contributed to set the basis for a successful PhD study.

I would also like to thank Prof. Euan K. Brechin and Dr. Sergio Sanz at The University of Edinburgh for their invaluable work on collection and analysis of magnetic data for the compounds presented in this thesis. Dr Simon J. Teat and Dr Kevin J. Gagnon at the Advanced Light Source in Berkeley, California, for their work on collecting *X*-ray data. Prof. Andrew I. Cooper and Mr. Rob Clowes at The University of Liverpool, for their hard work on gas sorption studies. Prof Martin J. Paterson and Mr. Paul Murphy at Heriot-Watt University for the computational studies.

Special thanks go to previous and current PhD students at Heriot-Watt University for making these years enjoyable. I have many good and happy memories that I will jealously carry with me in the future.

Finally, I would like to thank my family and friends for the unlimited support and encouragement throughout my PhD.

TABLE OF CONTENTS

Symbols and abbreviations

Å	Ångström (0.1 nm)
ASU	Asymmetric Unit
^{t}Bu	*tert*-butyl
Et	Ethyl
Me	Methyl
Pr	Propyl
Ph	Phenyl
ºC	Degrees Celsius
dc	Direct current
K	Kelvin
M	Molar
mol	mol
L	Litre
g	Gram
mins	Minutes
TLC	Thin Layer Chromatrography
NMR	Nuclear Magnetic Resonance
Hz	Hertz
J	Coupling constant (Hz)
br s	broad singlet
m	multiplet
s	singlet
t	triplet
M^{+}	Molecular ion peak
MS	Mass spectrometry
m/z	mass/charge ratio
ppm	parts per million
RT	Room temperature

$H_4C[4]$	Calix[4]arene
$H_4TBC[4]$	*p-tert*-butyl-calix[4]arene
$TM^{III/II}$	Transition metal ion
Ln^{III}	Lanthanide metal ion
R_f	Retention factor
MW	Molecular weight
FW	Formula weight
π	pi
s.e.	Symmetry equivalent
SMM	Single Molecule Magnet
MCE	Magnetocaloric effect
MR	Molecular refrigerant/refrigeration
NMR	Nuclear Magnetic Resonance
SQUID	Superconducting Quantum Interference Device
H_2pdm	2,6-pyridinedimethanol
Hhmp	2-pyridinemethanol
$CDCl_3$	Deuterated chloroform
CD_3CN	Deuterated acetonitrile
$CHCl_3$	Chloroform
DCM	Dichloromethane
H_3DEA	Diethanolamine
dmf	*N*,*N*-dimethylformamide
Et_2O	Diethyl ether
Et_3N	Triethylamine
EtOAc	Ehtyl Acetate
EtOH	Ethanol
H_2O	Water
HCHO	Formaldehyde
Hex	Hexane
H_2MDEA	*N*-methyldiethanolamine

MeCN	Acetonitrile
MeOH	Methanol
n-BuLi	*n*-butyllithium
NaH	Sodium hydride
NaOH	Sodium hydroxide
PET	Petroleum ether 40-60 ºC
Ph_2O	Diphenyl ether
THF	Tetrahydrofuran
Tol	Toluene

Chapter 1: Introduction

1.1. Calix[*n*]arenes and related macrocycles.

1.1.1. History of calixarenes.

Calixarene chemistry dates back to 1872 when Adolph von Baeyer began the study of reactions involving condensation between formaldehyde and phenolic derivatives. The outcome of this research was the publication of a series of papers[1] in which he described the condensation products as resinous materials or "cement-like" substances. Unfortunately, von Baeyer never managed to obtain or isolate a pure product; it was therefore impossible for him to conduct any further analysis that would have allowed for the identification of the product of the phenol-formaldehyde condensation, even though he suggested a possible product of the reaction. Some years later Baekeland began to investigate analogous reactions using small amounts of base to promote condensation between the phenolic derivative and formaldehyde, obtaining the same resinous materials. He patented this reaction and with its product, named Bakelite©, kick-started the industrial production of plastics.[2]

It was not clear yet what kind of product was obtained from these reactions, and in 1944 Zinke and Ziegler investigated these processes in more detail, performing a series of reactions using exclusively *para*-substituted phenols. The choice of using solely *para* isomers was due to the fact that, at that time, it was known that the condensation between phenols and formaldehyde occurred at the *ortho* and *para* positions. An unsubstituted phenol would therefore have led to a cross-linked polymer without any preferential direction of polymerisation. A *para*-substituted phenol would result in lower cross-linking given that the two phenolic *ortho* positions are the only reaction sites. With this knowledge, Ziegler and Zinke managed to isolate a crystalline product with a melting point > 300 °C. [3] At that time, the structure of these condensation products was yet to be determined, although elemental analysis and other analytical techniques suggested that the product was in fact a cyclic tetramer.

Following Zinke's work, other researchers studied similar reactions following slightly different procedures, and in all cases obtained the same high-melting point, pure crystalline material, therefore supporting the idea that the product isolated by Zinke *et al.* was indeed a cyclic tetramer.[4] The development of novel and improved analytical techniques, such as nuclear magnetic resonance spectroscopy (NMR), infrared spectroscopy

(IR) and single crystal *X*-ray crystallography (SCXRD), were intended to shed light on the nature of these products, whereas the result was actually doubtful of their cyclic tetrameric nature. Lacking a reasonable reaction mechanism for the condensation of phenols and formaldehyde and their cyclisation into tetramers, the experimental data were pointing towards a cyclic octamer form of these resinous materials or, at least, to a mixture of both tetramer and octamer.[5]

An important step forward in calixarene chemistry can be attributed to Gutsche and co-workers, who extensively investigated the phenol-formaldehyde chemistry with the initial idea of producing enzyme mimics. The cyclic nature and the presence of a cavity made these tetramers the perfect candidates for such an investigation. In addition, by that time, there was a very small number of cavity-containing macrocycles readily available *via* facile laboratory synthesis that could have been utilised as biomimetics. These molecules were cyclodextrins, naturally occurring products that are now obtained from action of the enzyme cyclodextrin glycosyltransferase on pre-treated starch-based sources. Crown ethers were also known and, even though possessing an annular-like shape, were lacking of the cavity necessary for them to act as enzyme mimics. In their preliminary experiments, Gutsche and co-workers acquired a deep understanding of the nature of phenol-formaldehyde condensation chemistry. This culminated in systematic screening of the optimum conditions to favour the isolation of one macrocycle over another, including changes in the solvent, temperature and base employed, as well as stoichiometry. The legacy of these efforts is the flawless and accurate synthetic protocols that researchers can now use to synthesise whichever macrocycle they desire.

In parallel to the development of the synthetic chemistry of these interesting macrocycles, they required an appropriate and attractive name. Several names were proposed throughout time, both common and systematic, but none were officially accepted. Based on a nomenclature system invented by Cram in 1951,[6] these compounds can be referred to as [1_n]meta-cyclophanes, but it is only thanks to Gutsche that these macrocycles are today known as calixarenes. Given the shape similarity between an ancient Greek vase and a space-filling model of Zinke's tetramer, in which all the phenol moieties are pointing in the same direction, Gutsche coined the term "calixarene". This name derives from *calix*, the Greek for "chalice" or "vase", and *arene*, indicating the presence of aryl moieties as part of the molecule. At first this name was not officially accepted from IUPAC but, shortly after, it gained its official status and is now used to include any molecule whose structure could have any remote similarity to the phenol-derived calixarenes.[7] Since then calixarene chemistry

rapidly expanded and led to several, often more complex products, which stressed the need for systematic nomenclature. Calixarenes are named using a [*n*] between the words calix and arene which indicates the number of phenolic units forming the macrocycle. In this way calix[4]arene refers to the macrocycle with four phenolic units, calix[8]arene to the one with eight and so on. As the word "chalice" suggests, these macrocycles are oriented in such way that the -OH groups are pointing down (*endo*) and the *para*-substituents are pointing up (*exo*). Commonly, it can be referred as to the *endo* face at the lower-rim of the calixarene, and as to the *exo* face at the upper-rim. The atoms are numbered in order that a calix[4]arene, in which each phenolic ring bears a *tert*-butyl group in *para* position, is named 5,11,17,23-tetra-*tert*-butyl-calix[4]arene-25,26,27,28-tetrol (Figure 1). The systematic nomenclature can become cumbersome and is commonly simplified to shorter forms. This thesis will exclusively present work undertaken on *p-tert*-butyl-calix[4]arenes and its derivatives, therefore, when not otherwise stated, it will be shortened to "H_4TBC[4]" hereafter to denote the level of protonation of the molecule relative to the lower-rim OH groups.[8] The same will apply to other ligands presented throughout this thesis.

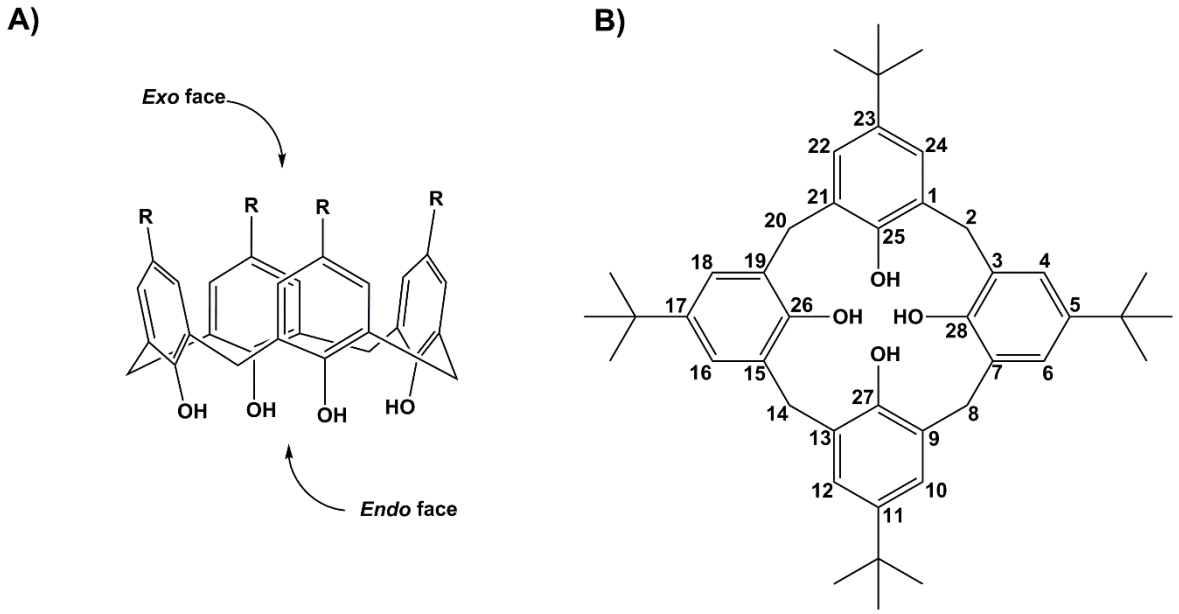

Figure 1. A) Representation of the *exo* and *endo* faces in a calix[4]arene. B) Numbering scheme of 5,11,17,23-tetra-*tert*-butylcalix[4]arene-25,26,27,28-tetrol, H_4TBC[4].

The development of a successful and reliable synthetic procedure to obtain calix[4]arenes required accurate screening of all the variables that could influence the outcome of the reaction.[9] Before Gutsche's work, the Zinke procedure was the most reliable, although in many cases it proved not to be completely reproducible. An in-depth investigation showed

that the main reason for the unpredictability of such a reaction was its extreme sensitivity towards the amount of base (sodium hydroxide) catalyst present. It appears that an ideal amount of base can maximise the yield of H_4TBC[4], whereas small deviations from such an optimum can lead to no yield at all, or favour the cyclic hexamer over the tetramer.[10] The nature of the cation coupled to the hydroxide anion also proved to be rather important,[11] as the reaction leads to the cyclic tetramer and/or the octamer when NaOH is used, while it yields mainly H_6TBC[6] with KOH. The reason of this is mainly a templating effect exerted by the cation in the reaction stage in which the polymer is broken and the fragments recombine to afford cyclic products. The temperature and, accordingly, the solvent used to reflux the reaction mixture is another critical factor that can heavily influence the outcome. This is because, depending on the nature of the solvent and the temperature, when the cation is the same, the thermodynamic product (e.g. H_4TBC[4]) can be favoured over the kinetic product (e.g. H_8TBC[8]) and vice-versa.

Calix[*n*]arenes with $n = 4, 6, 8$ are named as "major" calixarenes whilst those with $n = 5, 7$ are referred to as "minor" calixarenes. All can be synthesised using a base-catalysed process but, for the minor calixarenes, the synthetic routes are much more demanding and usually lead to low yields even if the reaction has been carried out by carefully following the highly reliable procedures available. The first synthesis of calix[5]arene, subsequently perfected by Gutsche,[12] was reported in 1982 by Ninagawa *et al.*,[13] and involved heating to reflux a mixture of 4-*tert*-butylphenol and paraformaldehyde in tetralin (i.e. 1,2,3,4-tetrahydronaphtalene). This afforded the cyclic pentamer in only a small quantity, with the major products being calix[4,8]arenes. In the same year, Nakamoto *et al.* reported the first one-pot synthesis of calix[7]arene, employing similar conditions and 1,4-dioxane/KOH system.[14] They obtained, albeit in low yield, the heptameric macrocycle as the major product along with calix[6,8]arenes, once again proving the sensitivity of these reaction towards the conditions employed. For some time, it was believed that the three major and two minor calixarenes exclusively represented the family of molecules. Relentless efforts by Gutsche's research group at the end of the 1980s culminated in the synthesis and the isolation of calix[9]arene and calix[10]arene, formed in a mixture with all of the other inferior homologues (Figure 2), as well as larger calixarenes reaching up to the eicosomer ($n = 20$).[15]

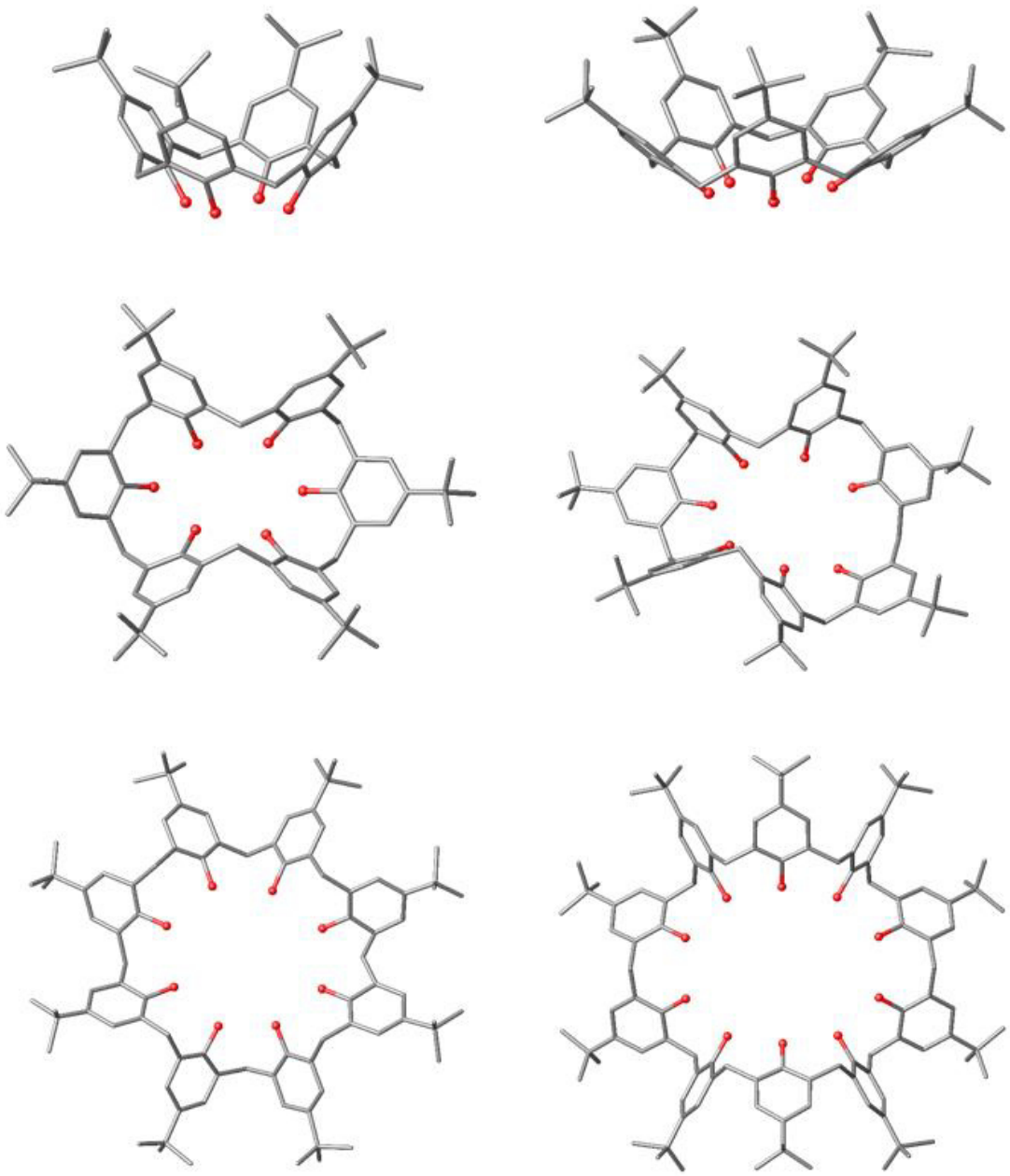

Figure 2. Partial single crystal *X*-ray structures of *p-tert*-butyl-calix[4,5,6,7,8,10]arenes. Solvent of crystallisation and hydrogen atoms omitted for clarity (Colour code: C – grey, O – red).

The most accepted procedure to obtain both major and minor calixarenes involved a base-catalysed process as discussed above; however, it was discovered that, in order to obtain larger calixarenes with higher yields, an acid-catalysed process was recommended. The reactions that lead to larger calixarenes are, however, not selective. This means that the

reaction inevitably yields a mixture of different calix[*n*]arenes that have to be separated *via* tedious, time- and solvent-demanding extractions, mainly relying on the slight solubility differences of one macrocycle over the others. In all cases, even if the reaction conditions are optimised, the overall yields for larger calixarenes are always lower than those for calix[4-8]arenes.

It is worth noting that, although *p-tert*-butylphenol is the most commonly used phenol in the synthesis of calixarenes, other *p*-substituted phenols can react similarly, such as *p-tert*-pentylphenol[16] and *p-tert*-octylphenol,[17] even though the isolation of the pure product is more complicated and the overall yields are lower. Reactions with other *p*-substituted phenols, especially those in which the *para* substituent is a deactivating group, afford untreatable mixtures and therefore do not represent a suitable choice. In general, the premise for the cyclisation process is to use a phenol bearing an alkyl group in the *para* position. Several products have been synthesised using other *p*-substitued phenols, such as *p*-cresol,[18] *p*-isopropylphenol and *p*-phenylphenol.[19] In all cases, the reactions deliver mixtures of calixarenes with lower yields compared to when *p-tert*-butylphenol is employed. Cyclisation is also possible when other phenol-like compounds are reacted with formaldehyde, such as 1-naphthol, the product of which was investigated by Georghiou *et al*. (Figure 3).[20] This base-promoted reaction leads to a mixture of macrocycles that have been called calixnaphthalenes in which, as opposed to the case with calixarenes, the OH groups are oriented on the outside of the annulus. Similar *exo*-annular compounds can be obtained when bis-phenols are condensed with formaldehyde.[21]

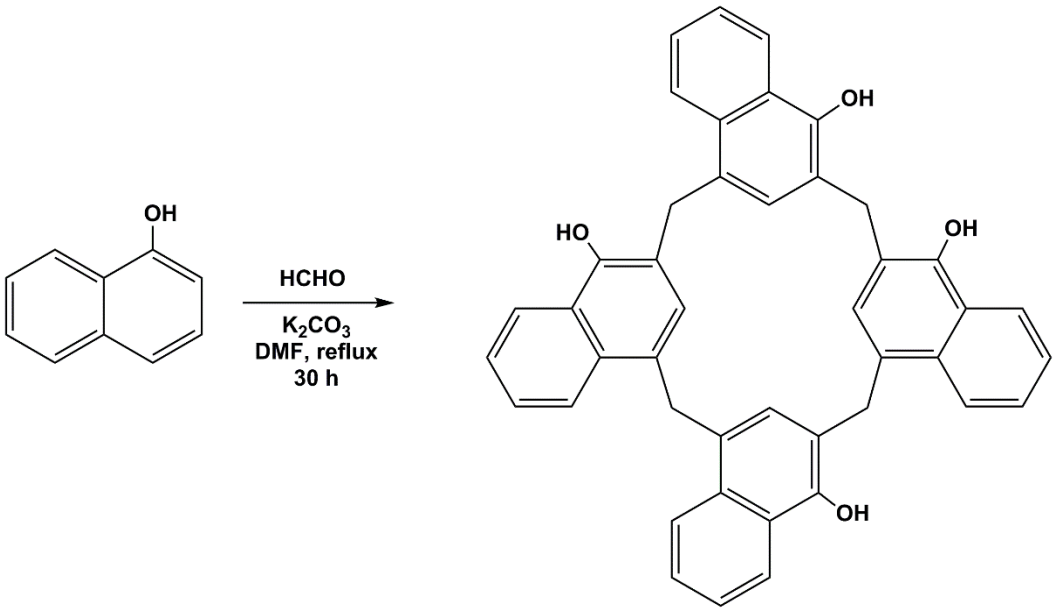

Figure 3. Synthetic scheme of calix[4]naphthalene.[20]

Work undertaken by Niederl and Vogel focused on acid-catalysed reactions using resorcinol (1,3-dihydroxybenzene) as the phenolic moiety and several aldehydes, with the exception of formaldehyde.[22] They obtained a series of products which, on the basis of rudimental molecular weight determinations, proved to be cyclic tetramers, namely calix[4]resorcarenes or, more simply, resorcinarenes. Depending on the aldehyde employed in the synthesis, conditions must be optimised by accurately choosing the Lewis acid that promotes the condensation reaction. These syntheses, quite interestingly and in contrast with what has been discussed so far regarding calixarenes, lead almost exclusively to the cyclic tetramer regardless of the steric hindrance and / or electronic properties of the aldehyde employed. The difference between these products and those obtained by Ziegler-Zinke is that the eight phenolic OHs are *extra*-annular, whilst the four OHs in Ziegler-Zinke's products are *intra*-annular. Similarly, pyrogallol (1,2,3-trihydroxybenzene) can be employed in the condensation reaction with aldehydes to afford the corresponding pyrogallol[4]arene (Figure 4).[23]

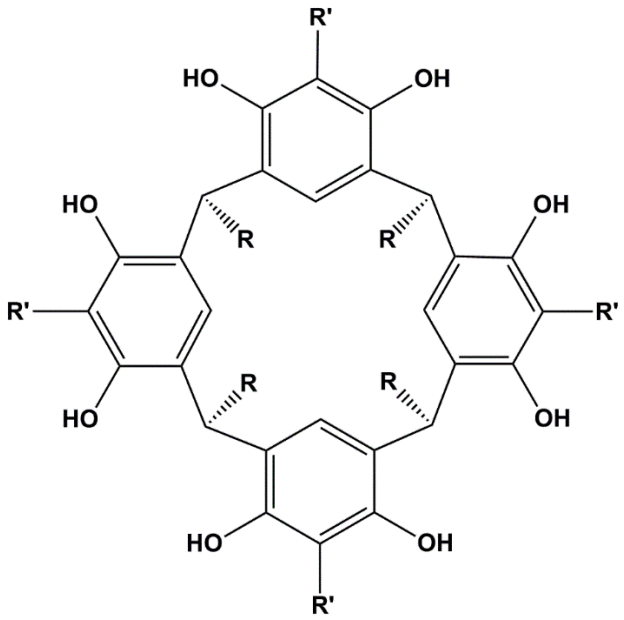

Figure 4. General structure of resorcin[4]arenes (R' = H) and pyrogallol[4]arenes (R' = OH).

In 2008, Ogoshi and Nakamoto reported the synthesis of a new class of macrocycles, obtained by condensation of hydroquinone (e.g. 1,4-dihydroxybenzene) derivatives and paraformaldehyde.[24] The products, containing five subunits, were named pillar[5]arenes and can be described as 1,4-disubstituted [1$_n$] cyclophanes linked by methylene bridges at the 2,5-positions (Figure 5A). These compounds rapidly caught the attention of the scientific

community for their wide-ranging potential applications. Although synthesised in the same way as calixarenes, pillararenes are quite different. First, they do not have a cone shape but are cylindrical; therefore, their shape resembles more that of cucurbit[*n*]urils[25] (Figure 5B) and makes it impossible to individuate an upper- and lower-rim. As discussed later for TBC[*n*]s, conformational isomers are generated by the rotation of aromatic rings through the macrocycle annulus. In addition, substitution at the positions 1- and 4- leads to two possible stereoisomers. Although still embryonic, pillar[5]arene chemistry has rapidly developed and it is now possible to synthesise these macrocycles in high yields and with a certain degree of functionalisation. This includes asymmetric pillar[5]arenes in which the substituents at the 1- and 4- positions are different, or the so-called copillar[5]arenes containing different hydroquinone moieties in a 4:1 ratio.[26] Pillar[5]arenes have displayed interesting host-guest properties, being able to form inclusion complexes with viologen derivatives such as alkyl substituted paraquats,[27] and also alkyldiamines.[28] Knowing these inclusion properties, some researchers have used polymers containing viologen subunits to build (pseudo)rotaxanes that act as a shuttle for electrons or as sensors for diamines.[29]

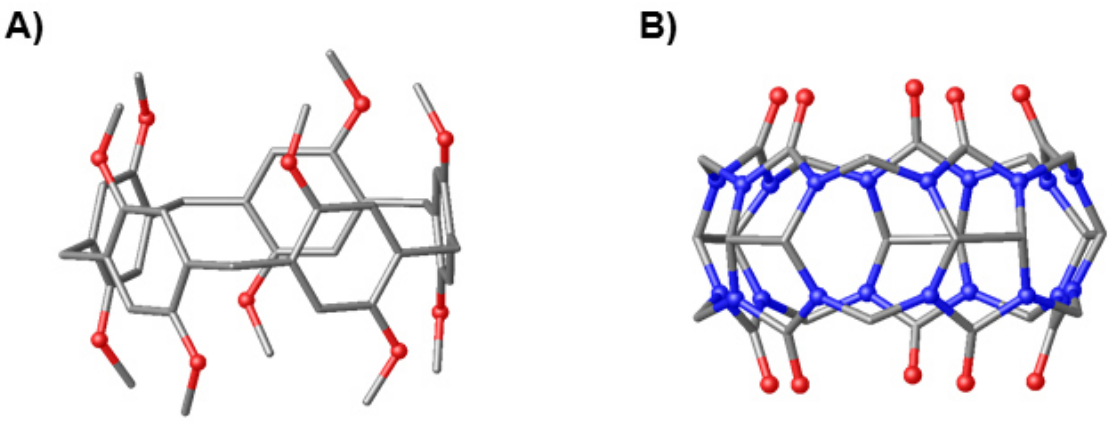

Figure 5. Partial single crystal *X*-ray structures of A) Ogoshi's dimethoxypillar[5]arene and B) Cucurbit[5]uril.[24-25] Solvent of crystallisation and hydrogen atoms omitted for clarity (Colour code: C – grey, O – red, N – blue).

The syntheses discussed so far all involve a one-pot condensation of phenolic-based compounds with aldehydes in a base- or acid-catalysed process. Although the one-pot synthesis is now widely employed to obtain different sized calixarenes and their derivatives, it used to lead in many cases to a mixture of products that had to be separated, often with tedious and time-consuming protocols. With this in mind, and with the determination of

achieving a better understanding of the cyclisation process, many researchers began to develop multi-step synthetic strategies. In general, these would involve the non-convergent synthesis of a linear oligomer of the appropriate size followed by intramolecular cyclisation into the desired calixarene product or, alternatively, in a convergent fashion, with the synthesis of fragments bearing functionalities of opposite reactivity that are reacted with each other to form the macrocycle. Hayes and Hunter, followed by Kämmerer, managed to synthesise a *p*-methylcalix[4]arene in a 10 step reaction that, although long and tiresome, features high yields in each reaction step, including the final cyclisation.[30]

A *p*-heptamethylcalix[7]arene was successfully synthesised in a similar fashion after 18 steps.[31] In order to reduce the large number of reaction steps required to synthesise these macrocycles, many groups began investigating convergent methods. Amongst others, Böhmer investigated the possibility of obtaining a cyclic tetramer *via* [3+1][32] and [2+2][33] condensations. Most of these fragment cyclisations require the presence of a catalyst such as $TiCl_4$ in order to obtain appreciable yields and avoid high dilution conditions that are normally employed in such reactions. The choice between a [3+1] or a [2+2] approach merely depends on the ease of synthesis of the respective fragments. Pursuing such a synthetic strategy can be advantageous because it allows the chemist to react fragments not necessarily of the same nature, therefore leading to calixarene products bearing moieties with different functional groups and reactivity.

Although this thesis will focus exclusively on calix[4]arene and its derivatives, it is worth briefly mentioning other synthetic possibilities available to researchers in order to obtain macrocyclic compounds that are closely related to the "standard" calixarenes. Reaction between bis-phenol and formaldehyde yields a mixture of a hexamer and an octamer in which, due to the absence of methylene bridges, some the phenolic moieties are directly linked to each other. These macrocycles are named "norcalixarenes" and have been synthesised in reasonable yields.[34] It is also possible to introduce more than one carbon between the phenolic moieties of the calixarene, obtaining the so-called homocalixarenes (Figure 6).[35]

Another attractive possibility for the chemist is the replacement of one or all methylene bridges between the phenolic moieties with heteroatoms such as oxygen, nitrogen or sulphur. These compounds, called "heteracalixarenes" and belonging to the family of calixarenes, are named oxa-, thia- and azacalixarenes respectively depending on the nature of the heteroatom bridging the phenol units (Figure 7).

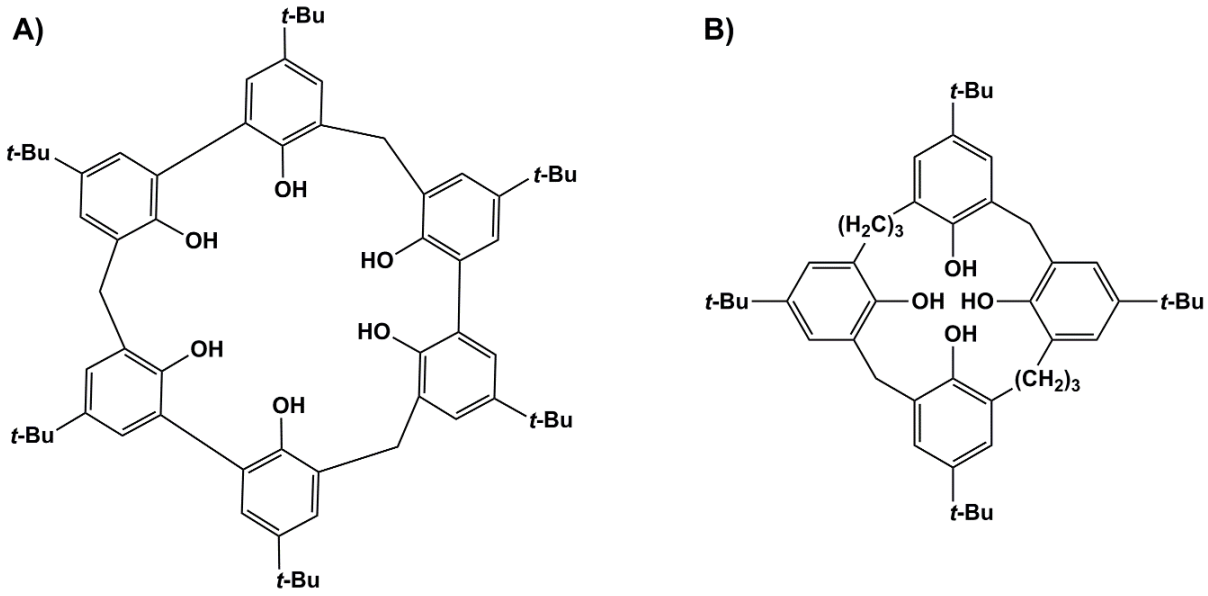

Figure 6. General structure of A) norcalix[6]arene and B) homocalix[4]arene.

The first oxacalixarenes were synthesised in modest to low yields around the 1950s by condensation of resorcinols with electron-poor arenes such as dihaloarenes[36] or dinitroarenes.[37] Although these compounds were fully characterised, their study was abandoned for several years because the extremely long one-pot reactions required harsh conditions and most of them led to low yielding mixtures of products. In addition, the scarce solubility of these products prevented any further application. Since the beginning of the new millennium, oxacalixarenes regained attention thanks to the efforts of several research groups that developed novel elegant synthetic procedures for asymmetric oxacalix[4]arenes; this is possible *via* a 3+1 macrocyclisation of a pre-synthesised linear trimer with a difunctional reagent. The reagents chosen to maximise the synthesis were, in general, heteroatomic electron-poor systems due to their higher reactivity in the nucleophilic aromatic substitution reaction.

In 2004, Wang *et al.* synthesised a series of aza- and / or oxo-bridged calix[2]arene[2]triazines through an efficient coupling reaction of a trimer, previously synthesised by reaction of cyanuric chloride and resorcinol, with a 1,3-bifunctionalised arene. The resulting macrocycles all adopt a specific conformation and, thanks to the nature of the bridging heteroatoms which can heavily influence and regulate the cavity size within the macrocycle, differ in chemical and physical properties from the "standard" calixarenes and have found use in molecular recognition.[38] A year later, several other oxacalix[4]arenes were synthesised by Katz *et al*., choosing 1,5-difluoro-2,4-dinitrobenzenes as the activated arene to react with resorcinol. Assuming formation of the same conformation, these

macrocycles were synthesised in such a way that they will still have reactive sites on the *exo* rim, which can be used to further functionalise the oxacalixarene.[39] Konishi investigated the nature of the cyclisation process by synthesising asymmetric oxacalix[4]arenes *via* [3+1] cyclisation, obtaining ABAC-type macrocycles.[40] He envisaged the possibility of performing CsF-catalysed disproportion reactions, therefore leading to an equilibrium mixture of the product and the ABAB and ACAC counterparts.

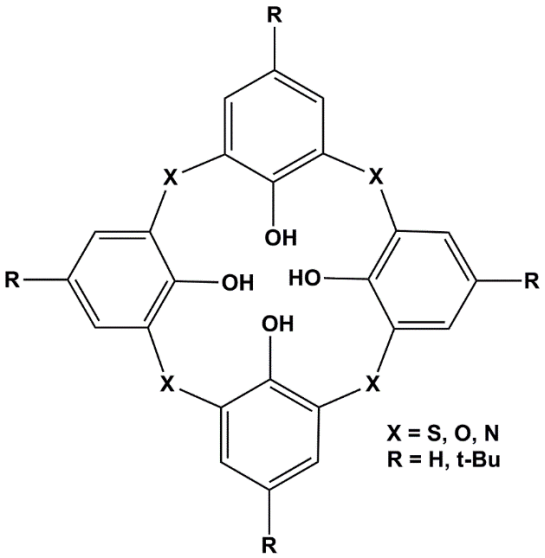

Figure 7. General structure of heteracalixarenes.

Since the following paragraph will describe the coordination chemistry of some thiacalix[4]arene derivatives, it is worth briefly mentioning their synthesis, properties and differences relative to calix[4]arenes. Thiacalixarenes have attracted significant attention and interest as alternatives to the classical calixarenes due to the presence of sulfur atoms which have dramatic effects on the prevailing conformation and reactivity of these macrocycles. They were synthesised in very low yield by Sone and coworkers through cyclisation of linear sulphur-bridged trimers with SCl_2, but were fully characterised.[41] This reaction was then improved, revealing a one-pot synthesis performed by heating a mixture of *p-tert*-butylphenol and elemental sulfur in a high boiling solvent and in the presence of NaOH.[42] It is now possible to synthesise these macrocycles in high yields by performing the same reaction but starting from a sulfur-bridged dimer. This reaction also yields small but isolable amounts of thiacalix[6,8]arenes.[43] It is worth mentioning that several synthetic protocols have been developed to synthesise thiacalix[4]arene derivatives containing -SO- and $-SO_2-$ groups at the methylene bridge positions, namely sulfinyl-[44] and sulfonylcalix[4]arenes.[45]

Another interesting class of macrocycles closely related to the classical calix[*n*]arenes is the family of heterocalixarenes, obtained by acid-catalysed condensation of ketones or aldehydes with heterocycles. The most important are the heterocalixarenes obtained from condensation of ketones and / or aldehydes with furans, pyrroles and thiophenes derivatives yielding, respectively, calixfurans,[46] calixpyrroles[47] and calixthiophenes,[48] the latter being less easily isolable. Other compounds that can be described as calixarenes, though less frequently encountered are, for example, calix[3]indoles,[49] silacalix[4]arenes,[50] calix[4]pyridines[51] and platinocalix[4]uracils (Figure 8).[52]

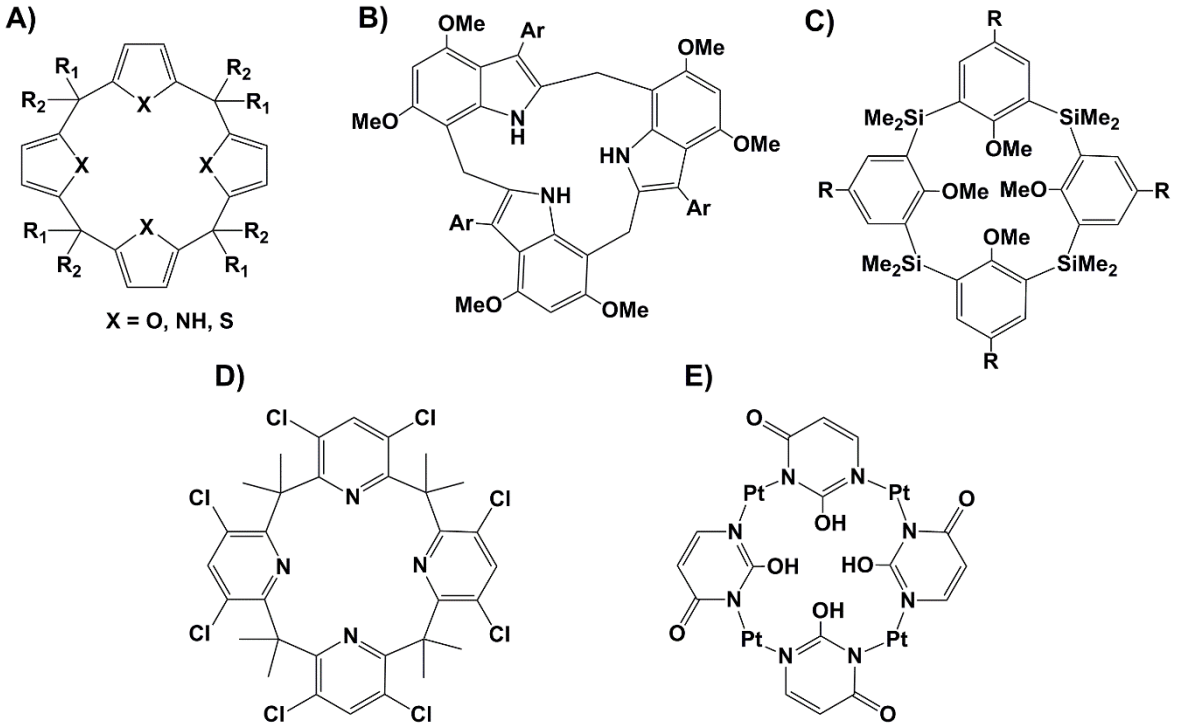

Figure 8. A) General structure of heterocalixarenes; B) Structure of calix[3]indole; C) Structure of silacalix[4]arene; D) Structure of calix[4]pyridine; E) Structure of platinocalix[4]uracil.

1.1.2. Calix[4]arene conformations and properties.

Calixarenes, along with the enormous family of their derivatives, have been synthesised with success and fully characterised with all available experimental techniques, including SCXRD, NMR spectroscopy and mass spectrometry. This greatly helped the further development of other synthetic protocols that aided researchers to obtain specific calixarene derivatives. Despite this enormous body of knowledge, the mechanism from which formaldehydes and phenols react with each other to produce linear oligomers and, then, cyclise into the final product has been the subject of debate for some time. In the base-catalysed process, it is very likely that the base deprotonates the phenol, leading to a phenoxide anion that undergoes nucleophilic addition to the carbonyl of the formaldehyde. Under the relatively harsh conditions employed in the synthesis of calixarenes, the reaction likely proceeds to the formation of an *o*-quinonemethide intermediate capable of reacting with another phenoxide anion in a Michael-like addition to yield a diarylmethyl species. The aforementioned step repeats, leading to the formation of a linear oligomer. In the Cornforth synthesis of H_4TBC[4] the linear oligomer obtained is broken down by addition of toluene to the reaction mixture with vigorous stirring. This addition, along with the template effect exerted by the sodium ions present in solution, leads to the formation of the tetramer as the major, often exclusive product. As mentioned above, for some calixarene derivatives (e.g. resorcinarenes) as well as the larger calix[*n*]arenes the only viable pathway is an acid-catalysed reaction. This mainly occurs *via* formation of a cationic intermediate and a series of electrophilic aromatic substitutions.[8]

Calix[*n*]arenes can exist in different conformations, mainly depending on the bridging atoms between the phenolic moieties, the substituents on both the *exo* and the *endo* rim and on the number of the phenols units in the macrocycle. Therefore, calix[4]arene can have four possible conformers: cone, partial cone, 1,2- and 1,3-alternate (Figure 9).[53] Each name is associated with the position to which a phenol group is pointing (up or down) relative to the other phenols and an average plane defined by the bridging methylene groups. Given this, the number of possible conformers dramatically rises for larger macrocycles. Substitution of the upper- or lower-rim can affect the orientation of the phenolic moieties, thus favouring a specific conformation over the others. H_4C[4]s with four *endo* -OH groups are in a cone conformation at room temperature thanks to a network of hydrogen bonds between the lower-rim phenol groups. Increasing the temperature, in order to break the hydrogen-bonded network, or deprotonation and etherification of these groups gives access to the other conformers. These are in equilibrium and are interconverting by the flipping of

phenolic units through the calixarene annulus. Theoretically, this process would involve a calix[4]arene molecule in a cone conformation to undergo conformational changes until it assumes its inverted-cone conformer.

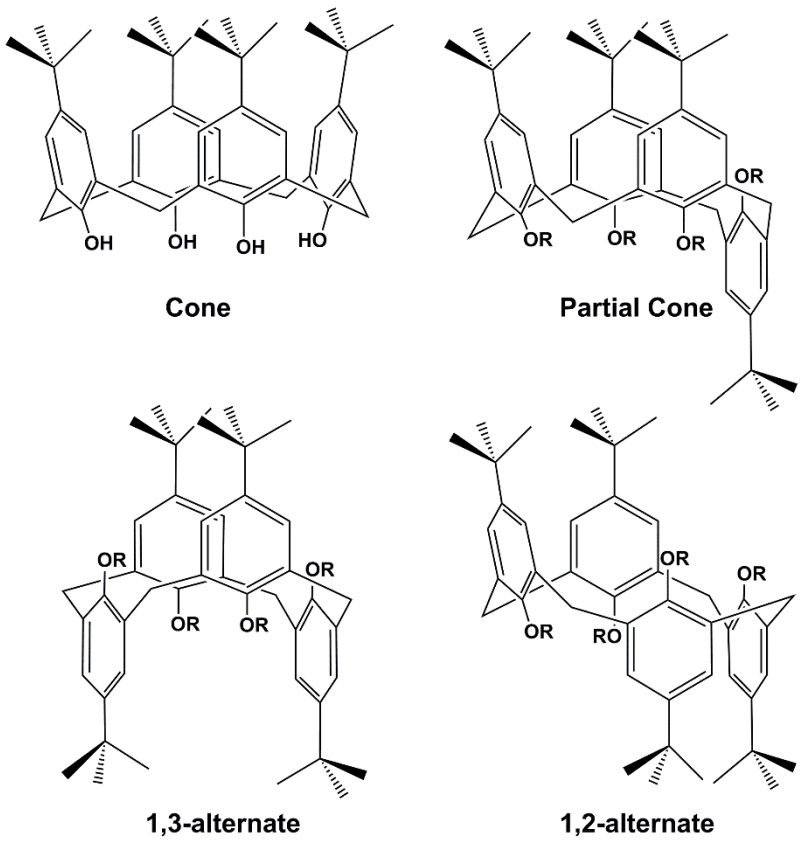

Figure 9. Four possible conformers adopted by H_4TBC[4].

The mechanism under which this interconversion occurs was debated for some time, and two main routes have been proposed. The first involves a concerted pathway in which the four phenolic moieties perform a through-annulus flipping at the same time, generating the inverted cone conformer without any intermediate and only one transition state. The second suggests a stepwise process in which a single phenolic moiety of the initial cone conformer undergoes through-annulus flipping, generating the partial cone conformer as an intermediate. Such a process repeats itself through the 1,2- and 1,3- alternate intermediates, finally affording the inverted cone conformer.[54] Through-annulus flipping depends on the size of the substituent on the lower-rim and on the temperature. It occurs, for example, at room temperature with small groups such as -OMe, while higher temperatures are required for bulkier groups such as -OPr, -OBu etc.

1.2. Calix[*n*]arene upper- and lower-rim functionalisation.

The great potential of calix[*n*]arenes to act as candidates for a vast range of applications and devices was envisaged by many since the early stage of calixarene chemistry, contributing to a widespread interest in these macrocyles. These unique features are not only related to the cone-shape of the macrocycle, but also to the presence of the two rims, both of different size, and with each one bearing different functional groups that can readily undergo chemical functionalisation to afford a practically infinite series of calixarene derivatives. For the sake of brevity, only examples based on calix[4]arene will be described, although many of these apply, in principle, to the whole family of calix[*n*]arenes.

1.2.1. Lower-rim functionalisation.

Functionalisation at the lower-rim is possible thanks to the presence of phenolic OHs. It was possible to measure their pK_a values through the use of several experimental and computational studies. These were not as straightforward as one may think due to the poor solubility of calixarenes in common solvents used in the potentiometric and spectroscopic studies, which required indirect measurements using water-soluble derivatives.[55] From these studies it was observed that, in general, calixarenes are stronger acids than their phenolic monomer equivalents. The first deprotonation of calix[4]arene occurs, for example, at pH = 1 while the last proton is removed ad pH = 11. This is rather interesting because it means that calix[4]arene possesses a super-acidic proton and, at the same time, it is a very basic anion. The ease of first proton removal is due to the stabilisation energy gained by the formation of a stronger hydrogen bond of the oxyanion with the neighbouring OHs. Subsequent proton removals are increasingly difficult because of the destabilisation given by electrostatic repulsions. It was also observed that, upon deprotonation, the conformation of calix[4]arene changes significantly. The acidity of the phenolic proton is, of course, very susceptible to the electronic nature of the substituents in other areas of the macrocycle and also to the number of the remaining OH protons.

Given the above, the simplest functionalisation reaction that can be performed at the lower-rim is an alkylation *via* etherification using alkyl halides (*via* a Williamson reaction). Considering the huge gap in the pK_a values for the first and second proton, a very strong base would be required to perform tetra-alkylation and, in general, monoalkylation products would be the most favourable. With surprise, along with strong bases such as NaH, alkylation can be also performed by using weak bases such as K_2CO_3 in acetone or

acetonitrile when in the presence of a large excess of alkylating agent. The reason of this phenomenon is the similarity in pK_a values between H_4TBC[4] and the monoalkylated derivative. Since lower-rim functionalisation is a valuable tool in order to obtain precursors used in other derivatisations, etherification has been studied in detail to the point that it is now possible to obtain mono-,[56] di- (either 1,2 or 1,3),[57] tri-[53] and tetraethers[53] from one-pot or multi-step reactions based on partially alkylated starting materials. The latter synthetic strategy allows one to introduce different alkyl groups relative to the one-pot approach. Although etherification is now widely employed, esterification was historically the first type of lower-rim functionalisation to be performed. As for etherification, esterification normally leads to the tetrasubstituted derivative with a series of acyls of different nature,[58] as well as to partial substitution if the reaction is carried out with milder bases, different solvent or smaller quantities of acylating agent.[59]

Lower-rim functionalisation is most commonly used as a strategy aimed at protecting the phenolic OHs from reagents used for other reactions that may affect them. Alkylating agents that possess a secondary functional group, if used in the proper way, can also introduce further functionalities at the lower-rim of the calixarene. Some examples are the reactions of calix[4]arene with alkylating agents containing C=C and C≡C obtaining, respectively, allyl-[53] and propargyl-like[60] calix[4]arene derivatives. From the plethora of functionalising agents that can be used on the lower-rim, it is worth mentioning the use of polyethylene glycol chains to intramolecularly bridge two OHs at the lower-rim, giving rise to the small family of calixcrowns (Figure 10).[61]

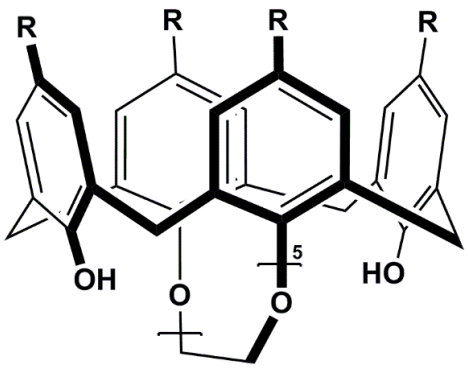

Figure 10. The first calixcrown synthesised by Ungaro *et al.*[61]

1.2.2. Upper-rim functionalisation.

Regarding the introduction of functionalities at the upper-rim, an obvious synthetic choice would be to synthesise the macrocycle in a multi-step fashion, using fragments already bearing the functionalities of interest. Although this may seem a wise strategy to pursue, it is worth remembering that the condensation of fragments is usually a reaction leading to lower yields and in most cases it is very time consuming. In addition, all the major and minor calixarenes are now accessible in high yields using one-pot approaches. The most high-yielding procedures are those from which the *para*-substituent can be easily removed by a reverse Friedel-Crafts reaction, thus rendering the *para*-position available for further functionalisation (Figure 11).[62]

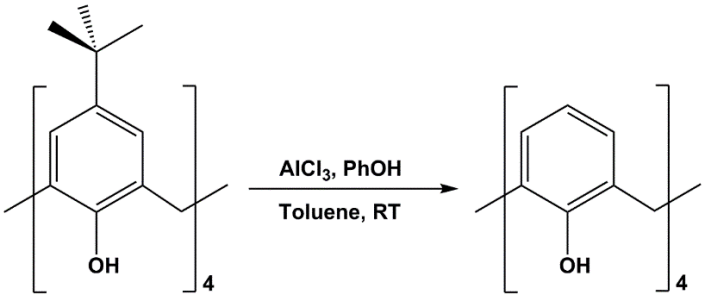

Figure 11. Reverse Friedel-Crafts reaction to remove *p-tert*-butyl groups.[62]

Halocalixarenes are valuable intermediates for the introduction of further functionalities at the *para*-position. For instance, tetra-bromination can be easily achieved by reaction of tetramethoxycalix[4]arene with *N*-bromosuccinimide,[63] whereas selective bromination can be carried out using bromine on partially lower-rim etherified calixarenes.[64] Reaction with *t*-BuLi has the effect of generating a tetra-lithiated calix[4]arene at the upper-rim *para*-position, which represents another route to obtain several products. Amongst these, it is worth mentioning the formation of *para*-carboxylic acid[63] and *para*-formyl calixarene derivatives.[65] The possibility of introducing a nitro group in the *para*-position was not very successful at the early stages of calixarene chemistry. This issue was partially solved by Shinkai *et al*., who managed to perform such a reaction going through a *para*-sulfonato intermediate.[66] A more useful procedure for the *para* nitration of calixarenes is one developed by Reinhoudt and co-workers.[67] This procedure encompasses an *ipso*-substitution of the *tert*-butyl group with a -NO_2 group, with the obvious advantage of not having to remove the *tert*-butyl group in the first place, not considering the peculiar selectivity preferences that this reaction features. Nitrocalixarenes represent the perfect starting point

for the introduction of further functionalities on the calixarene scaffold, most often *via* reduction of the nitro to an amino group by employing H_2 or Raney/Ni, which have found use, for example, in the linkage to aminoacids to form peptidocalix[4]arenes.[68]

Another valuable functionality that can be introduced at the upper-rim is an allylic group, which can later be converted to other important functionalities. For example, photochemical addition of HBr can be undertaken to obtain *para* primary alkyl bromides, or ozonolysis can afford aldehydes that are able to undergo further functionalisation. Predicting the immense possibilities given by the introduction of the aforementioned double bond moiety, Gutsche and co-workers developed an elegant synthetic protocol that involves a *para*-Claisen rearrangement (Figure 12).[69] The *para*-allyl compound is obtained in two steps: the formation of a tetra-allyl ether at the lower-rim, followed by thermal rearrangement to the final product.

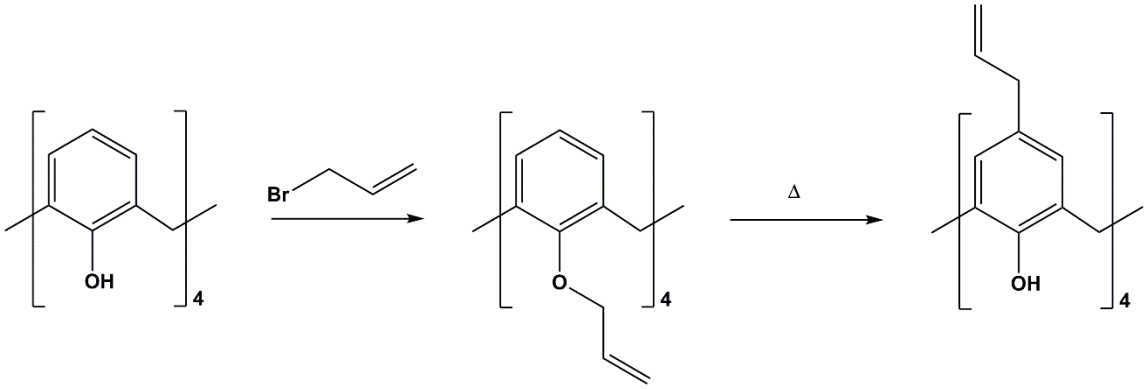

Figure 12. Lower-rim tetra-allyl formation followed by thermal *p*-Claisen rearrangement.[69]

1.3. Calix[*n*]arene functionalisation at the methylene bridge.

Since this thesis will describe the synthesis, characterisation and exploratory cluster formation of some calix[4]arenes linked through the methylene bridges by different spacers, it is worth dedicating a section to this type of functionalisation. Compared to the great variety of functionalisation that can be carried out on both the upper- and lower-rim of the calixarene, relatively little has been explored so far regarding the functionalisation of the methylene bridges (the 2,8,14,20-positions, Figure 1B). Exploration of this chemistry is attractive as the methylene-bridged substituted derivatives may possess different properties relative to their unsubstituted parents (e.g. enhanced solubility), or offer an extra site for linkage to a solid support, leaving both rims available for further functionalisation.

In the cone conformation $H_4C[4]$ has two protons on each methylene bridge that are positioned in equatorial and axial positions, akin to a cyclohexane ring. From the ^1H NMR spectrum of $H_4TBC[4]$ in $CDCl_3$ at room temperature it is possible to state that the methylene bridge protons give rise to two sets of doublets. On the basis of NOE experiments and chemical shifts induced by different solvents, Ungaro and co-workers assigned the lower field doublet to the axial protons, closer to the phenolic OHs, and the higher field doublet to the protons in the equatorial position, therefore closer to the aromatic rings.[70] In addition, as a result of the conformational mobility already discussed above, the aforementioned pattern of doublets tends to coalesce to a sharp singlet at around 60 ºC. Monosubstitution of one of the two protons with a generic R group would yield a product still adopting a cone conformation, but one that would coexist as two diastereoisomers interconverting into each other *via* the through-annulus flipping mechanism discussed earlier; this is because the substituent can either be located in an axial or equatorial position (Figure 13). In order to have quantitative information regarding the energy of the *cone*-to-*cone* ring inversion mechanism, Biali and co-workers performed molecular mechanics calculations.[71] These calculations indicate that alkyl substituents at the methylene bridge energetically prefer to sit in an equatorial position, whilst for aryl substituents this difference is less marked. The preference of aliphatic substituents for the equatorial position originates from the distortion of the tetrahedral arrangement of the methine carbon generated by the repulsion of the carbon attached to the bridge and the neighbouring OH groups.

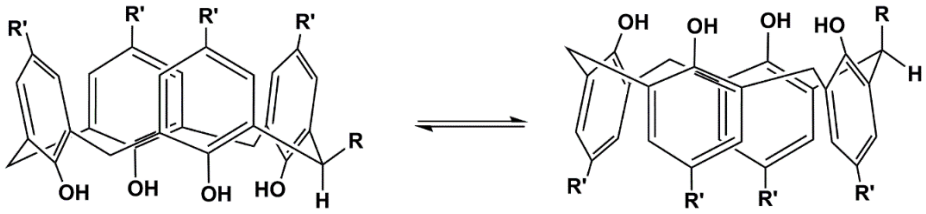

Figure 13. *Cone*-to-*cone* ring inversion mechanism on methylene bridge monosusbstituted calix[4]arenes (R = alkyl, aryl; R' = H, *t*-Bu).[71]

Whilst functionalisation on the upper- and lower-rim affords a derivative in which the substituents are oriented parallel to the central calixarene axis, modification at the methylene bridge by substitution of the equatorial position gives the possibility to expand the structures perpendicular to the macrocycle.[72] Biali and co-workers can be considered as pioneers of this type of chemistry, having managed to introduce several different functionalities at one, or all, C[4] methylene bridges. The routes available to perform such functionalisation are

varied but typically involve S_NAr or S_N1 reactions in a one-pot or multi-step fashion. S_N2-type reactions are rarer due to decomposition of the starting materials under the reaction conditions employed. Photochemical bromination of the methylene bridges, achieved by heating to reflux a solution of the selected calix[4]arene and *N*-bromosuccinimide in chloroform while irradiating with a spotlight, is often the starting point to synthesise methylene bridge-substituted calixarenes.[73] Once the tetra-brominated calix[4]arene is obtained, it is possible to replace the bromine atoms with several substituents. Regardless of the substituent chosen, all the reactions are performed under solvolytic conditions employing a solvent of high ionising power such as trifluoroethanol (TFE) or hexafluoroisopropanol (HFIP). The reason for this is that a high ionising power is required to produce an appreciable amount of the alleged carbocation generated by the dissociation of the C-Br bond. It is clear, however, that the nucleophilic power of the solvent must be lower than that of the chosen nucleophile, the former being present in larger amount.[74] Performing a solvolysis under such conditions leads to a series of TBC[4]OMe derivatived bearing groups such as -OMe, -OEt, $-OC_2H_4OH$ or $-N_3$ at the methylene bridge (Figure 14).[75]

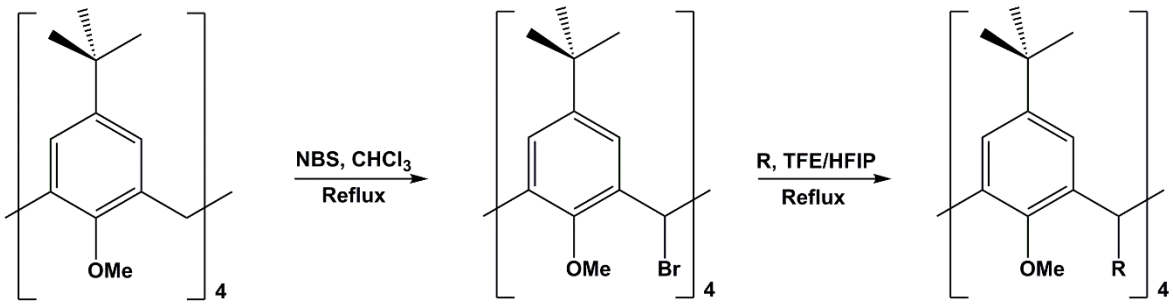

Figure 14. Synthetic scheme of tetrabromination of TBC[4]OMe at the methylene bridge and subsequent solvolysis (R = OMe, OEt, OC_2H_4OH or N_3). [75]

Hydroxyl groups can be also introduced at the methylene bridge in a two-step synthesis that involves solvolysis of the methylene-bridge tetrabromo derivative in glacial acetic acid, producing the tetra-acetoxy derivative, with subsequent reduction to -OHs using $LiAlH_4$ (Figure 15).[74]

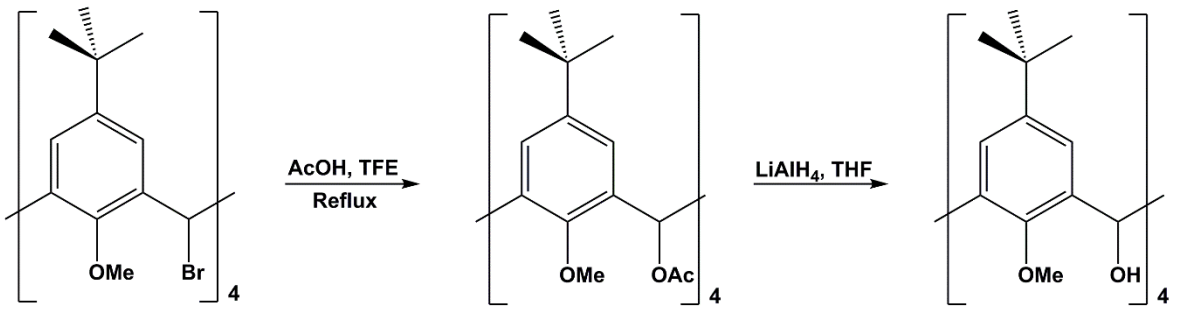

Figure 15. Synthetic scheme of tetraacetylation of TBC[4]OMe at the methylene bridge and subsequent reduction of the OAc moieties with $LiAlH_4$ to OHs.[74]

The methodologies discussed so far are also applicable to larger calixarenes,[76] and are generally not restricted to substitution at all the methylene bridges, but allow partial bridge functionalisation.[77] It is also worth mentioning that specific functionalisation of two distal methylene bridge positions can also occur by pursuing a different and more complicated synthetic route. This encompasses the preparation of a (bis)spirodienone derivative of the calixarene by reaction with mild oxidising agents,[78] followed by bromination/dehydrobromination. This inserts two exocyclic double bonds that subsequently undergo reaction with nucleophiles to afford the disubstituted (bis)spirodienone derivative. Reduction with $LiAlH_4$ restores the calixarene scaffold bearing two distal substituents at the methylene bridges.[79]

The Fantini group made an important contribution to methylene bridge functionalisation chemistry with the development of simple but elegant strategies in order to introduce different groups at this position. Exploration of the mechanism of methylene bridge substitution and its reactivity was inspired by the synthesis of calix[4]arene-based Mo and W complexes in which the metal centres are oxidatively inserted intramolecularly in the methine C-H bond, producing metalated complexes.[80] In their early work, the Fantini group produced TBC[4]s substituted with either methyl, ethyl, benzyl, *para*-bromobenzyl or carboxy at the methylene bridge, proving simultaneously that, under the reaction conditions employed, the reaction yields exclusively mono-substituted products. The monosubstitution occurs *via* lithiation of tetramethoxy-*p-tert*-butylcalix[4]arene (TBC[4]OMe), producing a supposed, non-isolable, bridge lithiated species, which is capable of reacting with electrophiles (Figure 16). [72]

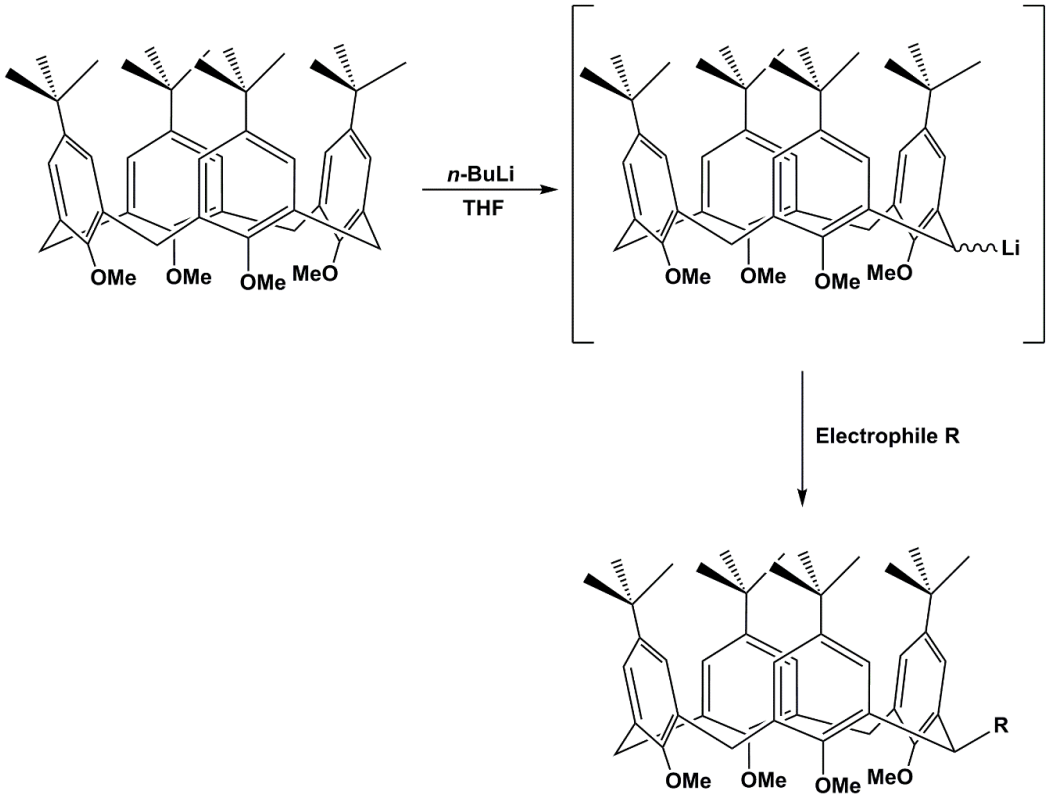

Figure 16. General synthetic scheme of TBC[4]OMe methylene bridge functionalisation.[72]

With this in mind, they began to investigate the possibility of installing secondary amines tethered at the methylene bridge through an alkyl chain. This was in order to obtain TBC[4]OMe derivatives that would, to some extent, retain classical well-known TBC[4]OMe properties.[81] In addition, the presence of a tether allows for coordination to metal centres or, alternatively, attachment to a solid support, giving the possibility to study these derivatives from a heterogeneous catalysis perspective. Since the bridge-lithiated species are quenched upon addition of amines, a two-step synthesis was thus required. The first step is the reaction of the bridge-lithiated species with a 1-bromo-ω-chloroalkane of different length to produce 2-(ω-chloroalkyl)-calix[4]arene. This product is subsequently reacted with alkyl or aryl amines (in the presence of a base such as Na_2CO_3 or KH) to afford the TBC[4]OMe derivative bearing a secondary amine (Figure 17).

Further investigation into methylene bridge functionalisation culminated in proof that the chloroalkyl derivative can undergo a standard Finkelstein reaction. Replacement of the terminal chlorine atom with an iodine is useful in order to introduce a better leaving group for any subsequent S_N2-type reactions. Another viable route to produce methylene-bridge substituted calix[4]arenes bearing solid support anchoring functionalities is to introduce azide tethers and perform Huisgen-type 1,3-dipolar cycloadditions with terminal

alkynes to produce 1,4-disubstituted-1,2,3-triazoles.[82] This is, of course, not a novel synthetic strategy, as the introduction of azides and alkynes has been applied in the past at either upper- and lower-rims.[83] The aforementioned derivatives are readily obtained by treatment of the corresponding (ω-chloroalkyl)calixarene with NaN_3/NaI in dmf, followed by "click reaction" with terminal alkynes, either aliphatic or aromatic, in a Cu^I catalysed reaction.

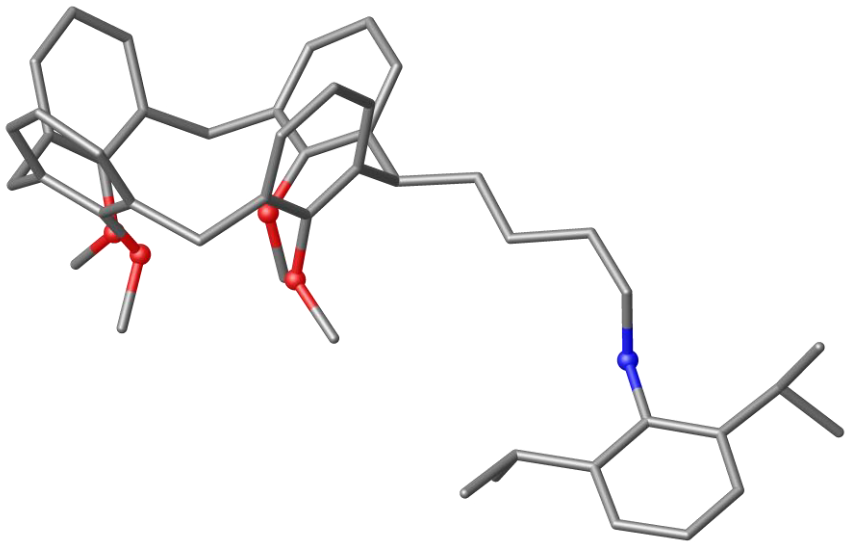

Figure 17. Partial single crystal *X*-ray structure of the diisopropylanilinobutyl-TBC[4]OMe derivative synthesised by Fantini.[81] ^{t}Bu groups, hydrogen atoms, ligated solvent molecules and solvent of crystallisation omitted for clarity (Colour code: C – grey, O – red, N – blue).

Not all functional groups can be introduced by pursuing the synthetic strategies discussed so far. Taking inspiration from Biali's work on calix[6,8]arene,[77] Fantini *et al*. synthesised a TBC[4]OMe bearing an electrophilic centre at a single methylene bridge.[84] Whereas the 2-chloro species of calix[6,8]arene derivatives were synthesised by a multi-step approach involving photochemical bromination and *in situ* hydrolysis of the bromide to hydroxyl, followed by chlorination of the resulting 2-hydroxy compound, simpler methodology was possible in the case of TBC[4]OMe thanks to the selectivity of the lithiation process towards mono-substitution. In this way, a 2-chloroTBC[4]OMe was synthesised by treatment of TBC[4]OMe with *n*-BuLi in dry THF, followed by addition to a solution of CCl_4, which represents the source of electrophilic chlorine (Cl^+) of choice. The aforementioned derivative proved to be reactive towards S_N1-type reaction with a wide range of different nucleophiles, giving the possibility to convert the chloro-derivative to hydroxy, isopropylamino and ethoxy derivatives (Figure 18).

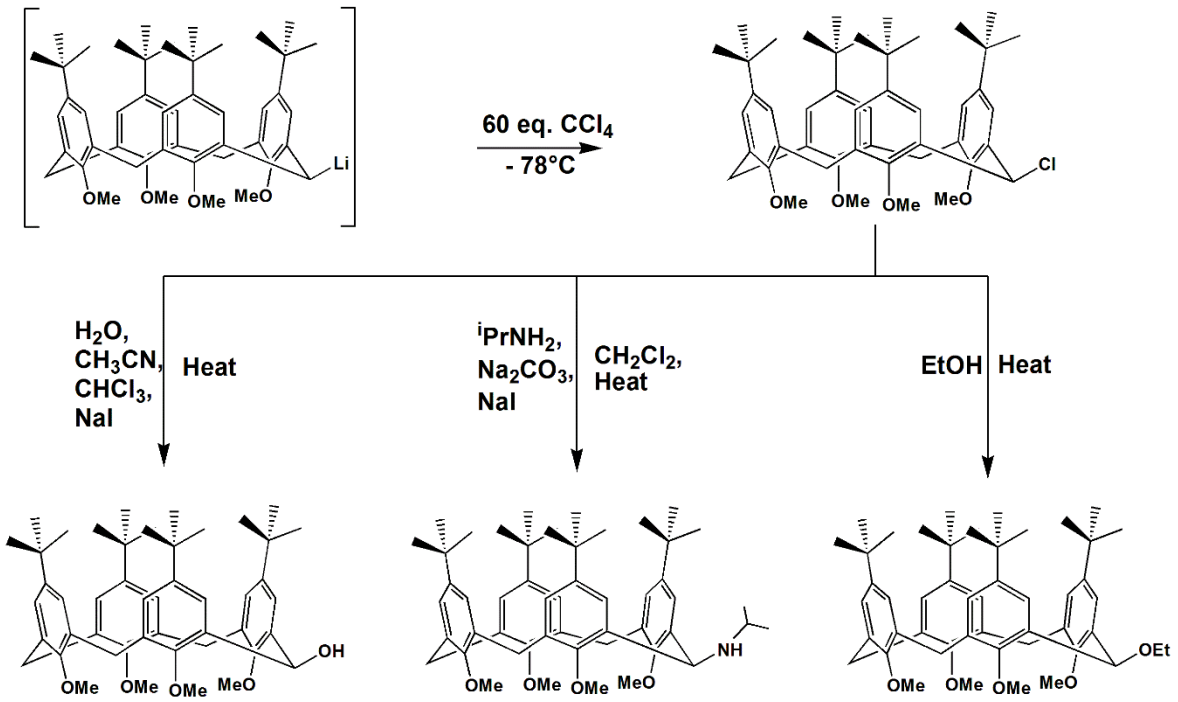

Figure 18. Synthesis of 2-chloroTBC[4]OMe and its reaction to yield the 2-hydroxy, 2-isopropylamino and 2-ethoxy derivative, respectively.[84]

While screening the best conditions to maximise the yield for 2-chlorocalix[4]arene, the Fantini group serendipitously isolated a side product which turned out to be a biscalix[4]arene, a species in which two macrocycles are directly linked *via* methylene bridges. Thanks to the acquired knowledge on methylene-bridge substitution chemistry, it was hypothesised that the biscalix[4]arene was the product of the reaction of 2-chlorocalix[4]arene with bridge-lithiated calix[4]arene still present in solution. It was therefore possible to outline a synthetic protocol that leads exclusively to the 2,2'-biscalixarene without any side products. Rather than producing a 2-chlorocalix[4]arene, this time a more reactive, non-isolable, 2-bromocalix[4]arene was produced using 1,2-dibromoethane as a source of electrophilic bromine, which readily reacted with another equivalent of the lithiated calix[4]arene to afford the directly coupled product (Figure 19). As biscalix[4]arene plays a central role in this work of thesis its coordination properties and behaviour will be outlined in the following section. New results obtained with this ligand are presented in Chapters 2 and 3.

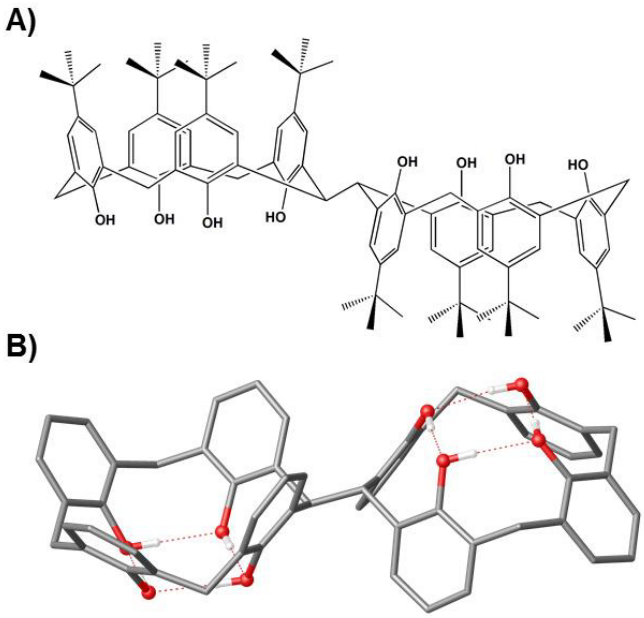

Figure 19. A) Schematic and B) Partial single crystal *X*-ray structure of 2,2'-Biscalixarene synthesised by Fantini and co-workers.[84] ^{t}Bu groups, hydrogen atoms not involved in hydrogen bonds, ligated solvent molecules and solvent of crystallisation omitted for clarity (Colour code: C – grey, O – red, H – white).

1.4. Single Molecule Magnets and Molecular Refrigerants.

The general aim of the work in this thesis is the synthesis of biscalix[4]arene-based 3*d* or 3*d*/4*f* polymetallic clusters that exhibit interesting magnetic behaviour as Single Molecule Magnets (SMMs) and Molecular Refrigerants (MRs). It is therefore pertinent to discuss this subject, in which the two topics will be briefly and qualitatively described, corroborated by important literature examples. Magnets are now employed in a wide range of applications and can be found anywhere in daily life. One the most fundamental and obvious application of magnetic materials is in information storage. The quest for miniaturisation of magnetic devices is ongoing, attempting to overcome the fact that it is impossible to permanently store information below a specific size of the magnet due to increasingly strong magnetisation fluctuations. In theory, smaller particles could be used for the same purposes by working at temperatures lower than ambient and / or by exploitation of the quantum size effect, thus making nanomagnets the perfect candidates for information storage nanodevices.[85] Molecules containing a number of transition metal ions have been proved to have magnetic behaviour somewhat similar to nanomagnets. Such polynuclear metal clusters showing remarkable superparamagnetic properties have therefore been termed single-molecule

magnets (SMMs). The interest in the magnetic behaviour of such polynuclear cluster dates back to 1985 when the Gatteschi group observed that there was a positive ferromagnetic interaction when copper(II) and gadolinium(III) were put in close contact within a crystal structure.[86] Initial work performed in this new era used mainly Schiff bases as polydentate ligands to bridge the magnetically active metal centres. The idea, that already had within itself the aim of rational ligand design that would be pivotal in the future of coordination chemistry, was to exploit the oxophilicity of the lanthanides whereas the copper centres would bind to the softer nitrogens. A plethora of Schiff bases have been used to obtain a series of different polynuclear Cu/Ln clusters, most often in a two-step coordination process (Figure 20).[87]

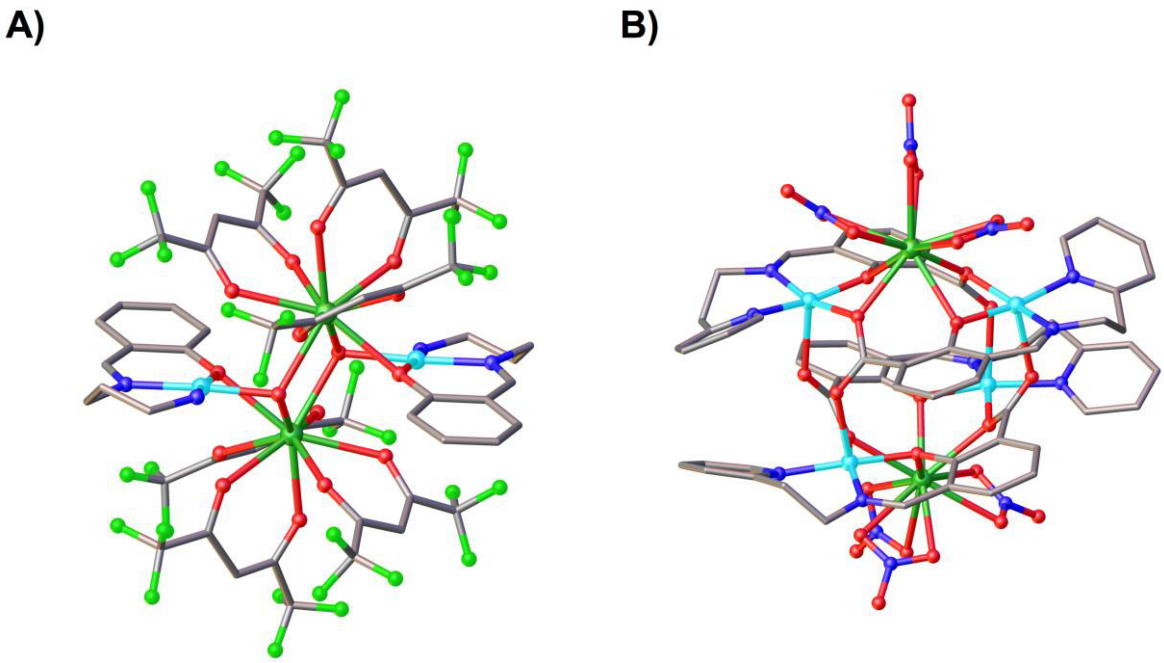

Figure 20. Partial single crystal *X*-ray structures of a A) $Cu^{II}_2Ln^{III}_2$ and B) $Cu^{II}_4Ln^{III}_2$ (Ln = Gd, Dy, Pr) clusters with Schiff base ligands.[87] Hydrogen atoms, ligated solvent molecules and solvent of crystallisation omitted for clarity (Colour code: Cu – light blue; Ln – green, C – grey, N – blue, O – red; F – light green).

Motivated by these results, researchers began looking at other types of ligand in order to construct different Cu / Ln polymetallic clusters with higher nuclearity and, more often, with unpredictable structures. The outcome of these efforts was the synthesis of $Cu^{II}_4Ln^{III}_2$ and $Cu^{II}_8Ln^{III}_2$ cages in which the cations were bound to 2-pyridone-like ligands (Figure 21).[88] Magnetic studies on these complexes showed that, as anticipated, there is a ferromagnetic interaction between the Cu^{II} and the Gd^{III} centres. Moreover, the substantial number of Cu /

Ln cages produced allowed for correlation between the structures of the aforementioned polymetallic clusters and the magnitude of the magnetic exchange interaction (*J*) occurring between the Cu-Ln centres. There is an exponential correlation between *J* and the Cu-Ln distances, which suggests that, although being an assumption based solely on empirical grounds, an increase of the exchange occurs as the distance between the metal centres becomes smaller. The experimental way to test such a correlation would be to synthesise a dinuclear CuLn species in which the antiferromagnetic exchange is reduced to zero, being this exchange occurring exclusively between cations of the same nature.[89] All the aforementioned metal clusters are characterised by a relatively small spin ground state, the highest value being of $S = 9/2$ in the case of the $Cu^{II}_2Ln^{III}_2$ cluster, but for large clusters the antiferromagnetic interactions between the copper centres are so strong that the molecule possesses an overall low spin or it is even diamagnetic.

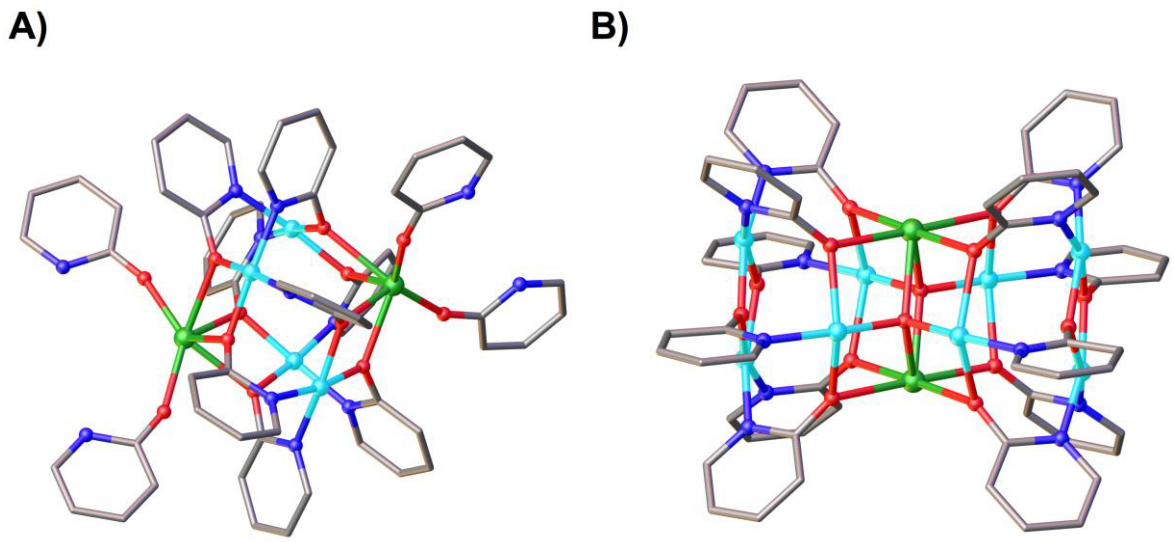

Figure 21. Partial single crystal *X*-ray structures of A) $Cu^{II}_4Ln^{III}_2$ and B) $Cu^{II}_8Ln^{III}_2$ (Ln = Gd, Dy, Nd, Y) clusters with 2-pyridone ligands.[88] Hydrogen atoms, ligated solvent molecules and solvent of crystallisation omitted for clarity (Colour code: Cu – light blue; Ln – green, C – grey, N – blue, O – red).

In 1993, the first true SMM was reported in the literature, comprising a $Mn^{IV}_4Mn^{III}_8$ cluster core.[90] This metal cluster has a spin ground state of $S = 10$, resulting from the antiferromagnetic interaction between the close Mn^{IV} ($S = 3/2$) and Mn^{III} ($S = 2$) ions, and an axial zero-field splitting that leads to the splitting of the $S = 10$ states into 21 different levels, each one characterised by an energy and a quantum number m_s where $-S \leq m_s \leq S$. For this cluster, the axial zero-field splitting parameter *D*, which is related to the axial

component of the dipole-dipole interaction, is negative. The negative value of *D* means that there is a potential barrier between the "spin-up" (m_s = -10) and "spin-down" (m_s = 10) orientation of the magnetic moment of each single molecule. The presence of this potential barrier means that energy is required in order to invert the moment from one orientation to the opposite one *via* perpendicular orientation in which the moment is zero (m_s = 0). If this energetic barrier is sufficiently large, the spin can be magnetised into one direction, and the time for reorientation of the magnetisation increases exponentially on the height of the potential-energy barrier. Calculations showed that the barrier for this cluster is around 70 K so, if it is magnetised at 2 K by applying and removing the magnetic field, the relaxation is so slow that after two months there is still 40 % of the net magnetic moment. The same measurements carried out at 1.5 K showed that the reorientation is so slow it could not be measured. These results clearly showed that the slow relaxation is given by individual molecules and not by long-range ordering, as in bulk magnets.

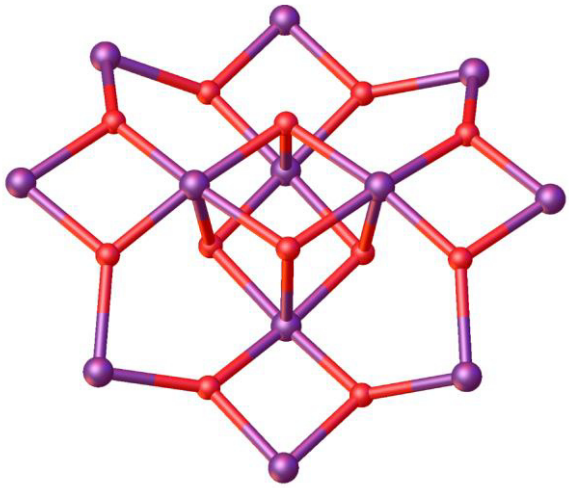

Figure 22. Partial single crystal *X*-ray structure showing $[Mn^{IV}_4Mn^{III}_8O_{12}]$ core (Colour code: Mn – purple, O – red).[90]

What is most important about SMMs is that when applying an external magnetic field, all the spins will align, exhibiting magnetisation. When the external field is removed, the magnetisation is blocked by the presence of the energy barrier that does not allow reordering. If a negative field is applied, it will reduce the barrier energy, thus giving the possibility to reverse the magnetisation, observing a hysteresis loop. Relying on this, in principle, information can be stored in a single molecule. Although being quite a rare phenomenon for macroscopic particles, it is worth mentioning that, in principle, these systems can also relax

through macroscopic quantum tunnelling (MQT) which, incidentally, is what has been observed for the $Mn^{IV}_4Mn^{III}_8$ cluster mentioned above.[90] The MQT is appreciable in the hysteresis loop for the presence of "steps" observed at regular intervals that are associated with an increase of the rate in magnetisation that occurs when there are two levels of similar energy belonging to two opposite sides of the potential barrier (Figure 23). Tunnelling is allowed for these values of energy, which translates into a visible increase of the relaxation rate.

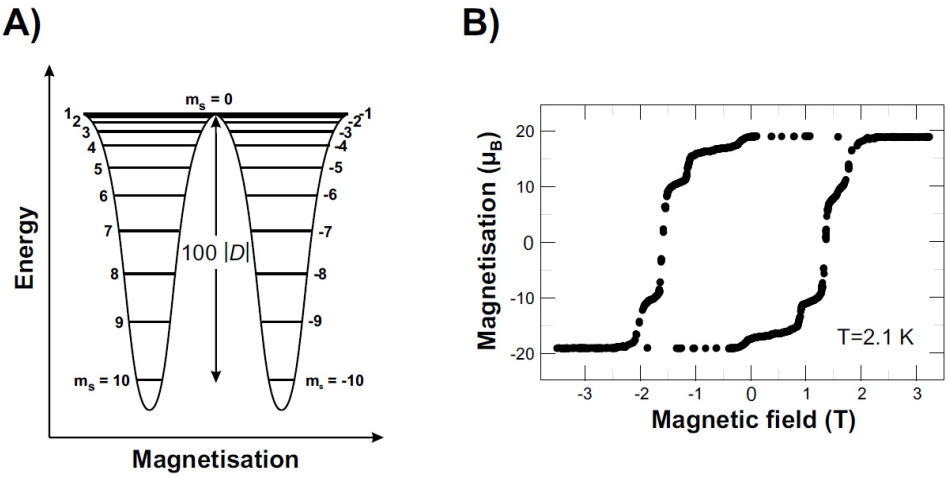

Figure 23. A) Plot of the potential energy versus the magnetisation direction for a SMM with $S = 10$. B) Magnetisation versus magnetic field hysteresis loop for the $Mn^{IV}_4Mn^{III}_8O_{12}$ cluster. The vertical jumps correspond to relaxation through quantum tunnelling.[85]

In general, SMMs should have a large S value with negative values of zero-field splitting. It is not easy to prepare large polynuclear clusters in a rational manner, with a definite number of metal centres and a large ground state. Whichever synthetic route is chosen, it is always important to increase the ground spin state, considering that it is not only the number of metal centres that contribute to the spin, but also antiferromagnetic interaction and magnetic exchange with neighbouring ligands; the metal ions and ligands have to be carefully designed and arranged. In addition, a high spin ground state does not assure SMM behaviour, as it depends also on the symmetry of the cluster.

Another important application that is rapidly gaining wide interest amongst the scientific community is the use of molecular magnets for low- and ultra-low temperature cooling (1.8 - 20 K). A cooling technique that relies exclusively on the use of magnetic fields is naturally quite attractive and, moreover, greener than the traditional ways of vapour / gas compression.[91] Applications of cryocoolers are not limited to everyday life, but also reach

into more advanced areas such as the condensation of light gases (including H_2, CH_4 etc.) and obtainment of sub-Kelvin and sub-milliKelvin temperatures. Currently, the only means to obtain such temperatures is to rely on H_2 / He liquefiers and superconducting magnets that can produce strong and permanent magnetic fields. These devices are often cooled at low temperatures by superfluid liquid helium in order to exhibit superconducting behaviour. There is a great deal of interest regarding the use of helium, since in each operation of maintenance of the magnets, the loss by evaporations are substantial, economically affecting these procedures. In addition, the aforementioned cryocoolers employ ^{3}He, an expensive isotope of helium that can reach a temperature of 0.5 K, whereas for gas compression ^{4}He is typically employed, having a 2 K limit. Successes have also been obtained with a $Gd_3Ga_5O_{12}$ (GGG) garnet,[92] a $Dy_3Al_5O_{12}$ garnet (DAG)[93] and $DyVO_4$[92]; this was followed by other researchers showing that rare earth orthoaluminates could be better refrigerants compared to the aforementioned examples.[94] Materials containing nanosized magnetic particles should exhibit an enhanced MCE compared to bulk material thanks to superparamagnetism. This is the case for a Gd / Ga / Fe garnet, in which the MCE enhancement is related to Gd-Gd interactions occurring *via* superexchange through Fe atoms.[95] Some materials capable of cooling down to 20 K have been synthesised in the past, but molecule-based magnetic refrigerants have recently been proposed as valid and more efficient alternatives. Cooling to temperatures lower than 20 K is theoretically possible but this would require that there is not long range magnetic order at the desired temperature, meaning that each magnetic centre responsible of the cooling effect must be separated.

A better way of cooling to extremely low temperature is to produce a magnetic material that can exploit the magnetocaloric effect (MCE), which is the cooling or heating upon exposure of said material to a variable magnetic field. The MCE is the result of the coupling of the magnetic moment to the temperature of the lattice, through variations of entropy resulting from variations of the external magnetic field. Since entropy is a measure of disorder, the magnetic entropy within the lattice is related directly to the order of the magnetic spins. When such a magnetic material is exposed to an external field the spins will align, producing a more ordered system with a reduced entropy. When the magnetic field is removed, assuming that the material is under adiabatic conditions (the total entropy of the system remains unchanged during the variation of the magnetic field), no energy is allowed to migrate into the material to induce the demagnetisation or reorientation of the spins. Therefore, the order decreases and, consequently, the magnetic entropy within the lattice

must increase. In order to balance the increase in entropy, energy must be removed from the lattice, leading to a lowering of the temperature of the material.

$$\Delta T_{ad} = -\int_{H0}^{H1}\left(\frac{T}{C(T,H)}\right)_H\left(\frac{\partial M(T,H)}{\partial T}\right)_H dH \quad \textbf{(1)}$$

This is shown in equation **(1)** where T is the temperature in K, H is the applied magnetic field, C is the heat capacity of the working magnet (refrigerant) and M is the magnetization of the refrigerant. The general rule is to design structures with little anisotropy (isotropic clusters), which makes it hard to polarise the net molecular spin. This leads to a large magnetic entropy change with low excited spin states, which allows one to gain extra magnetic entropy. Moreover, the material must respond quickly to magnetisation / demagnetisation loops.

The first magnetic clusters to be investigated were $[Mn_{12}]$[96] and $[Fe_8]$[97] due to their high ground spin state (S = 10) and large magnetic entropy. The large anisotropy displayed by these systems makes it hard to reorient the spins at very low temperature (below 4 K), thus making them perfect SMMs thanks to the slow relaxation of magnetisation, but also poor magnetic coolers. The first isotropic metal cluster described was a $[Cr_7Cd]$ wheel which, unfortunately, is characterised by a low spin ground state (S = 3/2).[98] Exploitation of highly symmetric building blocks gave the possibility to yield three-dimensional metal clusters with a large value spin ground state. Examples could be a $[Fe_{14}]$ cluster (S = 25),[99] a $[Mn_{10}]$ supertetrahedron (S = 22)[100] and a $[Mn_{14}]$[101] disk (S = 7) (Figure 24), which display a large MCE enhancement thanks to a combination of large spin ground state values and high symmetry of the cluster (which translates into small magnetic anisotropy).

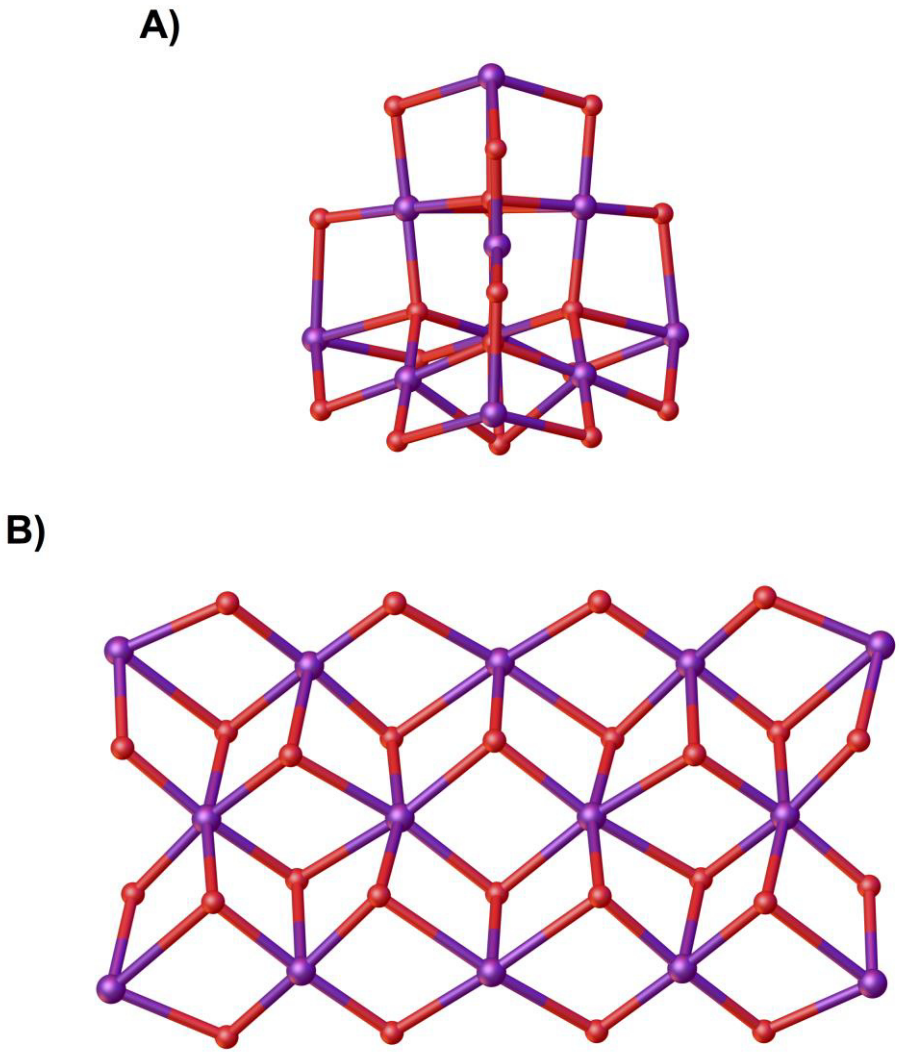

Figure 24. Partial single crystal *X*-ray structure of the cores of A) $Mn^{II}_6Mn^{III}_4$ supertetrahedron and B) $Mn^{II}_8Mn^{III}_6$ (Colour code: Mn – pink; O – red).[100] Figures not to scale.

A common strategy used in order to obtain high spin molecular clusters is to use tripodal polyalkoxide ligands which, upon reaction with transition metals, form triangular units that act as starting materials for more complex structures. [102] By pursuing this synthetic strategy a number of Mn- and Fe-based SMMs were produced, in addition to Ni and Co cubane-like structures,[103] the latter displaying no single-molecule magnet behaviour despite the Co^{II} being ferromagnetically coupled (Figure 25).

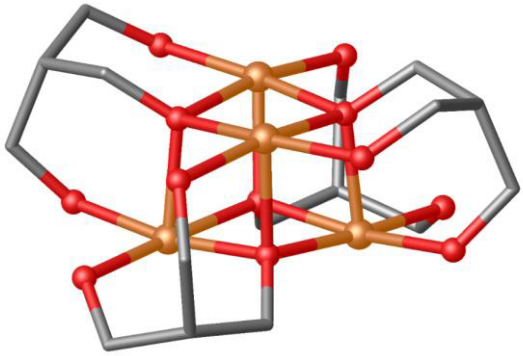

Figure 25. Partial single crystal *X*-ray structure of the core Ni^{II}/Co^{II} cubane-like (Colour code: Ni/Co – orange; O – red).[103] Hydrogen atoms, ligated solvent molecules and solvent of crystallisation omitted for clarity.

1.5. Calix[4]arene-supported metal clusters.

1.5.1. General calix[4]arene binding mode.

Calix[4]arenes are ideal potential candidates for the complexation of metal ions and, thanks to the bridging behaviour of the lower-rim phenolic oxygens and appropriate cavity size, the synthesis of paramagnetic clusters. When in the cone conformation, metal ions can be complexed by the lower-rim phenolic (or phenolate) oxygens atoms either inside or outside the macrocyclic cavity, referred to as *endo* and *exo* respectively (Figure 26).[104]

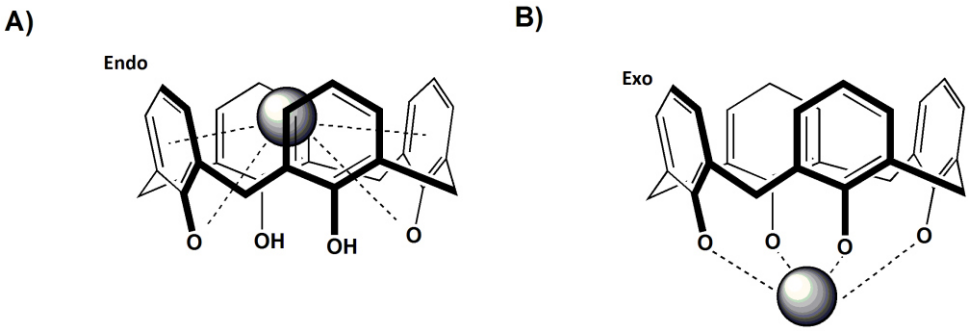

Figure 26. Schematics of A) *endo*-H_2C[4] metal ion binding and B) *exo*-C[4] metal ion binding at the lower-rim oxygens.

In *endo* binding, the metal ion is capable of interacting with the π faces of the macrocyle and with the lower-rim oxygens simultaneously, whereas in the *exo* case the cation is complexed by the four lower-rim oxygens, thus sitting just below the macrocycle plane. However, few cations are large enough to participate in multiple metal-π interactions, thus making *endo* complexation less favourable, especially when bonding by the four phenolic oxygens and

additional solvent interactions are considered. In general, alkaline and alkaline-earth metals tend to be complexed in the calix[4]arene cavity because, in this way, the metal ion can interact in an *endo* fashion with both the phenolic units and through cation- π interactions. The clusters presented in this paragraph, as well as in the following chapters, exclusively involve *exo*-binding (Figure 26).

The first high-nuclearity calix[4]arene-supported transition metal (TM) cluster was reported in by Luneau *et al.* in 2008.[105] This comprised a mixed valence $V^{III}V^{IV}_5O_{19}$ Lindqvist-like polyoxovanadate cluster capped by a TBC[4] moiety, obtained under anaerobic and solvothermal conditions (Figure 27). As is common, the interaction between the V^{III} and V^{IV} centres is weakly ferromagnetic whereas the exchange between the V^{IV} is of antiferromagnetic nature.

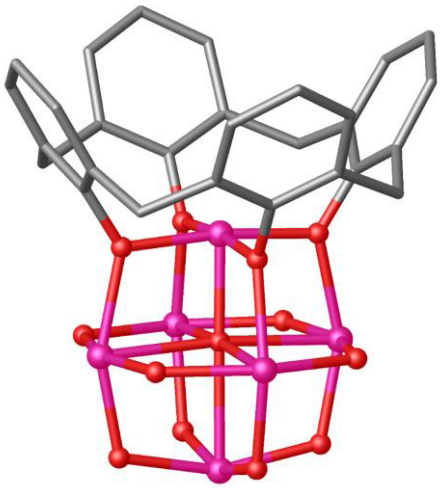

Figure 27. Partial single crystal *X*-ray structure of polyoxovanadate-TBC[4] cluster (Colour code: V – pink; O – red).[105] ^{t}Bu groups, hydrogen atoms, ligated solvent molecules and solvent of crystallisation omitted for clarity.

Recently, there has been growing interest in calix[4]arene-supported metal clusters, whereas in the past more attention has been addressed to coordination chemistry of the thia-, sulfinyl- and sulfonycalix[4]arenes.[106] While methylene-bridged calix[4]arenes are capable of binding one metal ion *via exo* complexation at the lower-rim, the presence of heteroatoms or heteroatom-containing groups such as S, SO and SO_2 at the bridging positions offers additional binding sites that can potentially affect the complexation of cations, resulting in markedly different cluster topologies (Figure 28).

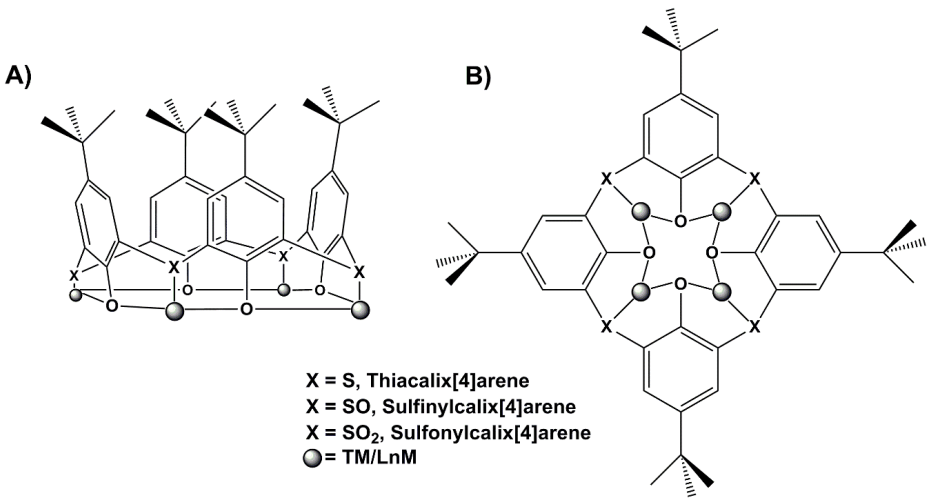

Figure 28. A) Metal ion binding motif and B) Schematic top view of thia-, sulfinyl- and sulfonylcalix[4]arene binding modes.[106]

The C-S bonds in thiacalix[4]arene (hereafter termed tC[4]) are longer than the C-C bonds in H_4TBC[4], and therefore each heteroatom generates a characteristic binding environment that comprises one soft sulfur bridging atom and two neighbouring hard oxygens. Although there are several examples in the literature in which the tC[4]s display coordination behaviour similar to the H_4TBC[4] analogues,[107] it has been shown that they behave differently when first row TM ions such as Mn^{II}, Co^{II}, Cu^{II} and Zn^{II} are involved.[108] The unique behaviour of tC[4] is retained with heavier TM ions such as Hg^{II}, forming the so-called "koiland" clusters, and Ln ions such as Nd^{III} (Figure 29).[109]

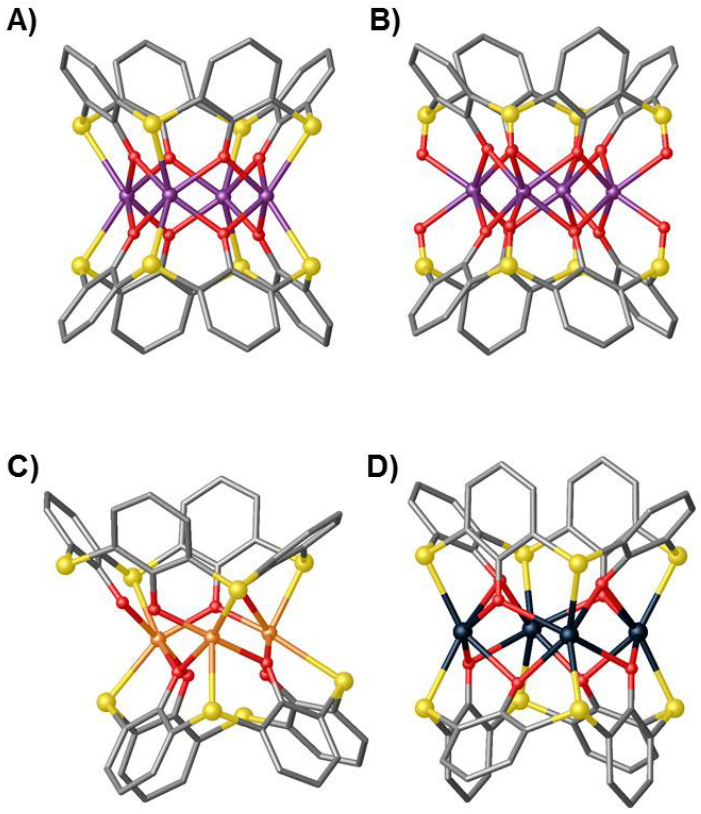

Figure 29. Partial single crystal *X*-ray structures of A) a tC[4]-supported tetranuclear Mn cluster showing coordination to the bridge atoms as well as to the lower-rim oxygens, B) a sulfinylcalix[4]arene-supported Mn_4 cluster, C) a tC[4]-supported trinuclear Co/Zn cluster and D) a tetranuclear koiland (Colour code: C – grey; O – red; S – yellow, Mn – purple, Co/Zn – orange, Hg – black).[108-109] ^{t}Bu groups, hydrogen atoms, ligated solvent molecules and solvent of crystallisation omitted for clarity.

In all of the examples mentioned above the tetra- and trinuclear clusters follow the same coordination behaviour, with the TMs or Ln ions sandwiched between tC[4]s (or sulfinylC[4]) that are fully or partially deprotonated, and in which the four sulfur and four oxygen atoms are near coplanar. Thiacalix[4]arene-based clusters have recently been used to produce a range of stable metal-organic polyhedra (MOPs) in which the TM_4tC[4] moieties are linked together thanks to topologically directing ligands such as benzene tricarboxylic acid (Figure 30).[110]

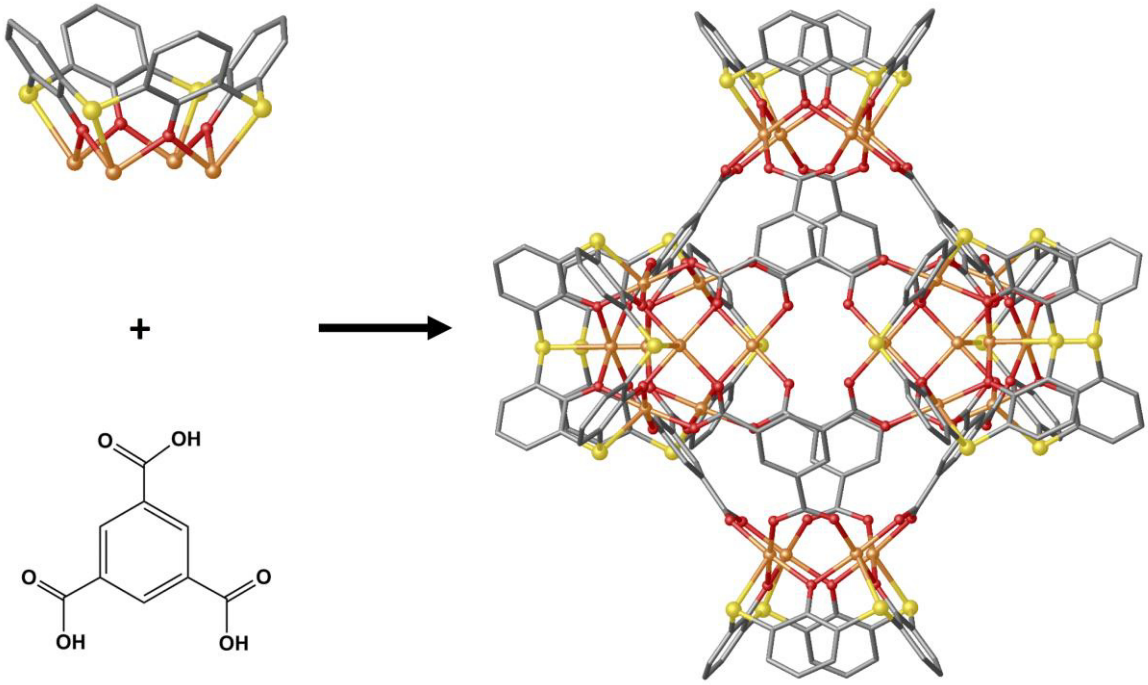

Figure 30. Directed assembly of a metal-organic octahedron using directing units and a $TM_4tC[4]$ bulding block (Colour code: C – grey; O – red; S – yellow, Co – orange).[110] ^{t}Bu groups, hydrogen atoms, ligated solvent molecules and solvent of crystallisation omitted for clarity.

1.5.2. TBC[4]-supported metal clusters.

The binding preference of $H_4TBC[4]$ and $H_4C[4]$ towards one metal ion at the lower-rim has been of particular interest within our group, as coordination could afford metal-organic building units from which it would be possible to construct larger systems. In the absence of additional donors at the methylene bridges, complexation always occurs at the lower-rim *via* interaction of the metal ion with the polyphenolic pocket. In addition, oxygens are also able to bridge to additional cations in the same way as in the polyoxovanadate TBC[4]-supported cluster mentioned above (Figure 27).[105]

Initial efforts within the research group with first row transition metal and aerobic bench top conditions culminated in the synthesis of several new calix[4]arene-based assemblies. The first example is a group of mixed valence $[Mn^{III}_2Mn^{II}_2(C[4])_2(\mu_3\text{-}OH)_2(dmf)_6]$ clusters (**1**, Figure 31) in which the metallic core is arranged to form a planar diamond-like or butterfly-like shape.[111] All four $Mn^{II/III}$ cations are arranged in distorted octahedral geometry, are occupying the wing-tip and body portions respectively and are bridged to each other *via* C[4] lower-rim oxygens and μ_3-hydroxides. Although this cluster

motif is not entirely new in Mn chemistry, it is noteworthy that the oxidation states in this case are reversed relative to those previously reported.[112]

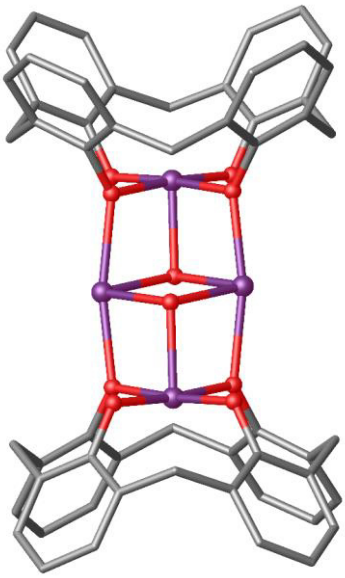

Figure 31. Partial single crystal *X*-ray structure of **1** showing the $[Mn^{III}_2Mn^{II}_2(OH)_2(C[4])_2]$ core (Colour code: Mn – purple; O – red; C – grey).[111] ^{t}Bu groups, hydrogen atoms, ligated solvent molecules and solvent of crystallisation omitted for clarity.

With respect to the magnetic properties, this cluster showed dominant but weak intramolecular ferromagnetic exchange. The ground state is $S = 7$ with various excited states which differentiate very little in energy, thus describing a quasi-continuum of states. Magnetisation *vs* field experiments showed that M increases slowly and does not reach saturation quickly as it would for an isolated ground state. Hysteresis loop measurements confirmed SMM behaviour, with no intercluster interactions, even though there are many excited states mixed with the ground state. Similar results have been obtained using $H_4C[4]$ in which the upper-rim *tert*-butyl groups were removed, with the only difference being in the packing observed; the result of this is a more compact bilayer due to the absence of the bulky *tert*-butyl groups. This proved that manipulation of the calix[4]arene upper-rim can dramatically affect the packing, resulting in a degree of structural control over the system.

Another type of assembly was isolated upon reaction of $H_4TBC[4]$ with Cu^{II} salts of differing nature, yielding enneanuclear Cu^{II} metal clusters of general formula $[Cu^{II}_9(C[4]_3)X_3]$ (**2**, Figure 32);[113] the main difference here is the nature of the counterions present as well as peripheral ligated solvent. This cluster can be described as having a tri-capped trigonal prismatic topology, with three hydroxides located in the core, bridging the

Cu^{II} ions at the vertices of the prism. A point of note is that there is a $[Cu^{II}(C[4])]^{2-}$ capping unit / moiety on each of the rectangular faces of the prism. Moving from **1** to **2** demonstrates the versatility of calix[4]arene to accommodate first row TMs in either the second or third oxidation state.

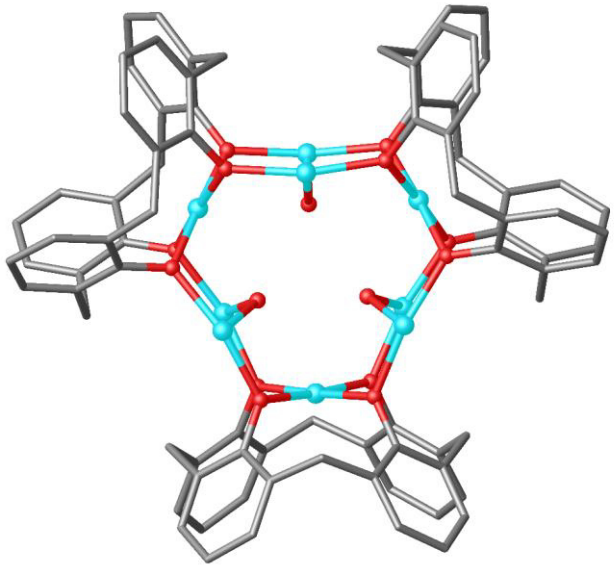

Figure 32. Partial single crystal *X*-ray structure of **2** showing the $[Cu^{II}_9(OH)_3(C[4])_3]$ core (Colour code: Cu – light blue; O – red; C – grey).[113] ^{t}Bu groups, hydrogen atoms, ligated solvent molecules and solvent of crystallisation omitted for clarity.

Dc magnetic susceptibility measurements on **2** suggest strong antiferromagnetic interactions between the Cu centres, with a spin ground state value of $S = 3/2$, confirmed by variable field magnetisation measures. From this is possible to rationalise that the ground state is given by a "spin-up" configuration of the Cu^{II} ions in the trigonal prism skeleton, whereas the capping ions are "spin-down". Another structurally analogous enneanuclear cluster was synthesised, this time comprising a Co^{II}_9 core.[114]

Rigorous screening with Ln ions resulted in the isolation of a family of clusters having general formula $[Ln^{III}_6(C[4]_2(\mu\text{-}OH)_4(\mu\text{-}O)_2(HCO)_2(dmf)_8]^+$ (Ln = Gd, Tb or Dy, **3**, Figure 33), with a disordered bridging counterion.[115] The topology of these clusters is significantly different to those described above regarding TMs, with the Ln ions arranged at the vertices of an octahedron. The Ln ions bound to the tetraphenolic pocket reside slightly out of the plane defined by the four lower-rim oxygens, whereas the remaining Ln cations form the central square of the octahedral structure. As already described for the clusters above, capping behaviour is also observed, in this case as a $[Ln^{III}(C[4])]^-$ moiety. As will be

clear in the following cluster descriptions, capping is a recurring theme for these systems. The magnetic behaviour of this family of clusters, obtained through dc magnetic susceptibility measurements, is indicative of weakly antiferromagnetic interactions between the Ln-Ln centres, which fits perfectly with the simulations obtained employing a model that considers the values of the magnetic exchange interaction (*J*) between the magnetic centres as equivalent.

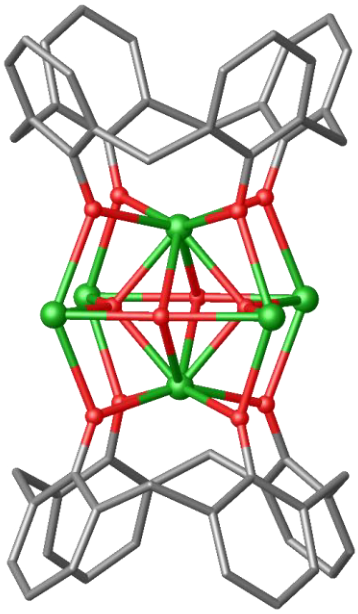

Figure 33. Partial single crystal *X*-ray structure of **3** showing the $[Ln^{III}_6(OH)_2(O)_2(C[4])_2]$ core (Colour code: Ln – green; O – red; C – grey).[115] ^{t}Bu groups, hydrogen atoms, ligated solvent molecules and solvent of crystallisation omitted for clarity.

Considering the ability of calix[4]arenes to support clusters containing TM or Ln ions, the next step was the synthesis of TBC[4]-supported 3*d*/4*f* metal clusters. By adding stoichiometric amounts of Ln^{III} salt to a reaction that normally would have led to the Mn_4 butterfly (**1**), it was possible to isolate a series of calix[4]arene-supported 3*d*/4*f* clusters of general formula $[Mn^{III}_4Ln^{III}_4(C[4])_4(\mu_3\text{-}OH)_4(NO_3)_2(dmf)_6(H_2O)_6](OH)_2$ (Ln = Gd, Tb or Dy, **4**, Figure 34).[116] These clusters can be readily visualised as a square of octacoordinate coplanar Ln^{III} ions in a distorted square antiprismatic geometry, within a square of $[Mn^{III}(C[4])]^-$ capping moieties, and in which the Mn^{III} ions are in a Jahn-Teller distorted octahedral geometry.

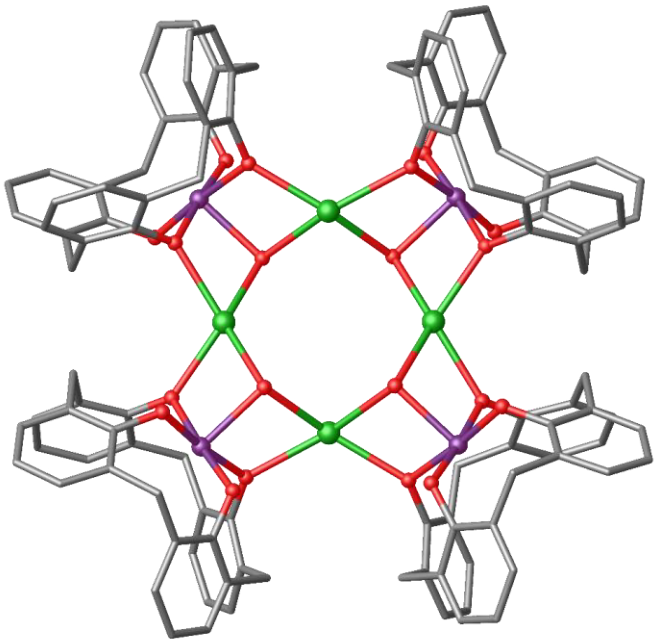

Figure 34. Partial single crystal *X*-ray structure of **4** showing the $[Mn^{III}_4Ln^{III}_4(C[4])_4(\mu_3\text{-}OH)_4(NO_3)_2(dmf)_6(H_2O)_6](OH)_2$ core (Colour code: Mn – purple; Ln – green; O – red; C – grey).[116] Hydrogen atoms, ligated solvent molecules and solvent of crystallisation omitted for clarity.

Magnetic studies on the Gd-containing cluster revealed that, at the temperatures investigated (5 - 300 K), a vast number of molecular spin states are populated, with predominantly weak intramolecular exchange. The ferromagnetic interactions given by $S = 22$ are reached exclusively at very large applied fields, meaning that the low-lying levels become depopulated when a large field is applied, making this cluster a perfect candidate for molecular refrigeration. Magnetic entropy changes were therefore determined and were found to increase gradually with increasing magnetic fields, reaching the highest values reported at that time. Moreover, the magnetic entropy change is larger than the maximum allowed for an isolated cluster having $S = 22$, confirming the presence of low-lying excited states that positively contribute to the large MCE. Selective replacement of the Gd^{III} ions, which have a zero-orbital moment, with Tb^{III} and Dy^{III}, that are instead anisotropic, has a dramatic effect on the magneto-thermal properties of structurally analogous molecules. Because of the overall anisotropy induced by Tb^{III} and Dy^{III}, each cluster has a net magnetic moment at low temperatures that has the general effect of inducing a slow relaxation of the magnetisation, resulting in SMM behaviour.

Expansion of the 3*d*/4*f* cluster library was successful with the synthesis of a series of TBC[4]-supported $Fe^{III}_2Ln^{III}_2$ clusters of general formula

$[Fe^{III}_2Ln^{III}_2(C[4])_2(\mu_4\text{-}O)(\mu\text{-}OH)(dmf)_4(MeOH)_2(H_2O)_2]Cl$ (Ln = Gd, Tb or Dy, **5**, Figure 35).[117] The metallic skeleton of these clusters is a distorted tetrahedron in which all the metal centres are connected *via* μ_4-oxide anions. Again, capping behaviour is observed with $[Fe^{III}(TBC[4])]^-$ moieties that act in a similar fashion to the $[Mn^{III}(TBC[4])]^-$ units seen above. Regarding the magnetic properties of this cluster, magnetisation measurements on the Gd^{III} derivative showed that, at low temperature, the two Fe^{III} ions are blocked in a non-magnetic singlet state and therefore the whole molecule behaves as two paramagnetic weakly interacting Gd^{III} ions. For the Dy^{III} and Tb^{III} derivatives, there is an expected magnetic anisotropy although no SMM behaviour is encountered.

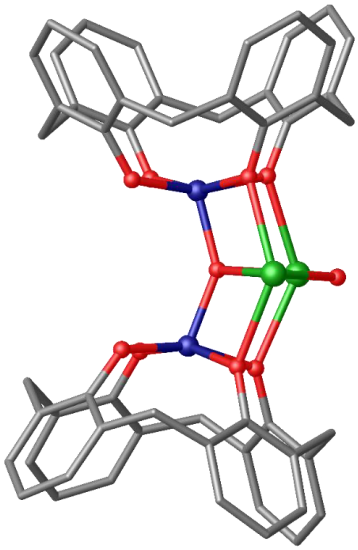

Figure 35. Partial single crystal *X*-ray structure of **5** showing the $[Fe^{III}_2Ln^{III}_2(C[4])_2(\mu_4\text{-}O)(\mu\text{-}OH)(dmf)_4(MeOH)_2(H_2O)_2]Cl$ (Ln = Gd, Tb or Dy) core (Colour code: Fe – dark blue; Ln – green; O – red; C – grey).[117] ^{t}Bu groups, hydrogen atoms, ligated solvent molecules and solvent of crystallisation omitted for clarity.

Another important achievement of our group in relation to TBC[4]-supported 3*d*/4*f* clusters was the isolation of two more clusters of general formula $[Mn^{III}_2Mn^{II}Ln^{III}(C[4])_2(\mu_3\text{-}OH)_2(NO_3)(dmso)_6]$ (**6**) and $[Mn^{III}_2Ln^{III}_2(C[4])_2(\mu_3\text{-}OH)_2(dmso)_8]Cl_2$ (**7**, Ln = Gd, Tb or Dy, Figure 36).[118] This family of clusters was elegantly obtained by tuning the reaction conditions (metal salt, stoichiometry and solvents), demonstrating an unusual example of TM / Ln ion interchange with retention of the major structural connectivities.

By inspection of the partial single crystal *X*-ray structures in Figure 36 it is possible to appreciate the small, yet important structural differences derived by such an interchange. The presence of a larger, more highly coordinated Ln^{III} ion in place of Mn^{II} in Figure 36B

has the effect of distorting the co-planarity of the C[4] moieties present in Figure 36A. This co-planarity is restored in Figure 36C upon interchange of the second Mn^{II} ion with another Ln^{III} ion.

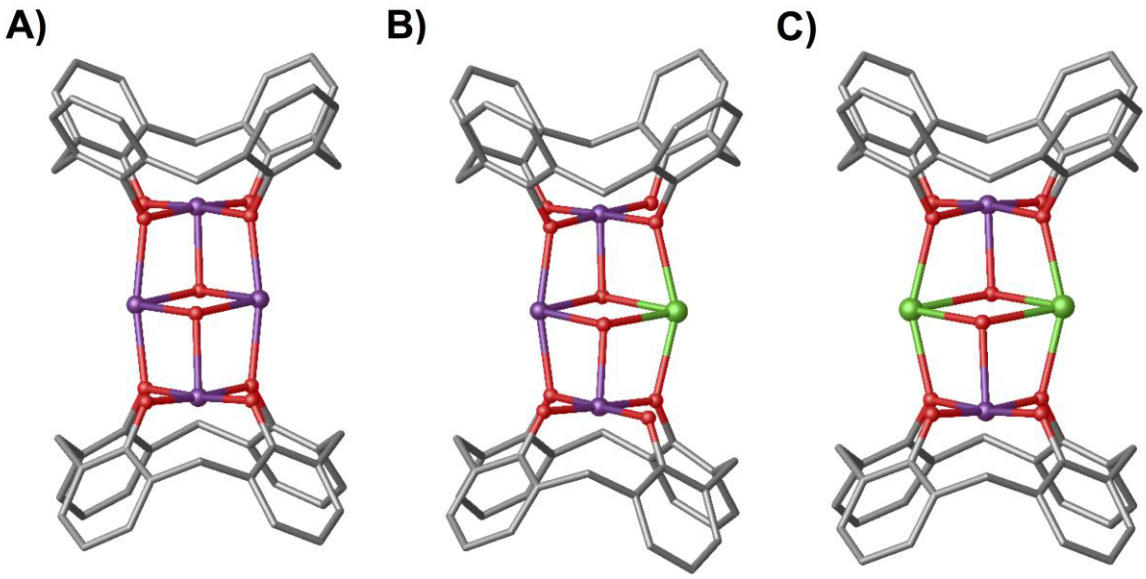

Figure 36. Partial single crystal *X*-ray structures comparing A) **1** $[Mn^{III}_2Mn^{II}_2(OH)_2(C[4])_2]$, B) **6** $[Mn^{III}_2Mn^{II}Ln^{III}(C[4])_2(\mu_3\text{-}OH)_2]$ and C) **7** $([Mn^{III}_2Ln^{III}_2(C[4])_2(\mu_3\text{-}OH)_2]$. Figures not to scale (Colour code: Mn – purple; Ln – green; O – red; C – grey).[118] ^{t}Bu groups, hydrogen atoms, ligated solvent molecules and solvent of crystallisation omitted for clarity.

Compound **1** shows important magnetic exchange between the metal centres, both ferro- and antiferromagnetic, and these interactions become progressively weaker for **6** and **7**, which is expected for the introduction of one or two 4*f* metal ions as the cluster becomes increasingly isotropic. Moving from **1** to **6** to **7**, two and four relatively strong ferromagnetic interactions (Mn^{III}-Mn^{II}) are removed and replaced with two (**6**) and four (**7**) weak ferromagnetic interactions that are at least one order of magnitude smaller than the former. Moreover, the antiferromagnetic interaction of the Mn^{II}-Mn^{II} is replaced by the two weaker antiferromagnetic interactions between the Mn^{II}-Gd^{III} and Gd^{III}-Gd^{III}. The result of these changes is the presence of more pathways through which the net magnetisation can relax. On moving to Tb and Dy for both **6** and **7**, a weak antiferromagnetic exchange becomes evident between the Mn^{II}-Tb^{III}/Dy^{III}, replacing the weak ferromagnetic interaction of the Mn^{II}-Gd^{III} centres.

Another viable route to influence the cluster composition and its geometry is to alter the size and/or the shape of the lower-rim phenolic pocket involved in metal binding. This

approach has been accurately followed with the preparation of a homooxacalix[4]arene (hoC[4]) in which, with respect to the classical calix[4]arene, one ethereal oxygen has been introduced between the phenolic moieties within the macrocycle. Reaction of this ligand with Ln^{III} ions yielded clusters of general formula $[Ln^{III}_5(hoC[4])_2(NO_3)_3(\mu\text{-}MeO)(\mu\text{-}O)(\mu_3\text{-}OH)(dmf)_7(H_2O)]$ (Ln = Gd, Tb or Dy, **8**, Figure 37).[119] If the Ln^{III}_6 octahedron described above (**3**, Figure 33) is taken as starting point,[115] the distortion generated by the introduction of a bridging heteroatom has the effect of expelling one Ln^{III} ion, resulting in a Ln^{III}_5 cluster in which two $[Ln^{III}(hoC[4])]^-$ moieties are capping a triangle, producing a distorted square pyramidal metallic core as a result.

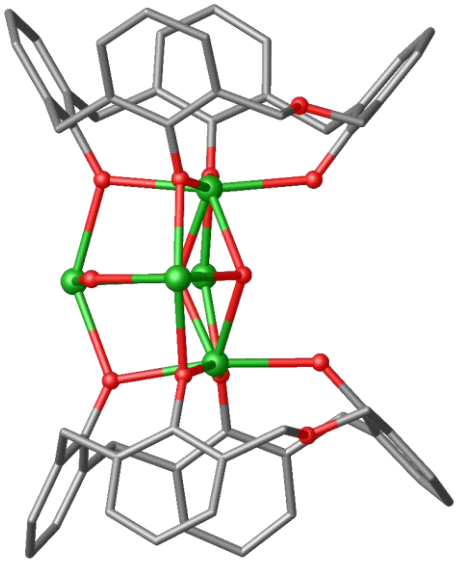

Figure 37. Partial single crystal *X*-ray structure of **8** showing the $[Ln^{III}_5(hoC[4])_2(NO_3)_3(\mu\text{-}MeO)(\mu\text{-}O)(\mu_3\text{-}OH)(dmf)_7(H_2O)]$ core (Ln = Gd, Tb or Dy) (Colour code: Ln – green; O – red; C – grey).[119] ^{t}Bu groups, hydrogen atoms, ligated solvent molecules and solvent of crystallisation omitted for clarity.

The magnetic data for the cluster containing Gd showed very weak intramolecular antiferromagnetic interactions and, considering all the Gd-Gd interactions as equivalent, presents a behaviour that is similar to the Gd_6 octahedron. In contrast, the Tb and Dy analogues show no small magnetisation relaxation and hence no SMM behaviour, which is surprising considering that similar Dy_5 pyramids are characterised by a large thermal barrier regarding the magnetisation relaxation.[120]

From the exploratory cluster-formation studies described so far, it is possible to observe constant structural trends, coordination preferences and common cluster motifs; therefore, the following empirical rules were established:

- TM^{II}/TM^{III} cations are always bound within the C[4] tetraphenolic pocket, producing $[TM(C[4])]^{-/2-}$ capping units (Figure 38);
- Ln^{III} cations are bound within the C[4] tetraphenolic pocket, producing $[Ln(C[4])]^{-}$ capping units;
- In the case of reaction mixtures involving 3*d*/4*f* metals, the TM ion is always bound preferentially by the C[4] tetraphenolic pocket;
- All clusters have a geometry in which the core metals are linked to each other to form a 3D (frequently polygonal) assembly, the edges or faces of which are capped by the aforementioned $[TM(C[4])]^{-/2-}$/$[Ln(C[4])]^{-}$ moieties.

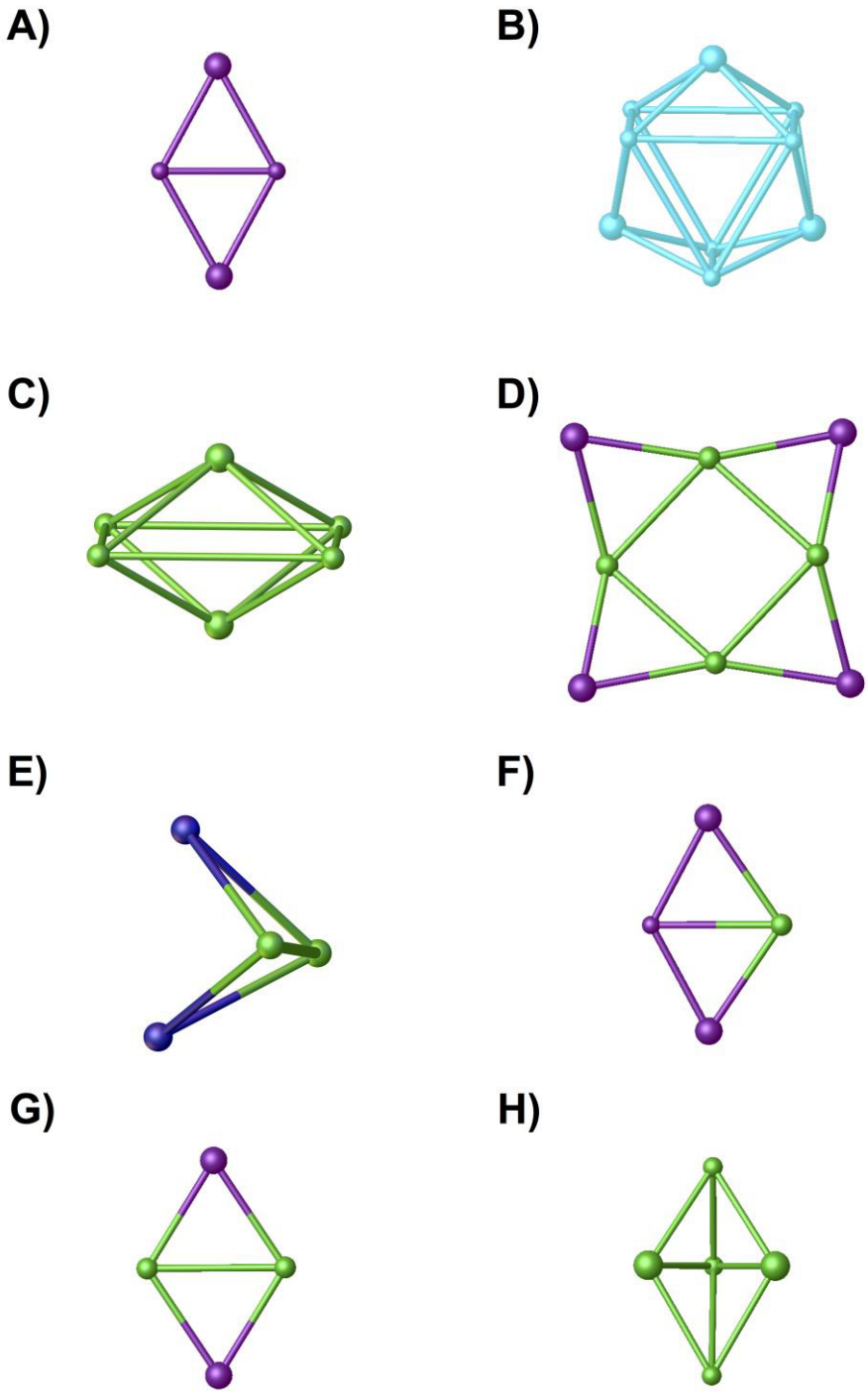

Figure 38. Capping behaviour in the structures of **1** – **8**. Capping by $[TM^{III} / Ln^{III}(TBC[4])]^-$ moieties are shown as large spheres (Colour code: Mn – purple; Cu – light blue; Fe – dark blue; Ln – green).

1.5.3. BisTBC[4]-supported metal clusters.

As described in section 1.3 (*vide supra*), functionalisation of calix[4]arenes at the methylene bridge represents an excellent route in order to obtain novel molecular entities that can be exploited in coordination chemistry, since this functionalisation leaves the lower-rim phenolic pocket free for metal complexation. The efforts of the Biali and Fantini groups have been extremely important in this context, because the methylene bridge-functionalised molecules offer the possibility to influence, enhance and / or direct the cluster topology. The compound 2,2-biscalixarene (H_8BisTBC[4]) was found to be an excellent building block, capable of yielding a plethora of novel polymetallic clusters that are structurally related to the aforementioned TBC[4] analogues. Some are described here, whereas the rest are discussed in more detail in Chapters 2 and 3, as they were obtained during the doctoral period of which this thesis represents the outcome.

Upon conformational change to *syn*-, BisTBC[4] generates two additional binding sites for $TM^{II/III}$ / Ln^{III} cations; this occurs thanks to the proximity of four lower-rim oxygens belonging in pairs to the two constituent TBC[4] moieties in the ligand scaffold. It is possible in this way to identify two different binding sites or modes: Type I, in which the $TM^{II/III}$ / Ln^{III} cations are classically residing in the calix[4]cavity, and Type II, in which the cations are bound in the aforementioned binding sites generated upon configurational inversion of the ligand from *anti* to *syn* (Figure 39).[121]

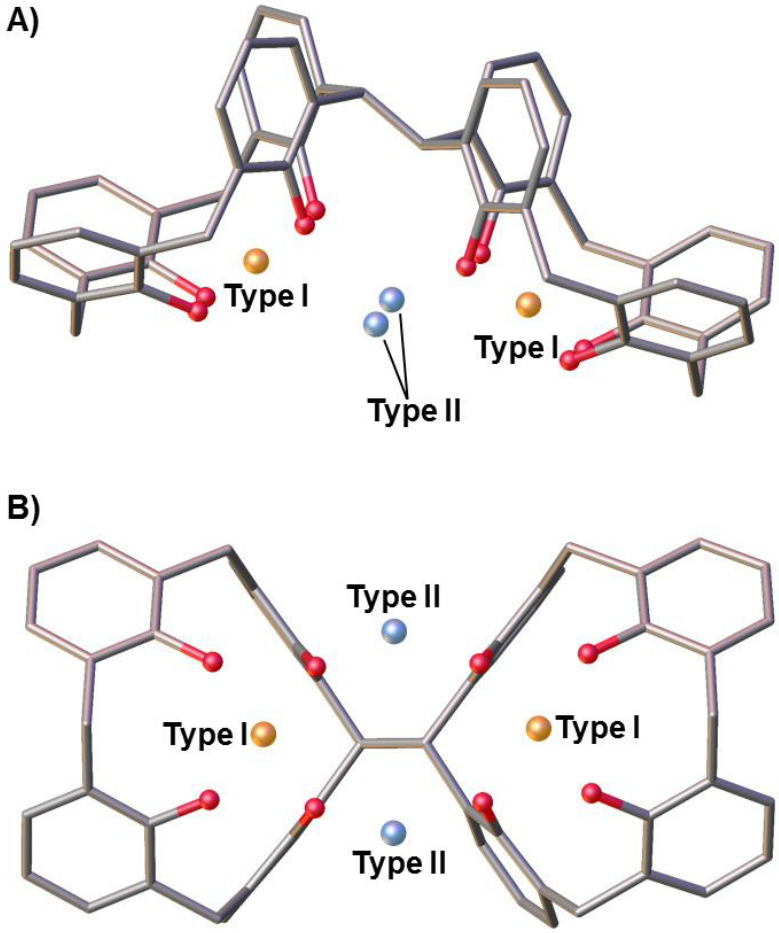

Figure 39. Plan (A) and elevation (B) views of a partial single crystal *X*-ray structure containing BisTBC[4] showing the two different binding types when the ligand is in the *syn*-configuration.

Reaction of H_8BisTBC[4] with Mn(II) chloride under analogous conditions used to synthesise the Mn_4 butterfly afforded a new cluster of formula $[Mn^{III}_4Mn^{II}_4(BisTBC[4])_2(\mu_3\text{-}OH)_2(\mu\text{-}Cl)(H_2O)(MeOH)(dmf)_4$ (**9**, Figure 40).[122] This cluster comprises a mixed valence Mn^{III}/Mn^{II} metallic skeleton that is closely related to the $Mn^{III}_2Mn^{II}_2$ butterfly obtained with TBC[4]. Four Mn^{III} ions are bound within each cavity of the two BisTBC[4] molecules in a Type I coordination mode, whereas the four Mn^{II} are housed in the Type II binding sites generated by ligand inversion. Each metal ion is hexacoordinate, is in a distorted octahedral geometry and is connected with its neighbour by bridging phenolates, hydroxides and chlorides. As a result, the cluster can be described as two fused and highly distorted $Mn^{III}_2Mn^{II}_2$ butterflies, further stressing the structural relation to TBC[4], as $[Mn^{III}_2(BisTBC[4])]^{2-}$ capping moieties are present (Figure 43).

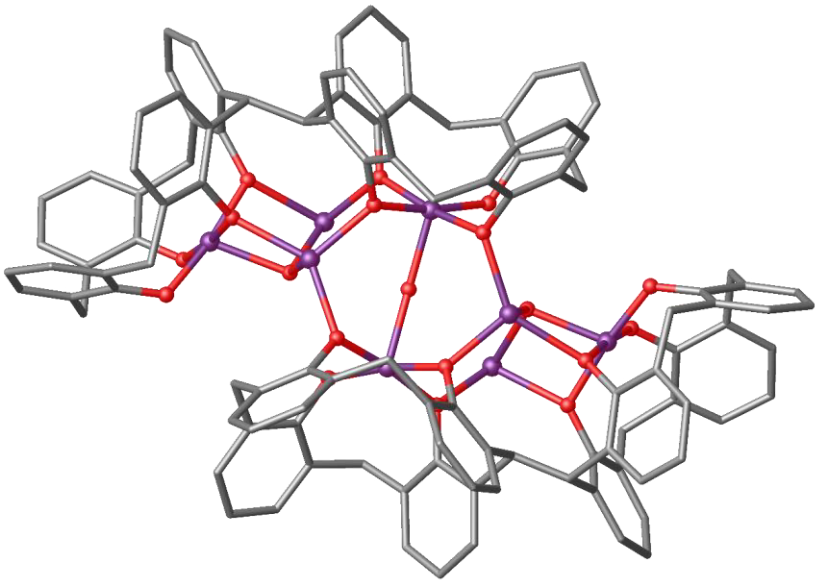

Figure 40. Partial single crystal *X*-ray structure of **9** showing the $[Mn^{III}_4Mn^{II}_4(BisTBC[4])_2(\mu_3\text{-}OH)_2(\mu\text{-}Cl)(H_2O)(MeOH)(dmf)_4$ core (Colour code: Mn – purple; O – red; C – grey).[122] ^{t}Bu groups, hydrogen atoms, ligated solvent molecules and solvent of crystallisation omitted for clarity.

Temperature-dependent dc magnetic susceptibility studies show that, at 300 K, the magnetisation (expressed as the product χT, where $\chi = M/B$, M is the magnetisation and B is the applied magnetic field) is exclusively dependent on the spin-only contribution from both Mn^{II} and Mn^{III}, although smaller than the calculated value. On lowering the temperature, χT remains essentially constant until the temperature of 150 K is reached, at which point it begins to rapidly decrease. The complexity of **9** makes modelling of the overall magnetic behaviour challenging, and algorithms were required in order to find a best fit of the data. The data are consistent with parameters calculated for topologies containing the same inverted butterfly. From this, the calculated ground state has a value of $S = 0$, with numerous excited spin-states with energies very close to the ground state.

Screening of the coordination behaviour of H_8BisTBC[4] with other TM ions resulted in the isolation of a Cu-based cluster having formula $[Cu^{II}_{13}(BisTBC[4])_2(NO_3)(\mu\text{-}OH)_8(dmf)_7](OH)$ (**10**, Figure 41).[122] The metallic core of the cluster can be described as a tetra-capped square prism at the centre of which is located the thirteenth Cu^{II} cation, disordered over several positions. The square prism is formed by eight Cu^{II} ions, four residing in the BisTBC[4] binding pockets and four located between the two Cu^{II}_4-BisTBC[4] sections, with four Cu^{II}-TBC[4] moieties capping each edge (Figure 43). The

clusters demonstrate a remarkable extension to the tri-capped trigonal prismatic Cu^{II}_9 species obtained using TBC[4] (**2**, Figure 32, Section 1.5.2).

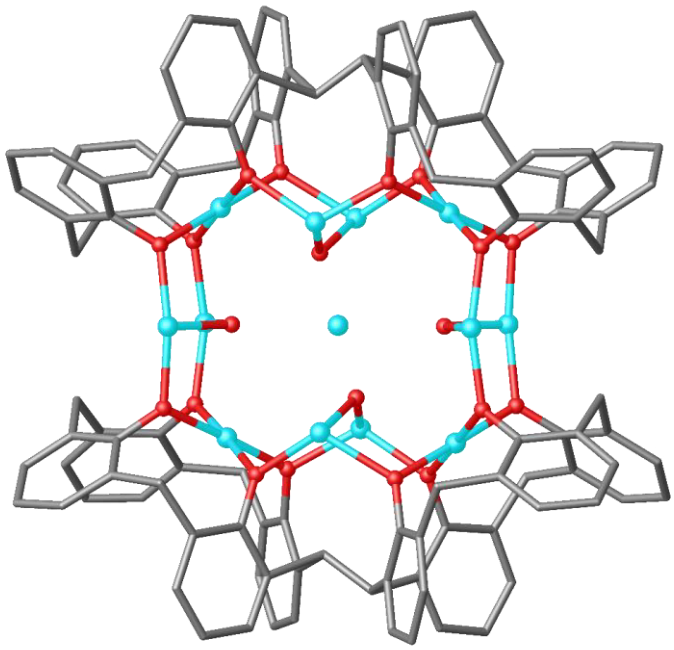

Figure 41. Partial single crystal *X*-ray structure of **10** showing the $[Cu^{II}_{13}(BisTBC[4])_2(NO_3)(\mu\text{-}OH)_8(dmf)_7](OH)$ core (Colour code: Cu – light blue; O – red; C – grey).[122] ^{t}Bu groups, hydrogen atoms, ligated solvent molecules and solvent of crystallisation omitted for clarity.

Compound **10** has a χT value lower than that calculated, which is indicative of strong antiferromagnetic interactions. On lowering the temperature, the magnetisation monotonically decreases and reaches a plateau at around 25 K and then a minimum at 5 K. The calculated spin state is a quadruply degenerate $S = 1/2$, with the first excited state being a doubly degenerate $S = 1/2$, energetically separated from the ground state.

Implementation of the reaction conditions that yielded TBC[4]-supported 3*d*/4*f* clusters was also successful with H_8BisTBC[4]. In the first instance, reaction of H_8BisTBC[4] with Mn(II) and Gd(III) chlorides afforded the first BisTBC[4]-supported 3*d*/4*f* cluster of formula $[Mn^{III}_4Mn^{II}_2Gd^{III}_2(BisTBC[4])_2(Cl)_2(\mu_3\text{-}OH)_4(MeOH)_2(dmf)_8]$ (**11**, Figure 42).[122] The cluster has a striking similarity to the $Mn^{III}_4Mn^{II}_4$ described above, the key difference being replacement of two Mn^{II} ions with two Gd^{III} ions. The butterfly motif is retained to some extent, although with some distortion originating from the larger size and higher coordination number of the gadolinium cations, and is represented by a $Mn^{III}_2Mn^{II}Gd^{III}$ moiety. The whole structure can therefore be described, in analogy with the

$Mn^{III}_4Mn^{II}_4$ species, as the fusion of two distorted $Mn^{III}_2Mn^{II}Gd^{III}$ butterflies, with expected capping exerted by the $[Mn^{III}_2(BisTBC[4])]^{2-}$ units (Figure 43).

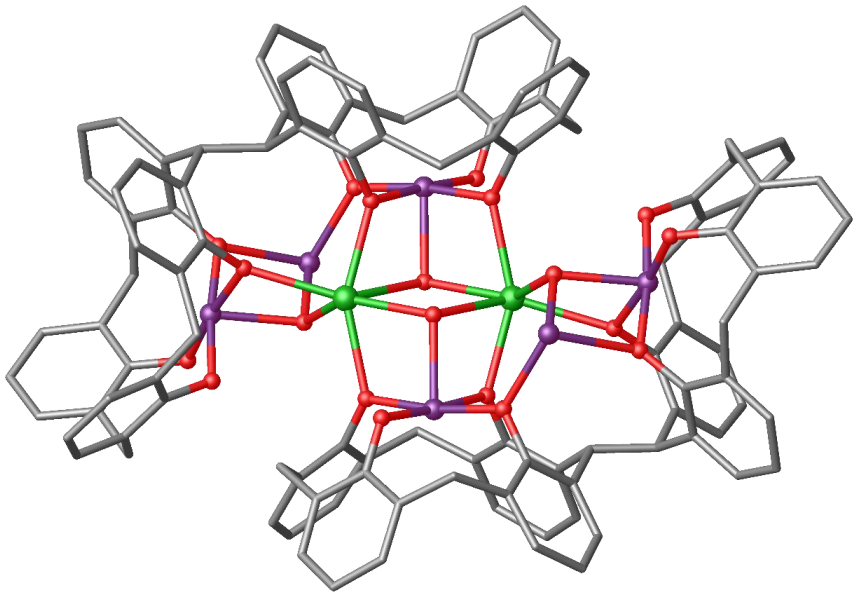

Figure 42. Partial single crystal *X*-ray structure of **11** showing the $[Mn^{III}_4Mn^{II}_2Gd^{III}_2(bisTBC[4])_2(Cl)_2(\mu_3\text{-}OH)_4(MeOH)_2(dmf)_8]$ core (Colour code: Mn – purple; Gd – green, O – red; C – grey).[122] ^{t}Bu groups, hydrogen atoms, ligated solvent molecules and solvent of crystallisation omitted for clarity.

Analogous experiments carried out on **11** showed that, at 300 K, the χT product has a value slightly higher than that calculated. Similar behaviour is observed upon lowering the temperature, with the magnetisation product remaining constant until 150 K, at which point it increases reaching a maximum at 5 K. An analogous algorithm to that used to model **9** was applied to the data obtained for **11**, with calculated parameter sets that reproduce the experimental data accurately. With these parameters, it was calculated that the ground spin state has a value of $S = 9$, with several low-lying excited spin states in close proximity to the ground state.

Considering the preliminary results obtained using H_8BisTBC[4] as a ligand, we envisaged that the binding rules established for H_4TBC[4] would broadly apply to H_8BisTBC[4]. The octa-anionic nature of BisTBC[4] allows for an enhanced nuclearity of the resulting clusters compared to those obtained with TBC[4], with capping behaviour that is systematically respected (Figure 43). This represents a promising feature as the greater

rigidity of the H_8BisTBC[4] ligand, along with more facile bridging behaviour, allows one to introduce a higher degree of control over the resulting assembly.

With this in mind, the overarching aims of the work in this thesis are:

- Further investigation of the binding properties of H_8BisTBC[4] (Chapter 2);
- Investigation into the effect of *N*,*O*-coligands on BisTBC[4]-supported metal clusters (Chapter 3);
- The synthesis of a range of flexible alkyl chain-tethered BisTBC[4]s (Chapter 4) and rigid spacer-tethered BisTBC[4]s (Chapter 5), and their use in exploratory cluster formation.

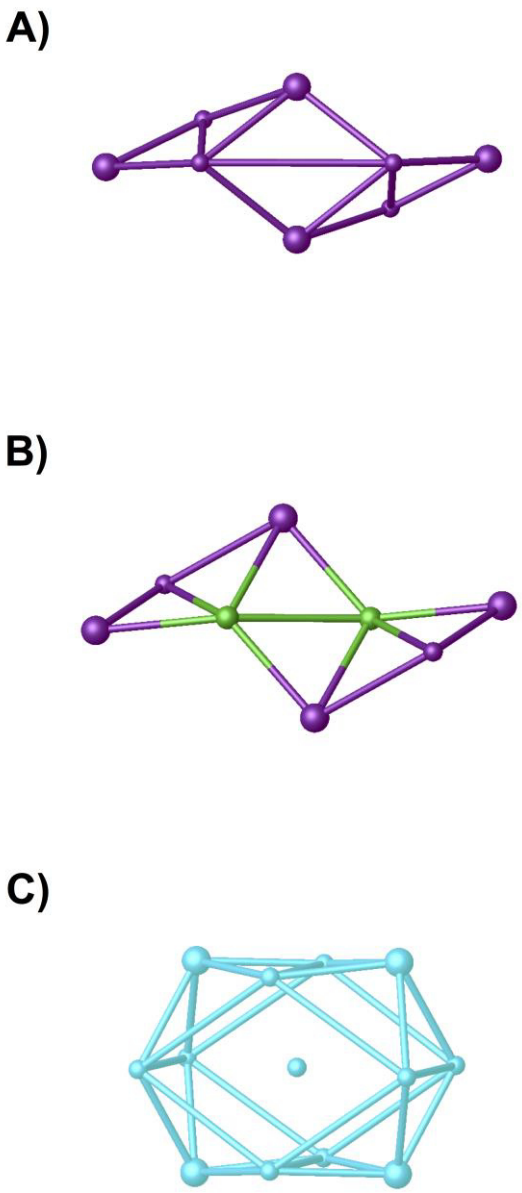

Figure 43. Capping behaviour the structures of **9** – **11**. Capping by $[TM^{III} / Ln^{III}(TBC[4])]^{-}$ moieties are shown as large spheres (Colour code: Mn – purple; Cu – light blue; Ln – green).

1.6. References.

1. Baeyer, A.; *Ber.*; **1872**, *5*, 280 – 282 and 1094 – 1100.

2. L. H. Baekeland US Patent 942,699; October **1908**.

3. Zinke, A.; Ziegler, E.; *Ber.*; **1944**, *77*, 264 – 272.

4. Hayes, B., T.; Hunter, R., F.; *J. Appl. Chem.*, **1958**, *8*, 743 – 748.

5. Cornforth, J., W.; Morgan, E., D.; Potts, K., T., Rees, R., J., W.; *Tetrahedron*, **1973**, *29*, 1659 – 1667.

6. Cram, D., J.; Steinberg, H.; *J. Am. Chem. Soc.*, **1951**, *73*, 5691 – 5704.

7. Gutsche, C., D.; Muthukrishnan, R.; *J. Org. Chem.*, **1978**, *43*, 4905 – 4906.

8. C. D. Gutsche, *Calixarenes – An Introduction*, 2nd edn., RSC, **2008** (and references therein).

9. Gutsche, C., D.; Iqbal, M., *Org. Synth.*, **1990**, *68*, 234 – 235.

10. Gutsche, C., D.; Dhawan, D.; No, K., H.; Muthukrishnan, R.; *J. Am. Chem. Soc.*, **1981**, *103*, 3782 – 3792.

11. Dhawan, B.; Chen, S., -I.; Gutsche, C., D.; *Makromol. Chem.*, **1987**, *188*, 921 – 950.

12. Stewart, D., R.; Gutsche, C., D., *Org. Prep. Proc. Int.*, **1993**, *25*, 137 – 139.

13. Ninegawa, A., Matsuda, H.; *Makromol. Chem. Rapid Commun.,* **1982**, *3*, 65 – 67.

14. Nakamoto, Y.; Ishida, S., I.; *Makromol. Chem. Rapid Commun.*, **1982**, *25*, 705 – 707.

15. Stewart, D., R.; Gutsche, C., D., *J. Am. Chem. Soc.* **1999**, *121*, 4136 – 4146.

16. Izatt, S., R.; Hawkins, R., T.; Christensen, J., J.; Izatt, R., M.; *J. Am. Chem. Soc.*, **1985**, *107*, 63 – 66.

17. Bocchi, V.; Foina, D.; Pochini, A.; Ungaro, R., *Tetrahedron*, **1982**, *38*, 373 – 378.

18. Asfari Z.; Vicens, J., *Makromol. Chem. Rapid. Commun.*, **1989**, *10*, 181 – 183.

19. Makha M., Raston, C., L.; *Tetrahedron Lett.*, **2001**, *42*, 6215 – 6217.

20. Georghiou, P., E.; Li, Z.; *Tetrahedron Lett.*, **1993**, *34*, 2887 – 2890.

21. Chasar, D., W.; *J. Org. Chem.*, **1985**, *59*, 545 – 546.

22. Niederl, J., B.; Vogel, H., J.; *J. Am. Chem. Soc.*, **1940**, *62*, 2512 – 2514.

23. Weinelt, F.; Schneider, H.; *J. Org. Chem.*, **1991**, *56*, 5527 – 5535.

24. Ogoshi, T.; Kanai, S.; Fujinami, S.; Yamagishi, T., A.; *J. Am. Chem. Soc.*, **2008**, *130*, 5022 – 5023.

25. Kim, J.; Jung, I.; Kim, S.; Lee, E.; Kang, J.; Sakamoto, S.; Yamaguchi, K.; Kim, K.; *J. Am Chem Soc.*, **2000**, *122*, 540 – 541.

26. Cragg, P., J.; Sharma, K.; *Chem. Soc. Rev*, **2012**, *41*, 597 – 607 and references therein.

27. Li, C.; Xu, Q.; Li, F.; Yao, F.; Jia, X.; *Org. Biomol. Chem.*, **2010**, *8*, 1568 – 1576.

28. Strutt, N., J.; Forgan, R., S.; Spruell, J., M.; Botros, Y., Y.; Stoddart, J., F.; *J. Am. Chem. Soc.*, **2011**, *133*, 5668 – 5671.

29. Ogoshi, T.; Nishida, Y.; Yamagishi, T., A.; Nakamoto, Y.; *Macromolecules*, **2010**, *43*, 7068 – 7072.

30. Kammerer, H.; Happel, G.; Caesar, F.; *Makromol. Chem.*, **1972**, *162*, 179 – 197.

31. Kammerer, H.; Happel, *Makromol. Chem.*, **1980**, *181*, 2049 – 2062.

32. Bohmer, V.; Chhim, P.; Kammerer, H.; *Makromol. Chem.*, **1979**, *180*, 2503 – 2506.

33. Bohmer, V.; Merkel, L.; Kunz, U.; *J. Chem. Soc. Chem. Commun.*, **1987**, 896 – 897.

34. Yamato, T.; Hasegawa, K.; Saruwatari, Y.; Doamekpor, L., K.; *Chem. Ber.*, **1993**, *126*, 1435 – 1439.

35. Yamato, T.; Saruwatari, Y.; Nagayama, S.; Maeda, K.; Tashiro, M.; *J. Chem. Soc. Chem. Commun.*, **1992**, 861 – 862.

36. Sommer, N.; Staab, H., A.; *Tetrahedron Lett.*, **1966**, 2837 – 2841.

37. Lehman, P., A.; *Tetrahedron*, **1974**, *30*, 727 – 733.

38. Wang, M.-X.; Yang, H.-B.; *J. Am. Chem. Soc.*, **2004**, *126*, 15412 – 15422.

39. Katz, J., L.; Feldman, M., B.; Conry, R., R.; *Org. Lett.*, **2005**, *7*, 91 – 94 and Katz, J., L.; Selby, K., J.; Conry, R., R.; *Org. Lett.*, **2005**, *16*, 3505 – 3507.

40. Konishi, H.; Mita, T.; Morikawa, O.; Kobayashi, K., *Tetrahedron Lett.*, **2007**, *48*, 3029 – 3032.

41. Sone, T.; Ohba, Y.; Moriya, K.; Kumada, H.; Kazuski, I.; *Tetrahedron*, **1997**, *53*, 10689 – 10698.

42. Iki, N.; Kabuto, C.; Fukushima, T.; Kumagai, H.; Takeya, H.; Miyanari, S.; Miyashi, T.; Miyano, S.; *Tetrahedron*, **2000**, *56*, 1437 – 1443.

43. Kon, N.; Iki, N.; Miyano, S.; *Tetrahedron Lett.*, **2002**, *41*, 2231 – 2234.

44. Morohashi, N.; Katagiri, K.; Iki, N.; Yamane, Y.; Kabuto, C.; Hattori, T.; Miyano, S.; *J. Org. Chem.*, **2003**, *68*, 2324 – 2333.

45. Morohashi, N.; Iki, N.; Sugawara, A.; Miyano, S.; *Tetrahedron*, **2001**, *57*, 5557 – 5563.

46. Musau, R., M.; Whiting, A.; *J. Chem. Soc. Chem. Commun.*, **1993**, 1029 – 1031.

47. Gale, P. A.; Sessler, J., L.; Kral, V.; Lynch, V.; *J. Am. Chem. Soc.*, **1996**, *118*, 5140 – 5141.

48. Komatsu, N.; Taniguchi, A.; Suzuki, H.; *Tetrahedron Lett.*, **1999**, *40*, 3749 – 3752.

49. Black, D., St., C.; Craig, D., C.; Kumar, N.; McConell, D., B.; *Tetrahedron Lett.*, **1996**, *37*, 241 – 244.

50. Koenig, B.; Rodel, M.; Bubenitschek, P.; Jones, P., G.; *Angew. Chem. Int. Ed. Engl.*, **1995**, *34*, 661 – 662.

51. Kral, V.; Gale, P., A.; Anzenbacher Jr., P.; Jursikova, K.; Lynch, V.; Sessler, J., L.; *Chem. Commun.*, **1998**, 9 – 10.

52. Rauter, H.; Hillgeris, E., C.; Erxleben, A., S.; Lippert, B.; *J. Am. Chem. Soc.*, **1994**, *116*, 616 – 624.

53. Gutsche, C., D.; Dhawan, B.; Levine, J., A.; No, K., H.; Bauer, L.; *Tetrahedron*, **1983**, *39*, 409 – 426.

54. Fischer, S.; Grootenhuis, P., D., J.; Groenen, L., C.; van Hoorn, W., P.; van Veggel, F., C., J., M.; Reinhoudt, D., N.; Karplus, M.; *J. Am. Chem. Soc.*, **1995**, *117*, 1611 – 1620.

55. Shinkai, S.; Araki, K.; Koreishi, H.; Tsubaki, T.; Manabe, O., *Chem. Lett.*, **1986**, 1351 – 1354.

56. Groenen, L., C.; Ruel, B., H., M.; Casnati, A.; Verboom, W.; Pochini, A.; Ungaro, R.; Reinhoudt, D., N.; *Tetrahedron*, **1991**, *47*, 8379 – 8384.

57. van Loon, J., -D.; Arduini, A.; Coppi, L.; Verboom, W.; Pochini, A.; Ungaro, R.; Harkema, S.; Reinhoudt, D., N.; *J. Org. Chem.*, **1990**, *55*, 5639 – 5646; Groenen, L., C.; Ruel, B., H., M.; Casnati, A.; Timmerman, P.; Verboom, W.; Harkema, S.; Pochini, A.; Ungaro, R.; Reinhoudt, D., N.; *Tetrahedron Lett.*, **1991**, *12*, 2675 – 2678.

58. No, K.; Koo, H., J.; *Bull. Korean Chem. Soc.*, **1994**, *15*, 483 – 488.

59. Shu, C., -M.; Liu, W., -C.; Ku, M., -C.; Tan, F., S.; Yeh, M., -L.; Lin, L., -G.; *J. Org. Chem.*, **1994**, *59*, 3730 – 3733.

60. Kanamathareddy S.; Gutsche, C., D.; *J. Org. Chem.*, **1995**, *60*, 6070 – 6074.

61. Alfieri, C.; Dradi, E.; Pochini, A.; Ungaro, R.; Andreetti, C., D.; *J. Chem. Soc. Chem. Commun.*, **1983**, 1075 – 1076.

62. Bohmer, V.; Rathay, D.; Kammerer, H.; *Org. Prep. Proced. Int.*, **1978**, *10*, 113 – 121.

63. Gutsche, C., D.; Pagoria, P., F.; *J. Org. Chem.*, **1985**, *50*, 5795 – 5802.

64. Linnane, P.; James, D.; Shinkai, S.; *J. Chem. Soc. Chem. Commun.*, **1995**, 1997 – 1998.

65. Lhotak, P.; Shinkai, S.; *Tetrahedron Lett.*, **1996**, *37*, 645 – 648.

66. Shinkai, S.; Usubaki, T.; Sone, T.; Manabe, O.; *Tetrahedron Lett.*, **1985**, *26*, 3343 – 3344.

67. Verboom, W.; Durie, A.; Egberink, R., J., M.; Asfari, Z.; Reinhoudt, D., N.; *J. Org. Chem.*, **1992**, *57*, 1313 – 1316.

68. Lazzarotto, M.; Sansone, F.; Baldini, L.; Casnati, A.; Cozzini, P.; Ungaro, R.; *Eur. J. Org. Chem.*, **2001**, 595 – 602.

69. Gutsche, C., D.; Levine, J., A.; *J. Am. Chem. Soc.*, **1982**, *104*, 2652 – 2653.

70. Arduini, A.; Pochini, A.; Reverberi, S.; Ungaro, R.; *J. Chem. Soc. Chem. Commun.*, **1984**, 981 – 982.

71. Biali, S., E.; Bohmer, V.; Cohen, S.; Ferguson, G.; Gruttner, C.; Grynszpan, F.; Paulus, E., F.; Thondorf, I.; Vogt, W.; *J. Am. Chem. Soc.*, **1996**, *118*, 12938 – 12949.

72. Scully; P., A.; Hamilton; T., M.; Bennett, J., L.; *Org. Lett.*, **2001**, *17*, 2741 – 2744.

73. Kumar, S.; Chawla, H., M.; Varadarajan, R.; *Tetrahedron Lett.*, **2002**, *43*, 7073 – 7075.

74. Columbus, I.; Biali, S., E.; *J. Org. Chem.*, **2008**, *73*, 2598 – 2606.

75. Columbus, I.; Biali, S., E.; *Org. Lett.*; **2007**, *15*, 2927 – 2929.

76. For examples see: 1) Kogan, K.; Biali, S., E.; *J. Org. Chem.*, **2009**, *74*, 7172 – 7175; 2) Kogan, K.; Columbus, I.; Biali, S., E.; *J. Org. Chem.*, **2008**, *73*, 7327 – 7335; 3) Kogan, K.; Biali, S., E.; *J. Org. Chem.*, **2011**, *76*, 7240 – 7244.

77. For examples see: 1) Poms, D.; Itzhak, N.; Kuno, L.; Biali, S., E.; *J. Org. Chem*, **2014**, *79*, 538 – 545; 2) Kuno, L.; Biali, S., E.; *J. Org. Chem*., **2011**, *76*, 3664 – 3675; 3) Itzhak, N.; Biali, S., E.; *J. Org. Chem.*, **2010**, *75*, 3437 – 3442; 4) Itzhak, N.; Kogan, K.; Biali, S., E.; *Eur. J. Org. Chem.*, **2011**, *32*, 6581 – 6585.

78. Litwak, A., M.; Grynszpan, F.; Aleksiuk, O.; Cohen, S.; Biali, S., E.; *J. Org. Chem.*, **1993**, *58*, 393 – 402.

79. Samah, S.; Agbaria, K.; Biali, S., E.; *J. Org. Chem.*, **2002**, *67*, 6136 – 6142.

80. Buccella, D.; Parkin, G.; *J. Am. Chem. Soc.*, **2006**, *128*, 16358 – 16364.

81. Hertel, M., P.; Behrle, A., C.; Williams, S., A.; Schmidt, J., A., R.; Fantini, J., L.; *Tetrahedron*, **2009**, *65*, 8657 – 8667.

82. Hardman, M., J.; Thomas, A., M.; Caroll, L., T.; Williams, L., C.; Parkin, S.; Fantini, J., L.; *Tetrahedron*, **2011**, *67*, 7027 – 7034.

83. For examples see: 1) Bew, S., P.; Brimage, R., A.; L'Hermite, N.; Sharma, S., V.; *Org. Lett.*, **2007**, *19*, 3713 – 3716; 2) Morales-Sanfrutos, J.; Ortega-Muñoz, M.; Lopez-Jaramillo, J.; Henandez-Mateo, F.; Santoyo-Gonzales, F.; *J. Org. Chem.*, **2008**, *73*, 7768 – 7771.

84. Carroll, L., T.; Hill, P., A.; Ngo, C., Q.; Klatt, K., P.; Fantini J., L.; *Tetrahedron*, **2013**, *69*, 5002 – 5007.

85. Christou, G.; Gatteschi, D.; Hendrickson, D., N.; Sessoli, R.; *MRS Bulletin*, **2000**, 25, 66 – 71 and references therein.

86. Bencini, A.; Benelli, C.; Caneschi, A.; Carlin, R., L.; Dei, A.; Gatteschi, D.; *J. Am. Chem. Soc.*, **1985**, *107*, 8129 – 8136.

87. Benelli, C.; Caneschi, A.; Gatteschi D.; Guillou, O.; Pardi, L.; *Inorg. Chem.*, **1990**, *29*, 1750 – 1755 and Andruh, M.; Ramade, I.; Codjovi, E.; Guillou, O.; Kahn, O.; Trombe, J., C.; *J. Am. Chem. Soc.*, **1993**, *115*, 1822 – 1829.

88. Goodgame, D., M., L.; Williams, D., J.; Winpenny, R., E., P.; *Polyhedron*, **1989**, *8*, 1531 – 1536 and Wang, S.; Pang, Z.; Wagner, M., J.; *Inorg. Chem.*, **1992**, *31*, 5381 – 5388.

89. Winpenny, R., E., P.; *Chem. Soc. Rev*, **1998**, *27*, 447 – 452 and references therein.

90. Sessoli, R.; Tsai, H., -L.; Schake, A., R.; Wang, S.; Vincent, J., B.; Folting, K.; Gatteschi, D.; Christou, G.; Hendrickson, D., N.; *J. Am. Chem. Soc.*, **1993**, *115*, 1804 – 1816.

91. Zheng, Y., -Z.; Zhou, G., -J.; Zheng, Z.; Winpenny, R., E., P.; *Chem. Soc. Rev.*, **2014**, *43*, 1462 – 1475 and references therein.

92. Barclay, J., A.; Moze, O.; Paterson, L.; *J. Appl. Phys.*, **1979**, *50*, 5870 – 5877.

93. Kuz'min, M., D.; Tishin, A., M.; *J. Phys. D: Appl. Phys*, **1991**, 2*4*, 2039 – 2044.

94. Kimura, H.; Numazawa, T.; Sato, M.; Ikeya, T.; Fukuda, T.; Fujioka, K.; *J. Mater. Sci.*; **1997**, *32*, 5743 – 5747.

95. McMichael, R., D.; Ritter, J., J.; Shull, R., D.; *J. Appl. Phys.*, **1993**, *73*, 6946 – 6948.

96. Caneschi, A.; Gatteschi, D.; Sessoli, R.; *J. Am. Chem. Soc.*, **1991**, *113*, 5873 – 5874.

97. Delfs, C.; Gatteschi, D.; Pardi, L.; Sessoli, R.; Wieghardt, K.; Hanke, D.; *Inorg. Chem.*, **1993**, *32*, 3099 – 3103.

98. Affronte, M.; Ghirri, A.; Carretta, S.; Amoretti, G.; Piligkos, S.; Timco, G., A.; Winpenny R., E., P.; *Appl. Phys. Lett.*, **2004**, *84*, 3468 – 3470.

99. Evangelisti, M.; Candini, A.; Ghirri, A.; Affronte, M.; Brechin, E. K.; McInnes, E. J. L.; *Appl. Phys. Lett.*, **2005**, *87*, 072504.

100. Manoli, M.; Johnstone, R. D. L.; Parsons, S.; Murrie, M.; Affronte, M.; Evangelisti, M.; Brechin, E. K.; *Angew. Chem., Int. Ed.,* **2007**, *46*, 4456 – 4460.

101. Manoli, M.; Collins, A.; Parsons, S.; Candini, A.; Evangelisti, M.; Brechin, E., K.; *J. Am. Chem. Soc.*, **2008**, *130*, 11129 – 11139.

102. Brechin, E., K.; *Chem. Commun.*; **2005**, 5141 – 5153.

103. Moragues-Canovas, M.; Helliwell, M.; Ricard, L.; Riviere, E.; Wernsdorfer, W.; Brechin, E., K.; Mallah, T.; *Eur. J. Inorg. Chem.*, **2004**, 2219 – 2222.

104. Petrella, A., J.; Raston, C., L.; *J. Organomet. Chem.,* **2004**, *689*, 4125 – 4136.

105. Aronica, C.; Chastanet, C.; Zueva, E.; Borshch, S., A.; Clemente-Juan, J., M.; Luneau, D.; *J. Am. Chem. Soc.*; **2008**, *130*, 2365 – 2371.

106. Kajiwara, T.; Iki, N.; Yamashita, M.; *Coordination Chemistry Reviews*, **2007**, *251*, 1734 – 1746 and references therein.

107. For examples regarding tC[4] metal cluster with alkali metals see: 1) Fischer, R.; Görls, H.; Walther, D.; *Eur. J. Inorg. Chem*., **2004**, *6*, 1243 – 1252 and 2) Bilyk, A.; Hall, K. A.; Harrowfield, J. M.; Hosseini, M. W.; Skelton, B. W.; White, A. H.; *Inorg. Chem*., **2001**, *40*, 672 – 686.

108. See: 1) For MnII clusters: Desroches, C.; Pilet, G.; Borshch, S., A.; Parola, S.; Luneau, D.; *Inorg. Chem.*, **2005**, *44* , 9112 – 9120; 2) For CoII and ZnII clusters: Bilyk, A.; Hall, K., A.; Harrowfield, J., M.; Hosseini, M., W.; Mislin, G.; Skelton, B., W.; Taylor, C.; White, A., H.; *Eur. J. Inorg. Chem.*, **2000**, 823 – 826 and 3) For CuII clusters: Mislin, G.; Graf, E.; Hosseini, M., W.; Bilyk, A.; Hall, A., K., Harrowfield, J., M.; Skelton, B., W.; White, A., H.; *Chem. Commun*., **1999**, 373 – 374.

109. See: 1) Akdas, H.; Graf, E.; Hosseini, M., W.; De Cian, A.; Bilyk, A.; Skelton, B., W.; Koutsantonis, G., A.; Murray, I.; Harrowfield, J., M.; White, A., H.; *Chem. Commun.*, **2002**, 1042 – 1043 and 2) Bilyk, A.; Hall, A., K., Harrowfield, J., M.; Hosseini, M., W.; Skelton, B., W.; White, A., H., *Aust. J. Chem*., **2000**, *53*, 895 – 898.

110. Liu, M.; Liao, W.; Hu, C.; Du, S.; Zhang, H., *Angew. Chem. Int. Ed.*, **2012**, *51*, 1585 – 1588.

111. 1) Karotsis, G.; Teat, S., J.; Wernsdorfer, W.; Piligkos, S.; Dalgarno, S., J.; Brechin, E., K.; *Angew. Chem. Int. Ed.*; **2009***, 48*, 8258 – 8288 and 2) Taylor, S., M.; Karotsis, G.; McIntosh, R., D.; Kennedy, S.; Teat, S., J; Beavers, C., M.; Wernsdorfer, W.; Piligkos, S.; Dalgarno, S., J.; Brechin, E., K.; *Chem. Eur. J.*, **2011**, *17*, 7521 – 7530.

112. Brechin, E., K., Yoo, J.; Nakano, M.; Huffman, J., C.; Hendrickson, D., N.; Christou, G.; *Chem. Commun.*, **1999**, 783 – 784.

113. Karotsis, G.; Kennedy, S.; Dalgarno, S., J.; Brechin, E., K.; *Chem. Commun*., **2010**, *46*, 3884 – 3886.

114. Su, K.; Jiang, F.; Qian, J.; Zhou, K.; Pang, J.; Basahel. S.; Mokhtar, M.; Al-Thabaiti, S., A.; Hong, M.; *Inorg. Lett.*, **2014**, *1*, 1 – 8.

115. Sanz, S.; McIntosh, R., D.; Beavers, C., M.; Teat, S., J.; Evangelisti, M.; Brechin, E., K., Dalgarno, S., J.; *Chem. Commun.*, **2012**, *48*, 1449 – 1451.

116. Karotsis, G.; Kennedy, S.; Teat, S., J.; Beavers, C., M.; Fowler, D., A.; Morales, J., J.; Evangelisti, M.; Dalgarno, S., J.; Brechin, E., K.; *J. Am. Chem. Soc*., **2010**, *132*, 12983 – 12990.

117. Sanz, S.; Ferreira, K.; McIntosh, R., D.; Dalgarno, S., J.; Brechin, E., K.; *Chem. Commun.*, **2011**, *47*, 9042 – 9044.

118. Palacios, M., A.; McLellan, R.; Beavers, C., M.; Teat, S., J.; Weihe, H.; Piligkos, S.; Dalgarno, S., J.; Brechin, E., K.; *Chem. Eur. J*. **2015**, *21*, 11212 – 11218.

119. Fairbairn, R., E.; McLellan, R.; McIntosh, R., D.; Taylor, S., M.; Brechin, E., K.; Dalgarno, S., J.; *Chem. Commun*., **2012**, *48*, 8493 – 8495.

120. Blagg, R., J.; Muryn, C., A.; McInnes, E., J., L.; Tuna, F.; Winpenny, R., E., P.; *Angew. Chem. Int. Ed.*, **2011**, *56*, 6530 – 6533.

121. Murphy, P.; Dalgarno, S., J.; Paterson, M., J.; *J. Phys. Chem. A*, **2014**, *118* (36), 7986 – 8001.

122. McLellan, R.; Palacios, M., A.; Beavers, C., M.; Teat, S., J.; Piligkos, S.; Brechin, E., K.; Dalgarno, S., J., *Chem. Eur. J.*, **2015**, *21*, 2804 – 2812.

Chapter 2: Biscalix[4]arene-supported metal clusters

The following chapter presents a series of results that were obtained by employing 2,2'-biscalix[4]arene (H_8BisTBC[4]) as a ligand in exploratory coordination chemistry. The synthesis of calixarene starting materials is presented prior to the associated coordination chemistry. With respect to the latter, a general description of the methods used to synthesise 3*d* and 3*d*/4*f* BisTBC[4]-supported clusters is given, along with crystallisation methods employed to obtain single crystals suitable for *X*-ray diffraction studies. The crystal structures obtained are described in detail, with a particular emphasis on the structural similarities or differences with respect to the clusters obtained previously within this research group, as presented in Chapter 1 (Section 1.5.2).

2.1. Synthesis of precursors and 2,2'-biscalix[4]arene.

The synthesis of a methylene-bridge directly coupled 2,2'-biscalix[4]arene was carried out according to literature procedures.[84] This building block was obtained following a multi-step synthetic pathway encompassing the synthesis of *p-tert*-butylcalix[4]arene (H_4TBC[4], **12**) as a starting material, as well as lower-rim functionalisation in order to "protect" the phenolic groups in the methylene-bridge functionalisation step. Compound **12** was obtained by following a modified procedure developed by Gutsche *et al.*,[9] in which *p-tert*-butylphenol is reacted with formaldehyde in a base catalysed process by the addition of NaOH (Figure 44).

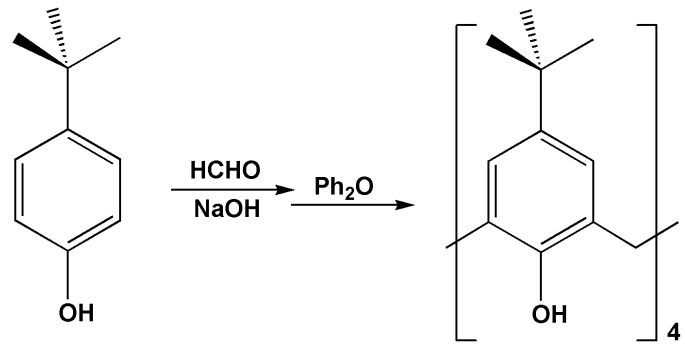

(12)

Figure 44. Synthetic scheme for the synthesis of *p-tert*-butylcalix[4]arene (H_4TBC[4], **12**).[84]

The reaction leads to the formation of an intermediate, called a "precursor", which consists of a thick viscous mass of condensation product between the two aforementioned reagents.

The precursor is readily broken down through the addition of Tol and subsequent prolonged heating in Ph_2O at reflux. This affords a precipitate consisting of a mixture of both H_4TBC[4] and H_8TBC[8], which is purified by washing with EtOAc, affording the product as a microcrystalline powder.

As described in Chapter 1, in order to connect two calix[4]arenes together *via* the methylene bridge, it is necessary to remove an equatorial proton on the methylene bridge using a strong base such as *n*-BuLi. Given that the lower-rim phenolic hydroxyls are rather acidic, it is first necessary to protect these with a base-resistant group. The most obvious protection reaction is to perform a lower-rim alkylation in order to create a tetra-ether. The alkylating agent must be chosen carefully, because it has been proven that some may favour a different conformation from the desired cone, which would be undesirable considering that the formation of polymetallic clusters requires the presence of all four lower-rim phenolic oxygens. For the same reason, said protecting group must be easily cleaved in order to restore the phenolic functionalities involved in metal-ion binding. Etherification is therefore carried out to introduce methoxy groups at the lower-rim. The reaction is carried out by addition of NaH to **12** in a THF/dmf mixture, causing the deprotonation of the lower-rim hydroxyl groups, followed by a nucleophilic substitution using methyl iodide (MeI) as an electrophile (Figure 45).[53]

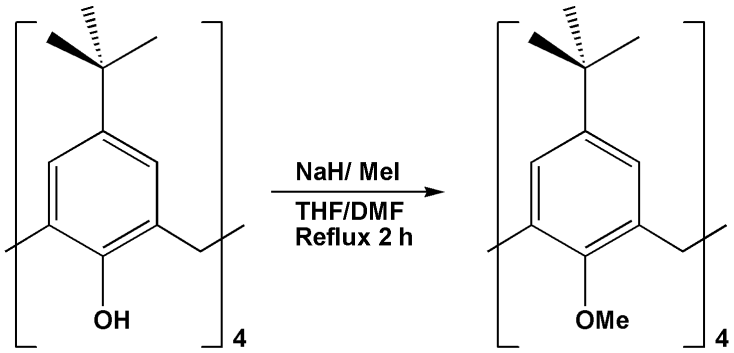

Figure 45. Synthetic scheme for the synthesis of tetramethoxycalix[4]arene (TBC[4]OMe, **13**).

The ^{1}H NMR spectrum of the crude product shows that the reaction reaches completion after 2 hours at reflux based on a) the disappearance of the -OH resonance at 10.5 ppm and b) the appearance of an additional resonance generated by the introduction of methyl groups at the lower-rim. In addition, the ^{1}H NMR spectrum shows considerable broadening of all the resonances as a result of the formation of the tetramethoxy derivative (TBC[4]OMe, **13**).

Lower-rim alkylation has the effect of disrupting the hydrogen-bonding network between the OHs at the lower-rim that are responsible for stabilising the cone conformation of **12**. Compound **13** therefore exists as a mixture of rapidly interconverting conformers in solution, even at low temperatures. The coexistence of these conformers is responsible of the broadening of the resonances in the proton NMR spectrum.

The synthesis of octamethoxy-2,2'-biscalix[4]arene (BisTBC[4]OMe, **14**, Figure 46) was performed by drying **13** under vacuum for at least 2 hours, after which time the compound was dissolved in dry THF, affording a pale yellow solution.[84] *n*-BuLi was added through a septum under an N_2 atmosphere. Upon addition of *n*-BuLi the solution turns blood red due to the formation of a bridge-lithiated **13-Li** (see Chapter 1, Section 1.3). Subsequent addition of a solution of α,ω-dibromoethane in dry THF, which acts as an electrophilic bromine (Br^+) source, leads to the formation of a small, but not isolable, quantity of 2-bromoTBC[4]OMe (**13-Br**). Thanks to the pseudo-high dilution conditions employed, this species is capable of reacting readily with one equivalent of **13-Li** to afford the directly coupled BisTBC[4]OMe.

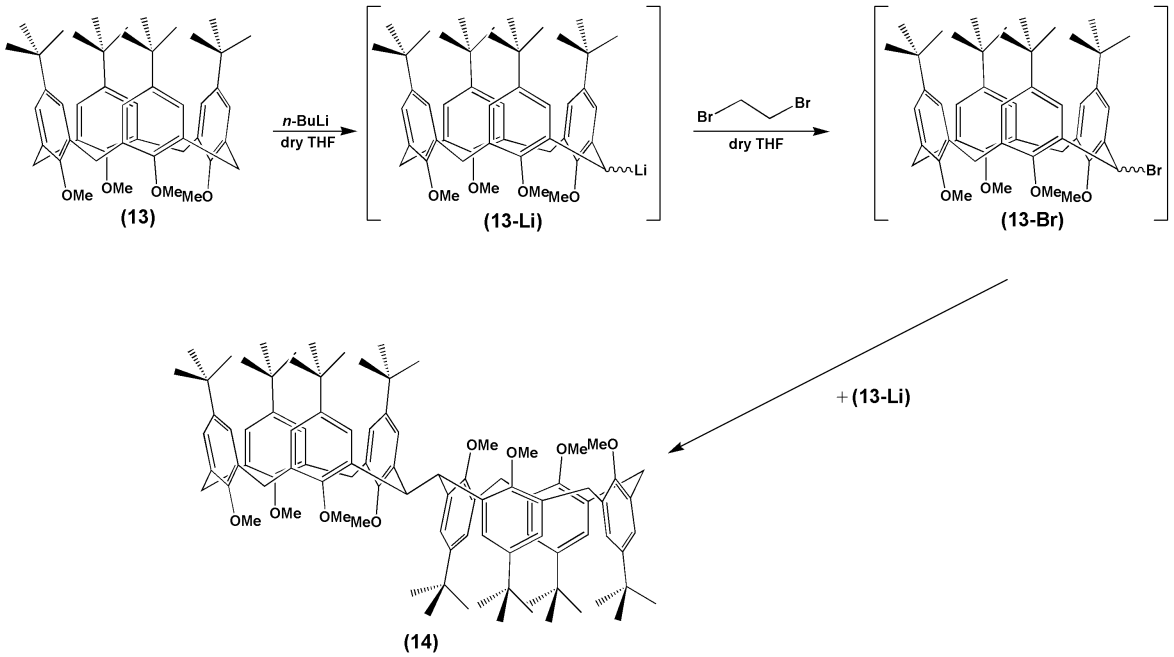

Figure 46. Synthetic scheme for the synthesis of octamethoxy-2,2'-biscalix[4]arene (BisTBC[4]OMe, **14**).

The ^{1}H NMR spectrum of **14** was not interpretable as a result of the fluxionality due to the aforementioned lower-rim methoxy groups. Attempts at acquiring ^{1}H NMR spectra in a $CDCl_3/CD_3CN$ 3:1 mixture in the presence of small amounts of NaI were unsuccessful. With

NaI present, calixarenes would adopt a cone conformation, enforced by the binding of the lower-rim ethereal oxygens to the Na^+ ion thus giving sharpened and interpretable signals.[123]

In order to employ H_8BisTBC[4] as a ligand in the formation of polymetallic clusters, the lower-rim methoxy groups must be removed to restore the phenolic functionalities. This reaction was carried out by heating a solution of **14** in dmf at reflux in presence of iodocyclohexane.[124] The choice of iodocyclohexane as a demethylating agent rather than classical Lewis acids such as BBr_3 or trimethylsilyl iodide (TMSI) offers several advantages such as shorter reaction times, milder conditions and higher yields. As for other iodoalkanes, iodocyclohexane is a hydriodic acid source, which is produced *in situ* through an E_1 elimination reaction. The reaction generally requires dmf as a solvent, since it is a strongly basic medium, although not strong enough to neutralise the evolving HI. Hydriodic acid reacts with a methoxy group *via* an S_N2 reaction, producing CH_3I and therefore restoring the phenolic functionalities at the BisTBC[4] lower-rim, affording compound **$H_8$15** as a result (Figure 47).

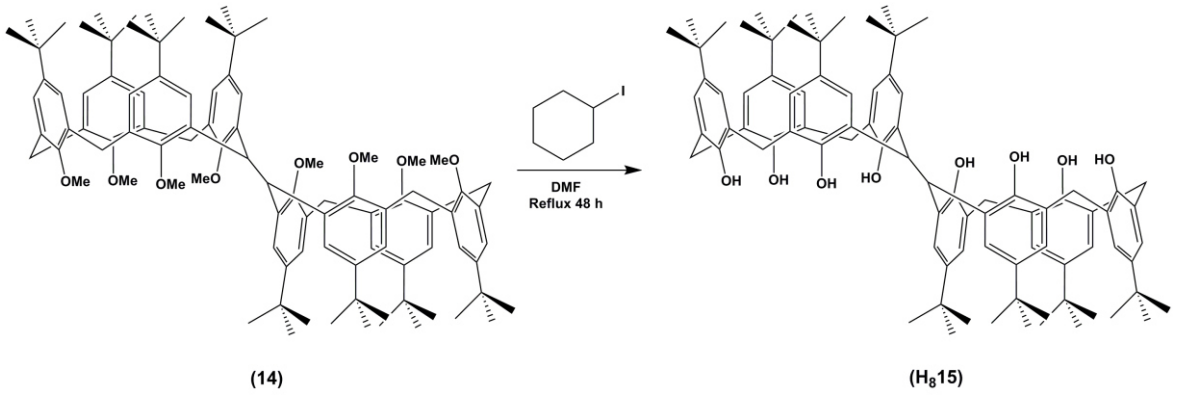

Figure 47. Demethylation of **14** to afford 2,2'-biscalix[4]arene (BisTBC[4], **$H_8$15**).

The successful synthesis of **$H_8$15** was confirmed by analysis of both ^1H and ^{13}C NMR spectra, with the former showing a series of resonances that are consistent with the targeted product; two calix[4]arene moieties in the cone conformation and linked together *via* the methylene bridge. The singlet at 10.41 ppm refers to the eight phenolic protons at the lower-rim. From 7.18 ppm to 6.81 there is a set of four doublets with a coupling constant value between 2.2 Hz and 2.6 Hz, given by the aryl groups of the TBC[4] moieties. The resonance at 5.82 ppm is generated by the methine proton on the monosubstituted methylene bridge. The doublets at 4.29 ppm and 4.19 ppm, with ^2J of 13.9 Hz and 13.6 Hz respectively, refer to the methylene bridge protons in axial positions, whereas the same pattern of doublets can be found at 3.5 ppm and 3.4 ppm, which relate to the protons in equatorial positions. The

two singlets at 1.21 ppm and 1.11 ppm are given by the ^{t}Bu groups on the upper-rim. The presence of additional resonances for the methylene bridge protons and for the ^{t}Bu groups is due to the lower symmetry of **H$_8$15** compared to **12**, the former possessing a mirror plane that bisects the two calix[4]arene moieties through the C-C bond at the 2,2' positions.

2.2. Biscalix[4]arene-supported metal clusters.

In order to explore the coordination properties of **H$_8$15** a simple reaction protocol was followed systematically. ***General procedure:*** Compound **H$_8$15** was accurately weighed out in the presence of different equivalents of TM (Mn^{II}, Cu^{II}, Fe^{II}), Ln (Gd^{III}, Dy^{III} and Tb^{III}) and 3*d* / 4*f* salt mixtures. All of the salts employed were either chlorides or nitrates, making sure in the case of mixed 3*d* / 4*f* systems that the counterion was the same for both species (i.e. both chlorides or nitrates). This mixture was dissolved in a 1:1 solution of dmf / MeOH and stirred at RT for 10 minutes, after which time an excess of 9 equivalents (relative to **15**) of Et_3N was added in order to deprotonate the lower-rim phenolic oxygens. Prior to the addition of the base the solutions were cloudy and contain undissolved ligand. However, upon addition of the base, the solution changed colour and became clear, going (for example) from white to deep purple for the Mn^{II} or Mn^{II} / Ln^{III} reactions. The solutions were stirred for a further 2 hrs after which time the mother liquor was filtered in order to remove unreacted ligand or inorganic salts. Aliquots of the mother liquor were transferred into small vials, and these were placed into larger vials containing volatile solvents such as MeCN, Et_2O and PET, in the attempt of growing single crystals suitable for *X*-ray diffraction studies upon vapour diffusion of the solvent into the mother liquor. One of the aforementioned solvents often proved to be better with respect to growing suitable single crystals, although slow evaporation of the dmf / MeOH mother liquor was also found to produce good quality single crystals. For reactions that produced suitable crystals, *X*-ray analysis was performed using either a standard Mo-Kα radiation source in the laboratory or synchrotron radiation in the case of weakly diffracting crystals in order to obtain data of publishable quality. In some cases only partial structural analyses could be performed due to the very weakly diffracting nature of the crystals, even with the use of synchrotron radiation.

2.2.1. $[Cu^{II}_4Ln^{III}_5(15)_2(\mu_3\text{-}OMe)(\mu\text{-}OMe)(\mu_3\text{-}OH)(\mu_4\text{-}NO_3)(\mu_5\text{-}NO_3)(MeOH)(dmf)(H_2O)_4](OH)_2(dmf)_6(H_2O)$, 16.

Reaction of **H$_8$15** with Cu(II) nitrate trihydrate and Ln(III) nitrate hexahydrate afforded a series of new clusters of general formula $[Cu^{II}_4Ln^{III}_5(\mathbf{15})_2(\mu_3\text{-}OMe)(\mu\text{-}OMe)(\mu_3\text{-}OH)(\mu_4\text{-}NO_3)(\mu_5\text{-}NO_3)(MeOH)(dmf)(H_2O)_4](OH)_2(dmf)_6(H_2O)$, **16** (Ln = Gd, Tb or Dy, **16Tb** being shown in Figure 48) upon slow evaporation of the mother liquor. The crystals were found to be in monoclinic cell and structure solution was carried out in the space group $P2_1/n$. The structure described is the Tb derivative (**16Tb**), although the Gd and Dy analogues (**16Gd** and **16Dy** respectively) proved to be isostructural, as determined by unit cell measurements on several different single crystals. Compound **16Tb** can be summarised as two $Cu^{II}_2Tb^{III}_2$-(BisTBC[4]) butterflies linked together by a central octacoordinate Tb^{III} ion that is in a square antiprismatic geometry. Bridging anions such as μ_4- and μ_5- nitrates are also present between the two aforementioned butterflies. A detailed structural description is given below.

The asymmetric unit (ASU) in **16Tb** comprises two molecules of **15** housing a $Cu^{II}_4Tb^{III}_5$ core in which the metal cations are bridged *via* hydroxide and nitrate anions. Four Cu^{II} ions reside in the Type I binding sites of the two molecules of **15**, and all are in a distorted square pyramidal geometry. This is in perfect accordance to the known Cu^{II} coordination chemistry of **15**, as seen in Chapter 1 (Section 1.5.2, Figure 32 and Section 1.5.3, Figure 41).[113, 122] Cu1 is bound in the TBC[4] cavity through coordination to the lower-rim oxygen atoms O1 – O4 (Cu1–O range 1.943(7) – 2.002(7) Å). Two of these oxygens, O1 and O4, bridge to Tb2 and Tb1 respectively (Tb2–O1, 2.357(7) Å and Tb1–O4, 2.383(7) Å). The Cu1 coordination sphere is completed by a μ_3-methoxide (Cu1–O17, 2.221(7) Å), which bridges to both the Tb1 and Tb2 ions (Tb1–O17, 2.322(7) Å and Tb2–O17, 2.346(7) Å). Cu2 has the same coordination environment, as it is residing in a Type I binding site (Cu2–O range 1.920(8) – 1.977(7) Å), the only exception being the different nature of the oxygen atom (O20) forming the apex of the square pyramid. In this case, the oxygen atom belongs to a μ_5-nitrate anion with a Cu2–O20 distance of 2.239(7) Å. This anion bridges to the Tb2 and Tb3 ions residing in the Type II binding pockets of one molecule of **15** (Tb2–O20, 2.383(6) Å, Tb3–O20, 2.461(7) Å and Tb3–O21, 2.494(7) Å). Tb3 acts as the bridging cation between the two halves of the cluster and is discussed in detail below. Tb1 is heptacoordinate, is in a distorted pentagonal bipyramidal geometry and, in addition to the aforementioned coordination with O4 and O17, is bound to a phenolic oxygen of the other TBC[4] cavity O5 (Tb1–O5, 2.290(7) Å), O19 of the μ_5-nitrate anion (Tb1–O19, 2.378(7) Å), two ligated dmf molecules (Tb1–O25, 2.369(10) Å and Tb1–O27, 2.324(7) Å) and an

aqua ligand (Tb1–O26, 2.338(7) Å). The Tb2 coordination sphere is similar to that of Tb1, as it is bound to the aforementioned O17 and O20, to the phenolic oxygens O1 and O8 (Tb2–O1, 2.357(7) Å Tb2–O8, 2.291(7) Å) and a ligated dmf molecule (Tb2–O28, 2.353(9) Å). The main differences are the presence of a ligated MeOH molecule (Tb2–O29, 2.361(7) Å) and bridging to Tb3 *via* a μ-methoxide (Tb2–O30, 2.259(7) Å).

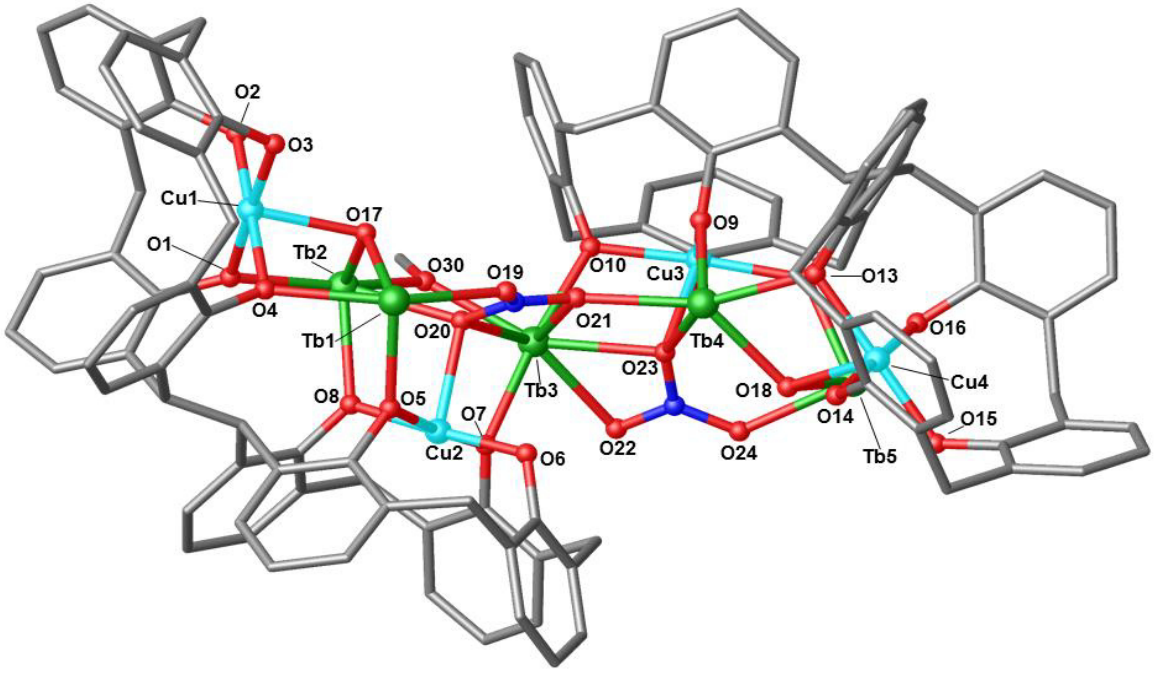

Figure 48. Partial single crystal *X*-ray structure showing the $[Cu^{II}_4Tb^{III}_5(\mathbf{15})_2(\mu_3\text{-OMe})(\mu\text{-OMe})(\mu_3\text{-OH})(\mu_4\text{-NO}_3)(\mu_5\text{-NO}_3)(MeOH)(dmf)(H_2O)_4](OH)_2(dmf)_6(H_2O)$ cluster, **16Tb**, and selected labels according to discussion (Colour code: Cu – light blue, Tb – green, O – red, N – blue, C – grey). ^{t}Bu groups, hydrogen atoms, ligated solvent molecules and solvent of crystallisation omitted for clarity.

Tb3 is octacoordinate, in a distorted square antiprismatic geometry and is the metal centre acting as a bridge between the two $Cu^{II}_2Tb^{III}_2$-**15** butterflies. It is coordinated to the O20 and O21 of the μ_5-nitrate anion in a chelate as mentioned above. A second μ_4-nitrate anion from the second half of **16Tb** is coordinated to Tb3 in a similar manner, bonding through O22 and O23 (Tb3–O22, 2.438(8) Å and Tb3–O23, 2.456(7) Å) as shown in Figure 48. Two phenolic oxygens of two different **15** ligand complete the coordination sphere of Tb3 (Tb3–O7, 2.322(7) Å and Tb3–O10, 2.304(7) Å). Tb3 is located almost equidistant from the two $Cu^{II}_2Tb^{III}_2$-**15** butterflies, as found by measuring the distance between the central lanthanide ion and centroids generated at the centre of each $Cu^{II}_2Tb^{III}_2$-**15** butterfly; the respective

distances between Tb3 and the Cu1-Tb1-Cu2-Tb2 and Cu3-Tb4-Cu4-Tb5 butterfly centroids were found to be 4.655 Å and 4.747 Å. Cu3 resides in a Type I binding site, being bound to the lower-rim phenolic oxygens O9 – O12 (Cu3–O range, 1.907(7) – 2.029(7) Å) and its coordination sphere is completed by O23 of a μ_5-nitrate anion (Cu3–O23, 2.330(7) Å). The coordination of Cu4 is similar (Cu4–O range, 1.938(7) – 2.012(7) Å), with the presence of a μ_3-hydroxide on the apex of a distorted square pyramid (Cu4–O18, 2.205(7) Å) that acts as a linker to Tb4 and Tb5 (Tb4–O18, 2.308 Å and Tb5–O18, 2.338(7) Å). The Tb4 and Tb5 coordination modes are similar, as they are both residing in a Type II binding pocket. They are both bound to phenolic oxygens belonging to two separate TBC[4] moieties (Tb4–O9, 2.279(6) Å, Tb4–O13, 2.348(7) Å and Tb5–O12, 2.285(7) Å, Tb5–O16, 2.365(7) Å), to ligated dmf molecules (Tb4–O32, 2.303(7) Å and Tb5–O34, 2.326(7) Å) and aqua ligands (Tb4–O33, 2.360(7) Å and Tb5–O36, 2.342(7) Å). The main difference in the coordination of Tb4 and Tb5 is that Tb4 is bound to O21 and O23, belonging respectively to μ_5- and μ_4-nitrate anions (Tb4–O21, 2.350(7) Å and Tb4–O23, 2.384(7) Å) whereas Tb5 is bound to O24 of the aforementioned μ_4-nitrate anion (Tb5–O24, 2.344(7) Å) and an aqua ligand (Tb5–O35, 2.399(8) Å).

As was the case for compound **10** described in Chapter 1 (Section 1.5.3, Figure 41), similar capping behaviour is observed and this occurs through the $[Cu^{II}_2$-**15**$]^{4-}$ moieties (capping defined by large light blue spheroids, Figure 49). Structural expansion does not show any significant interaction between the metal clusters, with the presence of co-crystallised dmf molecules along the *a* and *c* axes (Figure 50). The closest metal-metal intercluster distance found is along the *b* axis and was found to be 12.892 Å between Cu1 of one metal cluster and Cu4 of its neighbour.

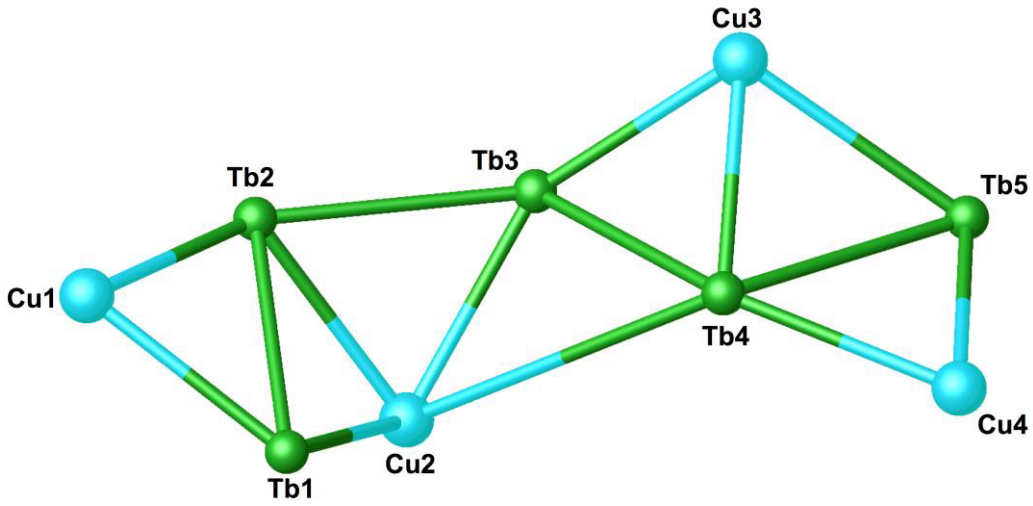

Figure 49. Capping behaviour in the structure of **16Tb**. Capping by $[Cu^{II}(TBC[4])]^{2-}$ moieties are shown as large spheres (Colour code: Cu – light blue; Tb – green).

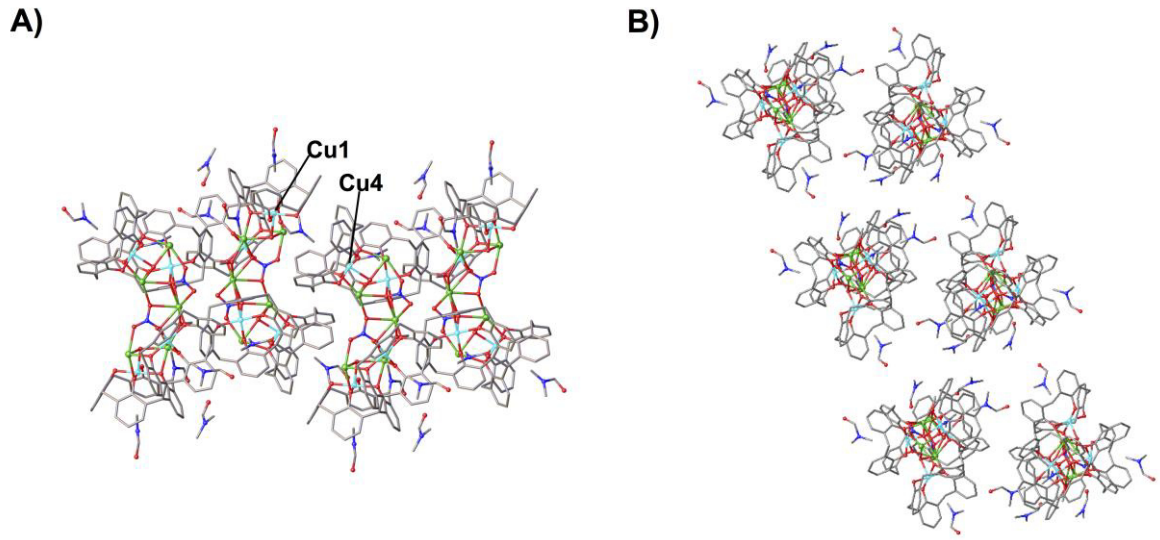

Figure 50. Views of the extended structure of **16Tb**. A) The *ac* plane and B) *ab* plane showing co-crystallised dmf molecules and closest ions labelled according to discussion (Colour code: Cu – light blue; Tb – green; O – red; N – blue; C – grey). ^{t}Bu groups, hydrogen atoms and ligated solvent molecules omitted for clarity.

2.2.2. $[Fe^{III}_5Ln^{III}_4(15)_2(\mu_4\text{-}O)_2(\mu_3\text{-}O)_2(\mu_3\text{-}NO_3)_2(dmf)_8(H_2O)_6](OH)$, 17.

Analogous conditions were employed to synthesise a novel series of Fe^{III} / Ln^{III} clusters. These were obtained by reacting **H$_8$15** with iron(III) nitrate nonahydrate and lanthanide(III) nitrate hexahydrate and have general formula $[Fe^{III}_5Ln^{III}_4(\mathbf{15})_2(\mu_4\text{-}O)_2(\mu_3\text{-}O)_2(\mu_3\text{-}NO_3)_2(dmf)_8(H_2O)_6](OH)$, **17** (Ln = Gd, Tb or Dy, **17Gd** being shown in Figure 51), after slow evaporation of the mother liquor. The crystals were found to be in a triclinic cell and structure solution was carried out in the space group *P*-1. The structure described is of the Gd derivative (**17Gd**), although the Tb and Dy analogues (**17Tb** and **17Dy** respectively) proved to be isostructural, after having determined the unit cell dimensions of several different single crystals of each compound.

The asymmetric unit in **17Gd** comprises of a $Fe^{III}_2Gd^{III}_2$ butterfly contained in an octa-anionic **15**, and a Fe^{III} cation linked to the aforementioned butterfly *via* μ_4-nitrates and μ_4-oxygens. Symmetry expansion of the ASU reveals a large assembly, composed of two $Fe^{III}_2Gd^{III}_2$-**15** butterflies linked together by the aforementioned central Fe^{III} ion which is disordered over two positions. The disorder, which also affects the nitrate anion bridges, was modelled successfully at half occupancy and, for the sake of brevity, only one position will be discussed here. The Fe^{III} cations are all hexacoordinate and have octahedral geometry. Fe1 and Fe2 (and s.e.) reside in the tetraphenolic cavity of the TBC[4] moieties in a Type I binding fashion (oxygen atoms O1 – O4 and O5 – O8, Fe1–O range 1.961(5) – 2.024(4) Å, Fe2–O range 1.952(4) – 2.029(4) Å). Both are also bound to a ligated dmf molecule (Fe1–O11, 2.098(7) Å, Fe2-O12, 2.116(4) Å) and to μ_4-oxide (Fe1–O9, 1.946(4) Å) and μ_3-oxide (Fe2–O10, 1.935(4) Å). These are binding to the two Gd ions residing in Type II binding pockets generated by inversion of the ligand conformation from *anti* to *syn* (Gd1–O9, 2.405(4) Å, Gd1 – O10, 2.376(4) Å, Gd2–O9, 2.400(6) Å and Gd2–O10, 2.376(4) Å).

Both Gd1 and Gd2 (and s.e.) are octacoordinate and are in a distorted square antiprismatic geometry. Gd1 is bound to two phenolic oxygens belonging to separate TBC[4] moieties of the same **15** unit (Gd1–O1, 2.353(4) Å and Gd1–O8, 2.374(4) Å). The μ_4-oxide unit acts as a bridge to Gd2, Fe2 and the central Fe3, and is positioned at the centre of a tetrahedron described by the four cations. The Gd1 coordination sphere is completed by two oxygens of a μ_4-nitrate (Gd1–O21, 2.553(4) Å and Gd1–O25, 2.284(8) Å), a ligated dmf molecule (Gd1–O13, 2.360(5) Å) and an aqua ligand (Gd1–O14, 2.493(7) Å).

Gd2 has the same coordination environment, with slight differences in bond length and angles due to distortion.

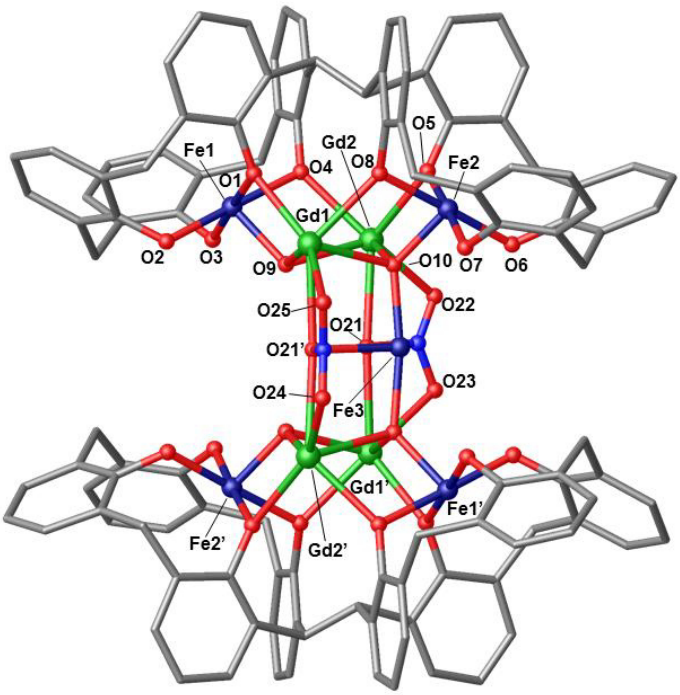

Figure 51. Partial single crystal *X*-ray structure showing the $[Fe^{III}_5Gd^{III}_4(\mathbf{15})_2(\mu_4\text{-}O)_2(\mu_3\text{-}O)_2(\mu_3\text{-}NO_3)_2(dmf)_8(H_2O)_6](OH)$ cluster, **17Gd**, and selected labels according to discussion (Colour code: Fe – dark blue; Gd – green; O – red; N – blue; C – grey). ^{t}Bu groups, hydrogen atoms, ligated solvent molecules and solvent of crystallisation omitted for clarity.

In addition to the aforementioned bonds with O9 and O10 (Gd2–O10, 2.376(4) Å), it is in fact bound to the phenolic oxygens O4 and O5, that are part of two separate TBC[4] units forming a molecule of **15** (Gd2–O4, 2.351(5) Å and Gd2–O5, 2.376(4) Å), two oxygen atoms of a μ_4-nitrate (Gd2–O21, 2.547(4) Å and Gd2–O24, 2.349(8) Å), a ligated dmf molecule (Gd2–O26, 2.359(5) Å) and an aqua ligand (Gd2–O19, 2.540(8) Å). Fe3 is located at the centre of the metallic skeleton, forming the cap on the side of the square described by the Gd^{III} ions. It also acts as a bridge between the two $[Fe^{III}_2Gd^{III}_2\text{-}\mathbf{15}]$ moieties of the cluster. It is axially bound to two μ_4-oxides (Fe3–O10, 1.983(4) Å and Fe3–O9', 2.040(5) Å), and equatorially to two oxygens atoms belonging to two μ_3-nitrates (Fe3–O21, 2.235(5) Å and Fe–O21', 2.269(5) Å) and two aqua ligands (Fe3–O16, 2.017(10) Å and Fe3–O17, 2.025(10) Å). The equatorial bond distances of Fe3 are longer compared to those of the Fe^{III} ions residing in Type I binding regions, with a difference of ca 0.2 Å due to the rigidity of the ligand binding sites.

An alternative way of describing **17** is to focus on the square described by the Gd^{III} ions, that is capped on each edge by a $[Fe^{III}_2\text{-}\mathbf{15}]^{2-}$ moiety, with the fifth Fe^{III} ion capping one side of

the square, along with the aforementioned nitrates and oxygen (Figure 52). The capped square of Gd^{III} is a recurring structural motif observed already for TBC[4]-supported metal clusters (e.g. compound **4** in Section 1.5.2., Figure 34) and was also found in another BisTBC[4]-supported 3*d* / 4*f* clusters that will be described in a following section.

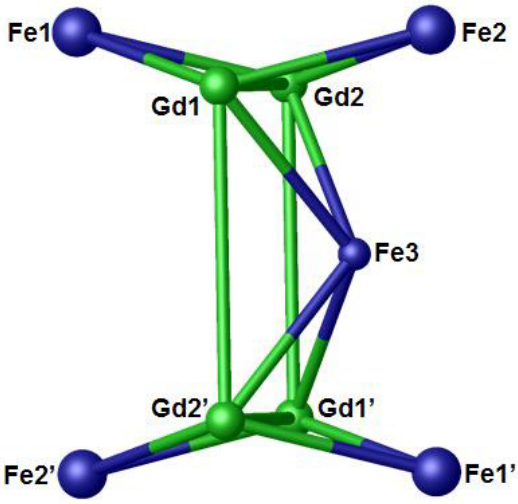

Figure 52. Capping behaviour in the structure of **17Gd**. Capping by $[Fe^{III}(TBC[4])]^-$ moieties are shown as large spheres (Colour code: Fe – dark blue; Gd – green).

Structure expansion reveals weak Van der Waals interactions along the *c* axis between the dmf molecule ligated to Gd2, with a distance between the nitrogen atoms N4 of 3.698 Å (Figure 53). The shortest metal-metal intercluster distances were found to be along the *c* axis, occurring between the Gd2 centres of two neighbouring clusters, with a Gd2…Gd2 distance of 11.179 Å. Along the *b* axis, the shortest metal-metal distance worth of mention is between the capping Fe3 and Gd2 (Fe3…Gd2, 13.914 Å).

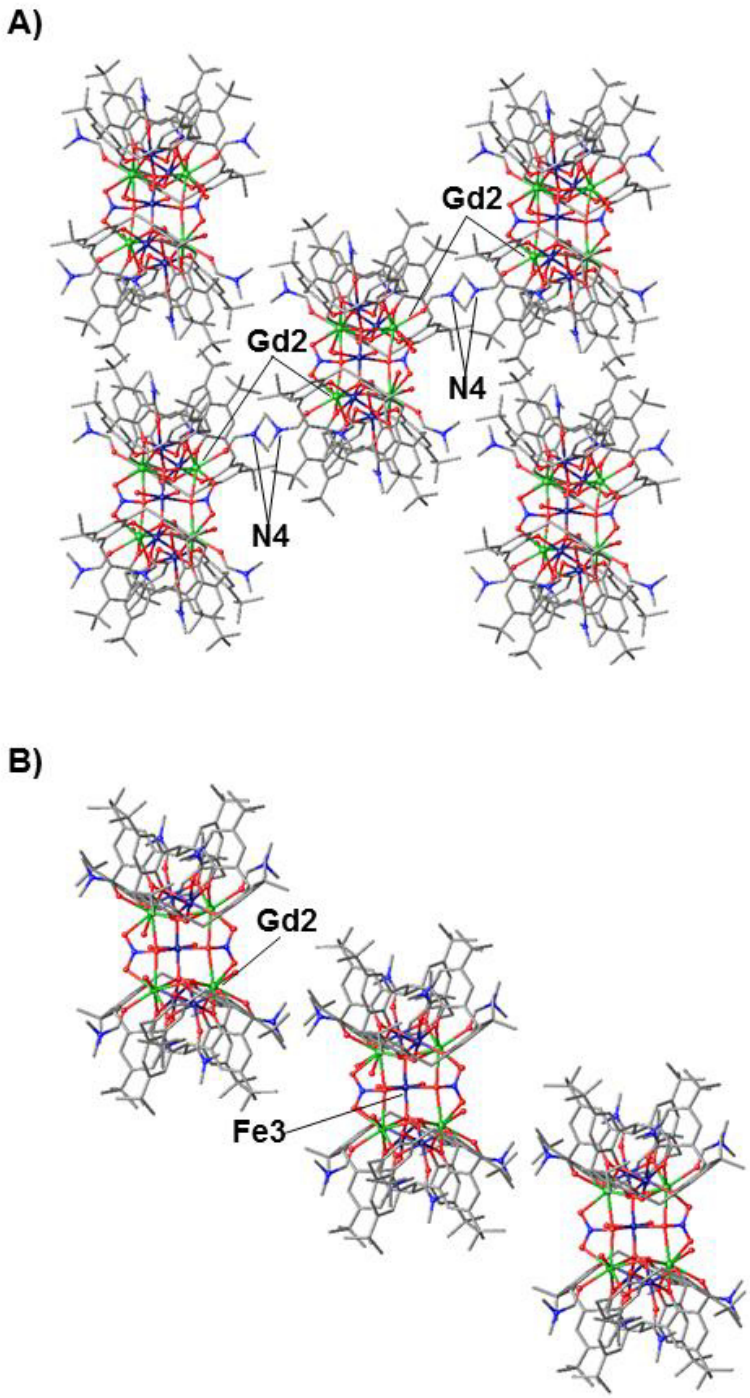

Figure 53. Views of the extended structure of **17Gd**. A) The *ab* plane showing the VdW interaction. B) The *ac* plane with closest ions labelled according to discussion (Colour code: Fe – dark blue; Gd – green; O – red; N – blue; C – grey). Hydrogen atoms, ligated solvent molecules and solvent of crystallisation omitted for clarity.

2.3. Stoichiometric control over cluster composition.

H_8BisTBC[4] proved to be a remarkably versatile ligand for the synthesis of 3*d* and 3*d* / 4*f* polymetallic clusters, in a similar fashion to H_4TBC[4]. As discussed for TBC[4]-supported metal clusters (Chapter 1, Section 1.5.2), small variations in the stoichiometries employed can have a dramatic effect on the composition of the polymetallic core, such as facile interchange of 3*d* and 4*f* ions. This section focuses on an analogous chemistry, employing **H$_8$15** as a ligand. The outcome of this investigation was the isolation of three novel BisTBC[4]-supported clusters in which it was possible to "expand" the cluster core and alter its composition by variation in reactant ratios and crystallisation conditions.

2.3.1. $[Mn_6^{III}Mn_4^{II}(15)_2(\mu_3\text{-}O)_2(\mu_3\text{-}OH)_4(\mu\text{-}CH_3O)_4(H_2O)_4(dmf)_8](dmf)_4$, 18.

The first cluster in this section was obtained by variation in the stoichiometry employed to synthesise the $[Mn^{III}_4Mn^{II}_4(\mathbf{15})_2(\mu_3\text{-}OH)_2(\mu\text{-}Cl)(H_2O)(MeOH)(dmf)_4]$ species presented in Chapter 1 (Section 1.5.2, Figure 40).[122] Reaction of **H$_8$15** with manganese(II) dichloride tetrahydrate, followed by slow evaporation of the mother liquor afforded singe crystals suitable for *X*-ray diffraction studies of formula $[Mn_6^{III}Mn_4^{II}(\mathbf{15})_2(\mu_3\text{-}O)_2(\mu_3\text{-}OH)_4(\mu\text{-}CH_3O)_4(H_2O)_4(dmf)_8](dmf)_4$, **18** (Figure 54). The crystals were found to be in a triclinic cell and structure solution was carried out in the space group *P*-1. The metallic core of **18** is similar to that of **9** and can be described as three fused butterflies, but with incorporation of two additional μ-methoxy-bridged Mn^{III} ions.

The ASU comprises half of the cluster (Mn1–Mn5) due to the presence of an inversion centre located within the rhomboidal area described by Mn5-O14-Mn5'-O14' (Mn5/Mn5'–centroid distance 1.444 Å, O14/O14'–centroid distance 1.265 Å), therefore only half of the cluster will be discussed in detail. Mn1 is bound in a TBC[4] lower-rim tetraphenolic pocket in a Type I fashion (oxygen atoms O1 – O4, Mn–O range 1.907(5) – 1.935(4) Å) and, as expected considering the well-established TBC[4] binding rules, is in the third oxidation state. The coordination sphere of Mn1 is completed by a ligated dmf molecule residing within the TBC[4] cavity (Mn1–O9, 2.348(3) Å) and a μ_3-hydroxide (Mn1–O13, 2.107(5) Å) which is also binding to Mn3 and Mn4 (Mn3–O13, 2.192(5) Å and Mn4–O13, 2.187(5) Å). The vector along O9-Mn1-O13 defines the Jahn-Teller axis, with an angle of 170.3(9)º due to distortion. Both Mn3 and Mn4 are in a second oxidation state and, as already discussed for other BisTBC[4]-supported clusters (*vide supra*), are residing in Type II binding pockets. Mn3 is bonded to a dmf molecule (Mn3–O11, 2.166(6) Å), two

μ-phenoxide oxygens (Mn3–O1, 2.436(4) Å and Mn3–O8, 2.109(4) Å), an aqua ligand (Mn3–O15, 2.241(5) Å) and a μ-methoxide (Mn3–O16, 2.154(5) Å). The coordination sphere of Mn2 (3+) and Mn4 (2+) are near identical to those of the aforementioned Mn1 (3+) and Mn3 (2+) ions respectively, with only negligible differences observed in the bond lengths. Mn2 is bound to the O5 – O8 phenolic oxygens (Mn2–O range 1.923(5) – 1.936(4) Å), a ligated dmf molecule (Mn2–O10, 2.236(5) Å) and a μ_3-hydroxide (Mn2–O14, 2.146(4) Å), whereas Mn4 is bound to O4 and O5, two phenolic oxygens belonging to two separate TBC[4] moieties of the same ligand (Mn4–O4, 2.377(5) Å and Mn4–O5, 2.145(4) Å), the aforementioned μ_3-hydroxide (Mn4–O13, 2.187(5) Å), a μ-methoxide (Mn4–O17, 2.138(6) Å) and a ligated dmf molecule (Mn4–O12, 2.161(6) Å).

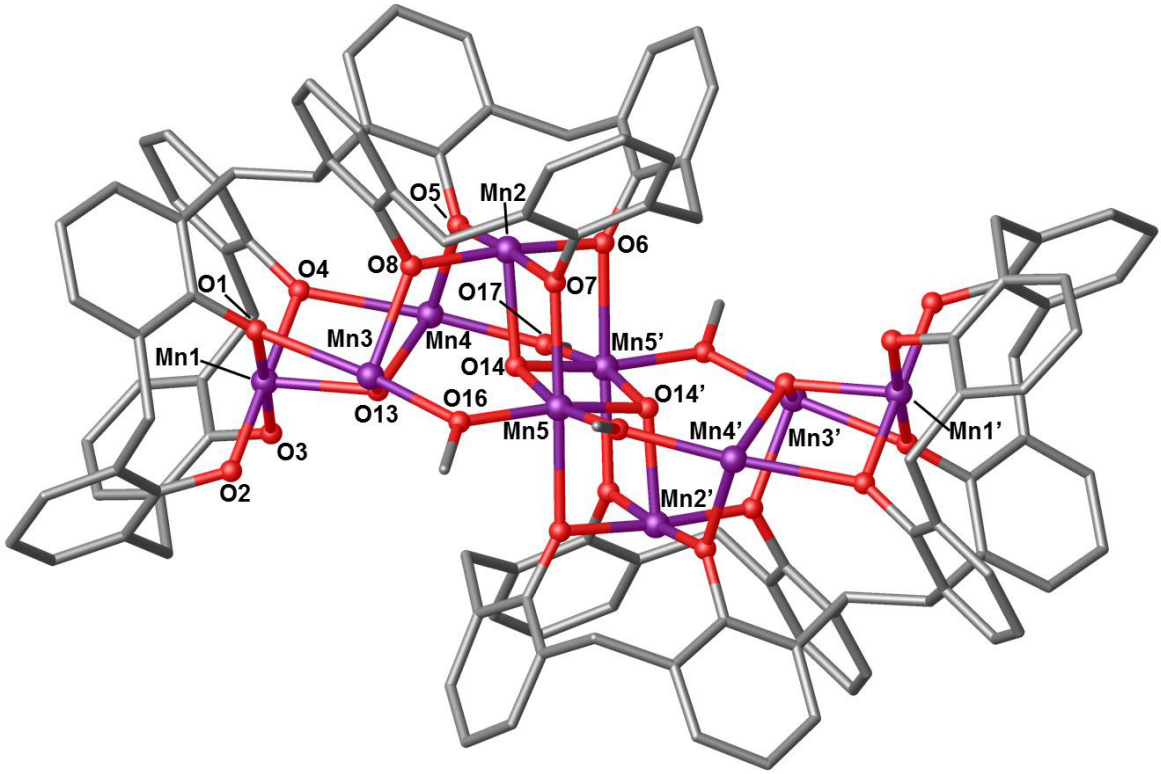

Figure 54. Partial single crystal *X*-ray structure showing the $[Mn_6^{III}Mn_4^{II}(\mathbf{15})_2(\mu_3\text{-}O)_2(\mu_3\text{-}OH)_4(\mu\text{-}CH_3O)_4(H_2O)_4(dmf)_8](dmf)_4$ cluster, **18**, and selected labels according to discussion (Colour code: Mn – purple; O – red; C – grey). ^{t}Bu groups, hydrogen atoms, ligated solvent molecules and solvent of crystallisation omitted for clarity.

Mn5 and Mn5' are the metal centres that, along with ligated molecules, contribute to the horizontal expansion of the polymetallic skeleton from $Mn^{III}_4Mn^{II}_4$ to $Mn^{III}_6Mn^{II}_4$. Mn5 (and its s.e. Mn5') is in a third oxidation state with distorted octahedral geometry and a Jahn-Teller axis along the O7-Mn5-O6' vector (Mn5–O7, 2.296(5) Å and Mn5–O6', 2.335(5) Å,

175.15(17)º). Two μ_3-oxides and two μ-methoxides complete the Mn5 coordination sphere (Mn5–O14, 1.920(5) Å, Mn5–O14', 1.921(5) Å, Mn5–O16, 1.926(6) Å and Mn5–O17', 1.925(6) Å). As expected, **18** shows capping behaviour, with a $[Mn^{III}(TBC[4])]^-$ units that are 'encapsulating' Mn3, Mn4 and Mn5 (and related s.e.). Moreover, the Mn2(TBC[4]) unit (and s.e.) are located at the apex of a distorted square pyramid (Figure 55).

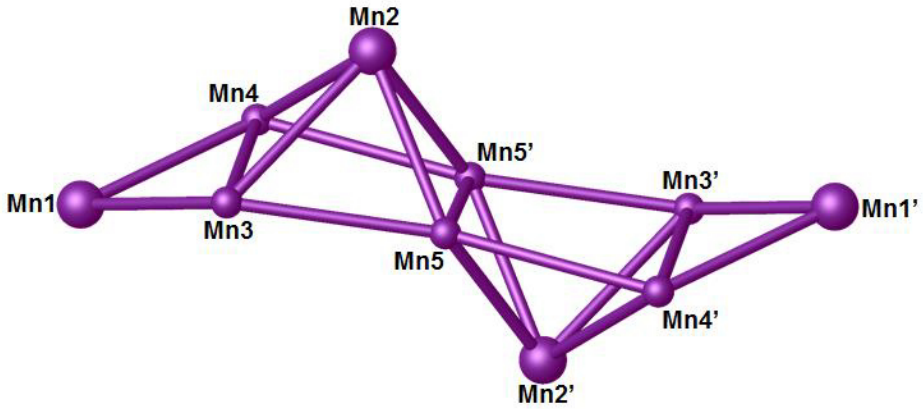

Figure 55. Capping behaviour in the structure of **18**. Capping by $[Mn^{III}(TBC[4])]^-$ moieties are shown as large spheres (Colour code: Mn – Purple).

Structure expansion of **18** shows that the clusters pack closer together compared to the other clusters discussed above (Figure 56). There are significant CH-π interactions along the *b* axis between the methyl group (C96) of the dmf molecule (N3) ligated to Mn3 and the π system located on the calix[4]arene aromatic ring described by C8-C13 (C-H96a…centroid distance of 3.671 Å). Another interaction worthy of mention is the hydrogen bond occurring between the hydrogen atom belonging to the aforementioned methyl group of the dmf molecule and O15 (H96a…O15, 3.082 Å). The shortest metal-metal intercluster distance was found to be between Mn3 and Mn3' (Mn3…Mn3', 8.519 Å) and is considerably shorter compared to the other intercluster distances presented so far.

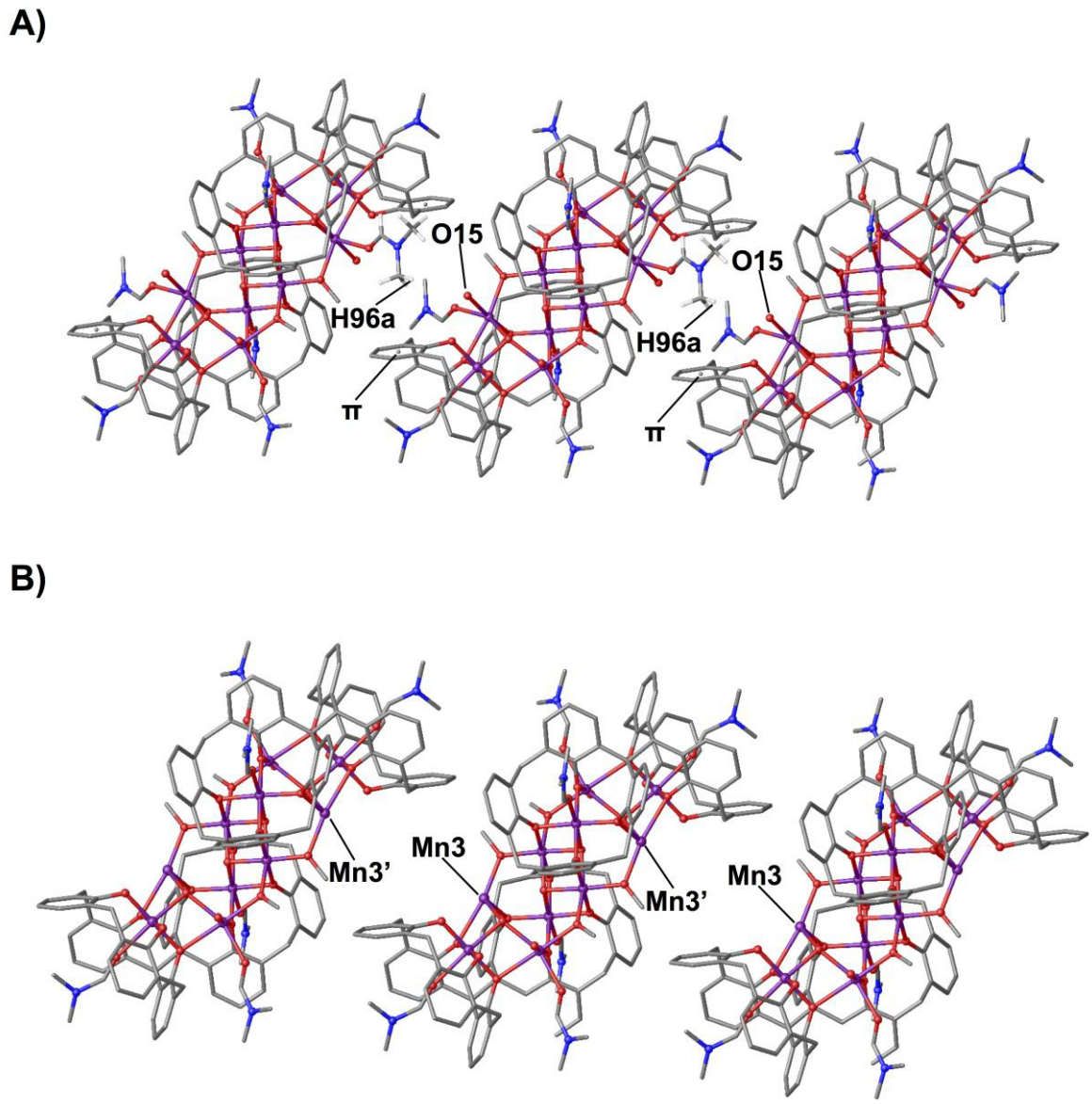

Figure 56. View of the *ac* plane in the extended structure of **18** showing A) the CH- π interaction and hydrogen bond with O15 and B) the closest ions labelled according to discussion (Colour code: Mn – purple; O – red; N – blue; C – grey). ^{t}Bu groups, hydrogen atoms not involved in any interaction, ligated solvent molecules and solvent of crystallisation omitted for clarity.

2.3.2. $[Mn^{III}_6Mn^{II}_2Ln^{III}_2(15)_2(\mu_4\text{-}O)_2(\mu_3\text{-}OH)_2(\mu\text{-}CH_3O)_2(\mu\text{-}OH)_2(MeOH)_4(dmf)_8](NO_3)_2(H_2O)_2$, 19.

Reaction of **H$_8$15** with Mn(II) nitrate hydrate and Ln(III) nitrates hexahydrate (Ln = Gd, Tb, Dy), followed by slow evaporation of the mother liquor, afforded a series of clusters of general formula $[Mn^{III}_6Mn^{II}_2Ln^{III}_2(\mathbf{15})_2(\mu_4\text{-}O)_2(\mu_3\text{-}OH)_2(\mu\text{-}CH_3O)_2(\mu\text{-}OH)_2(MeOH)_4(dmf)_8](NO_3)_2(H_2O)_2$, **19** (Ln = Gd, Tb, Dy, **19Gd** being shown in Figure 57). The crystals are in a monoclinic cell and structure solution was carried out in the space group $P2_1/n$. The structure described is of the Gd derivative (**19Gd**), although the Tb and Dy analogues (**19Tb** and **19Dy** respectively) proved to be isostructural, after having determined the unit cell dimensions of several single crystals of the compounds.

The ASU comprises half of the cluster, with disorder present in the positions of the Mn^{II} and Gd^{III} ions. This was modelled assigning half occupancy to each disordered Mn^{II} / Gd^{III} ion and, for the sake of brevity, only one position will be discussed. Cluster **19Gd** has a striking structural similarity to **18**, due to the interchange of one Mn^{II} ion with one Gd^{III} ion. It is also related to compound **11**, differing in the presence of two additional Mn^{III} cations. Mn1 in **19Gd** resides in the TBC[4] lower-rim, coordinated to the 4 phenolic oxyges O1 – O4 in a Type I binding mode (Mn1–O range 1.920(5) – 1.969(5) Å) and it is in the third oxidation state with a distorted octahedral geometry. The coordination sphere is completed by a ligated dmf molecule (Mn1–O9, 2.229(5) Å) residing in the calix[4]arene cavity and a μ_3-hydroxide (Mn1–O13, 2.174(6) Å). The O9-Mn1-O13 vector defines the Jahn-Teller axis, with considerable deviation from linearity (173.3(2)º) due to the aforementioned disorder. The Mn3 ion is in the second oxidation state and is disordered over two positions located in the Type II binding sites. It has a distorted octahedral geometry and it is bound to two phenolic oxygen atoms (Mn3–O1, 2.346(4) Å and Mn3–O8, 2.193(4) Å), a ligated dmf molecule (Mn3–O11, 1.998(6) Å), a ligated MeOH molecule (Mn3–O15, 2.241(5) Å), the aforementioned μ_3-hydroxide (Mn3–O13, 2.246(5) Å) and a μ-hydroxide (Mn3–O17, 2.170(4) Å) linking to Mn4.

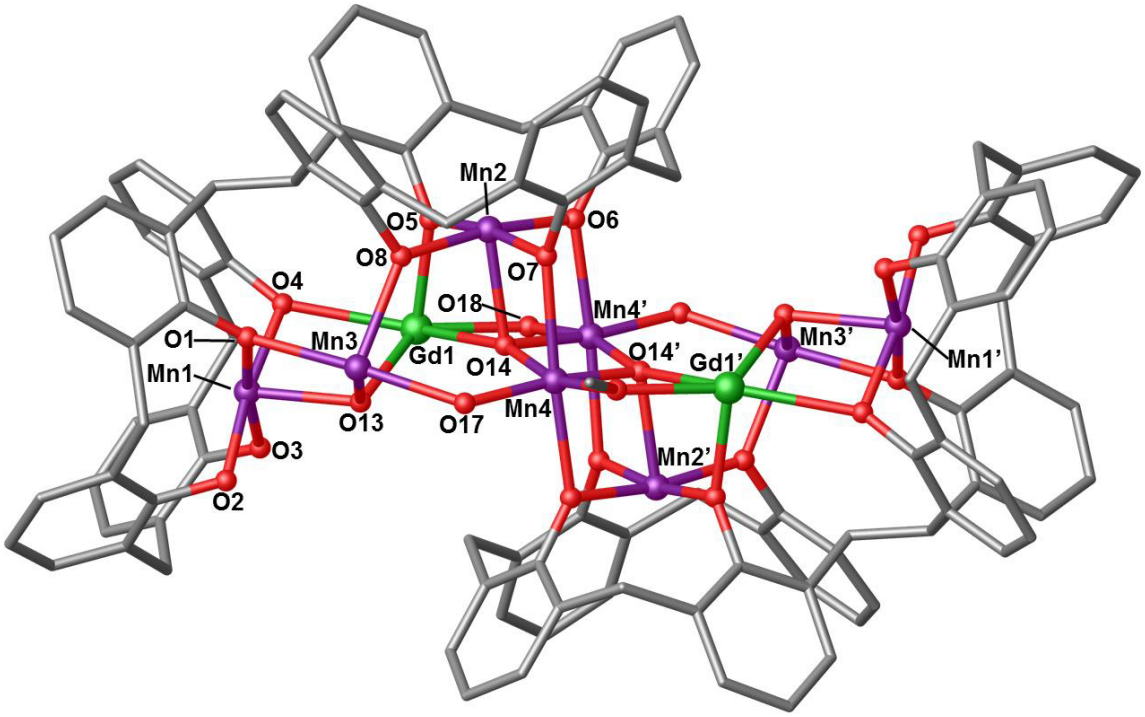

Figure 57. Partial single crystal *X*-ray structure showing the $[Mn^{III}_6Mn^{II}_2Gd^{III}_2(\mathbf{15})_2(\mu_4\text{-}O)_2(\mu_3\text{-}OH)_2(\mu\text{-}CH_3O)_2(\mu\text{-}OH)_2(MeOH)_4(dmf)_8](NO_3)_2(H_2O)_2$ cluster, **19Gd**, and selected labels according to discussion (Colour code: Mn – purple; Gd – green; O – red; C – grey). ^{t}Bu groups, hydrogen atoms, ligated solvent molecules and solvent of crystallisation omitted for clarity.

Gd1 is in the third oxidation state, is heptacoordinate with a distorted pentagonal bipyramidal geometry and, in a similar fashion as for Mn3, is disordered at half-occupancy over two positions. The coordination is defined by two μ-phenoxides (Gd1–O4, 2.493(4) Å and Gd1–O5, 2.201(4) Å), a μ_3-hydroxide (Gd1–O13, 2.299(7) Å), a ligated dmf molecule (Gd1–O12, 2.473(7) Å), a ligated MeOH molecule (Gd1–O16, 2.361(6) Å), a μ-methoxide (Gd1–O18, 2.184(5) Å) connected to Mn4, and a μ_4-oxide (Gd1–O14, 2.497(4) Å) that is binding Mn2, Mn4 and Mn4'. Mn2 (3+) has a near identical coordination mode compared to Mn1 (3+), as it is bound in a Type I binding pocket defined by O5 – O8 (Mn2-O range 1.901(4) – 1.950(4) Å) and to a ligated dmf molecule residing in the TBC[4] cavity (Mn2–O10, 2.250 Å). The only difference relative to Mn1 coordination sphere is the coordination to O14 (Mn2 - O14, 2.229(4) Å). Finally, Mn4 is in a third oxidation state and has a distorted octahedral geometry with a Jahn-Teller axis along the O7-Mn4-O6' vector (Mn4–O7, 2.354(4) Å and Mn4–O6', 2.256(4) Å, 175.79(14)º). The coordination sphere is completed by the aforementioned μ_4-oxides (Mn4–O14, 1.925(4) Å and Mn4–O14', 1.901(5) Å), the μ-hydroxide (Mn4–O17, 1.914(5) Å) and the μ-methoxide (Mn4–O18', 1.917(4) Å) mentioned above.

Being symmetrically analogus to **18**, **19Gd** shows identical capping behaviour (Figure 58), with four $[Mn^{III}(TBC[4])]^-$ encapsulating Mn3, Mn4 and Gd1 (and related s.e.) and the $[Mn2\ /Mn2'(TBC[4])]^-$ units at the vertex of a square pyramid (Figure 55). Examination of the extended structure shows that, as a result of symmetry, **19Gd** packs along the *a* axis in layers in which each of these is oriented in the opposite direction to the other, in a fishbone manner (Figure 59). There are no noteworthy interactions between neighbouring moieties, and the shortest metal-metal intercluster distance identified is along the *b* axis, occurring between Mn3 and Mn2 (Mn3…Mn2, 12.676 Å).

Temperature-dependent dc magnetic susceptibility studies carried out on polycrystalline samples of **18** and **19** show that, at room temperature, the χT value is in excellent agreement with that expected from spin-only contribution to the magnetism. On lowering the temperature, the χT product remains essentially the same until reaching 100 K for **18**, at which point it begins to decrease rapidly. The χT product for **19** remains essentially the same until reaching 50 K, at which point it slowly increases until the temperature of 20 K is reached, below which it has a more drastic increase. The overall magnetic behaviour proved hard to model due to structural complexity although, given the respective similarities of **18** and **19** to **9** and **11** (Chapter 1, Section 1.5.3), it is therefore safe to assume a similar qualitative behaviour. This is characterised by both ferro- and antiferromagnetic exchange interactions.

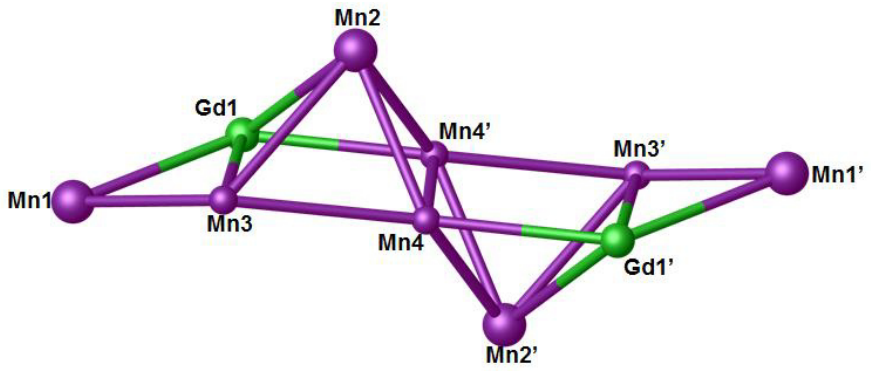

Figure 58. Capping behaviour in the structure of **19Gd**. Capping moieties by $[Mn^{III}(TBC[4])]^-$ moieties are shown as large spheres (Colour code: Mn – Purple, Gd – green).

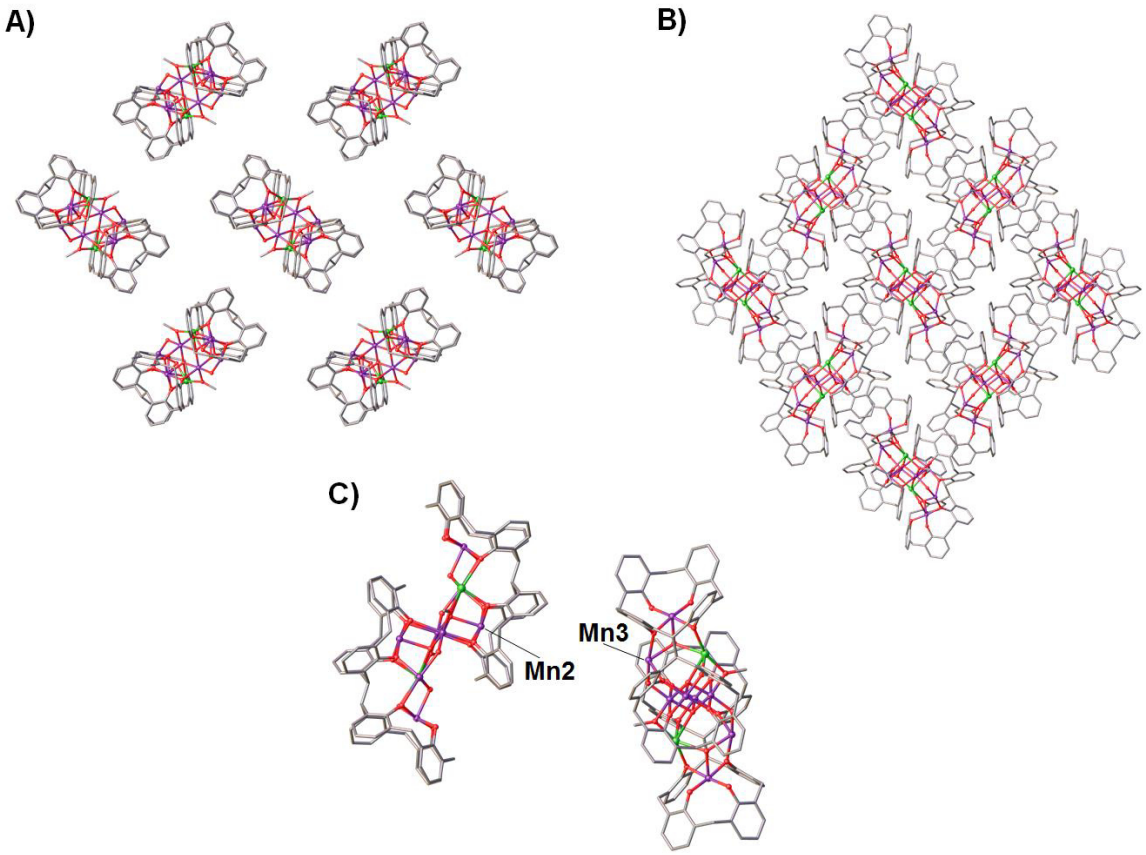

Figure 59. Views of the extended structure of **19Gd**. A) The *bc* and B) *ab* planes and C) closest ions labelled according to discussion (Colour code: Mn – purple; Gd – green; O – red; C – grey). ^{t}Bu groups, hydrogen atoms, ligated solvent molecules and solvent of crystallisation omitted for clarity.

2.3.3. $[Mn_4^{III}Ln_4^{III}(15)_2(\mu_3\text{-}OH)_4(\mu\text{-}CO_3)_2(dmf)_8(H_2O)_4](MeOH)(dmf)_2$, 20.

The last family of clusters obtained by variation of stoichiometry and crystallisation conditions was synthesised by reaction of **H$_8$15** with manganese(II) chloride tetrahydrate and lanthanide(III) chloride hexahydrate (Ln = Gd, Tb and Dy). Single crystals were obtained by slow evaporation of the mother liquor and SCXRD revealed that they are of general formula $[Mn_4^{III}Ln_4^{III}(\mathbf{15})_2(\mu_3\text{-}OH)_4(\mu\text{-}CO_3)_2(dmf)_8(H_2O)_4](MeOH)(dmf)_2$, **20** (Ln = Gd, Tb, Dy, **20Gd** being shown in Figure 60). The crystals were found to be in a monoclinic cell and structure solution was carried out in the space group $P2_1/n$. The structure described is of the Gd derivative (**20Gd**), although the Tb and Dy analogues (**20Tb** and **20Dy** respectively) proved to be isostructural, after having determined the unit cell dimensions of several single crystals of each compound.

The ASU is composed by two distorted $Mn^{III}_2Gd^{III}_2$ butterfly-like moieties connected together *via* μ-carbonates, the presence of which arises from incorporation of atmospheric

CO_2 into the structure, a fairly common phenomenon in coordination cluster chemistry.[125] Mn1 is bound to the calix[4]arene lower-rim phenolic oxygens O1 – O4 in a Type I binding fashion (Mn1–O range 1.919(7) – 1.969(7) Å) and it is in the third oxidation state with octahedral geometry. Its coordination sphere is completed by a ligated dmf molecule (Mn1–O21, 2.203(9) Å) and a μ_3-hydroxide (Mn1–O17, 2.073(7) Å). The Jahn-Teller axis is defined by the O21-Mn1-O17 vector with small deviation from linearity (177.1(2)°). Mn2 has an analogous oxidation state, geometry and coordination sphere, being coordinated to the phenolic oxygens O5 – O8 (Mn2–O range 1.905(8) – 1.989(7) Å), a ligated dmf molecule (Mn2–O22, 2.220(8) Å) and a μ_3-hydroxide (Mn2–O18, 2.127(6) Å). In this case the Jahn-Teller axis defined by the O22-Mn2-O18 vector is more distorted, deviating further from the linearity (166.9(2)°). The aforementioned μ_3-hydroxides are connecting to Gd1 and Gd2 (Gd1–O17, 2.387(5) Å; Gd2–O17, 2.342(5) Å; Gd1–O18, 2.408(5) Å; Gd2–O18, 2.409 Å), both of which are octacoordinate, in a distorted pentagonal bipyramidal geometry and residing in Type II binding sites. Gd1 is also bound to the phenolic oxygens O1 and O8, belonging to two separate TBC[4] fragments (Gd1–O1, 2.444(6) Å and Gd1–O8, 2.366(6) Å respectively), a ligated dmf molecule (Gd1–O25, 2.349(8) Å), an aqua ligand (Gd1–O26, 2.406(7) Å) and two oxygen atoms of a μ-carbonate (Gd1–O33, 2.419(7) Å and Gd1–O34, 2.438(6) Å). The other μ-carbonate anion is instead binding Gd2 (Gd2–O36, 2.391(7) and Gd2–O37, 2.481(6) Å), which has a coordination sphere identical to Gd1, being bound the aforementioned μ_3-hydroxide (Gd2–O18, 2.409(7) Å), two μ-phenoxides (O4 and O5, Gd2–O4, 2.523(6) Å and Gd2–O5, 2.333(6) Å), a ligated dmf molecule (Gd2–O27, 2.370(10) Å) and an aqua ligand (Gd2–O28, 2.415(7) Å).

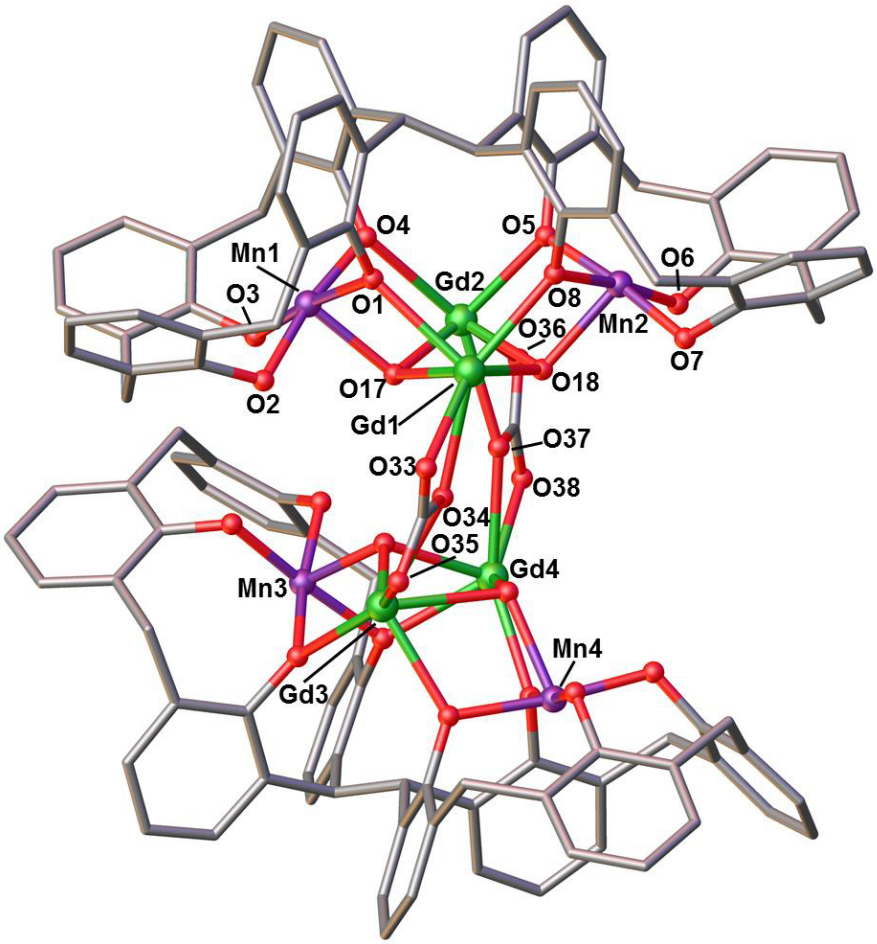

Figure 60. Partial single crystal *X*-ray structure showing the $[Mn_4^{III}Gd_4^{III}(\mathbf{15})_2(\mu_3\text{-}OH)_4(\mu\text{-}CO_3)_2(dmf)_8(H_2O)_4](MeOH)(dmf)_2$ cluster, **20Gd**, and selected labels according to discussion (Colour code: Mn – purple; Gd – green; O – red; C – grey). ^{t}Bu groups, hydrogen atoms, ligated solvent molecules and solvent of crystallisation omitted for clarity.

Mn3 and Mn4 are in a Type I binding site (Mn3–O range 1.917(7) – 1.960(7) Å and Mn4–O range 1.889(7) – 1.986(7) Å) and their coordination spheres are completed by ligated dmf molecules residing within the TBC[4] cavity (Mn3–O23, 2.153(8) Å and Mn4–O24, 2.239(7) Å) and μ_3-hydroxides (Mn3–O19, 2.000(7) Å and Mn4–O20, 2.130(6) Å). In Type I binding sites, Mn3 and Mn4 are in the third oxidation state with Jahn-Teller axes defined by the O23-Mn3-O19 (173.0(2)°) and O24-Mn4-O20 (168.5(2)°) vectors, both of which are far from linearity due to distortion. The aforementioned μ_3-hydroxides are the linked to Gd3 and Gd4, which are octacoordinate and in Type II binding sites (Gd3–O19, 2.325(7) Å, Gd4–O19, 2.359(7); Gd3–O20, 2.438(6) Å; Gd4–O20, 2.394(6) Å). Their coordination spheres, similar to those of Gd1 and Gd2, are completed by phenolic oxygens (Gd3–O12, 2.504(6) Å; Gd3–O13, 2.349(6) Å; Gd4–O9, 2.420(6) Å; Gd4–O16, 2.388(6) Å), ligated dmf

molecules (Gd3–O29, 2.365(9) Å and Gd4–O31, 2.355(8) Å), aqua ligands (Gd3–O30, 2.418(6) Å and Gd4–O32, 2.433(7) Å), and oxygens belonging to the μ-carbonate (Gd3–O34, 2.469(6) Å; Gd3–O35, 2.397(7) Å; Gd4–O37, 2.441(6) Å, Gd4–O38, 2.414(7) Å).

Once again, the presence of Ln^{III} instead of Mn^{II} ions in the binding region between the two TBC[4] macrocycles is confirmation of the interchangeability between these two ions with such systems, given the correct stoichiometry and crystallisation conditions employed. The metallic core is a distorted square of Ln^{III} ions that is capped on the edges by $[Mn^{III}_2$-**15**$]^{2-}$ moieties (Figure 61), which is a structural feature that can be observed for **17** discussed above, as well as for compound **4** in Chapter 1 (Section 1.5.2, Figure 34).

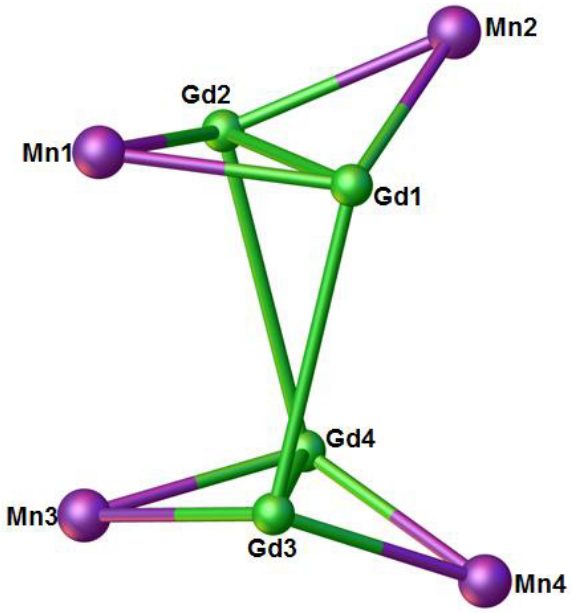

Figure 61. Capping behaviour in the structure of **20Gd**. Capping by $[Mn^{III}$(TBC[4])$]^-$ moieties are shown as large spheres (Colour code: Mn – Purple, Gd – green).

Structural expansion of **20Gd** reveals that there are no significant intermolecular interactions occurring between the clusters. Along the *a* axis, the shortest metal-metal intercluster distances measured are between Gd1 and Gd4 (Gd1…Gd4, 12.783 Å) followed by Mn2 and Mn3 (Mn2…Mn3, 12.969 Å) along the *b* axis (Figure 62).

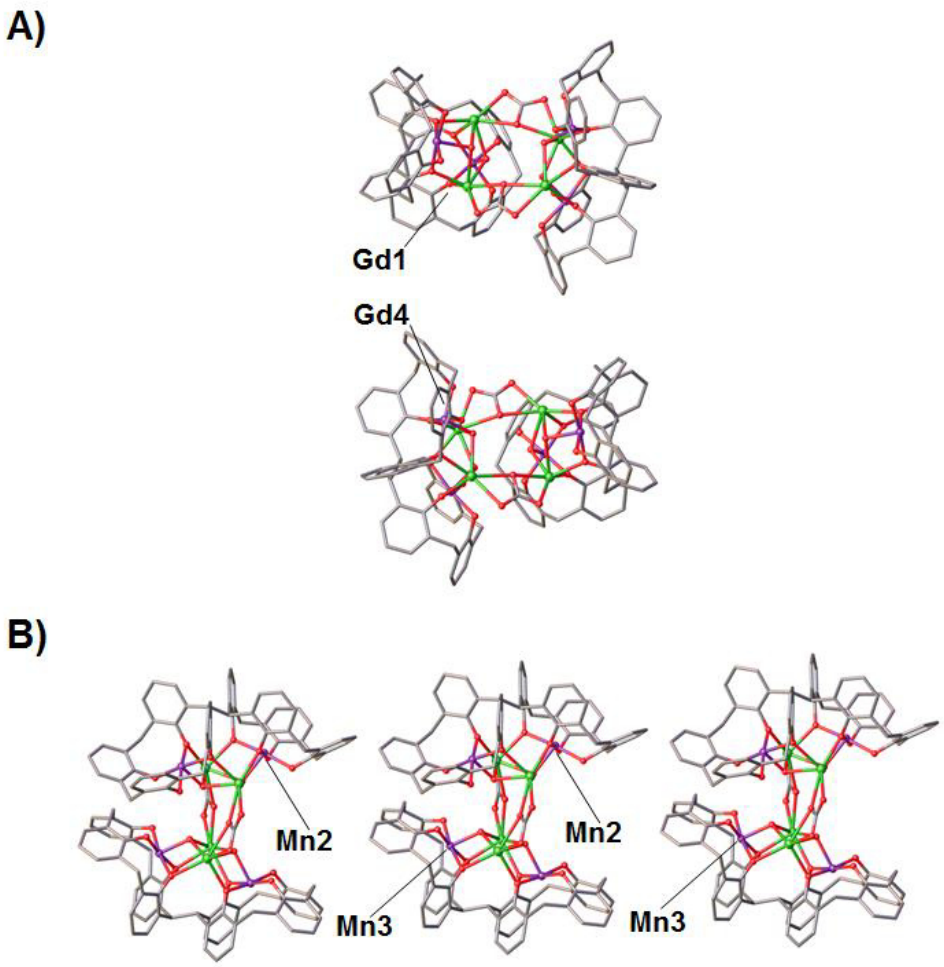

Figure 62. Views of the extended structure of **20Gd.** A) The *bc* and B) *ac* planes with closest ions labelled according to discussion (Colour code: Mn – purple; Gd – green; O – red; C – grey). ^{t}Bu groups, hydrogen atoms, ligated solvent molecules and solvent of crystallisation omitted for clarity.

2.4. Summary.

A search of the Cambridge Structural Database (CSD) was conducted in order to confirm the novelty of the topologies obtained as a consequence of the versatility of the H_8BisTBC[4] ligand (Table 1). This has revealed 7 entries for $[Cu_4Ln_5]$ clusters (where Ln = Gd, Dy and Tb) but none have a topology similar to **16**. No hits were obtained for $[Fe_5Ln_4]$ clusters, suggesting that compound **17** is indeed a new topology. On the contrary, Mn_{10} clusters are very common in coordination chemistry, with 156 entries for clusters in which the Mn ions possess different oxidation states; some of these clusters incorporate other metal ions. Despite the great number of clusters containing ten Mn cations, none have a topology comparable to **18**. Compound **19** appears to be a novel addition to cluster chemistry, as the CSD search for compounds containing the same number and composition of the core returned zero results. Finally, a search for $[Mn_4Ln_4]$-containing clusters (where Ln = Gd, Dy and Tb) returned 15 entries, three of which are represented by compound **4** (Chapter 1, Section 1.5.2.) which, although having the same core composition and featuring the same square of Ln^{III} within a square of Mn^{III} ions motif as compound **20**, is topologically different from the latter.

Considering the clusters discussed so far it is clear that H_8BisTBC[4] is a versatile ligand that allows the formation of several polymetallic clusters. Furthermore, the coordination modes, motifs and topologies of compounds **16** – **20** follow the same binding rules observed for the BisTBC[4]-supported parent clusters as well as for those supported by the TBC[4] ligand (Chapter 1, Sections 1.5.2 and 1.5.3). Evidence for the extension of these structural trends suggests that one should be able to ultimately construct highly complex assemblies in a logical fashion. This hypothesis is based on the systematic introduction of a tailored number of TBC[4] moieties in a target building block, and represents potential future research in this area.

	Mn^{II} / Mn^{III}	Cu^{II}	Fe^{III}	$Mn^{II/III}$ / Ln^{III}	Cu^{II} / Ln^{III}	Fe^{III} / Ln^{III}	Ln^{III}
$H_8$15	✓	✓	✗	✓	✓	✓	✗
Cluster no.	**9, 18**	**10**	–	**11, 19, 20**	**16**	**17**	–

Table 1. Summary of the attempted reactions of BisTBC[4], **$H_8$15**, with TM and Ln metal ions and relative compound number.

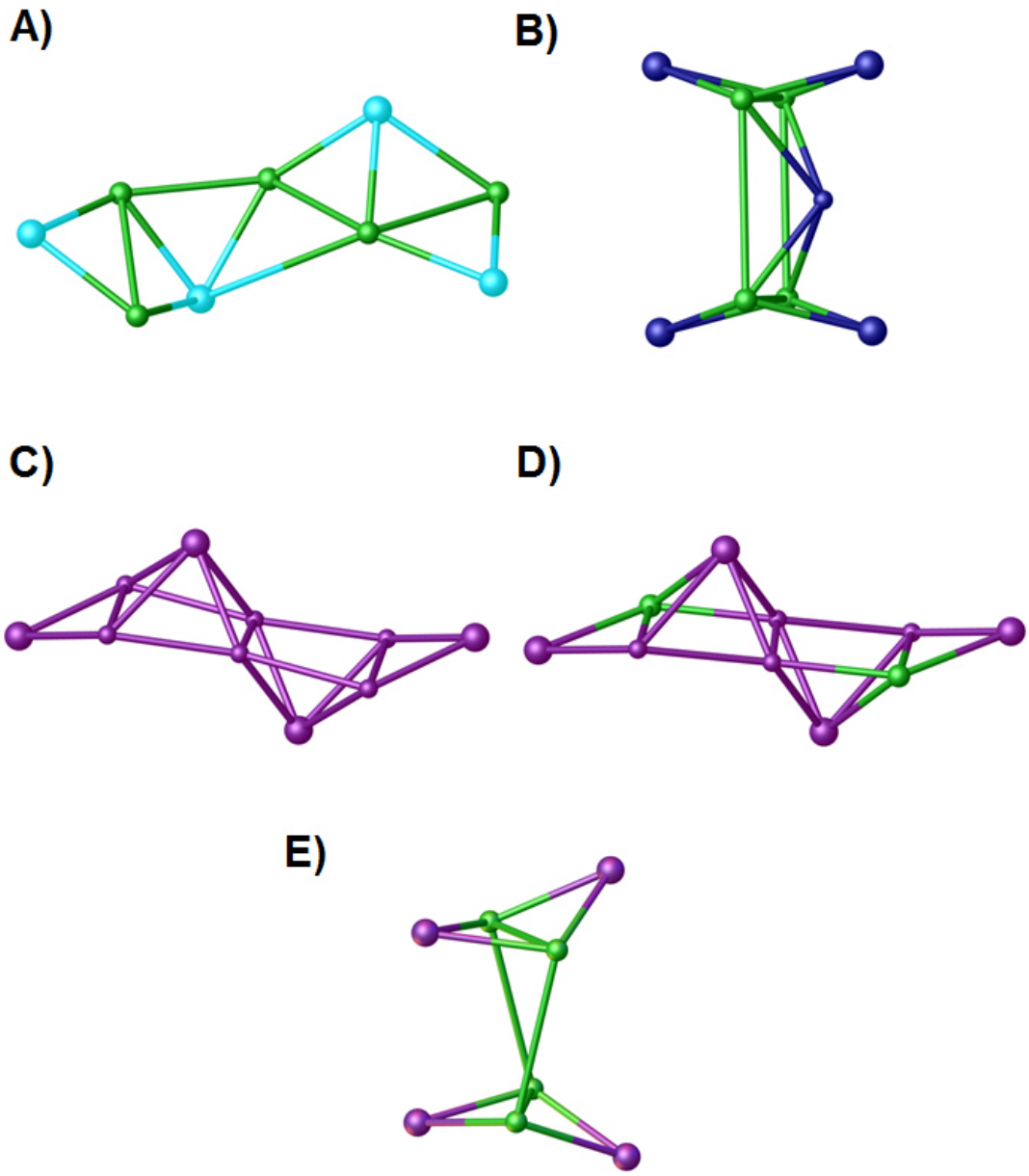

Figure 63. Capping behaviour in the structures of BisTBC[4]-supported clusters **16** – **20**. Capping by $[TM^{III} / Ln^{III}(TBC[4])]^{-}$ moieties are shown as large spheres (Colour code: Mn – purple; Cu – light blue; Fe – dark blue; Ln – green).

2.5. Experimental.

Precursors for compound **H8 15** and all the chemical reagents used in subsequent syntheses were purchased from Aldrich and used without further purification. Analytical thin layer chromatography was performed on precoated silica gel plates (Merck, 60 F_{254}) and column chromatography was performed with silica gel (Merck, particle size , mesh). ^{1}H NMR and $^{13}C\{^{1}H\}$ NMR spectra were collected on Bruker Avance^{III} 300 MHz for routine experiments and on a Bruker AVI 400 MHz for an accurate characterisation. All chemical shifts are expressed in ppm. Electrospray ionisation mass spectra were recorded on a Thermofisher LTQ Orbitrap XL Hybrid ion trap mass spectrometer. All the single crystals were analysed on a Bruker Apex II with a graphite monochromated Mo-Kα radiation source (0.71073 Å) or on a Bruker D8 equipped with a PHOTON 100 detector with a synchrotron radiation source (0.77490 Å).

Synthesis of *p-tert*-butylcalix[4]arene, H_4TBC[4], 12.

Compound **12** was synthesised according to literature procedure,[84] adopting and scaling-up the quantities. In a 3 neck 10 L reactor equipped with mechanical stirrer, *p-tert*-butylphenol (500 g, 3.3 mol), formaldehyde (37%, 300 mL), and a solution of sodium hydroxide (2.4 g, 60 mmol) dissolved in deionised water (20 mL) were added, and the reaction mixture was refluxed with stirring, while under N_2, at 120ºC until polymer was formed. The water formed by the reaction is removed by means of a Dean-Stark apparatus. Polymer was then cooled down to room temperature and toluene (2 L) and diphenyl ether (4 L) were added. The reaction mixture was heated until toluene was removed, kept under reflux at 260ºC for 4 hours, and then left to cool down. Next, ethyl acetate (3 L) was added and the solution was stirred at room temperature for 2 hours. The solution was filtered and the material collected was washed with ethyl acetate to afford 314 g of **12** as white crystals (Yield: 14.7%). ^{1}H NMR ($CDCl_3$): 10.35 (s, 4 H, O<u>H</u>), 7.06 (s, 8 H, Ar<u>H</u>), 4.26 (d, J = 12.8 Hz, 4 H, Ar-<u>CH_2</u>-Ar), 3.50 (d, J = 11.7 Hz, 4 H, Ar-<u>CH_2</u>-Ar), 1.22 (s, 36 H, C(<u>CH_3</u>)$_3$).

Synthesis of tetramethoxy-*p-tert*-butylcalix[4]arene, TBC[4]OMe, 13.

p-tert-butylcalix[4]arene **12** (20 g, 30.8 mmol) was dissolved in a 10:1 THF/dmf mixture (100 mL + 10 mL). NaH (5g, 0.21 mol) was slowly added while stirring the solution. MeI (20 mL, 0.32 mol) was added using a disposable syringe and the solution heated at reflux for 2 hours, after which it was cooled at RT and MeOH was added to destroy unreacted NaH.

Solvents were eliminated under reduced pressure and the resulting solid was collected and washed with H_2O. The crude was dissolved in $CHCl_3$ and the resulting yellow solution was dried over $MgSO_4$, filtered and concentrated under reduced pressure. The product was recrystallised from hot $CHCl_3$/MeOH to afford 17.2 g of **13** as a white powder (Yield: 79.2%).

Synthesis of 2,2'-bis(5,11,17,23-tetra-*p-tert*-butyl-25,26,27,28-tetramethoxycalix[4]arene), BisTBC[4]OMe, 14.

n-BuLi (2.5 M in hexane, 11.3 mL, 28.37 mmol, 2 eq.) was added to a stirred solution of tetramethoxycalix[4]arene **13** (10 g, 14.18 mmol, 1 eq.) in dry THF (50 mL) under an N_2 atmosphere, causing a rapid colour change from pale yellow to blood red. After ten minutes of stirring 1,2-dibromoethane (3.05 mL, 35.46 mmol, 2.5 eq.) was added dropwise over 40 minutes as a solution in 30 mL of dry THF, with concomitant change in colour from blood red to yellow. The reaction mixture was stirred for a further 12 hours before being quenched by the addition of H_2O. Volatiles were removed and the resulting solid was dried under vacuum. The crude material was then dissolved in CH_2Cl_2 (300 ml) and washed with brine (3 × 100 ml). The organic layer was separated, dried over $MgSO_4$, and the solvent was removed under reduced pressure to afford a gummy yellow solid that was dried under vacuum. The resulting yellow solid was recrystallised from hot $CHCl_3$/MeOH to afford a white powder of the pure target **14**. Yield: 7.07 g (35%). The ^{1}H NMR spectrum of the product is very difficult to interpret due to fluxionality caused by the presence of lower-rim methoxy groups. Although this is the case it was possible to gauge reaction completion for these synthetic intermediates by the disappearance of the characteristic -OH groups for the TBC[4] lower-rim.

Synthesis of 2,2'-bis(5,11,17,23-tetra-*p-tert*-butyl-tetrahydroxy-calix[4]arene, BisTBC[4], $H_8$15.

Cyclohexyl iodide (29.2 mL, 226 mmol, 45 eq.) was added to a dmf (150 ml) solution of **14** (7.07 g, 5.02 mmol, 1 eq.) and the resulting mixture was heated at reflux for 48h with a concomitant change in colour from pale yellow to dark orange. The solution was poured into H_2O (250 mL), causing the precipitation of an orange solid. The orange precipitate was collected, was washed several times with water, and stirred in MeOH for 15 minutes to afford a white solid. The white solid was filtered, washed several times with MeOH, collected under

reduced pressure and recrystallised from hot $CHCl_3$/MeOH to afford pure **$H_8$15**. Yield: 4.27 g (66%). ^1H, ^{13}C NMR spectra and MS were found to be consistent with the published data.

Synthesis of [$Cu^{II}_4Ln^{III}_5$(15)$_2$(μ_3-OMe)(μ-OMe)(μ_3-OH)(μ_4-NO_3)(μ_5-NO_3)(MeOH)(dmf)$_6$(H_2O)$_4$](OH)$_2$(dmf)$_6$(H_2O), 16.

$Cu^{II}_4Gd^{III}_5$, 16Gd: **$H_8$15** (350 mg, 0.27 mmol, 1 eq.) and $Cu(NO_3)_2{\cdot}3H_2O$ (65 mg, 0.27 mmol, 1 eq.), $Gd(NO_3)_3{\cdot}6H_2O$ (244 mg, 0.54 mmol, 2 eq.) were suspended in a 1:1 dmf / MeOH mixture (20 mL) and stirred for 10 minutes. Et_3N (0.35 mL) was added and the resulting brown solution was stirred for additional 2 h and filtered. Elemental Analysis (%) calculated for **16Gd**, $C_{215}H_{308}Cu_4Gd_5N_{14}O_{45}$ (M = 4849.35): C, 53.25%; H, 6.4%; N, 4.04%. Found: C, 52.91%; H, 6.17%; N, 3.78%. **Yield** 218 mg (16.6 %).

$Cu^{II}_4Dy^{III}_5$, 16Dy: **$H_8$15** (350 mg, 0.27 mmol, 1 eq.) and $Cu(NO_3)_2{\cdot}3H_2O$ (65 mg, 0.27 mmol, 1 eq.), $Dy(NO_3)_3{\cdot}5H_2O$ (237 mg, 0.54 mmol, 2 eq.) were suspended in a 1:1 dmf / MeOH mixture (20 mL) and stirred for 10 minutes. Et_3N (0.35 mL) was added and the resulting brown solution was stirred for additional 2 h and filtered. Elemental Analysis (%) calculated for **16Dy**, $C_{215}H_{308}Cu_4Dy_5N_{14}O_{45}$ (M = 4875.6): C, 52.97%; H, 6.37%; N, 4.02%. Found: C, 52.64%; H, 5.98%; N, 3.78%. **Yield** 422 mg (32 %).

$Cu^{II}_4Tb^{III}_5$, 16Tb: **$H_8$15** (350 mg, 0.27 mmol, 1eq.), $Cu(NO_3)_2{\cdot}3H_2O$ (65 mg, 0.27 mmol, 1 eq.) and $Tb(NO_3)_3{\cdot}6H_2O$ (245 mg, 0.54 mmol, 2 eq.) were suspended in a 1:1 dmf / MeOH mixture (20 mL) and stirred for 10 minutes. Et_3N (0.35 mL) was added and the resulting brown solution was stirred for additional 2 h and filtered. The mother liquor was allowed to slowly evaporate, affording crystals suitable for *X*-ray diffraction studies. Elemental Analysis (%) calculated for **16Tb**, $C_{215}H_{308}Cu_4Tb_5N_{14}O_{45}$ (M = 4857.73): C, 53.16%; H, 6.39%; N, 4.04%. Found: C, 52.84%; H, 6.21%; N, 3.78%. **Yield** 292 mg (22.1%). **Crystal data for 16Tb:** $C_{215}H_{308}Cu_4Tb_5N_{14}O_{45}$, M = 4857.73, Orange needles, 0.3 x 0.02 x 0.02 mm^3, monoclinic, space group $P2_1/n$ (No. 14), a = 19.0415(7), b = 55.063(2), c = 25.3349(9) Å, β = 97.974(2)º, V = 26306.3(17) $Å^3$, Z = 4, Bruker D8 diffractometer equipped with a PHOTON 100 detector, synchrotron radiation, λ = 0.7749 Å, T = 100(15) K, $2\theta_{max}$ = 48.34º, 475428 reflections collected, 32366 unique (R_{int} = 0.0986). Final *GooF* = 0.849, R_1 = 0.0874, wR_2 = 0.2276.

Synthesis of [$Fe^{III}_5Ln^{III}_4$(15)$_2$(μ_4-O)$_2$(μ_3-O)$_2$(μ_3-NO_3)$_2$(dmf)$_8$(H_2O)$_6$](OH), 17.

$Fe^{II}_5Gd^{III}_4$, 17Gd: **$H_8$15** (350 mg, 0.27 mmol, 1 eq.), $Fe(NO_3)_3{\cdot}9H_2O$ (109 mg, 0.27 mmol, 1 eq.) and $Gd(NO_3)_3{\cdot}6H_2O$ (488 mg, 1.08 mmol, 4 eq.) were suspended in a 1:1 dmf / MeOH

mixture (20 mL) and stirred for 10 minutes. Et_3N (0.35 mL) was added and the resulting orange/brown solution was stirred for additional 2 h and filtered. The mother liquor was allowed to slowly evaporate, affording crystals suitable for *X*-ray diffraction studies. Elemental Analysis (%) calculated for **17Gd**, $C_{200}H_{274}Fe_5Gd_4N_{10}O_{41}$ (M = 4382.69): C, 54.81%; H, 6.3%; N, 3.2%. Found: C, 54.56%; H, 6.09%; N, 3.18%. **Yield** 240 mg (20.3 %). **Crystal data for 17Gd:** $C_{200}H_{274}Fe_5Gd_4N_{10}O_{41}$, M = 4382.69, Orange plate, 0.11 x 0.08 x 0.03 mm^3, triclinic, space group *P*-1 (No. 2), a = 16.926(2), b = 19.634(2), c = 20.203(2)Å, α = 114.498(2)º, β = 99.345(2)º, γ = 99.663(2), V = 5847.7(11) $Å^3$, Z = 2, Bruker D8 diffractometer equipped with a PHOTON 100 detector, synchrotron radiation, λ = 0.7749 Å, T = 100(15) K, $2\theta_{max}$ = 58º, 65628 reflections collected, 23888 unique (R_{int} = 0.0597). Final *GooF* = 1.026, R_1 = 0.0794, wR_2 = 0.2648.

$Fe^{II}_5Dy^{III}_4$, 17Dy: **H8L15** (350 mg, 0.27 mmol, 1 eq.) and $Fe(NO_3)_2{\cdot}9H_2O$ (109 mg, 0.27 mmol, 1 eq.), $Dy(NO_3)_3{\cdot}5H_2O$ (474 mg, 1.08 mmol, 4 eq.) were suspended in a 1:1 dmf / MeOH mixture (20 mL) and stirred for 10 minutes. Et_3N (0.35 mL) was added and the resulting brown solution was stirred for additional 2 h and filtered. Elemental Analysis (%) calculated for **17Dy**, $C_{200}H_{274}Fe_5Dy_4N_{10}O_{41}$ (M = 4403.69): C, 54.55%; H, 6.27%; N, 3.18%. Found: C, 54.19%; H, 5.96%; N, 2.87%. **Yield** 278 mg (23.4 %).

$Fe^{II}_5Tb^{III}_4$, 17Tb: **H8L15** (350 mg, 0.27 mmol, 1eq.), $Fe(NO_3)_2{\cdot}3H_2O$ (109 mg, 0.27 mmol, 1 eq.) and $Tb(NO_3)_3{\cdot}6H_2O$ (489 mg, 1.08 mmol, 4 eq.) were suspended in a 1:1 dmf / MeOH mixture (20 mL) and stirred for 10 minutes. Et_3N (0.35 mL) was added and the resulting brown solution was stirred for additional 2 h and filtered. Elemental Analysis (%) calculated for **17Tb**, $C_{200}H_{274}Fe_5Tb_4N_{10}O_{41}$ (M = 4389.19): C, 54.73%; H, 6.29%; N, 3.19%. Found: C, 54.38%; H, 6.17%; N, 2.82%. **Yield** 236 mg (19.8%).

Synthesis of $[Mn_6^{III}Mn_4^{II}(15)_2(\mu_3\text{-}O)_2(\mu_3\text{-}OH)_2(\mu\text{-}CH_3O)_4(H_2O)_4(dmf)_8](dmf)_4$, 18.

H8L15 (175 mg, 0.135 mmol, 1eq.) and $MnCl_2{\cdot}4H_2O$ (214 mg, 1.08 mmol, 8 eq.) were suspended in a 1:1 dmf / MeOH mixture (20 mL) and stirred for 10 minutes. Et_3N (0.2 mL) was added and the resulting purple solution was stirred for additional 2 h and filtered. The mother liquor was allowed to slowly evaporate, affording arrow-headed crystals suitable for *X*-ray diffraction studies. Elemental Analysis (%) calculated for **18**, $C_{216}H_{310}Mn_{10}N_{12}O_{40}$ (M = 4264.14): C, 60.84%; H, 7.33%; N, 3.94%. Found: C, 60.68%; H, 7.26%; N, 3.77%. **Yield** 140 mg (24.3%). **Crystal data for 18:** $C_{216}H_{310}Mn_{10}N_{12}O_{40}$, M = 4264.14, Dark Violet, 0.1 x 0.06 x 0.01 mm^3, triclinic, space group *P*-1 (No. 2), a = 14.9101(5), b = 17.9438(5), c = 22.3792(7) Å, V = 5424(6) $Å^3$, Z = 1, Bruker D8 diffractometer equipped with a PHOTON

100 detector, synchrotron radiation, λ = 0.7749 Å, T = 100(15) K, $2\theta_{max}$ = 48.252º, 54412 reflections collected, 13284 unique (R_{int} = 0.0696). Final *GooF* = 1.045, R_1 = 0.1116, wR_2 = 0.2297.

Synthesis of $[Mn^{III}_6Mn^{II}_2Ln^{III}_2(15)_2(\mu_4\text{-}O)_2(\mu_3\text{-}OH)_2(\mu\text{-}OCH_3)_2(\mu\text{-}OH)_2(MeOH)_4(dmf)_8](NO_3)_2(H_2O)_2$, 19.

$Mn^{III}_6Mn^{II}_2Gd^{III}_2$, 19Gd: **H8 15** (50 mg, 0.039 mmol, 1 eq.) and $Mn(NO_3)_2{\cdot}xH_2O$ (41.4 mg, 0.234 mmol, 6 eq.), $Gd(NO_3)_3{\cdot}6H_2O$ (35 mg, 0.078 mmol, 2 eq.) were suspended in a 1:1 dmf / MeOH mixture (20 mL) and stirred for 10 minutes. Et_3N (0.05 mL) was added and the resulting purple solution was stirred for additional 2 h and filtered. The mother liquor was allowed to slowly diffuse with diethyl ether vapour, affording dark purple crystals suitable for *X*-ray diffraction studies. Elemental Analysis (%) calculated for (**19Gd**), $C_{206}H_{280}Mn_8Gd_2N_{10}O_{44}$ (M = 4354.40): C, 56.82%; H, 6.48%; N, 3.22%. Found: C, 56.59%; H, 6.21%; N, 2.98%. **Yield** 34.3 mg (20.2%). **Crystal data for 19Gd:** $C_{206}H_{280}Mn_8Gd_2N_{10}O_{44}$, M = 4354.40, Dark Violet Block, 0.4 x 0.35 x 0.3 mm^3, monoclinic, space group $P2_1/n$ (No. 14), a = 22.090(7), b = 19.1570(6), c = 27.0764(9) Å, β = 105.149(2)º, V = 11063.0(6) $Å^3$, Z = 2, Bruker D8 diffractometer equipped with a PHOTON 100 detector, λ = 0.7749 Å, T = 100(15) K, $2\theta_{max}$ = 59.772º, 136715 reflections collected, 24604 unique (R_{int} = 0.0542). Final *GooF* = 1.077, R_1 = 0.1061, wR_2 = 0.2740.

$Mn^{III}_6Mn^{II}_2Dy^{III}_2$, 19Dy: **H8 15** (50 mg, 0.039 mmol) and $Mn(NO_3)_2{\cdot}xH_2O$ (41.4 mg, 0.234 mmol), $Dy(NO_3)_3{\cdot}5H_2O$ (33.8 mg, 0.078 mmol) were suspended in a 1:1 dmf / MeOH mixture (20 mL) and stirred for 10 minutes. Et_3N (0.05 mL) was added and the resulting purple solution was stirred for additional 2 h and filtered. Elemental Analysis (%) calculated for **19Dy**, $C_{206}H_{280}Mn_8Dy_2N_{10}O_{44}$ (M = 4365.07): C, 56.68%; H, 6.46%; N, 3.21%. Found: C, 56.41%; H, 6.22%; N, 2.98%. **Yield** 22.86 mg (13.4 %).

$Mn^{III}_6Mn^{II}_2Tb^{III}_2$, 19Tb: H8 15 (50 mg, 0.039 mmol) and $Mn(NO_3)_2{\cdot}$(41.4 mg, 0.234 mmol), $Tb(NO_3)_3{\cdot}6H_2O$ (35 mg, 0.078 mmol) were suspended in a 1:1 dmf / MeOH mixture (20 mL) and stirred for 10 minutes. Et_3N (0.05 mL) was added and the resulting purple solution was stirred for additional 2 h and filtered. Elemental Analysis (%) calculated for **19Tb**, $C_{206}H_{280}Mn_8Tb_2N_{10}O_{44}$ (M = 4357.92): C, 56.78%; H, 6.48%; N, 3.21%. Found: C, 56.39%; H, 6.33%; N, 3.01%. **Yield** 40 mg (23.5 %).

Synthesis of $[Mn_4^{III}Ln_4^{III}(15)_2(\mu_3\text{-}OH)_4(\mu\text{-}CO_3)_2(dmf)_8(H_2O)_4](MeOH)(dmf)_2$, 20.

$Mn_4^{III}Gd_4^{III}$, 20Gd: **$H_8$15** (350 mg, 0.27 mmol, 1 eq.), $MnCl_2{\cdot}4H_2O$ (107 mg, 0.54 mmol, 2 eq.) and $Gd(NO_3)_3{\cdot}6H_2O$ (71 mg, 0.27 mmol, 1 eq.) were suspended in a 1:1 dmf / MeOH mixture (20 mL) and stirred for 10 minutes. Et_3N (0.35 mL) was added and the resulting purple solution was stirred for additional 2 h and filtered. The mother liquor was allowed to slowly evaporate, affording crystals suitable for *X*-ray diffraction studies. Elemental Analysis (%) calculated for **20Gd**, $C_{209}H_{290}Mn_4Gd_4N_{10}O_{41}$ (M = 4447.44): C, 56.44%; H, 6.57%; N, 3.15%. Found: C, 56.15%; H, 6.26%; N, 2.98%. **Yield** 396 mg (33 %). **Crystal data for 20Gd:** $C_{209}H_{290}Mn_4Gd_4N_{10}O_{41}$, M = 4447.44, Dark Violet Block, 0.3 x 0.07 x 0.01 mm^3, monoclinic, space group $P2_1/n$ (No. 14), a = 17.7206(8), b = 41.6212(17), c = 33.0584(14) Å, β = 102.014(2)º, V = 23848.3(18) $Å^3$, Z = 4, Bruker D8 diffractometer equipped with a PHOTON 100 detector, synchrotron radiation, λ = 0.7749 Å, T = 100(15) K, $2\theta_{max}$ = 54.448º, 295606 reflections collected, 40784 unique (R_{int} = 0.0793). Final *GooF* = 1.086, R_1 = 0.0690, wR_2 = 0.1752.

$Mn_4^{III}Dy_4^{III}$, 20Dy: **$H_8$15** (350 mg, 0.27 mmol, 1 eq.), $MnCl_2{\cdot}4H_2O$ (107 mg, 0.54 mmol, 2 eq.) and $Dy(NO_3)_3{\cdot}5H_2O$ (102 mg, 0.27 mmol, 1 eq.) were suspended in a 1:1 dmf / MeOH mixture (20 mL) and stirred for 10 minutes. Et_3N (0.35 mL) was added and the resulting purple solution was stirred for additional 2 h and filtered. Elemental Analysis (%) calculated for **20Dy**, $C_{209}H_{290}Mn_4Dy_4N_{10}O_{41}$ (M = 4468.44): C, 56.18%; H, 6.54%; N, 3.13%. Found: C, 55.87%; H, 6.22%; N, 2.96 %. **Yield** 431 mg (35.6%).

$Mn_4^{III}Tb_4^{III}$, 20Tb: **15** (350 mg, 0.27 mmol, 1 eq.), $MnCl_2{\cdot}4H_2O$ (107 mg, 0.54 mmol, 2 eq.) and $Tb(NO_3)_3{\cdot}6H_2O$ (101 mg, 0.27 mmol, 1 eq.) were suspended in a 1:1 dmf / MeOH mixture (20 mL) and stirred for 10 minutes. Et_3N (0.35 mL) was added and the resulting purple solution was stirred for additional 2 h and filtered. Elemental Analysis (%) calculated for **20Tb**, $C_{209}H_{290}Mn_4Tb_4N_{10}O_{41}$ (M = 4454.14): C, 56.36%; H, 6.56%; N, 3.14%. Found: C, 55.92%; H, 6.29%; N, 2.97 %. **Yield** 700 mg (58.3%).

2.6. References.

123. Bott, S., G.; Coleman, A. G.; Atwood, J., L.; *J. Am. Chem. Soc.*, **1986**, *108*, 1709 – 1710.

124. Zuo, L.; Yao, S.; Wang, W.; Duan, W.; *Tetrahedron Lett.*, **2008**, *49*, 4054 – 4056.

125. For examples see: 1) Wang, L.; Li, Y.; Peng, Y.; Liang, Z.; Yu, J.; Xu, R.; *Dalton Trans.*, **2012**, *41*, 6242 – 6246; 2) McLellan, R.; Rezé, J.; Taylor, S., M.; McIntosh, R., D.; Brechin, E., K.; Dalgarno, S., J.; *Chem. Comm.*, **2014**, *50*, 2202 – 2204.

Chapter 3: The effect of *N*,*O*–bi- and tri-dentate ligands on biscalix[4]arene-supported metal clusters

Chapter 3 covers a series of results obtained from exploratory cluster formation carried out with both H_8BisTBC[4] and a selection of *N*,*O*–bi- and tri-dentate co-ligands. This investigation was performed in order to study the possibility of obtaining hybrid polymetallic clusters with enhanced nuclearity, all of which may show coordination motifs typical of both BisTBC[4] and and the co-ligands employed. Prior to the discussion of the results obtained, the coordination properties of such *N*,*O*–co-ligands will be briefly described in relation to a) results present in the literature that employ just these ligands and b) a hybrid co-ligand TBC[4]-supported metal cluster that was obtained by implementing an analogous synthetic strategy.

3.1. *N*,*O*–bi- and tri-dentate ligands in coordination chemistry.

Exploitation of tripodal ligands bearing functionalities of different nature is a common strategy in the synthesis of high-spin paramagnetic clusters, as already discussed in Section 1.4; this can be achieved by taking advantage of the coordination modes of well-known building blocks. Amongst the plethora of bi- and tri-dentate ligands available, two classes of ligand proved to be interesting for their coordination properties, particularly because the cluster topologies observed are somewhat reminiscent of those formed with H_4TBC[4] and its derivatives. These ligands are *N*,*O*–chelates such as 2-pyridinemethanol (Hhmp), 2,6-pyridinedimethanol (H_2pdm), *N*-methyldiethanolamine (H_2MDEA) and diethanolamine (H_3DEA, Figure 64).

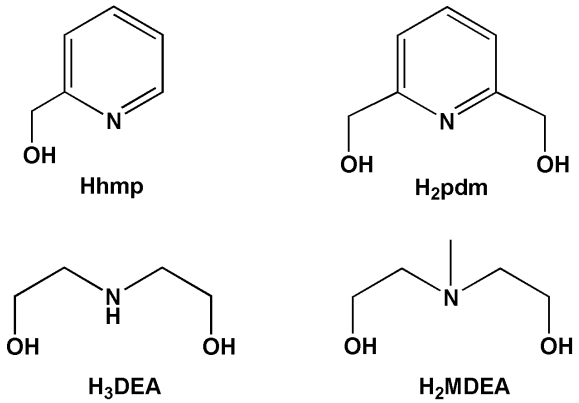

Figure 64. *N*,*O*–co-ligands chosen to explore coordination chemistry with H_8BisTBC[4].

To demonstrate this point, Hhmp typically acts as a μ-ligand, coordinating a $Mn^{II/III}$ ion *via* *N*- and *O*-atoms whilst bridging to a second metal ion through the alkoxide. This behaviour can be observed in the complex $[Mn^{III}_2Mn^{II}_2(hmp)_6Br_2(H_2O)_2]Br_2 \cdot H_2O$ (**21**, Figure 65A) and $[Mn_4(6me\text{-}hmp)_6Cl_4](H_2O)_4$.[126] The topology of the polymetallic core of this cluster is referred to as a butterfly, with a close relationship to those found in TBC[4]- and BisTBC[4]-supported polymetallic clusters.[111, 122] A similar pattern is observed when H_2pdm is employed. In this case, Brechin and co-workers obtained a mixed valence $Mn^{III}_2Mn^{II}_2$ cluster (**22**) supported by 2,6-pyridinedimethanol ligands that are only mono-deprotonated, with the remaining OH either binding a metal centre or being unbound (Figure 65B).[127] Employing unsubstituted and *N*-substituted diethanolamines afforded similar results, culminating in the isolation of a heptanuclear, six membered manganese wheel (**23**, Figure 65C) in which Mn^{II} and Mn^{III} cations alternate around a central Mn^{II} cation.[128] Alternatively, the topology of **23** can be viewed as two fused butterflies (compare Figure 65 A / B with C).

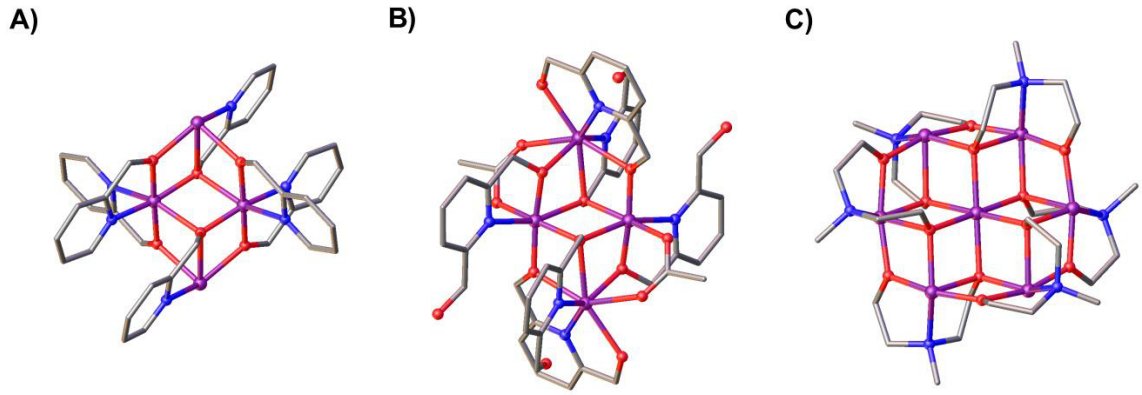

Figure 65. Partial single crystal *X*-ray structure showing A) a hmp–supported Mn_4 cluster, **21** B) a pdm–supported Mn_4 cluster, **22**, and C) a MDEA-supported Mn_7 wheel, **23** (Colour code: Mn – purple; O – red; N – blue, C – grey).[126-128] Hydrogen atoms, anions, ligated solvent molecules and solvent of crystallisation omitted for clarity.

The clusters obtained to date by employing the aforementioned *N*,*O*–ligands have clear similarities with the topologies formed with H_4TBC[4], making these two building blocks complementary to one another. Therefore, their concomitant employment should result in new cluster topologies that are in some way related to their parent complexes and ligand structure. With this in mind, Dalgarno and Brechin successfully synthesised a hybrid cluster that incorporates both moieties.[129] This was synthesised accordingly to the synthetic procedure

outlined in the previous chapter, and slow evaporation of the mother liquor afforded crystal of **24** which has formula $[Mn^{III}_3Mn^{II}_2(OH)_2(TBC[4])_2(hmp)_2(dmf)_6]$ $(H_3TBC[4])(dmf)_{2.6}(H_2O)_{1.4}$ (Figure 66). The ASU comprises of the entire cluster and the metallic skeleton is described by two $[Mn^{III}_2Mn^{II}]$ triangles sharing one vertex, in this case the central Mn^{III} cation in Figure 66; alternatively this can be described as two fused partial cubanes.

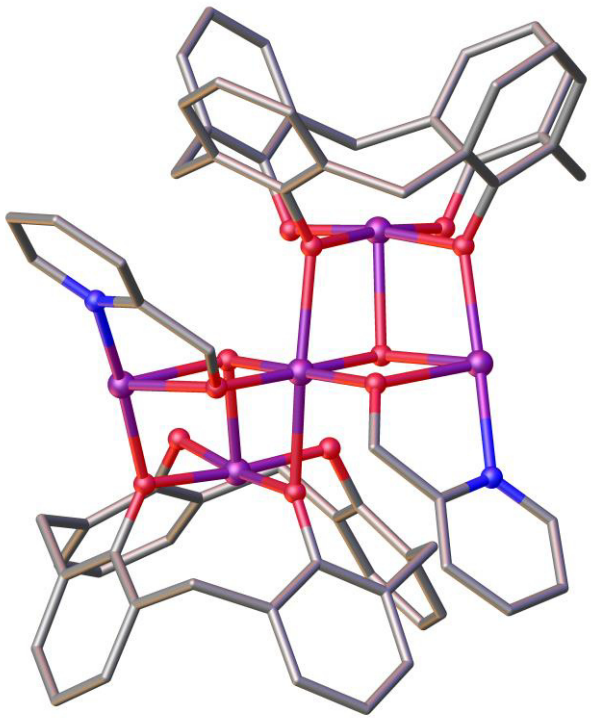

Figure 66. Partial single crystal *X*-ray structure of **24** showing the $[Mn^{III}_3Mn^{II}_2(OH)_2(TBC[4])_2(hmp)_2(dmf)_6](H_3TBC[4])(dmf)_{2.6}(H_2O)_{1.4}$ core (Colour code: Mn – purple; O – red; N – blue; C – grey).[129] ^{t}Bu groups, hydrogen atoms, anions, ligated solvent molecules and solvent of crystallisation omitted for clarity..

3.2. Biscalix[4]arene and *N*,*O*–ligands supported clusters.

Given that complementary and competitive *N*,*O*-ligands were successfully used to obtain new TBC[4]-supported metal clusters, it was worthwhile exploring the effect of these ligands in BisTBC[4] coordination chemistry and to draw comparison between the two systems.

3.2.1. $[Mn^{III}Mn^{II}Ln^{III}(H_315)(Hpdm)_2(MeOH)_2(dmf)](MeCN)_3(dmf)$, 25.

Reaction of **$H_8$15** with Mn(II) chloride tetrahydrate and Ln(III) chloride hexahydrate and H_2pdm afforded single crystals of $[Mn^{III}Mn^{II}Ln^{III}(\mathbf{H_3}\mathbf{15})(Hpdm)_2(MeOH)_2(dmf)](MeCN)_3$ (dmf), **25** (Ln = Gd, Tb or Dy, **25Gd** being shown in Figure 67), upon vapour diffusion of MeCN into the mother liquor. The crystals were found to be in a tetragonal cell and structure solution was carried out in the space group $P4_12_12$. The structure described is the Gd derivative (**25Gd**), although the Tb and Dy analogues (**25Tb** and **25Dy** respectively) proved to be isostructural, as determined by unit cell measurements on single crystals.

The ASU comprises the entire cluster, which has a $Mn^{III}Mn^{II}Gd^{III}$ polymetallic core in which the cations are in a near triangular arrangement or partial cubane. The BisTBC[4] octa-anion, according to the binding rules, has undergone conformational change although one of the Type I binding sites is unoccupied, perhaps due to the steric hindrance of one of the two neighbouring pdm molecules; these may be blocking binding sites that otherwise would have afforded already known topologies.

Notably this is the first time that a TBC[4] polyphenolic pocket has ever been found to be unoccupied in our studies of this coordination chemistry, perhaps a sign of the influence of the competing co-ligand present. Mn1 is in the third oxidation state and is bound in a Type I binding site (oxygen atoms O1 – O4, Mn–O range, 1.874(8) – 1.976(9) Å). Its coordination sphere is completed by a μ_3-oxygen belonging to a pdm molecule (Mn1–O9, 2.091(8) Å), which is also binding Mn2 and Gd1 (Mn2–O9, 2.277(8) Å and Gd1–O9, 2.476(8) Å). Mn2 is in the second oxidation state, adopting a distorted octahedral geometry and located in a Type II binding site. It is bound to two μ-phenoxides belonging to separate TBC[4] moieties (Mn2–O2, 2.223(8) Å and Mn2–O5, 2.152(8) Å), a μ-oxygen atom of another pdm molecule (Mn2–O12, 2.099(9) Å), a ligated dmf molecule (Mn2–O15, 2.187(11) Å) and a ligated methanol molecule (Mn2–O13, 2.225(10) Å).

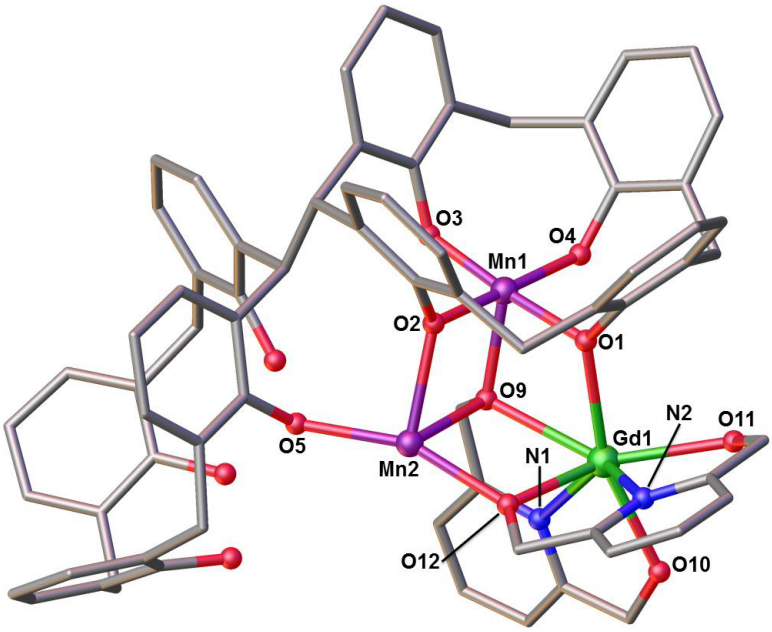

Figure 67. Partial single crystal *X*-ray structure showing the $[Mn^{III}Mn^{II}Gd^{III}(\mathbf{H_3 15})(pdm)_2(MeOH)_2(dmf)](MeCN)_3(dmf)$ cluster, **25Gd**, and selected labels according to discussion (Colour code: Mn – purple; Gd – green; O – red; N – blue; C – grey). ^{t}Bu groups, hydrogen atoms, ligated solvent molecules and solvent of crystallisation omitted for clarity.

Gd1 is heptacoordinate, is in a distorted pentagonal bypiramidal geometry and is bound to a phenolic oxygen (Gd1–O1, 2.392(9) Å), a ligated methanol molecule (Gd1–O14, 2.455(10) Å) and two pdm ligands (Gd1–N1, 2.521(11) Å; Gd1–O10, 2.330(9) Å; Gd1–O11, 2.406(9); Gd1–N2, 2.520(12) Å and Gd1–O12, 2.296(10) Å).

Capping behaviour in **25Gd** is observed with only one $[Mn^{III}(TBC[4])]^-$ moiety in this case, as the other Type I binding site is unoccupied (Figure 68). As stated above, this is likely attributable to the steric constraints of the vicinal Hpdm molecules, affording the triangular arrangement of three cations as a result.

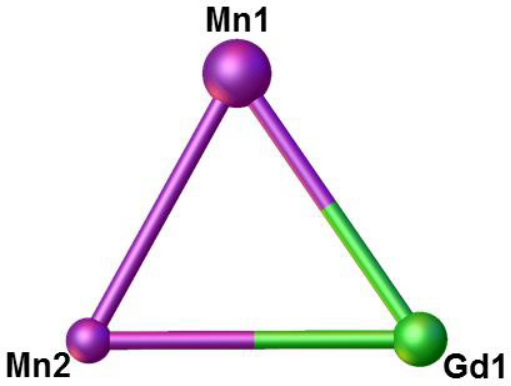

Figure 68. Capping behaviour in the structure of **25Gd**. Capping by a $[Mn^{III}(TBC[4])]^-$ moiety is shown as large sphere (Colour code: Mn – Purple, Gd – green).

Structure expansion reveals that the clusters pack close together, with the presence of strong H-bonding interactions along the *c* axis, occurring between the protonated OH groups of the pdm molecules (1.625(8) Å). The shortest measured metal-metal intercluster distance occurs along the *c* axis, between two neighbouring Gd1 ions was found to be ~ 5.9 Å (Figure 69).

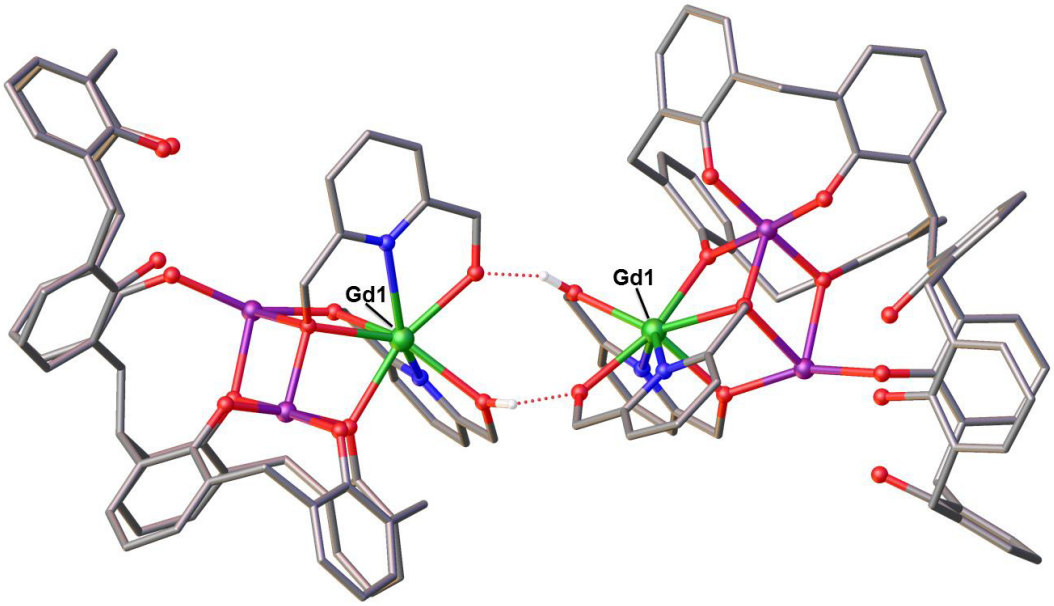

Figure 69. View of the *ab* plane in the extended structure of **25Gd** showing the H-bonding and the closest metal ions labelled according to discussion (Colour code: Mn – purple; Gd – green, O – red; N – blue; C – grey). ^{t}Bu groups, hydrogen atoms not involved in H-bonding, ligated solvent molecules and solvent of crystallisation omitted for clarity.

3.2.2. $[Mn^{III}_{10}Mn^{II}_4(15)_3(hmp)_4(\mu_3\text{-}O)_4(\mu_3\text{-}OH)_2(MeOH)_4(dmf)_6](dmf)_4$, 26.

Reaction of **H$_8$15** with Mn(II) chloride tetrahydrate and Hhmp afforded dark purple single crystals of formula $[Mn^{III}_{10}Mn^{II}_4(\mathbf{15})_3(hmp)_4(\mu_3\text{-}O)_4(\mu_3\text{-}OH)_2(MeOH)_4(dmf)_6](dmf)_4$, **26** (Figure 71), upon vapour diffusion of petroleum ether into the dmf / MeOH solvent mixture. The crystals were found to be in a monclinic cell and structure solution was carried out in the space group *C2/c*.

The ASU comprises one half of the title formula, presenting a $Mn^{III}_5Mn^{II}_2$ polymetallic core in which three Mn^{III} ions are located in a Type I binding sites, two Mn^{II} ions are in a Type II binding sites between the two TBC[4] moieties, and the remaining two Mn^{III} cations display a hybrid coordination pattern, both being supported by hmp ligands (Figure 70). Mn1 is bound to the four phenolic oxygens O1 – O4 of a Type I binding site (Mn1–O range 1.891(10) – 1.953(10) Å), is in the third oxidation state and has distorted square pyramidal geometry. Its coordination sphere is completed by a μ_3-hydroxide (Mn1–O13, 2.083(9) Å) that bridges to Mn4 and Mn5 (Mn4–O13, 2.191(9) Å and Mn5–O13, 2.187(10) Å). Mn2 is also in a Type I tetraphenolic binding site (O5–O8, Mn2–O range 1.917(9) – 1.946(9) Å) and it is in the third oxidation state with a distorted octahedral geometry. The O14–Mn2–O18 vector defines the Jahn-Teller axis and deviation from linearity is observed (174.9(4)º). Mn2 is also bound to a ligated dmf molecule located into a TBC[4] cavity (Mn2–O18, 2.206(11) Å) and a μ_3-oxide (Mn2–O14, 2.204(9) Å), the latter bridging to Mn6 and Mn7 (Mn6–O14, 1.896(9) Å and Mn7–O14, 1.865(8) Å).

Mn3 is in a Type 1 binding site, being coordinated to the lower-rim phenolic oxygens O9–O12 (Mn3–O range 1.916(9) – 1.981(9) Å), is in the third oxidation state and has distorted square pyramidal geometry. The Mn3 coordination sphere is completed by a μ_3-oxide (Mn3–O15, 2.119(9) Å) that bridges to Mn6 and Mn7 (Mn6–O15, 1.906(9) Å and Mn7–O15, 1.913(9) Å). Mn4 and Mn5 are both in Type II binding sites, in the second oxidation state and have distorted trigonal bipyramidal geometry; these have very similar coordination spheres. In addition to the aforementioned μ_3-oxide, they are bound to a phenolic oxygen (Mn4–O8, 2.116(9) Å and Mn5–O5, 2.128(9) Å), a ligated dmf molecule (Mn4–O19, 2.190(11) Å and Mn5–O20, 2.170(13) Å), a ligated MeOH molecule (Mn4–O21, 2.208(10) Å, Mn5–O22, 2.218(10) Å) and a μ-oxygen of a hmp ligand (Mn4–O16, 2.155(11) Å and Mn5–O17, 2.161(11) Å).

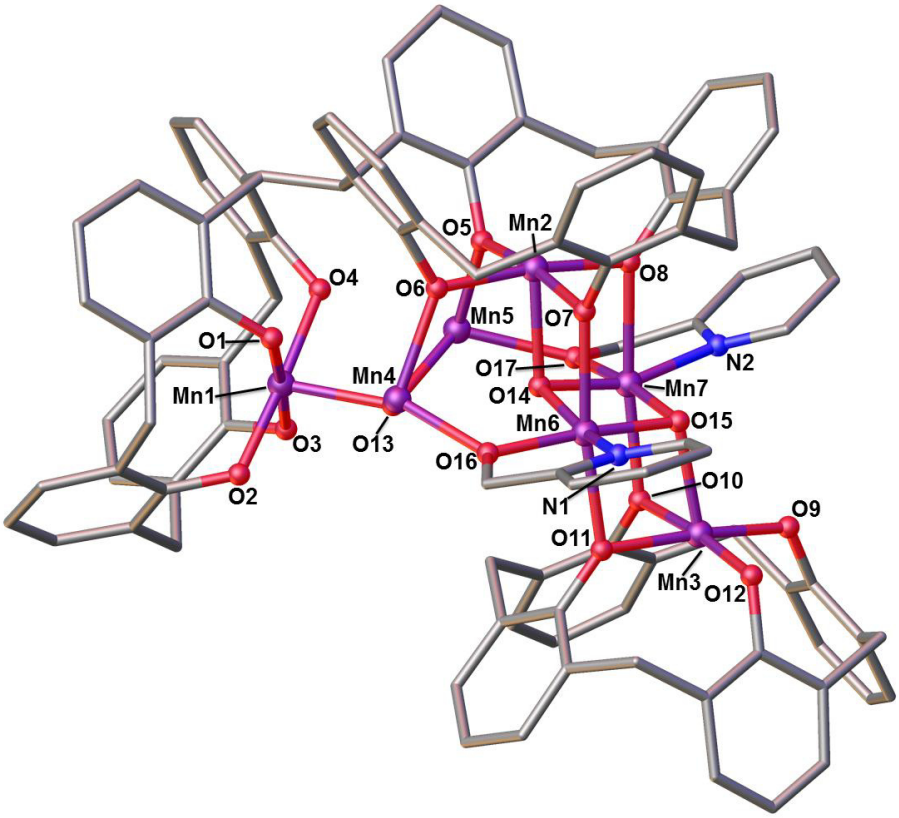

Figure 70. Partial single *X*-ray structure of **26** showing the asymmetric unit of $[Mn^{III}_{10}Mn^{II}_{4}(\mathbf{15})_3(hmp)_4(\mu_3\text{-}O)_4(\mu_3\text{-}OH)_2(MeOH)_4(dmf)_6](dmf)_4$ and selected labels according to discussion (Colour code: Mn – purple; O – red; N – blue; C – grey). ^{t}Bu groups, hydrogen atoms, ligated solvent molecules and solvent of crystallisation omitted for clarity.

Mn6 and Mn7 are both in the third oxidation state and have distorted octahedral geometries; the O7–Mn6–O11 and O6–Mn7–O10 vectors define the Jahn-Teller axes, both of which show deviation from linearity (172.3(3)º and 173.5(4)º respectively). Both Mn6 and Mn7 are bound to two phenolic oxygen atoms belonging to two separate TBC[4] moieties (Mn6–O7, 2.284(9) Å; Mn6–O11, 2.189(10) Å; Mn7–O6, 2.292(9) Å and Mn7–O10. 2.171(9) Å), the aforementioned μ_3-oxides (O14 and O15) and a ligated hmp molecule (Mn6–N1, 2.005(13) Å; Mn6–O16, 1.934(10) Å; Mn7–N2, 2.027(13) Å and Mn7–O17, 1.908(11) Å).

From symmetry expansion it is possible to appreciate the complexity of the cluster, which can be visualised as two $[Mn^{III}_{5}Mn^{II}_{2}(\mathbf{15})(hmp)_2]$ clusters that are linked / bridged by a central octa-anionic **15**, with a total of fourteen metal ions within the structure (Figure 71). Moreover, whereas two molecules of **15** are in a *syn* conformation, according to the now well-established empirical metal ion binding rules, the central **15** that links / bridges the two clusters is in an *anti* conformation, meaning that it has not undergone configurational inversion upon complexation. This is unprecedented compared to the BisTBC[4]-supported metal clusters

discussed so far, and by inspection of Figure 71, may also be due to the influence of the co-ligands present around the Mn6 and Mn7 centres. In this regard one can propose that, due to the competing nature of the two ligated hmp molecules, and also the proximity of these to the TBC[4] aromatic rings (~ 4.5 Å) some binding sites on Mn6 and Mn7 are not available to **15** for complexation as they normally may be. This may force the cluster to adopt a different and non-conventional topology as the structural fragments assemble, thus preventing the central **15** from undergoing configurational change. Hence, by understanding of the degree of complementarity between the two ligands, it is possible, to some extent, to exercise control over the cluster composition and geometry.

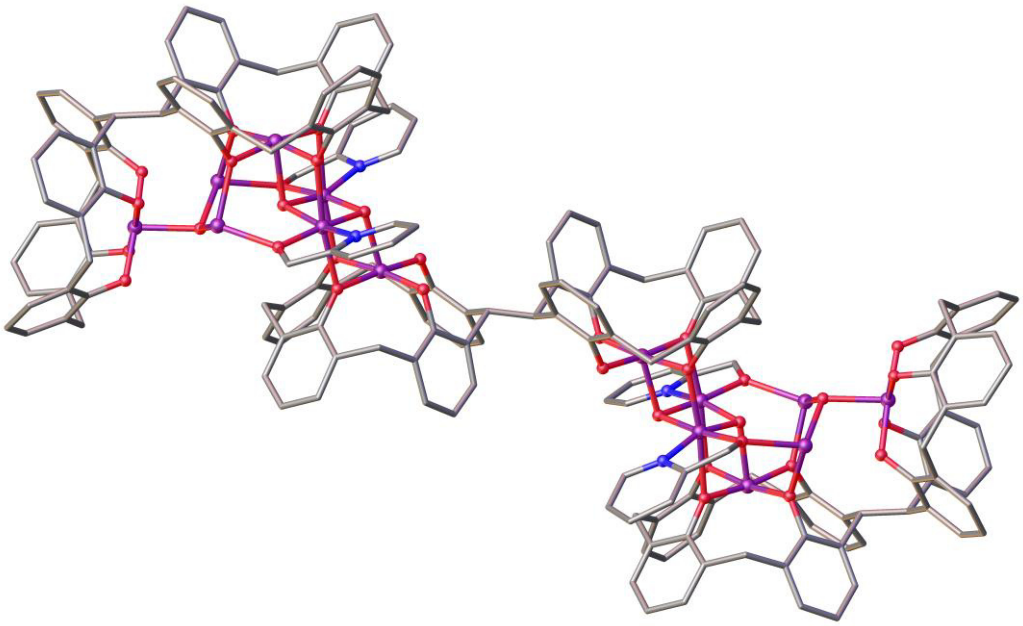

Figure 71. Symmetry-expanded structure of **26** showing the central bridging *syn*-**15** octa-anion (Colour code: Mn – purple; O – red; N – blue; C – grey). ^{t}Bu groups, hydrogen atoms, ligated solvent molecules and solvent of crystallisation omitted for clarity.

The metallic core in **26** can be described as two $[Mn^{III}(TBC[4])]^{-}$ butterflies fused on one edge by the Mn2 cation (Figure 72). The two butterflies are encapsulating Mn4 – Mn7 and Mn2 is located at the apex of a square-based pyramid formed by the 'encapsulated' ions in a similar manner to that observed in the structure of **18** (Figure 72).

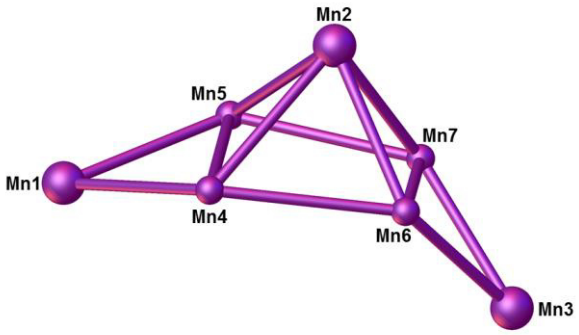

Figure 72. Capping behaviour in **26**. Capping by $[Mn^{III}(TBC[4])]^-$ moieties are shown as large spheres (Colour code: Mn – Purple).

Symmetry expansion of **26** shows a hydrogen bond interaction (CH…O, 2.525 Å) occurring along the *a* axis between the ligated dmf molecule on Mn5 and a dmf of crystallisation that has a CH-π interaction with a neighbouring TBC[4] moiety (CH…centroid, 2.735 Å).[130] The shortest metal-metal intercluster distance measured is 12.410 Å, which is between the Mn1 cations of two neighbouring clusters along the *a* axis (Figure 73).

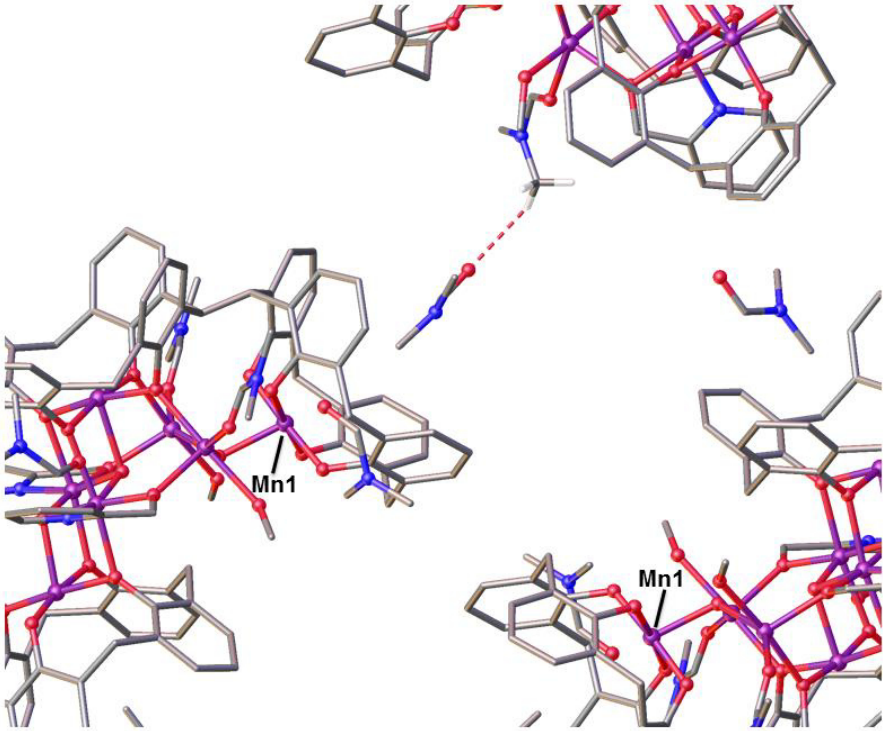

Figure 73. View of the *bc* plane in the extended structure of **26** showing the hydrogen bonding interaction occurring between two dmf molecules, represented as a dashed red line, with the closest ions labelled according to discussion (Colour code: Mn – purple; O – purple; N – blue; C – grey; H – white). ^{t}Bu groups, hydrogen atoms not involved in any interaction, ligated solvent molecules and solvent of crystallisation omitted for clarity.

3.2.3. $[Cu^{II}_{16}(15)_2(MDEA)_4(\mu_4\text{-}NO_3)_2(\mu\text{-}OH)_4(dmf)_3(MeOH)(H_2O)_2](H_615)(dmf)_{16}(H_2O)_4$, 27.

Treatment of **$H_8$15** with copper(II) nitrate trihydrate and H_2MDEA, followed by slow evaporation of the dmf / MeOH mother liquor, afforded dark brown crystals having formula $[Cu^{II}_{16}(\mathbf{15})_2(MDEA)_4(\mu_4\text{-}NO_3)_2(\mu\text{-}OH)_4(dmf)_3(MeOH)(H_2O)_2](\mathbf{H_6}\mathbf{15})(dmf)_{16}(H_2O)_4$, **27** (Figure 75). The crystals were found to be in a triclinic cell and structure solution was carried out in the space group *P*-1.

The ASU comprises half of the reported formula with a total of eight Cu^{II} cations located in binding regions of different nature, showing diversity in the coordination modes observed (Figure 74). Cu1 and Cu2 are in a distorted square planar geometry and are residing in Type I binding sites formed by the phenolic oxygen atoms (Cu1–O range 1.929(6) – 1.959(6) Å and Cu2–O range 1.905(6) – 1.975(6) Å). Cu3 is in a distorted square pyramidal geometry and is located in a Type II binding site. It is bound to two μ-phenolic oxygen atoms of two separate TBC[4] moieties (Cu3–O1, 1.967(7) Å and Cu3–O8, 2.173(7), a disordered ligated solvent molecule which is either methanol or dmf modelled at partial occupancy (Cu3–O18, 1.969(6) Å), an oxygen of a μ-nitrate (Cu3–O12', 1.983(7) Å) and a μ-hydroxide (Cu3–O9, 1.971(6) Å), the latter of which bridges to Cu4 (Cu4–O9, 1.971(4) Å).

Although Cu4 resides in a Type II binding site, as does Cu3, the coordination sphere differs to some extent. As for Cu3, Cu4 is connected to two lower-rim phenolic oxygen atoms (Cu4–O4, 1.953(6) Å and Cu4–O5, 2.044(6) Å), the aforementioned μ-hydroxide, an oxygen atom of a μ- nitrate (Cu4–O11, 2.272(6) Å) and an oxygen of a ligated MDEA molecule (Cu4–O14, 1.928(8) Å). Cu5 and Cu6 (and s.e.) reside in a region that allows connection between a $[Cu^{II}_4(BisTBC[4])]^-$ moiety and its symmetry equivalent, possible *via* O–Cu–O bridges. Cu5 is in a square pyramidal geometry and is bound to two lower-rim phenolic oxygens (Cu5–O7, 1.956(6) Å) and Cu5–O3', 1.983(6) Å) forming the aforementioned O–Cu–O link, a ligated dmf molecule (Cu5 – O20, 1.946(8) Å), an aqua ligand (Cu5–O19, 2.265(7) Å) and a μ-hydroxide (Cu5–O10, 1.957(6) Å), the latter bridging to Cu6 (Cu6–O10, 1.940(6).

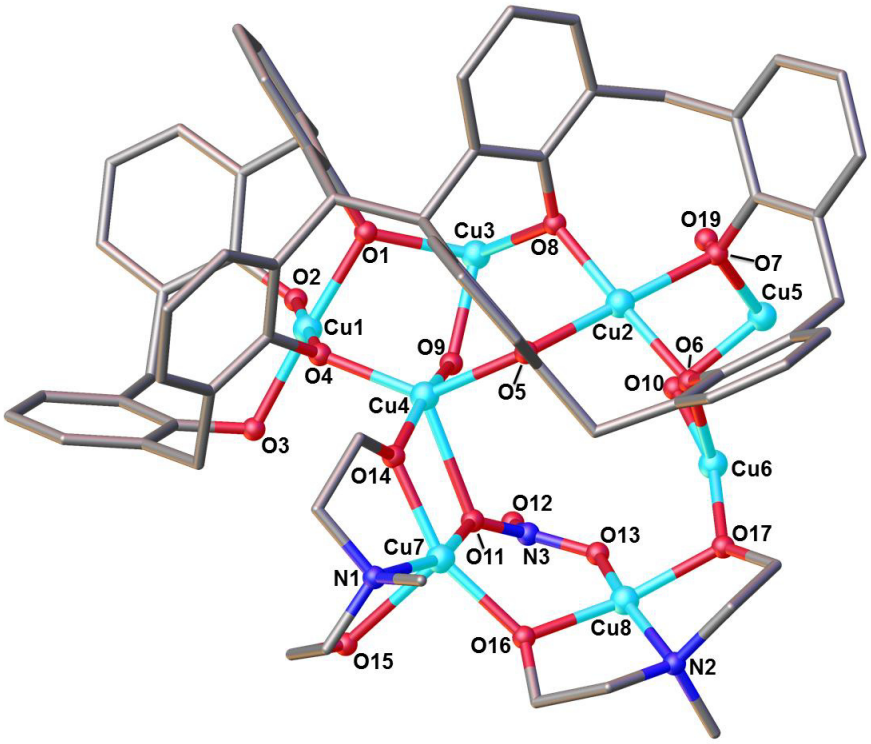

Figure 74. Partial single *X*-ray structure of **27** showing the asymmetric unit of $[Cu^{II}_{16}(\mathbf{15})_2(MDEA)_4(\mu_4\text{-}NO_3)_2(\mu\text{-}OH)_4(dmf)_3(MeOH)(H_2O)_2](\mathbf{H_6 15})(dmf)_{16}(H_2O)_4$ and selected labels according to discussion (Colour code: Cu – light blue; O – red; N – blue; C – grey). ^{t}Bu groups, hydrogen atoms not involved in any interaction, ligated solvent molecules and solvent of crystallisation omitted for clarity.

In contrast to Cu5, Cu6 is in a distorted square planar geometry and its coordination sphere is completed by a O-Cu-O link to the respective s.e. (Cu6–O6, 1.964(6) Å and Cu6–O2', 1.981(6) Å), as well as an oxygen of a ligated MDEA (Cu6–O17, 1.921(6) Å). Cu7 and Cu8 are fully MDEA-bound cations and are located external to the main Cu^{II}_6 polymetallic core (Figures 74 and 75).

Cu7 is in a distorted square pyramidal geometry, bound to an oxygen atom of a μ-nitrate (Cu7–O11, 1.953(7) Å), an oxygen of a ligated MDEA (Cu7–O16, 1.948(7) Å) and a full tridentate MDEA (Cu7–O14, 1.903(8) Å; Cu7–N1, 2.049(10) Å and Cu7–O15, 2.334(8) Å). Cu8 is in a distorted square planar geometry and is bound to an oxygen of a μ-nitrate (Cu8–O13, 1.891(6) Å) and a full tridentate MDEA (Cu8–O16, 1.912(7); Cu8–N2, 1.974(8) Å and Cu8–O17, 1.902(7) Å).

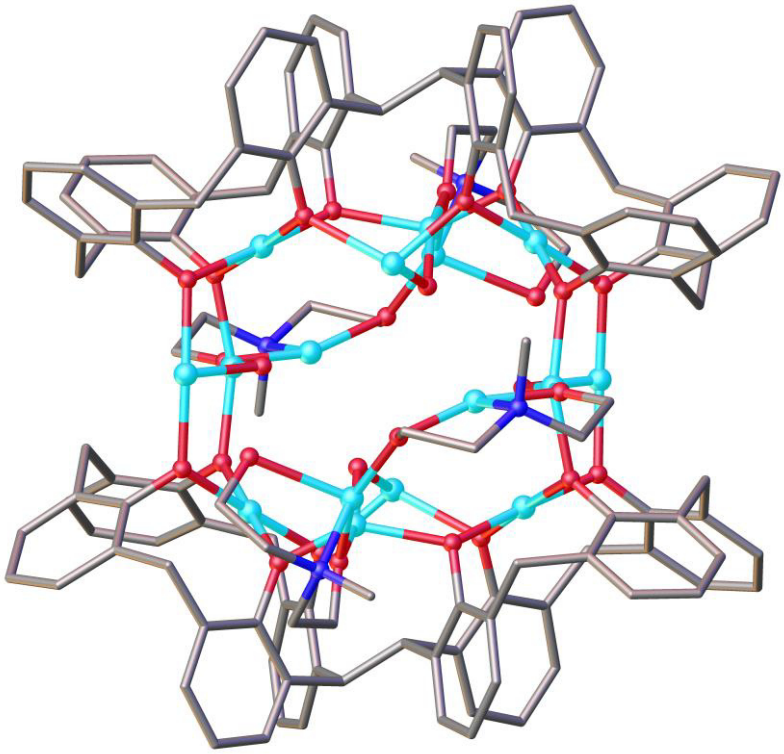

Figure 75. Symmetry-expanded partial *X*-ray structure of **27** showing the **15** / MDEA-supported Cu_{16} polymetallic core (Colour code: Cu – light blue; O – red; N – blue; C – grey). ^{t}Bu groups, hydrogen atoms not involved in any interaction, ligated solvent molecules and solvent of crystallisation omitted for clarity.

The Cu7–O15 bond is noticeably longer when compared to the 1.9 Å average encountered above for the same type of Cu–O bond, when O is an oxygen atom originating from a MDEA ligand. This appears to be due to the neighbouring MDEA molecule that prevents the oxygen atom from binding Cu7 at the binding site occupied by O16. This also reflects on the marked difference in angles between O14–Cu7–O15 (106.6(3)º) and O16–Cu8–O17 (162.6(3)º) and may explain the distorted square pyramidal geometry of Cu7 compared to the distorted square planar Cu8 (Figure 76). A search of the CSD revealed that this is a recurring trend for *N*-DEA-supported Cu^{II} clusters.[131]

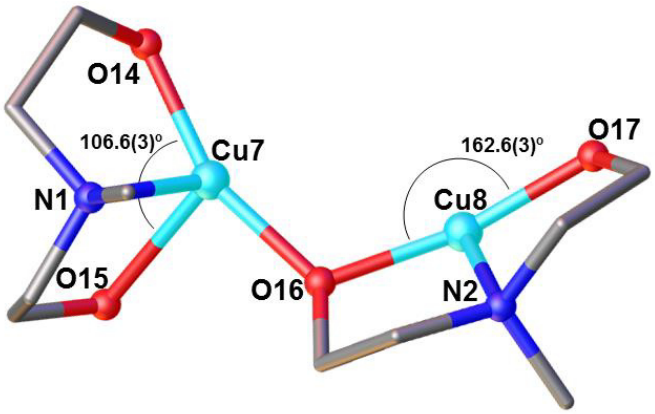

Figure 76. Fragment of the partial single *X*-ray structure of **27**, showing the diverse binding behaviour of MDEA towards the Cu centres (Colour code: Cu – light blue; O – red; N – blue; C – grey).

The entire cluster in Figure 75 is observed upon symmetry expansion around the inversion centre present within assembly. The cluster as a whole therefore comprises two capping $[Cu^{II}_2(\mathbf{15})]^{4-}$ moieties that 'encapsulate' four Cu^{II} ions in the Type II binding regions. These two capping moieties are linked to each other *via* four Cu–O–Cu bridges / links. The eight non-capping Cu^{II} ions are interconnected by μ-hydroxides, and there are four additional MDEA-supported Cu^{II} cations located around the periphery of the polymetallic core. Structure analysis reveals that the polymetallic core has a topology resembling a distorted tetra-capped square prism with four appended MDEA-supported Cu^{II} cations (Cu7 and Cu8 and related s.e.) as shown in Figure 77. The skeleton of the square prism is formed by the cations in the Type II binding site and those linking the two capping $[Cu^{II}_2(\mathbf{15})]^{4-}$ moieties (Cu3, Cu4, Cu5, Cu6 and respective s.e.). The topology, binding modes and assembly motifs displayed in **27** are strictly related to the analogous tetra-capped square prism seen previously in the structure of **10** (Chapter 1, Section 1.5.2, Figure 41) and are both related to the archetypal Cu^{II}-based tri-capped trigonal prism found in compound **2** (Chapter 1, Section 1.5.1, Figure 32). This trend further validates the empirical metal ion binding rules established for both H_4TBC[4] and H_8BisTBC[4], and is another example of how it is possible to obtain novel polymetallic clusters with enhanced nuclearity through the use of complementary and competitive ligands.

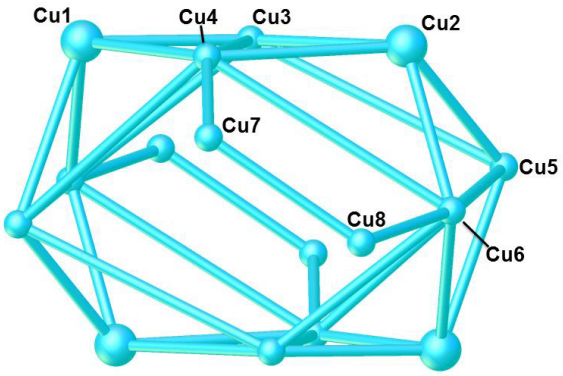

Figure 77. Metallic skeleton in **27** showing the tetra-capped square prismatic topology and four additional MDEA-bound Cu^{II} cations (Cu7, Cu8 and s.e.) around the periphery. Capping by $[Cu^{II}(TBC[4])]^{2-}$ moieties are shown as large spheres (Colour code: Cu – light blue).

Further symmetry expansion of **27** does not show any significant interactions with solvent of crystallisation, or the co-crystallised **$H_6$15** di-anion that provides charge balance to the overall di-cationic cluster. The individual clusters are thus well isolated with respect to each other; symmetry equivalents of **27** and **$H_6$15** alternate throughout the lattice. The shortest metal-metal intercluster distance was measured along the *c* axis and was found to occur between s.e. Cu8 cations bound to the MDEA ligands (12.260 Å, Figure 78).

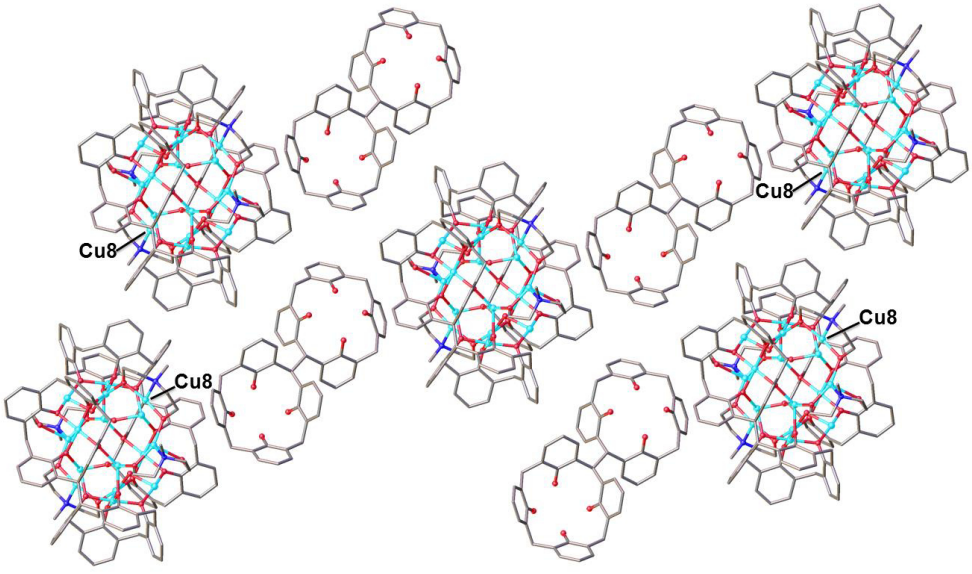

Figure 78. View of the *ab* plane in the extended structure of **27** with closest ions labelled according to discussion (Colour code: Cu – light blue; O – purple; N – blue; C – grey). ^{t}Bu groups, hydrogen atoms, ligated solvent molecules and solvent of crystallisation omitted for clarity.

3.2.4. $[Mn^{III}_3Mn^{II}Ln^{III}_2(15)(MDEA)_2(\mu_3\text{-}OH)(\mu_4\text{-}O)(H_2O)(dmf)_6(Cl)_2](dmf)(H_815)_{0.5}$, 28.

Treatment of **H815** with Mn(II) chloride tetrahydrate, lanthanide(III) chloride hexahydrates and H_2MDEA yielded dark purple crystals of formula $[Mn^{III}_3Mn^{II}Ln^{III}_2(\mathbf{15})(MDEA)_2(\mu_3\text{-}OH)(\mu_4\text{-}O)(H_2O)(dmf)_6(Cl)_2](dmf)(\mathbf{H_815})_{0.5}$, **28** (Ln = Gd, Tb or Dy, **28Gd** being shown in Figure 79) upon vapour diffusion of Et_2O into the dmf / MeOH mother liquor. The crystals were found to be in a triclinic cell and structure solution was carried out in the space group *P*-1. The structure described is the Gd derivative (**28Gd**), although the Tb and Dy analogues (**28Tb** and **28Dy** respectively) proved to be isostructural, as determined by unit cell measurements on single crystals.

The ASU comprises the entire cluster and a TBC[4] moiety that is half of a co-crystallised **H815**. The cluster can be described as a distorted BisTBC[4]-supported $[Mn^{III}_2Mn^{II}Gd^{III}]$ butterfly with the addition of two MDEA-bound cations. The aforementioned butterfly is structurally analogous to those seen in compound **19** (Chapter 2, Section 2.3.2, compare Figures 58 and 80) and the hybrid cluster results thanks to the competing nature of MDEA which, coordinating to a Mn^{II} and a Gd^{III} cation, appears to prevent further expansion of the metallic core to yield topologies similar to that of **19**.

Within the cluster, Mn1 resides in a Type I coordination site defined by the phenolic oxygens O1–O4 (Mn1–O range 1.884(4) – 1.987(4) Å). Mn1 is in the third oxidation state and has distorted octahedral geometry. The Jahn-Teller axis is defined by the O15–Mn1–O9 vector and has marked deviation from linearity (171.84(18)º). The Mn1 coordination sphere is completed by a ligated dmf molecule residing in a TBC[4] cavity (Mn1–O15, 2.252(5) Å) and a μ_3-hydroxide (Mn1–O9, 2.166(4) Å) that bridges to Mn3 and Gd1 (Mn3–O9, 2.176(4) Å and Gd1–O9, 2.321(4) Å). Mn2 has a coordination sphere similar to that of Mn1, as it is also bound in a tetraphenolic Type I binding site (generated by O5–O8, Mn2–O range 1.911(4) – 1.969(4) Å), is in the third oxidation state and has distorted octahedral coordination geometry. Its Jahn-Teller axis is along the O16–Mn2–O10 vector and is more distorted relative to that of Mn1 (168.73(16)º). The Mn2 coordination sphere is completed by a ligated dmf molecule (Mn2–O16, 2.277(4) Å) that resides in a TBC[4] cavity and a μ_4-oxide (Mn2–O10, 2.176(4) Å).

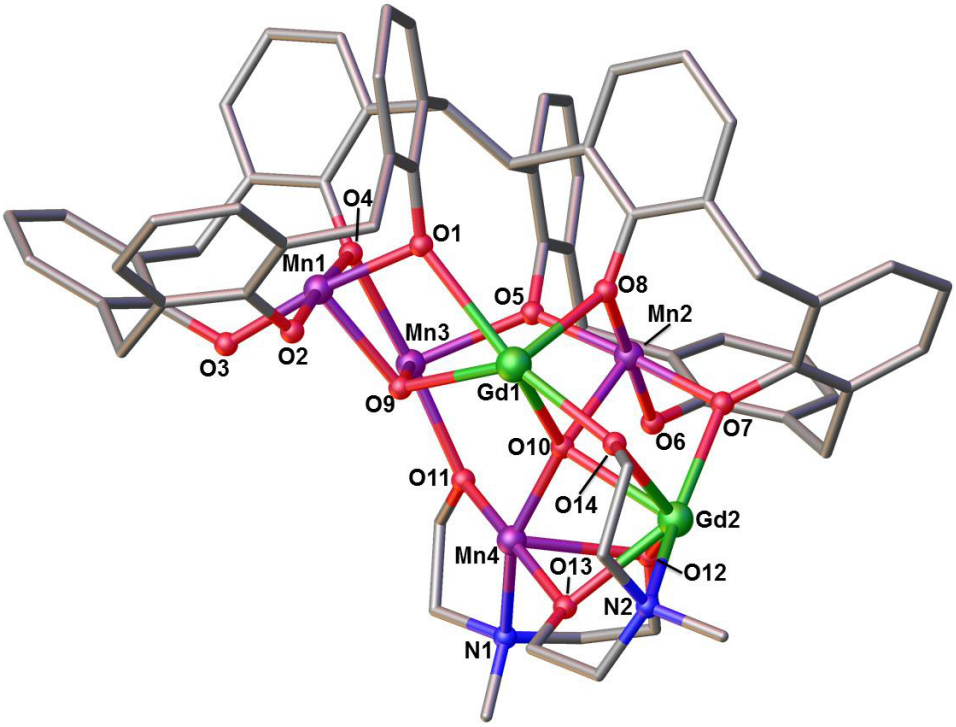

Figure 79. Partial single crystal *X*-ray structure showing the $[Mn^{III}_3Mn^{II}Gd^{III}_2(\mathbf{15})(MDEA)_2(\mu_3\text{-}OH)(\mu_4\text{-}O)(H_2O)(dmf)_6(Cl)_2](dmf)(\mathbf{H_8 15})_{0.5}$ cluster **28Gd**, and selected labels according to discussion (Colour code: Mn – purple; Gd – green; O – red; N – blue; C – grey). ^{t}Bu groups, hydrogen atoms, ligated solvent molecules and solvent of crystallisation omitted for clarity.

This bridging group is situated at the centre of a tetrahedron at the vertices of which are located Mn2, Mn4, Gd1 and Gd2. Mn3 resides in a Type II binding site, is in the second oxidation state and has distorted octahedral geometry. In addition to the aforementioned μ_3-hydroxide, it is also bound to two phenolic oxygen atoms of two separate TBC[4] moieties (Mn3–O4, 2.230(4) Å and Mn3–O5, 2.189(4) Å), a ligated dmf molecule (Mn3–O17, 2.156(5) Å), an aqua ligand (Mn3–O21, 2.315(4) Å) and an oxygen from a MDEA ligand (Mn3–O11, 2.142(4) Å). Gd1 is heptacoordinate, has distorted pentagonal bipyramidal geometry and resides in a Type II binding site in a similar manner to Mn3. Its coordination sphere is completed by two phenolic oxygens (Gd1–O1, 2.499(4) Å and Gd1–O8, 2.320(4) Å), two ligated dmf molecules (Gd1–O18, 2.353(5) Å and Gd1–O19, 2.368(5) Å), an oxygen of an MDEA ligand (Gd1–O14, 2.291(4) Å) and the aforementioned μ_3-hydroxide and μ_4-oxide bridges (Gd1–O10, 2.332(4) Å). The μ_4-oxide is also binding Mn4 (Mn4–O10, 1.902(4) Å), which is hexacoordinate an in a distorted octahedral geometry. It is also bound to an oxygen atom of an MDEA ligand (Mn4–O13 1.938(4) Å), a terminal chloride anion (Mn4–Cl1,

2.557(16) Å) and a tridentate MDEA (Mn4–O11, 1.899(4) Å; Mn4–N1, 2.179(5) Å; Mn4–O12, 2.402(4) Å). Gd2 is octacoordinate, is in a square antiprismatic geometry and is bound to the aforementioned μ_4-oxide (Gd2–O10, 2.415(4) Å), a phenolic oxygen atom (Gd2–O7, 2.360(4) Å), a terminal chloride anion (Gd2–Cl2, 2.737(15) Å), an oxygen atom of an MDEA (Gd2–O12, 2.546(4) Å) and a tridentate MDEA (Gd2–O13, 2.353(4) Å; Gd2–N2, 2.633(5) Å and Gd2–O14, 2.289(4) Å).

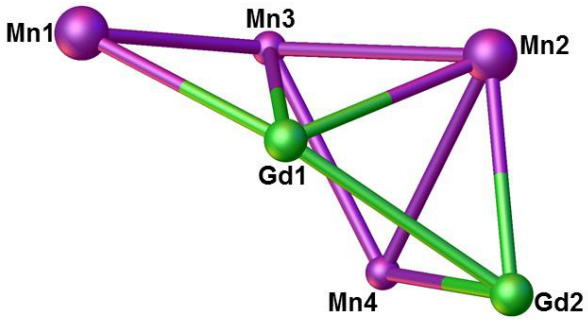

Figure 80. Capping behaviour in the structure of **28Gd**. Capping by $[Mn^{III}(TBC[4])]^-$ moieties are shown as large spheres (Colour code: Mn – Purple, Gd – green).

Capping behaviour is observed from the two $[Mn^{III}(TBC[4])]^-$ units that are 'encapsulating' Mn3, Gd1, Mn4 and Gd2. Moreover, Mn2 is located at the apex of a distorted square pyramid, in a similar fashion as observed in **18** and **19** (Figures 55 and 58). Mn4 and Gd2 are not 'encapsulated' within the BisTBC[4] framework, but are supported by two MDEA ligands (Figure 80).

Upon symmetry expansion it is possible to notice that the cluster packs close to the co-crystallised **$H_8$15**, which is interacting *via* hydrogen bonding between the hydrogen atoms of the methyl groups of the N8 dmf ligated to Gd2 and the lower-rim oxygens of a co-crystallised H_4TBC[4] moiety; this occurs with with an average distance of 2.6 Å. The shortest metal-metal intercluster distance measured can be found along the *c* axis, between the Gd2 cations (9.589 Å, Figure 81).

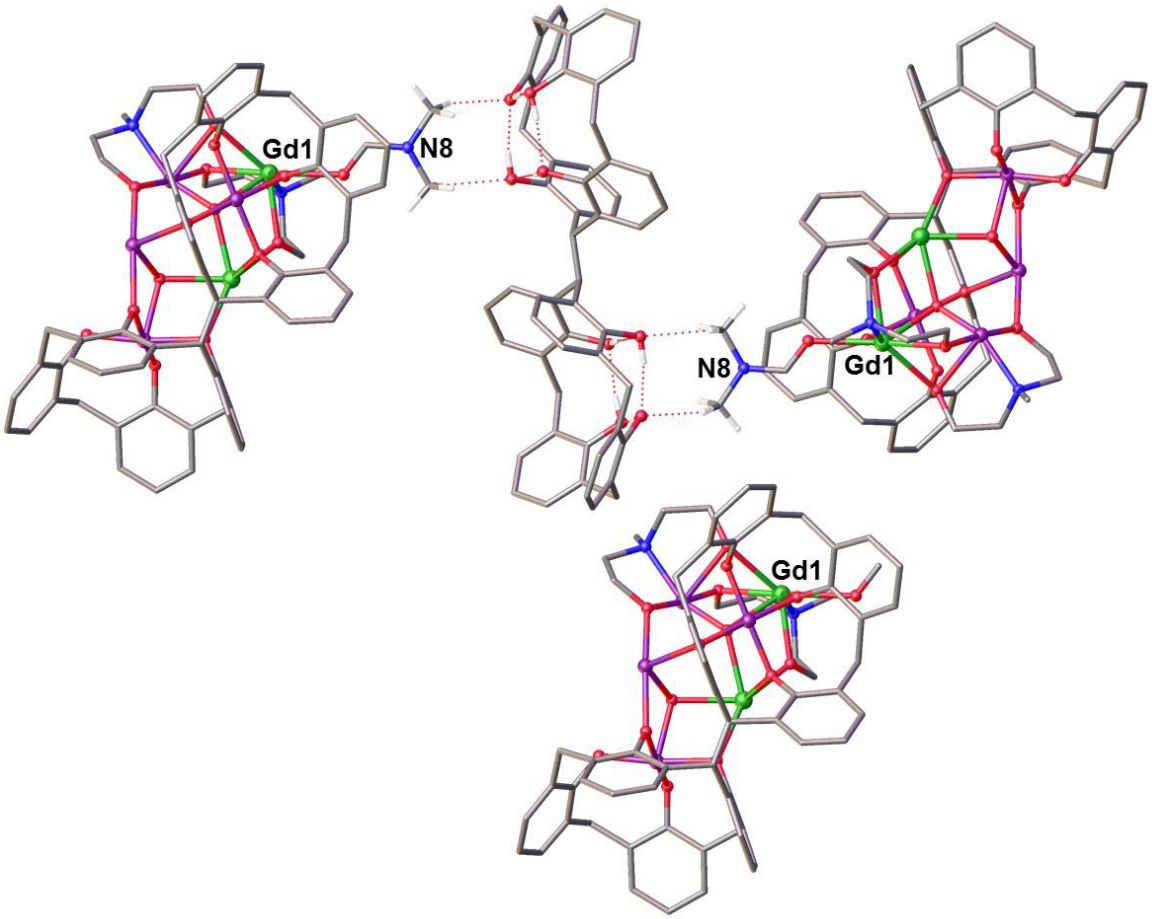

Figure 81. View of the *ab* plane in the extended structure of **28Gd** showing the hydrogen bond interactions occurring between the methyl groups of a ligated dmf molecule and the lower-rim phenolic oxygen atom, represented as dashed red lines, and the closest ions labelled according to discussion (Colour code: Mn – purple; Gd – green; O – purple; N – blue; C – grey; H – white). ^{t}Bu groups, hydrogen atoms not involved in any interaction, ligated solvent molecules and solvent of crystallisation omitted for clarity.

3.2.5. $[Mn^{III}_2Mn^{II}_2(15)(H_1MDEA)(\mu_3\text{-}OMe)(dmf)_2(H_2O)_2](MeCN)_2$, 29.

Reaction of **H$_8$15** with Mn(II) dichloride tetrahydrate and H_2MDEA, followed by vapour diffusion of MeCN in the mother liquor, afforded dark purple crystals of formula $[Mn^{III}_2Mn^{II}_2(\mathbf{15})(H_1MDEA)(\mu_3\text{-}OMe)(dmf)_2(H_2O)_2](MeCN)_2$, **29** (Figure 82). The crystals were found to be in a monoclinic cell and structure solution was carried out in the space group $P2_1/m$.

The ASU is composed of half of the cluster with disorder present in relation to the positions of the solvent ligated on the Mn^{II} centres; this is due to the presence of a plane of symmetry. The disorder was modelled successfully by assigning half-occupancy to the atoms involved and, therefore, only one position will be discussed here. Mn1 is in the third oxidation

state, has distorted square pyramidal geometry and is located in the tetraphenolic cavity of the TBC[4] moiety, bound in a Type I fashion (Mn1–O range 1.898(5) – 1.978(5) Å). Its coordination sphere is completed by an oxygen atom of the MDEA ligand, with an Mn1–O6 distance of 2.095(10) Å.

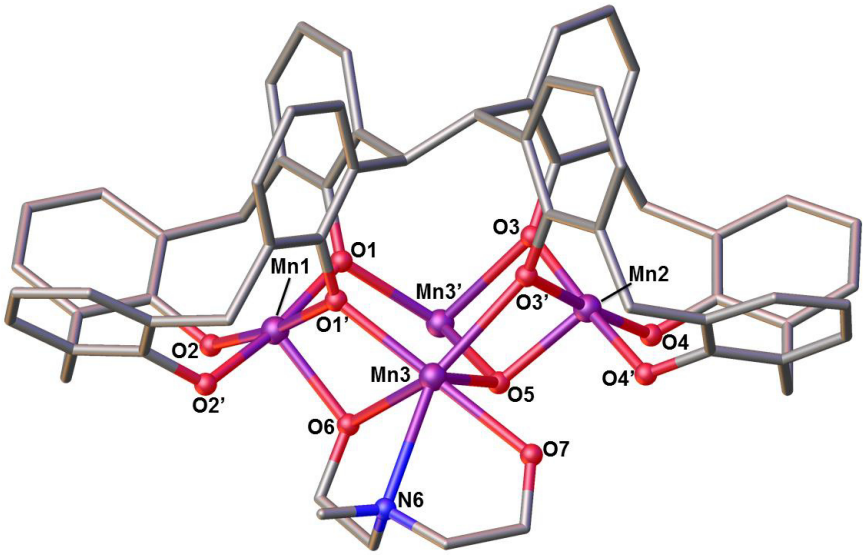

Figure 82. Symmetry-expanded structure of **29** showing the $[Mn^{III}_2Mn^{II}_2(\mathbf{15})(H_1MDEA)(\mu_3\text{-OMe})(dmf)_2(H_2O)_2](MeCN)_2$ cluster (Colour code: Mn – purple; O – red; N – blue; C – grey). ^{t}Bu groups, hydrogen atoms, ligated solvent molecules and solvent of crystallisation omitted for clarity.

Mn2 has analogous oxidation state, geometry and coordination to Mn1, as it is bound in a Type I coordination site (Mn2–O range 1.912(5) – 1.949(5) Å), with the only difference being the coordination to a μ_3-methoxide (Mn2–O5, 2.050(8) Å) which bridges to Mn3 and its s.e. (Mn3/Mn3'–O5, 2.241(5) Å). Mn3 is located in a Type II binding site, is in the second oxidation state and has pentagonal bipyramidal geometry. It is bound to two phenolic oxygen atoms belonging to two separate TBC[4] moieties (Mn3–O1', 2.171(4) Å and Mn3–O3', 2.406(5) Å), a ligated dmf molecule (Mn3–O10, 2.202(5) Å) and a tridentate MDEA (Mn3–O6, 2.349(10) Å; Mn3–N1, 2.534(13) Å and Mn3–O7, 2.234(11) Å). Mn3' has analogous coordination number and it is bound to the aforementioned μ_3-methoxide, two phenolic oxygen atoms (Mn3'–O1, 2.171(4) Å and Mn3'–O3, 2.406(5) Å), a ligated dmf molecule (Mn3'–O10, 2.202(5) Å) and two aqua ligands (Mn3'–O8, 2.251(10) Å and Mn3'–O9, 2.226(11) Å).

The now common capping behaviour is exerted by two $[Mn^{III}(TBC[4])]^-$ moieties that are 'encapsulating' the two Mn^{II} ions in a similar fashion to that seen for **18** (Figure 83).

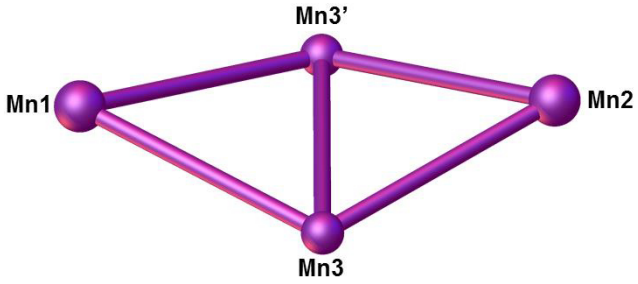

Figure 83. Capping behaviour in the structure of **29**. Capping by $[Mn^{III}(TBC[4])]^-$ moieties are shown as large spheres (Colour code: Mn – Purple).

Further symmetry expansion shows no significant intermolecular interactions within the structure, with the each cluster being well isolated from its neighbour. The shortest metal-metal intercluster distance was measured along the *c* axis, occurring between the Mn3 cations bound to the MDEA ligand (9.102 Å) (Figure 84).

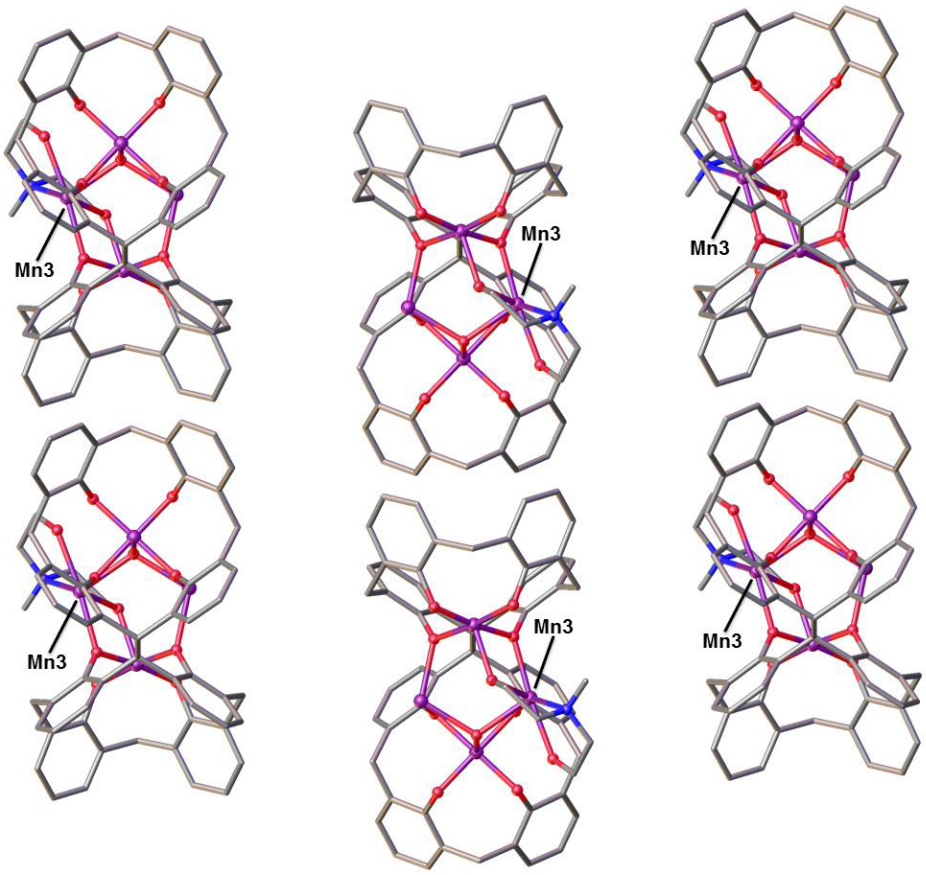

Figure 84. View of the *ab* plane in the extended structure of **29** with closest ions labelled according to discussion (Colour code: Mn – purple; O – purple; N – blue; C – grey). ^{t}Bu groups, hydrogen atoms, ligated solvent molecules and solvent of crystallisation omitted for clarity.

3.2.6. $[Mn^{IV}_2Mn^{III}_{10}Mn^{II}_8(15)_2(DEA)_6(\mu_4\text{-}O)_4(\mu_3\text{-}O)_6(dmf)_{10}(Cl)_6(H_2O)_2](dmf)_2(H_2O)_2$, 30.

Reaction of **H$_8$15** with Mn(II) chloride tetrahydrate and H_3DEA afforded dark purple single crystals of formula $[Mn^{IV}_2Mn^{III}_{10}Mn^{II}_8(\mathbf{15})_2(DEA)_6(\mu_4\text{-}O)_4(\mu_3\text{-}O)_6(dmf)_{10}(Cl)_6(H_2O)_2](dmf)_2(H_2O)_2$, **30** (Figure 86) upon vapour diffusion of Et_2O into the dmf / MeOH solvent mixture. The crystals were found to be in a monoclinic cell and structure solution was carried out in the space group *C2/c*.

The ASU comprises half of the reported formula, with ten mixed-valence Mn cations, two of which reside in the Type I binding sites of **15**. The remaining eight cations propagate horizontally from the BisTBC[4] moiety, forming a polymetallic core supported by DEA molecules, bridging hydroxides and chlorides (Figure 85). Mn1 is located in a Type I binding formed by the phenolic oxygen atoms of one TBC[4] moiety (Mn1–O range, 1.892(4) – 1.967

Å) and it is in the third oxidation state with distorted octahedral geometry. The Jahn-Teller axis is defined by the O8–Mn1–O10 vector that shows substantial deviation from linearity (170.79(15)º). The Mn1 coordination sphere is completed by a ligated dmf molecule residing in the TBC[4] cavity (Mn1–O10, 2.240(4) Å) and a μ_4-oxide (Mn1–O8, 2.141(3) Å) which bridges to Mn3, Mn4 and Mn6 (Mn3–O8, 2.417(4) Å; Mn4–O8, 1.896(3) Å; Mn6–O8, 1.858(4) Å).

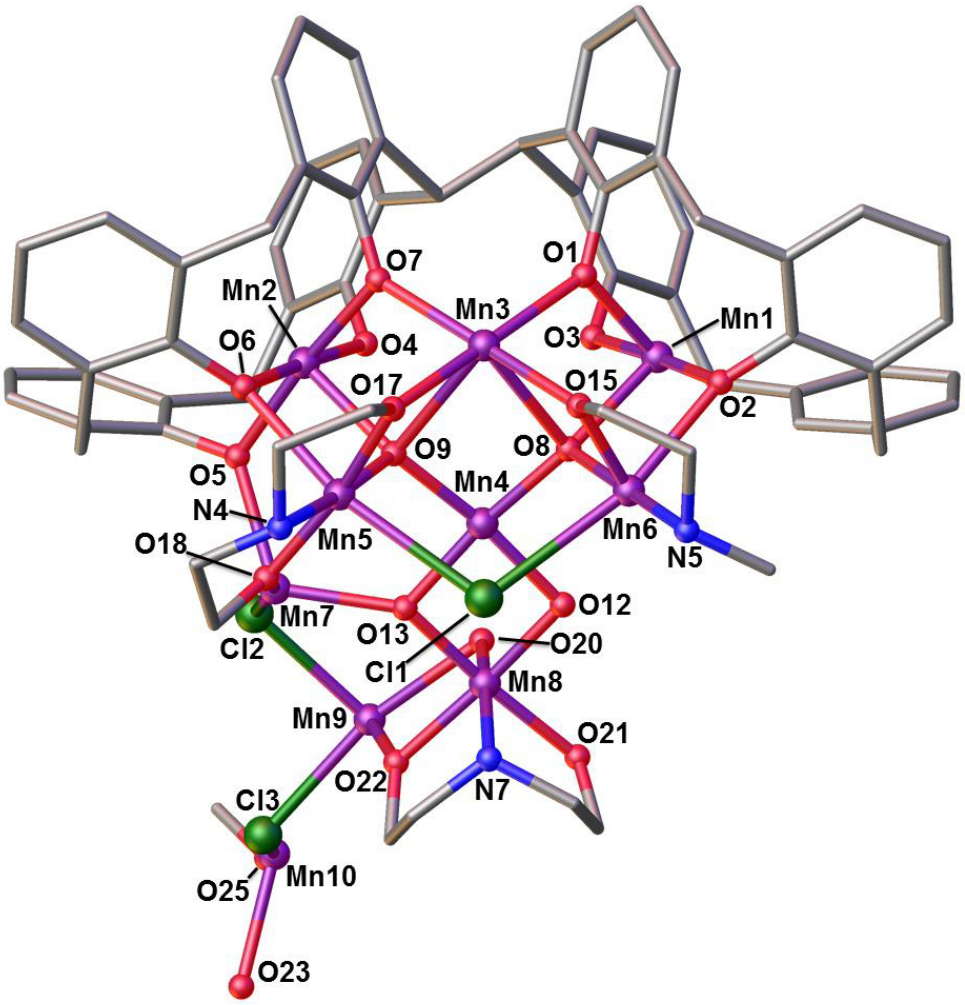

Figure 85. Partial single crystal *X*-ray structure of **30** showing the asymmetric unit in the structure of $[Mn^{IV}_2Mn^{III}_{10}Mn^{II}_8(\mathbf{15})_2(DEA)_6(\mu_4\text{-}O)_4(\mu_3\text{-}O)_6(dmf)_{10}(Cl)_6(H_2O)_2](dmf)_2(H_2O)_2$ and selected labels according to discussion (Colour code: Mn – purple; O – red; N – blue; C – grey; Cl – green). ^{t}Bu groups, hydrogen atoms, ligated solvent molecules and solvent of crystallisation omitted for clarity.

Mn2 has an analogous coordination environment, being bound in a Type I binding site (Mn2–O range 1.893(4) – 1.974(4) Å), to a ligated dmf molecule (Mn2–O11, 2.250(3) Å) and a

μ_4-oxide (Mn2–O9, 2.117(3) Å), the latter of which bridges to Mn3, Mn4 and Mn5 (Mn3–O9, 2.504(4) Å; Mn4–O9, 1.888(3) Å; Mn5–O9, 1.848(4) Å). Mn3 is heptacoordinate and in the second oxidation state and has distorted face-capped octahedral geometry and, in addition to the μ_4-oxides mentioned above, is also bound to two phenolic oxygen atoms belonging to the TBC[4] constituents of the octa-anionic **15** (Mn3–O1, 2.209(3) Å and Mn3–O7, 2.209(3) Å), a ligated dmf molecule (Mn3–O14, 2.200(3) Å) and two oxygens from different DEA ligands (Mn3–O15, 2.180(3) Å and Mn3–O17, 2.168(3) Å). Mn4 is in the third oxidation state, is penta-coordinate in has distorted square pyramidal geometry. The base of the pyramid is formed by the aforementioned O8, O9 and two μ_3-oxides (Mn4–O12, 1.866(3) Å and Mn4–O13, 1.866(3) Å), whilst an oxo bridge is located at the apex of the pyramid (Mn4–O16, 2.284(3) Å). Mn5 is in the third oxidation state, has distorted octahedral geometry and is bound to a μ-phenoxide (Mn5–O6, 2.232(3) Å), the aforementioned μ_4-oxide, a chloride anion (Mn5–Cl1, 2.781(15) Å) that bridges to Mn6 (Mn6–Cl1, 2.827(15) Å) and a tridentate DEA ligand (Mn5–O17, 1.864(3) Å; Mn5–N4, 2.019(4) Å; Mn5–O18, 1.891(4) Å). The distorted Jahn-Teller axis is located along the O6–Mn5–Cl1 vector and significant deviation from linearity is observed (165.27(10)º). A similar coordination environment is found for Mn6, being bound to both the μ_4-oxide and Cl1 mentioned above, a phenolic oxygen (Mn6–O2, 2.297(4) Å) and a ligated DEA (Mn6–O15, 1.868(4) Å; Mn6–N5, 2.022(5) Å; Mn6–O25', 1.897(4) Å). As for Mn5, Mn6 is in the third oxidation state and has distorted octahedral geometry; the Jahn-Teller axis was found along the O2–Mn6–Cl1 vector and significant deviation from linearity was also observed (164.77(11º). Mn7 is in the second oxidation state, is penta-coordinate and has distorted square pyramidal geometry. Mn7 is bound to a phenolic oxygen atom (Mn7–O5, 2.136(4) Å), a μ_3-oxide (Mn7–O13, 2.028(3) Å), an oxygen of a ligated DEA (Mn7–O18, 2.135(4) Å), a ligated dmf molecule (Mn7–O19, 2.136(4) Å) and a μ-Cl (Mn7–Cl2, 2.521(14) Å) that bridges to Mn9.

Mn8, Mn9 and their s.e. ions form a DEA-supported butterfly located at the centre of this large cluster, centrally linking the two Mn_8 moieties together (Figure 85). Mn8 is hexa-coordinate, is in a distorted octahedral geometry and is in the fourth oxidation state. It is bound to three μ_3-oxides (Mn8–O12, 1.820(3) Å; Mn8–O13, 1.828(3) Å; Mn8–O20, 1.917(3) Å) and to a ligated DEA molecule (Mn8–O21, 1.925(4) Å; Mn8–N7, 2.041(4) Å; Mn8–O22, 1.923(3) Å). Mn9 is in the second oxidation state with a distorted octahedral geometry and is bound to two μ_3-oxides (Mn9–O20, 2.239(3) Å and Mn9–O20', 2.254(3) Å), two oxygens from DEA ligands (Mn9–O21', 2.110(4) Å and Mn9–O22, 2.109(4) Å) and two μ-chlorides (Mn9–Cl2, 2.497(14) Å and Mn9–Cl3, 2.492(14) Å) that bridge to Mn7 and Mn10 (Mn7–Cl2 distance

given above, Mn10–Cl3, 2.531(15) Å). Finally, Mn10 is in the second oxidation state, has distorted trigonal bipyramidal geometry, and is bound to the aforementioned μ-chloride, a μ_3-oxide (Mn10–O12', 2.029(3) Å), an oxygen atom of a DEA ligand (Mn10–O25, 2.152(4) Å), a phenolic oxygen (Mn10–O23, 2.122(4) Å) and a ligated dmf molecule (Mn10–O24, 2.126(4) Å).

Symmetry expansion of the ASU affords the entire cluster (Figure 86), which can be visualised as two $Mn^{III}_5Mn^{II}_3$ moieties linked to a central DEA-supported $Mn^{IV}Mn^{II}$ fragment *via* μ-chloride anions. This moiety is displaying coordination motifs typical of this family of ligands (*vide supra*, Figure 65) and is an excellent example in which the nuclearity of BisTBC[4]-supported clusters can be augmented (or greatly increased) with the aid of complementary / competing co-ligands.

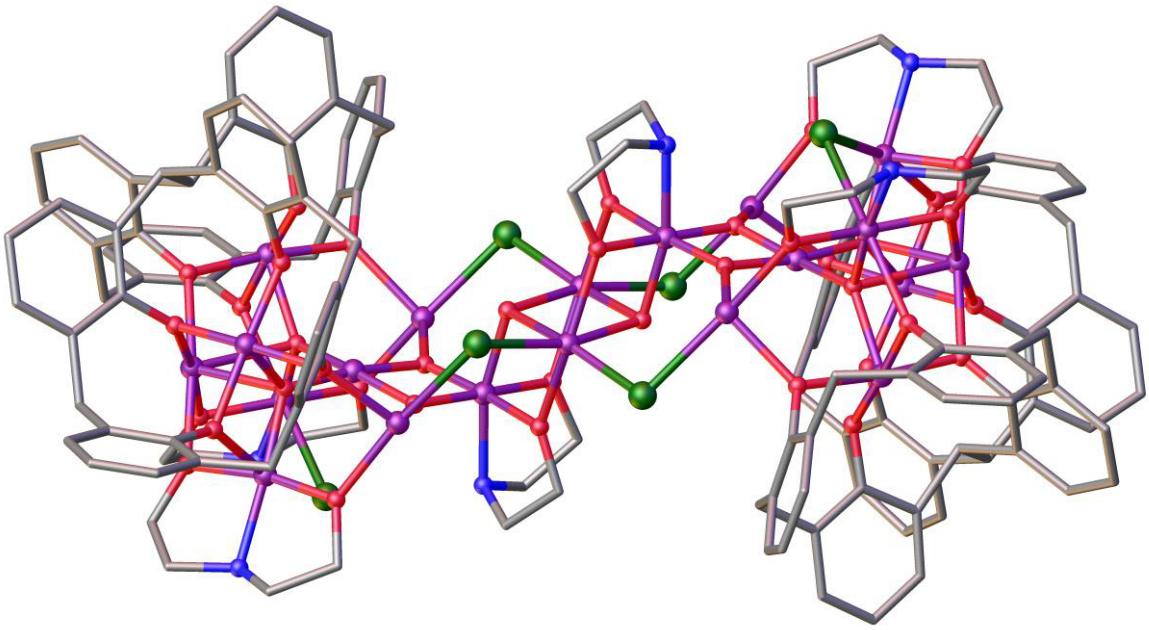

Figure 86. Symmetry-expanded partial *X*-ray structure of **30** (Colour code: Mn – purple; O – red; N – blue; C – grey; Cl – green). ^{t}Bu groups, hydrogen atoms, ligated solvent molecules and solvent of crystallisation omitted for clarity.

The polymetallic core of **30** has a very complex topology (Figure 87), with the presence of several recurring motifs that are typical of both BisTBC[4]- and DEA-supported metal cluster chemistry. Capping behaviour is observed with four $[Mn^{III}(TBC[4])]^-$ moieties (Mn1, Mn2 and s.e.) 'encapsulating' one Mn^{II} cation (Mn3) located in a Type II binding region, whereas the other Type II binding region is unoccpied. This is unprecedented and the reason for this is perhaps due to the presence of two additional DEA-supported Mn^{III} cations (Mn5 and Mn6)

that are creating steric hindrance, preventing that region from being occupied by a metal ion. This reflects also on the tetrahedral geometry of Mn4, which is unusual and unprecedented in BisTBC[4]-supported metal clusters to date.

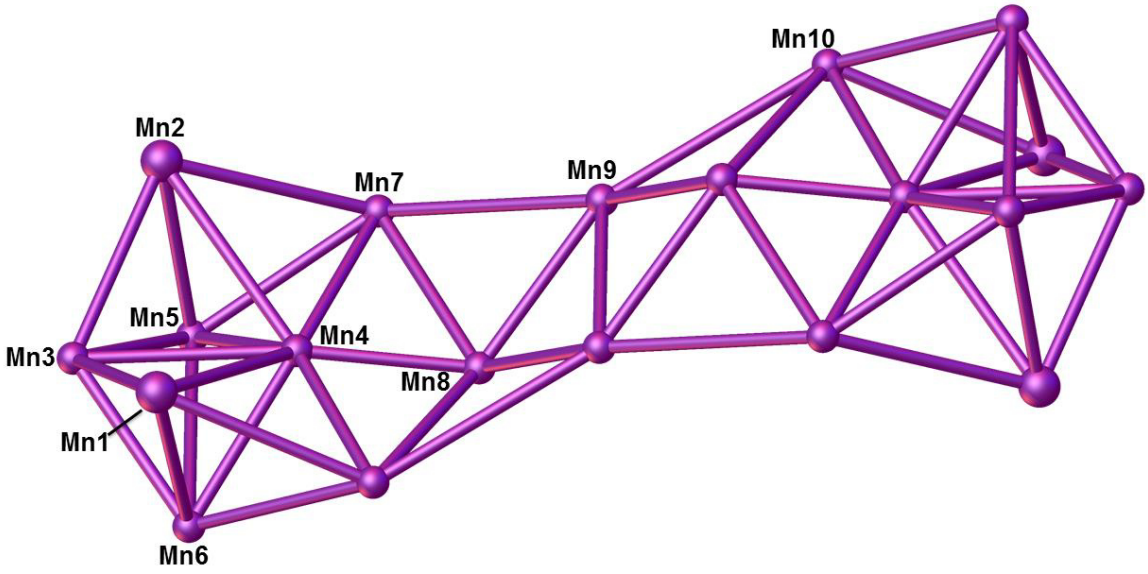

Figure 87. The complex topology of the metallic core found in **30**. Capping by $[Mn^{III}(TBC[4])]^-$ moieties are reported as large spheres (Colour code: Mn – Purple).

No significant intermolecular interactions were located upon further symmetry expansion, due to **30** packing in a well-isolated fashion. The shortest metal-metal intercluster distance (12.081 Å) was observed along the *b* axis, occurring between Mn1 and Mn7 (and relative s.e., Figure 88).

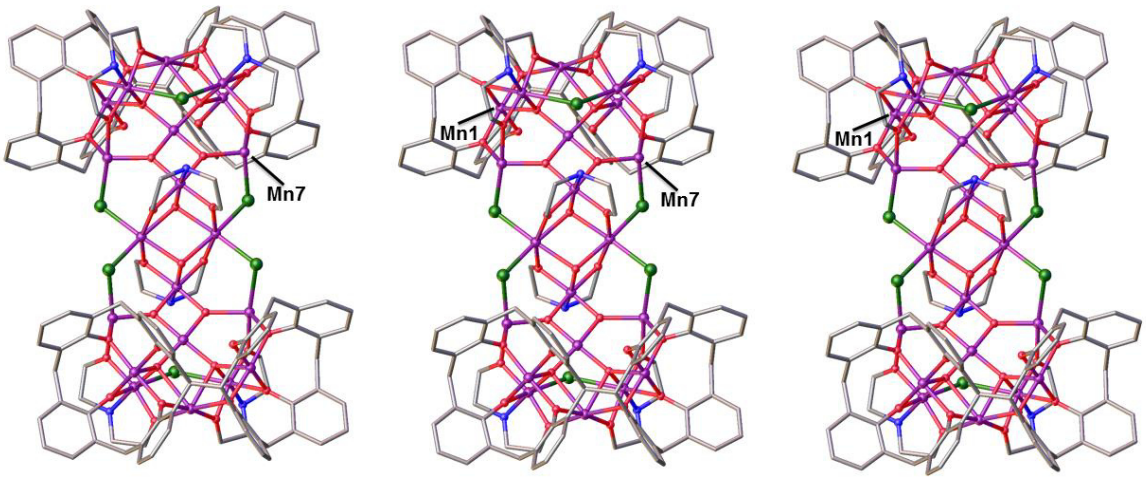

Figure 88. View of the *ac* plane in the extended structure of **30** with the closest ions labelled according to discussion (Colour code: Mn – purple; O – purple; N – blue; C – grey; Cl – green). ^{t}Bu groups, hydrogen atoms, ligated solvent molecules and solvent of crystallisation omitted for clarity.

3.3. Summary.

Given the enormous number of *N*,*O*-ligands-supported clusters present in the literature, a search of the Cambridge Structural Database (CSD) was conducted based on the number of the metal ions present as well as the nature of the polymetallic core presented in this chapter, in order to establish their uniqueness. This investigation revealed 10 hits for [Mn_2Ln] clusters (where Ln = Gd, Dy, and Tb) but none have a topology comparable to **25**. For [Mn_{14}]-containing clusters the CSD returned 17 entries, with none having a topology such as **26**. Clusters containing [Cu^{II}_{16}] were more abundant, with 29 hits, although none possess the tetra-capped square prismatic topology of **27**. A search for [Mn_4Ln_2] clusters (where Ln = Gd, Dy, Tb) returned 14 results, but none has a topology related to that of **28**. For clusters containing [Mn_4] fragments, the CSD returned an astounding 822 hits, one of which is compound **1**, the topology of which is markedly different from that of **29**. Finally, a search for [Mn_{20}]-containing clusters returned 8 results of clusters possessing a disparate topology relative to **30**.

The clusters presented in this chapter strictly relate to those described in Chapter 2, representing a logical synthetic development. It has been shown how it is possible to influence the composition of the polymetallic core using a small selection of *N*,*O*-tripodal ligands (Table 2). The synthesised species are a remarkable example of hybrid clusters, obtained thanks to

the complementarity and competitiveness of H_8BisTBC[4] and the co-ligands investigated. Clusters **25** – **30** still follow the binding rules observed for both H_4TBC[4] and H_8BisTBC[4], with the addition of binding modes and topologies classically linked to the aforementioned *N*,*O*-co-ligands. These results open up an infinite number of possibilities for future work, since hybrid clusters can potentially be synthesised with the addition of any tripodal ligand that varies in size, rigidity and diversity in the binding environment present.

The potential expansion of this chemistry is further evidenced by the fact that, from a selection of just 4 co-ligands, 6 new hybrid new clusters were obtained from 28 combinatorial reactions. The utilisation of a wide range of *N*,*O*-coligands would therefore likely yield many new hybrid clusters, the properties of which can potentially be tuned through an understanding of the magneto-structural correlation and the incorporation of typical (or well understood) metal ion / ligand fragments.

	Mn	Cu	Fe	Mn / Ln	Cu / Ln	Fe / Ln	Ln	Cluster no.
H_2pdm	✗	✗	✗	✓	✗	✗	✗	**25**
Hhmp	✓	✗	✗	✗	✗	✗	✗	**26**
H_2DEA	✓	✗	✗	✗	✗	✗	✗	**30**
H_2MDEA	✓	✓	✗	✓	✗	✗	✗	**29**, **27**, **28**

Table 2. Summary of the attempted reactions of BisTBC[4] with TM, Ln metal ions and co-ligands and relative compound number.

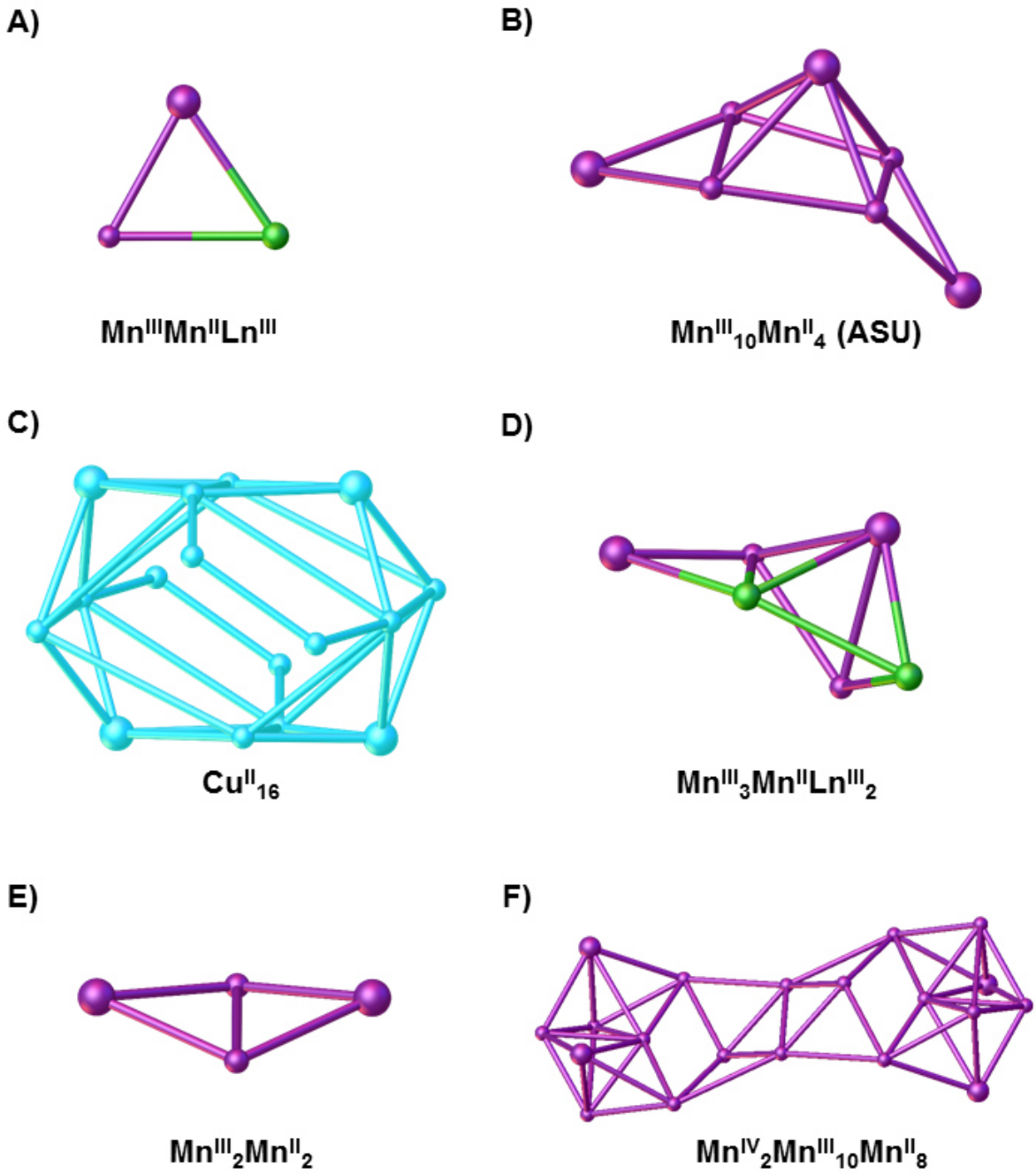

Figure 89. Capping behaviour of compounds **25** – **30**. Capping by $[TM^{III}$ / $Ln^{III}(TBC[4])]^{-}$ moieties are shown as large spheres (Colour code: Mn – purple; Cu – light blue; Ln – green).

3.4. Experimental.

Synthesis of $[Mn^{III}Mn^{II}Ln^{III}(H_3$15$)(pdm)_2(MeOH)_2(dmf)](MeCN)_3(dmf)$, 25.

$Mn^{III}Mn^{II}Gd^{III}$, 25Gd: $H_8$15 (150 mg, 0.116 mmol), $MnCl_2{\cdot}4H_2O$ (23 mg, 0.116 mmol), $GdCl_3{\cdot}6H_2O$ (35 mg, 0.116 mmol) and 2,6-pyridinedimethanol (32.2 mg, 0.232 mmol) were suspended in a 1:1 dmf / MeOH mixture (20 mL) and stirred for 10 minutes. Et_3N (0.15 mL) was added and the resulting purple solution was stirred for additional 2 hours and then filtered. The mother liquor was allowed to slowly diffuse with acetonitrile vapours, affording dark purple crystals suitable for *X*-ray diffraction studies. Elemental Analysis (%) calculated for **25Gd**, $C_{116}H_{151}Mn_2GdN_7O_{16}$ (M = 2166.6): C, 64.31%; H, 7.02%; N, 4.53%. Found: C, 64.24%; H, 6.83%; N, 4.23%. **Yield** 51 mg (20.3 %). **Crystal data for 25Gd:** $C_{116}H_{151}Mn_2GdN_7O_{16}$, M = 2166.6, 0.3 x 0.03 x 0.01 mm^3, tetragonal, space group $P4_12_12$ (no. 92), a = 23.2275(9) Å, c = 44.2459(18) Å, V = 23871.4(19) $Å^3$, Z = 8, Bruker D8 diffractometer equipped with a PHOTON 100 detector, synchrotron radiation, λ = 0.7749 Å, T = 100(15) K, $2\theta_{max}$ = 48.852º, 151662 reflections collected, 15095 unique (R_{int} = 0.0531). Final *GooF* = 1.278, R_1 = 0.0788, wR_2 = 0.2230.

$Mn^{III}Mn^{II}Dy^{III}$, 25Dy: $H_8$15 (150 mg, 0.116 mmol), $MnCl_2{\cdot}4H_2O$ (23 mg, 0.116 mmol), $DyCl_3{\cdot}6H_2O$ (43.6 mg, 0.116 mmol) and 2,6-pyridinedimethanol (32.2 mg, 0.232 mmol) were suspended in a 1:1 dmf / MeOH mixture (20 mL) and stirred for 10 minutes. Et_3N (0.15 mL) was added and the resulting purple solution was stirred for additional 2 hours and then filtered. Elemental Analysis (%) calculated for **25Dy**, $C_{116}H_{151}Mn_2DyN_7O_{16}$ (M = 2171.91): C, 64.15%; H, 7.01%; N, 4.51%. Found: C, 63.92%; H, 6.79%; N, 4.34%. **Yield** 14 mg (5.6 %).

$Mn^{III}Mn^{II}Tb^{III}$, 25Tb: $H_8$15 (150 mg, 0.116 mmol), $MnCl_2{\cdot}4H_2O$ (23 mg, 0.116 mmol), $TbCl_3{\cdot}6H_2O$ (43.2 mg, 0.116 mmol) and 2,6-pyridinedimethanol (32.2 mg, 0.232 mmol) were suspended in a 1:1 dmf / MeOH mixture (20 mL) and stirred for 10 minutes. Et_3N (0.15 mL) was added and the resulting purple solution was stirred for additional 2 hours and then filtered. Elemental Analysis (%) calculated for **25Tb**, $C_{116}H_{151}Mn_2TbN_7O_{16}$ (M = 2168.34): C, 64.26%; H, 7.02%; N, 4.52%. Found: C, 64.05%; H, 6.71%; N, 4.33%. **Yield** 21 mg (8.4 %).

Synthesis of $[Mn^{III}_{10}Mn^{II}_4(15)_3(hmp)_4(\mu_3\text{-}O)_4(\mu_3\text{-}OH)_2(MeOH)_4(dmf)_6](dmf)_4$, 26.

$H_8$15 (500 mg, 0.39 mmol), $MnCl_2{\cdot}4H_2O$ (610 mg, 3.08 mmol) and 2-pyridinemethanol (0.149 mL, 1.54 mmol) were suspended in a 1:1 dmf / MeOH mixture (20 mL) and stirred for 10 minutes. Et_3N (0.6 mL) was added and the resulting purple solution was stirred for additional 2 hours and then filtered. The mother liquor was slowly allowed to diffuse with

petroleum ether vapours, affording dark purple crystals suitable for *X*-ray studies. Elemental Analysis (%) calculated for **26**, $C_{322}H_{418}Mn_{14}N_{14}O_{48}$ (M = 6022.12): C, 64.22%; H, 7%; N, 3.26%. Found: C, 64.12%; H, 6.72%; N, 3.11%. **Yield** 431 mg (18.6 %). **Crystal data for 26:** $C_{322}H_{418}Mn_{14}N_{14}O_{48}$, M = 6022.12, 0.1 x 0.005 x 0.005 mm^3, purple needle, monoclinic, space group *C*2/*c* (no. 15), a = 59.816(8) Å, b = 18.706(2) Å, c = 30.329(4) Å, β = 104.498(3)°, V = 32856(7) $Å^3$, Z = 4, Bruker X8 Apex II CCD Diffractometer, MoKα radiation (λ = 0.71073 Å), T = 100(15) K, $2\theta_{max}$ = 37.904º, 33347 reflections collected, 12916 unique (R_{int} = 0.1430). Final *GooF* = 0.927, R_1 = 0.0990, wR_2 = 0.2779.

Synthesis of $[Cu^{II}_{16}(15)_2(MDEA)_4(\mu_4\text{-}NO3)_2(\mu\text{-}OH)_4(dmf)_3(MeOH)(H_2O)_2](H_615)(dmf)_{16}(H_2O)_4$, 27.

H_815 (150 mg, 0.115 mmol), $Cu(NO_3)_2{\cdot}3H_2O$ (168 mg, 0.69 mmol) and *N*-methyldiethanolamine (0.013 mL, 0.115 mmol) were suspended in a 1:1: dmf / MeOH mixture (20 mL) and stirred for 10 minutes. Et_3N (0.15 mL) was added and the resulting brown solution was stirred for additional 2 hours and then filtered. The mother liquor was slowly allowed to evaporate, affording dark brown crystals suitable for *X*-ray studies. Elemental Analysis (%) calculated for **27**, $C_{342}H_{509}Cu_{16}N_{25}O_{68}$ (M = 7075.73): C, 58.05%; H, 7.25%; N, 4.95%. Found: C, 57.82%; H, 6.93%; N, 4.69%. **Yield** 61 mg (7.4 %). **Crystal data for 27:** $C_{342}H_{509}Cu_{16}N_{25}O_{68}$, M = 7075.73, 0.15 x 0.2 x 0.02 mm^3, black rod, triclinic, space group *P*-1 (no. 92), a = 21.4369(9) Å, b = 21.9078(9) Å, c = 22.0660(9) Å, α = 105.596(3)º, β = 111.468(2)º, γ = 95.527(3)º, V = 9067.1(7) $Å^3$, Z = 1, Bruker D8 diffractometer equipped with a PHOTON 100 detector, synchrotron radiation, λ = 0.7749 Å, T = 100(15) K, $2\theta_{max}$ = 47.78º, 56658 reflections collected, 21581 unique (R_{int} = 0.0704). Final *GooF* = 1.062, R_1 = 0.0880, wR_2 = 0.2748.

Synthesis of $[Mn^{III}_3Mn^{II}Ln^{III}_2(15)(MDEA)_2(\mu_3\text{-}OH)(\mu_4\text{-}O)(H_2O)(dmf)_6(Cl)_2](dmf)(H_815)_{0.5}$, 28.

$Mn^{III}_3Mn^{II}Gd^{III}_2$, 28Gd: H_815 (100 mg, 0.077 mmol), $MnCl_2{\cdot}4H_2O$ (91.6 mg, 0.46 mmol), $GdCl_3{\cdot}6H_2O$ (81.4 mg, 0.31 mmol) and *N*-methyldiethanolamine (70.9 µL, 0.62 mmol) were suspended in a 1:1 dmf / MeOH mixture (20 mL) and stirred for 10 minutes. Et_3N (0.2 mL) was added and the resulting purple solution was stirred for additional 2 hours and then filtered. The mother liquor was allowed to slowly diffuse with diethyl ether vapours, affording dark purple crystals suitable for *X*-ray diffraction studies. Elemental Analysis (%) calculated for **28Gd**, $C_{163}H_{231}Mn_4Gd_2N_7O_{26}Cl_2$ (M = 3309.85): C, 59.15%; H, 7.03%; N, 2.96%. Found: C,

58.83%; H, 6.72%; N, 2.89%. **Yield** 42 mg (16.5 %). **Crystal data for 28Gd:** $C_{163}H_{231}Mn_4Gd_2N_7O_{26}Cl_2$, M = 3309.85, 0.1 x 0.01 x 0.02 mm^3, purple lath, triclinic, space group *P*-1 (no. 2), *a* = 21.3197(12) Å, *b* = 22.0763(12) Å, *c* = 27.1434(14) Å, α = 75.597(3)°, β = 79.680(3)°, γ = 61.784(3)°, *V* = 10875(11) Å^3, *Z* = 2, Bruker D8 diffractometer equipped with a PHOTON 100 detector, synchrotron radiation, λ = 0.7749 Å, *T* = 100(15) K, $2\theta_{max}$ = 54.558º, 114880 reflections collected, 36275 unique (R_{int} = 0.0610). Final *GooF* = 1.047, R_1 = 0.0690, wR_2 = 0.2054.

$Mn^{III}_3Mn^{II}Dy^{III}_2$, 28Dy: H8 15 (200 mg, 0.154 mmol), $MnCl_2 \cdot 4H_2O$ (183 mg, 0.96 mmol), $DyCl_3 \cdot 6H_2O$ (233 mg, 0.62 mmol) and *N*-methyldiethanolamine (0.14 mL, 1.23 mmol) were suspended in a 1:1 dmf / MeOH mixture (20 mL) and stirred for 10 minutes. Et_3N (0.2 mL) was added and the resulting purple solution was stirred for additional 2 hours and then filtered. Elemental Analysis (%) calculated for **28Dy**, $C_{163}H_{231}Mn_4Dy_2N_7O_{26}Cl_2$ (M = 3320.35): C, 58.96%; H, 7.01%; N, 2.95%. Found: C, 58.53%; H, 6.85%; N, 2.63%. **Yield** 69 mg (13.5 %).

$Mn^{III}_3Mn^{II}Tb^{III}_2$, 28Tb: H8 15 (200 mg, 0.154 mmol), $MnCl_2 \cdot 4H_2O$ (183 mg, 0.96 mmol), $TbCl_3 \cdot 6H_2O$ (231 mg, 0.62 mmol) and *N*-methyldiethanolamine (0.14 mL, 1.23 mmol) were suspended in a 1:1 dmf / MeOH mixture (20 mL) and stirred for 10 minutes. Et_3N (0.2 mL) was added and the resulting purple solution was stirred for additional 2 hours and then filtered. Elemental Analysis (%) calculated for **28Tb**, $C_{163}H_{231}Mn_4Tb_2N_7O_{26}Cl_2$ (M = 3313.2): C, 59.09%; H, 7.03%; N, 2.96%. Found: C, 58.82%; H, 6.74%; N, 2.52%. **Yield** 81 mg (15.9 %).

Synthesis of $[Mn^{III}_2Mn^{II}_2$(15)(H1MDEA)(μ3-OMe)(dmf)2(H2O)2](MeCN)2, 29.

H8 15 (500 mg, 0.39 mmol), $MnCl_2 \cdot 4H_2O$ (76.3 mg, 0.39 mmol) and *N*-methyldiethanolamine (0.27 mL, 2.31 mmol) were suspended in a 1:1: dmf / MeOH mixture (20 mL) and stirred for 10 minutes. Et_3N (0.6 mL) was added and the resulting purple solution was stirred for additional 2 hours and then filtered. The mother liquor was slowly allowed to diffuse with acetonitrile, affording dark purple crystals suitable for *X*-ray studies.

Elemental Analysis (%) calculated for **29**, $C_{108}H_{147}Mn_4N_7O_{15}$ (M = 2003.17): C, 64.76%; H, 7.4%; N, 4.89%. Found: C, 64.49%; H, 7.13%; N, 4.56%. **Yield** 98 mg (12.7 %). **Crystal data for 29:** $C_{108}H_{147}Mn_4N_7O_{15}$, M = 2003.17, 0.1 x 0.05 x 0.01 mm^3, purple plate, monoclinic, space group $P2_1/m$ (no. 11), *a* = 13.8645(6) Å, *b* = 23.1636(9) Å, *c* = 17.4875(7) Å, β = 107.315(2)°, *V* = 5361.6(4) Å^3, *Z* = 2, Bruker D8 diffractometer equipped with a PHOTON 100 detector, synchrotron radiation, λ = 0.7749 Å, *T* = 100(15) K, $2\theta_{max}$ =

51.032º, 7904 reflections collected, 7904 unique (R_{int} = 0.0375). Final *GooF* = 1.046, R_1 = 0.0864, wR_2 = 0.2388.

Synthesis of $[Mn^{IV}_2Mn^{III}_{10}Mn^{II}_8(15)_2(DEA)_6(\mu_4\text{-}O)_4(\mu_3\text{-}O)_6(dmf)_{10}(Cl)_6(H_2O)_2](dmf)_2(H_2O)_2$, 30.

$H_8$15 (500 mg, 0.39 mmol), $MnCl_2 \cdot 4H_2O$ (610 mg, 3.08 mmol) and diethanolamine (0.148 mL, 1.54 mmol) were suspended in a 1:1 dmf / MeOH mixture (20 mL) and stirred for 10 minutes. Et_3N (0.6 mL) was added and the resulting purple solution was stirred for additional 2 hours and then filtered. The mother liquor was slowly allowed to diffuse with diethyl ether, affording dark purple crystals suitable for *X*-ray studies. Elemental Analysis (%) calculated for **30**, $C_{236}H_{348}Mn_{20}N_{18}O_{56}Cl_6$ (M = 5644.97): C, 50.22%; H, 6.21%; N, 4.47%. Found: C, 49.87%; H, 5.89%; N, 4.16%. **Yield** 404 mg (18.5 %). **Crystal data for 30:** $C_{236}H_{348}Mn_{20}N_{18}O_{56}Cl_6$, M = 5644.97, 0.08 x 0.07 x 0.03 mm^3, dark orange block, monoclinic, space group C2/c (no. 15), a = 18.3953(7) Å, b = 45.6912(18) Å, c = 40.7908(16) Å, β = 99.212(2)°, V = 33843(2) $Å^3$, Z = 4, Bruker D8 diffractometer equipped with a PHOTON 100 detector, synchrotron radiation, λ = 0.7749 Å, T = 100(15) K, $2\theta_{max}$ = 58.238º, 165158 reflections collected, 34903 unique (R_{int} = 0.0608). Final *GooF* = 1.638 R_1 = 0.0824, wR_2 = 0.2435.

3.5. References.

126. Yoo, J.; Yamaguchi, A.; Nakano, M.; Krzystek, J.; Streib, W., E.; Brunel, L., -C.; Ishimoto, H.; Christou, G.; Hendrickson, D., N.; *Inorg. Chem.*, **2001**, *41*, 4604 – 4616.

127. Brechin, E., K.; Yoo, J.; Nakano, M.; Huffman, J., C.; Hendrickson, D., N.; Christou, G.; *Chem. Comm.*, **1999**, 789 – 784.

128. Saalfrank, R., W.; Nakajima, T.; Mooren, N.; Scheurer, A.; Maid, H.; Hampel, F.; Trieflinger, C.; Daub, J.; *Euro. J. Inorg. Chem.*, **2005**, 1149 – 1153.

129. Taylor, S, M.; McIntosh, R., D.; Piligkos, S.; Dalgarno, S., J.; Brechin, E., K.; *Chem. Comm.*, **2012**, *48*, 11190 – 11192.

130. Janiak, C.; *J. Chem. Soc., Dalton Trans*; **2000**, 3885 – 3896.

131. Nesterov, D., S.; Kokozay, V., N.; Jezierska, J.; Pavlyuk, O., V.; Boca, R.; Pombeiro, A., J., L.; *Inorg. Chem.*, **2011**, *50*, 4401 – 4411 and Krabbes, I.; Seichter, W.; Breuning, T.; Otschik, P.; Gloe, K.; *Z. Anorg. Allg. Chem.*, **1999**, *652*, 1562 – 1565.

Chapter 4: Alkyl chain-tethered biscalix[4]arenes

Chapter 4 focusses on the synthesis of a family of biscalix[4]arenes in which the two H_4TBC[4] moieties are spaced by flexible alkyl chains. The synthesis and characterisation of these ligands will be presented, as it encompasses a modification on the synthetic procedure outlined in Chapter 2, Section 2.1. The coordination chemistry of the alkyl chain-tethered ligands is also described, highlighting analogies with the structural chemistry of TBC[4]-supported metal clusters presented in Chapter 1.

4.1. Synthesis of alkyl chain-tethered biscalix[4]arenes.

A viable route to controlling and / or directing cluster composition and nuclearity with biscalix[4]arenes is to link TBC[4] moieties with organic spacers of differing chemical nature, size and shape. Preliminary cluster formation investigations with H_4TBC[4] functionalised at one methylene bridge with small alkyl groups (-Me and -Et) afforded $Mn^{III}_2Mn^{II}_2$ butterfly-like clusters (Compounds **31** and **32**, Figure 90) that have a topology equivalent to those formed when employing **12** as a ligand (Chapter 1, Section 1.5.2, Figure 31).

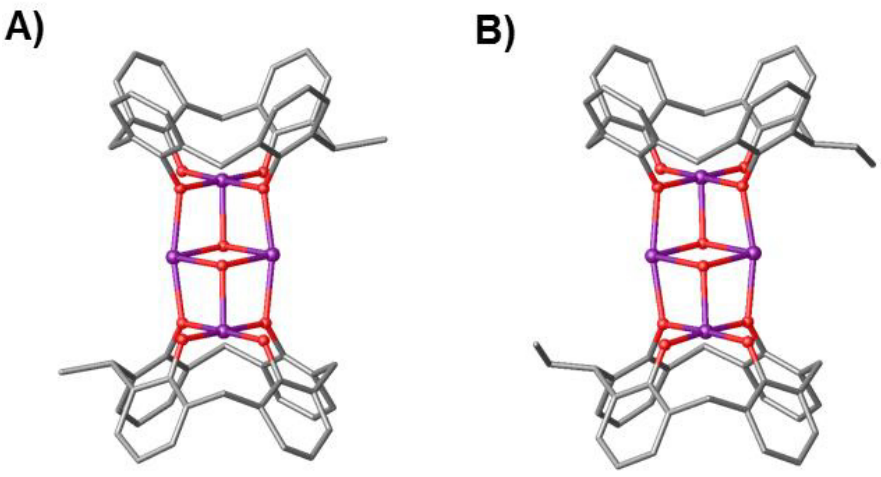

Figure 90. Partial single crystal *X*-crystal structures of compound **31** (A) and **32** (B) (Colour code: Mn – purple; O – red; C – grey). ^{t}Bu groups, hydrogen atoms, ligated solvent molecules and solvent of crystallisation omitted for clarity.

This result suggested that the presence of substituents at the methylene bridge has little effect on the coordination behaviour of the lower-rim oxygens. Therefore, it was pertinent to synthesise alkyl chain-tethered biscalix[4]arenes and explore their coordination chemistry in order to understand the effects of alkyl chain length on cluster formation. The synthesis of these new biscalix[4]arenes was accomplished via the same synthetic protocol discussed in Section 2.1. Reaction of **13** with *n*-BuLi leads to the formation of a methylene bridge lithiated species (**13-Li**) which is non-isolable and, upon addition of an α,ω-dibromoalkane, undergoes substitution, affording the targeted products **33** (Figure 91). In this case the electrophiles chosen to link the two TBC[4] moieties are a series of α,ω-dibromoalkanes, with an alkyl chain ranging from propyl to decyl in length. In order to maximise the yield of alkyl chain-tethered biscalix[4]arenes obtained over possible ω-bromoalkyl-TBC[4] side-products, it is necessary to operate under pseudo high-dilution conditions, by dropwise addition of a dry THF solution of the chosen electrophile.

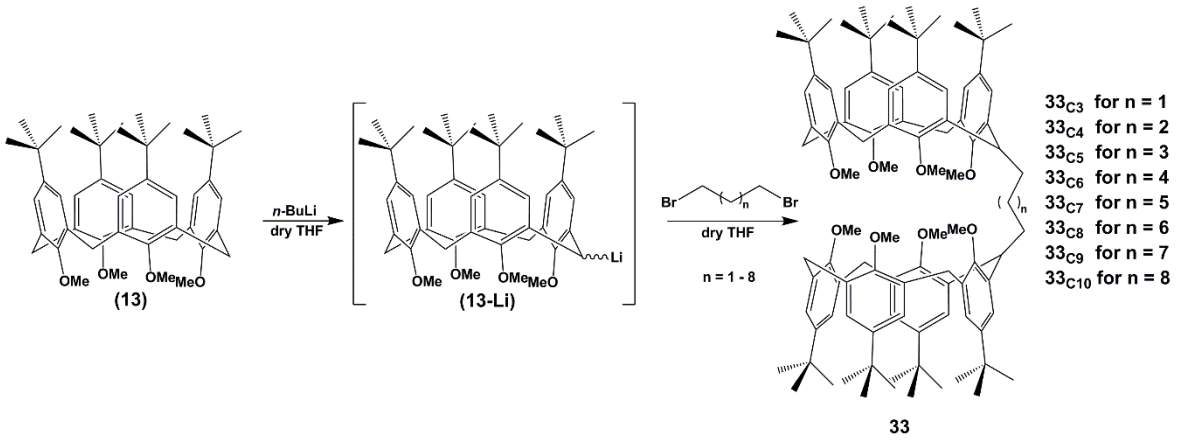

Figure 91. Synthesis of alkyl chain-tethered biscalix[4]arenes **33$_{C3}$** – **33$_{C10}$**.

As already discussed for **14**, the inherent fluxionality of these systems (due to the presence of lower-rim OMe groups) produces uninterpretable ^{1}H NMR spectra as a result of a fast dynamic interconversion between all possible conformations. Demethylation reactions analogous to those used to isolate **15** were carried out on compounds **33$_{C3-C10}$**. Heating dmf solutions of **33$_{C3-C10}$** at reflux for 48 hours in the presence of cyclohexyl iodide afforded the demethylated alkyl chain-tethered biscalix[4]arenes **H$_8$34$_{C3-C10}$** (Figure 92). Compounds **H$_8$34$_{C3-C10}$** were checked for purity by standard TLC ($CHCl_3$ / Hex 1:1) as they may contain small quantities of **12**, resulting from the previous synthetic step not being 100% efficient. Employing the aforementioned solvent system, it was noticed that **12** has a larger R_f value

than compounds **H834C3-C10**, therefore, if required, purification was carried out by column chromatography ($CHCl_3$ / Hex 1:1 → EtOAc).

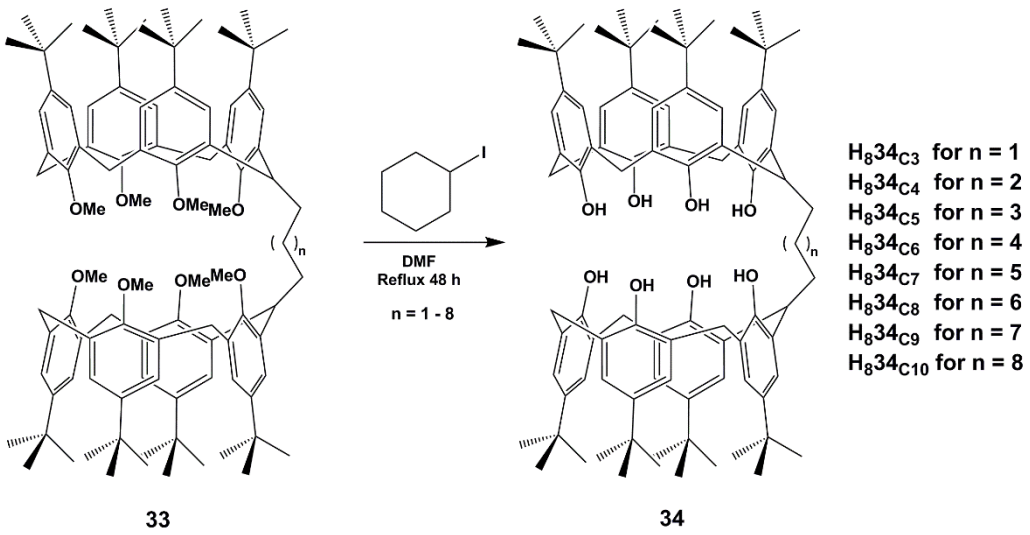

Figure 92. Demethylation reaction on **33C3-C10** to afford compounds **H834C3-C10**.

^{1}H NMR spectra confirmed the successful synthesis of all target compounds. Given the similar nature of compounds **H834C3-C10**, only a general ^{1}H NMR description will be provided. The eight -OH calix[4]arene lower-rim protons produce a sharp singlet at around 10.25 ppm which is also useful to estimate the purity of the sample, due to a different chemical shift of the phenolic protons of **12**. The aromatic protons of the macrocycle generate the multiplet between 7.1 ppm and 6.9 ppm, whereas the methine proton on the substituted methylene bridge linking the two calix[4]arenes gives rise to triplet at 4.47 - 4.40 ppm with a ^{3}J coupling constant of 8Hz. The protons located on the three unsubstituted methylene bridges give two multiplets between 4.29 - 4.17 ppm and 3.51 - 3.41 ppm. Moving to higher field, the singlet at 2.16 ppm is given by the coupling of the methylene protons on the alkyl chain adjacent methine proton on the TBC[4] macrocycles, whereas the rest of the alkyl chain protons resonate at circa 1.5 ppm. The ^{t}Bu groups on the upper-rim generate two distinct singlets at 1.23 - 1.21 ppm due to lower symmetry present as a result of substitution at the methylene bridge. Although products **H834C3-C10** were fully characterised through standard techniques, it was possible to isolate single crystals of suitable diffraction quality in one case, this being the MeCN solvate of compound **H834C3** (Figure 93). The ASU comprises one molecule of **H834C3** with four MeCN of crystallisation, two of which reside in the TBC[4] cavities, forming CH-π interactions with the aromatic rings. As expected, and as was the case for compounds **31** and **32** shown in Figure 88, the presence of the methylene

bridge tether in **H8340C3** does not interfere with the TBC[4] moieties adopting a cone conformation.

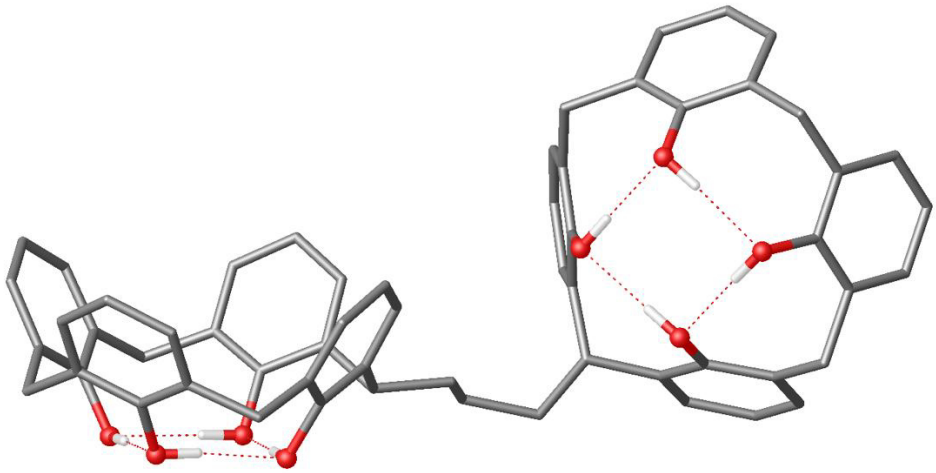

Figure 93. Partial single crystal *X*-ray structure of **H8340C3** (Colour code: C – grey, O – red, H – white). ^{t}Bu groups, hydrogen atoms not involved in hydrogen bonds, ligated solvent molecules and solvent of crystallisation omitted for clarity.

4.2. Alkyl chain biscalix[4]arene-supported metal clusters.

Exploratory coordination chemistry of compounds **H8340C3-C10** was carried out according to the general procedure outlined in Chapter 2, Section 2.2. From these studies it was possible to isolate four new polynuclear clusters. Three of these were obtained by employing compounds **H8340C8**, **H8340C9** and **H8340C10** in reactions with Mn(II) salts, whereas the fourth cluster was obtained using **H8340C9** and a Mn^{II} / Ln^{III} mixture.

4.2.1. $[Mn^{III}_2Mn^{II}_2(34_{C8})(\mu_3\text{-}OH)_2(dmf)_{5.5}(MeOH)_{0.5}](H_2O)_{1.5}$, 35.

Reaction of **H8340C8** with Mn(II) chloride tetrahydrate afforded crystals of $[Mn^{III}_2Mn^{II}_2(\mathbf{34_{C8}})(\mu_3\text{-}OH)_2(dmf)_{5.5}(MeOH)_{0.5}](H_2O)_{1.5}$ (**35**, Figure 94) upon slow evaporation of the mother liquor. The crystals were found to be in a monoclinic cell and structure solution was performed in the space group $P2_1/c$.

The ASU comprises the entire cluster along with solvent of crystallisation. Cluster **35** is structurally analogous to **1**, with the only substantial difference being the presence of an octyl alkyl chain tethering the two TBC[4] moieties (compare Figures 31 and 94). Mn1 is bound in the TBC[4] tetraphenolic binding pocket formed by O1 – O4 (Mn1–O range

1.919(9) – 1.974(9) Å) and is in the third oxidation state with Jahn-Teller distorted octahedral geometry; the Jahn-Teller axis defined by the O15-Mn1-O9 vector (167.3(4)º). Its coordination sphere is completed by a ligated dmf molecule residing in a TBC[4] cavity (Mn1–O15, 2.297(11) Å) and a μ_3-hydroxide (Mn1–O9, 2.141(9) Å) that acts as a bridge to Mn3 and Mn4 (Mn3–O9, 2.184(9) Å and Mn4–O9, 2.183(9) Å), both of which are in a 2+ oxidation state and have distorted octahedral geometry. Mn3 is also bound to two ligated dmf molecules (Mn3–O11, 2.138(10) Å and Mn3–O12, 2.124(11) Å), two phenolic oxygen atoms on the axial position of the octahedron, each one belonging to two separate TBC[4] subunits (Mn3–O4, 2.237(8) Å and Mn3–O8, 2.237(9) Å), and a μ_3-hydroxide (Mn3–O10, 2.155(9) Å) that bridges to Mn4 and Mn2, both of which have similar coordination spheres to Mn3 and Mn1, respectively. As is the case for Mn1, Mn2 is also in the third oxidation state and has distorted octahedral geometry; the Jahn-Teller axis is described by the O16-Mn2-O10 vector (170.1(4)º). Mn2 is equatorially bound to the TBC[4] phenolic oxygens O5 – O8 (Mn2–O range, 1.936(10) – 1.966(9) Å) where the axial vertices of the octahedron are constituted by a ligated dmf molecule (Mn2–O16, 2.254(13) Å) and the aforementioned μ_3-hydorxide (Mn2–O10, 2.157(9) Å). Mn4 has a coordination mode analogous to Mn3, being bound to two μ_3-hydroxides (Mn4–O9, 2.183(9) Å and Mn4–O10, 2.152(9) Å), two ligated dmf molecules (Mn4–O13, 2.049(17) Å and Mn4–O14, 2.108(15) Å) and two μ-phenolic oxygens (Mn4–O3, 2.156(9) Å and Mn4–O7, 2.208(9) Å).

As observed in **1**, $[Mn^{III}(TBC[4])]^-$ moieties are capping the cluster core in **35**, with the Mn^{III} and Mn^{II} ions occupying the wing-tip and body positions of the butterfly-like structure respectively. Examination of the extended structure shows no significant intermolecular interactions along the three crystallographic axes. Molecules of **35** are found to pack in layers and the closest metal-metal intercluster distance was found (along the *a* axis) to be 9.613 Å between Mn1 and a symmetry equivalent Mn2 (Figure 95).

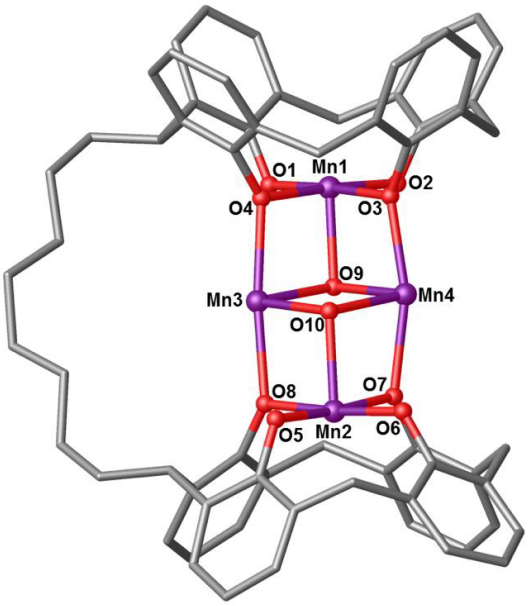

Figure 94. Partial single crystal *X*-ray structure showing the $[Mn^{III}_2Mn^{II}_2(\mathbf{34}\text{c8})(\mu_3\text{-}OH)_2(dmf)_{5.5}(MeOH)_{0.5}](H_2O)_{1.5}$ cluster, **35**, and selected labels according to discussion (Colour code: Mn – purple; O – red; C – grey). ^{t}Bu groups, hydrogen atoms, ligated solvent molecules and solvent of crystallisation omitted for clarity.

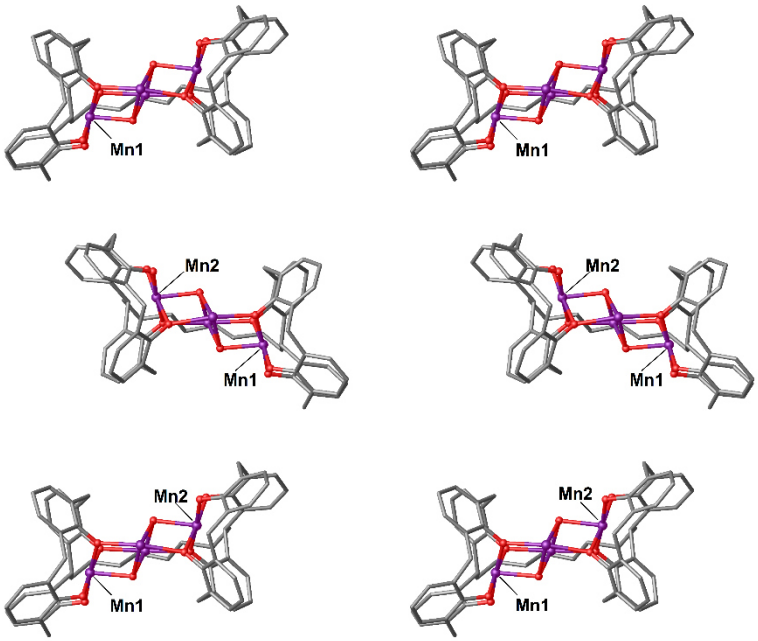

Figure 95. View of the *bc* plane in the extended structure of **35** with closest ions labelled according to discussion (Colour code: Mn – purple; O – red; C – grey). ^{t}Bu groups, hydrogen atoms, ligated solvent molecules and solvent of crystallisation omitted for clarity.

4.2.2. $[Mn^{III}_2Mn^{II}_2(\mathbf{34}_{C9})(\mu_3\text{-}OH)_2(dmf)_5(OMe)](MeOH)(dmf)(H_2O)_2$, 36.

Reaction of $\mathbf{H_8 34}_{C9}$ with Mn(II) chloride tetrahydrate yielded single crystals of formula $[Mn^{III}_2Mn^{II}_2(\mathbf{34}_{C9})(\mu_3\text{-}OH)_2(dmf)_5(OMe)](MeOH)(dmf)(H_2O)_2$ (**36**, Figure 96) upon slow evaporation of the mother liquor. The crystals were found to be in a triclinic cell and structure solution was performed in the space group *P*–1.

The ASU in **36** comprises the entire cluster and solvent of crystallisation. The nonyl tether in **36** was found to be disordered over two positions, but this was successfully modelled with the use of partial occupancies and suitable restraints (Figure 96). As anticipated, **36** is structurally related to the archetypal $[Mn^{III}_2Mn^{II}_2(TBC[4])](OH_2)$ cluster (**1**), as well as compound **35**. Mn1 in **36** is bound in the TBC[4] tetraphenolic binding pocket defined by O1 – O4 (Mn1–O range 1.916(8) – 1.962(7) Å) and is in the third oxidation state. Mn1 has distorted octahedral geometry and the Jahn-Teller axis is defined by the O10-Mn1-O12 vector with an angle of 166.3(3)º. The Mn1 coordination sphere is completed by a ligated dmf molecule that resides in the TBC[4] cavity (Mn1–O12, 2.291(8) Å) and a μ_3-hydroxide (Mn1–O10, 2.132(7) Å) that bridges to Mn3 and Mn4 (Mn3–O10, 2.418(7) Å and Mn4–O10, 2.189(8) Å), both of which are in the second oxidation state and have octahedral geometry. In addition to the aforementioned μ_3-hydroxide, Mn3 is also bound to two phenolic oxygens belonging to two separate TBC[4] moieties (Mn3–O3, 2.208(7) Å and Mn3–O7, 2.220(7) Å), a ligated dmf molecule (Mn3–O13, 2.127(12) Å), a ligated methanol molecule (Mn3–O15, 2.139(9) Å) and another μ_3-hydroxide that bridges to Mn2 and Mn4 (Mn3–O9, 2.164(8) Å, Mn2–O9, 2.153(7) and Mn4–O9, 2.182(8) Å). Mn4 has a similar coordination environment to Mn3, being bound to the two aforementioned bridging hydroxides, two phenolic oxygens at the axial positions of the geometric octahedron (Mn4–O4, 2.187(8) Å and Mn3–O8, 2.200(8) Å) and two ligated dmf molecules (Mn4–O14, 2.171(12) Å and Mn4–O16, 2.120(12) Å). Mn2 has a coordination sphere analogous to Mn1, is bound to the lower-rim oxygen atoms O5 – O8 (Mn2–O range 1.907(8) – 1.957(8) Å) and has a Jahn-Teller axis described by the O9-Mn2-O11 vector (169.5(3)º). Mn2 is bound to the aforementioned bridging hydroxide and a ligated dmf molecule that resides within the TBC[4] cavity (Mn2–O11, 2.252(8) Å).

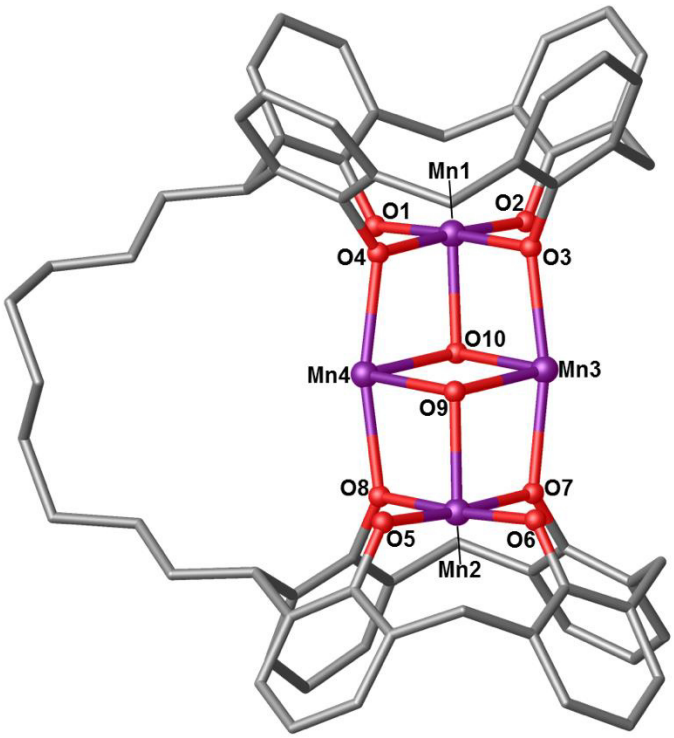

Figure 96. Partial single crystal *X*-ray structure showing the $[Mn^{III}_2Mn^{II}_2(\mathbf{34}_{C9})(\mu_3\text{-}OH)_2(dmf)_5(OMe)](MeOH)(dmf)(H_2O)_2$ cluster, **36**, and selected labels according to discussion (Colour code: Mn – purple; O – red; C – grey). ^{t}Bu groups, hydrogen atoms, ligated solvent molecules and solvent of crystallisation omitted for clarity.

The capping behaviour in **36** is, as expected, analogous to those found in both **1** and **35**, with the two $[Mn^{III}(TBC[4])]^-$ moieties being present. Structure expansion shows that the clusters packs in an interdigitated fashion, with the hydrocarbon tethers oriented towards each other along the *b* axis (Figure 97A). There are no significant intermolecular interactions between the clusters, and the shortest metal-metal intercluster distance was found to be along the *c* axis; this occurs between two symmetry equivalent Mn3 cations (Mn3…Mn3, 9.071 Å) (Figure 97B).

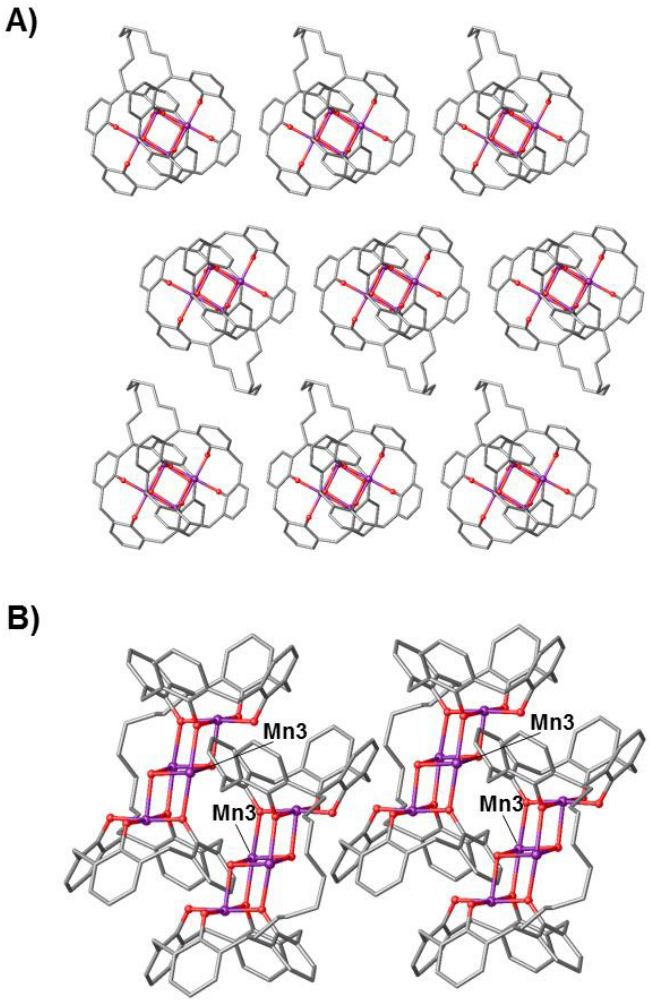

Figure 97. Views of the extended structure of **36**. A) The *ac* plane showing the interdigitated packing. B) The *ab* plane with closest ions labelled according to discussion (Colour code: Mn – purple; O – red; C – grey). ^{t}Bu groups, hydrogen atoms, ligated solvent molecules and solvent of crystallisation omitted for clarity.

4.2.3. $[Mn^{III}_4Gd^{III}_4(\mathbf{34}_{C9})(\mu_3\text{-}CO_3)_2(\mu_3\text{-}OH)_4(H_2O)_6(dmf)_6](dmf)_6(MeOH)_4$, 37.

Reaction of $\mathbf{H_8 34}_{C9}$ with Mn(II) chloride tetrahydrate and gadolinium(III) chloride hexahydrate afforded single crystals of $[Mn^{III}_4Gd^{III}_4(\mathbf{34}_{C9})(\mu_3\text{-}CO_3)_2(\mu_3\text{-}OH)_4(H_2O)_6(dmf)_6](dmf)_6(MeOH)_4$ (**37**, Figure 98) upon slow evaporation of the mother liquor. Single crystals of **37** were found to be in a triclinic cell and structure solution was performed in the space group *P*–1.

The ASU comprises of half assembly related to its s.e. through an inversion centre. The two Mn^{III} ions are bound to the phenolic oxygens of the TBC[4] moieties with Mn1–O and Mn2–O distances in the range 1.900(7) – 1.988(6) and 1.913(6) – 1.986(6) Å

respectively. Both are in a distorted octahedral geometry with Jahn-Teller axes described by the O9-Mn1-O12 and O10-Mn2-O13 vectors, both with an angle of 167.9(3)°. The Mn1 and Mn2 coordination spheres are completed by ligated dmf molecules (Mn1–O9, 2.263(6) Å and Mn2–O10, 2.263(6) Å) and μ_3-hydroxides (Mn1–O12, 2.245(5) Å and Mn2–O13, 2.233(6) Å), the latter bridging to octacoordinate Gd^{III} ions that are in square antiprismatic geometry (Gd1–O12, 2.419(5) Å, Gd1–O13, 2.427(6) Å, Gd2–O12, 2.379(6) Å and Gd2–O13, 2.390(6) Å). Gd1 is also bound to two μ-phenoxides of two TBC[4] moieties (Gd1–O3, 2.375(6) Å and Gd1–O7, 2.393(6) Å), two ligated water molecules (Gd1–O14, 2.410(7) Å and Gd1–O15, 2.428(6) Å) and two μ_3-carbonates (Gd1–O16, 2.397(6) Å and Gd1–O18, 2.394(6) Å). These carbonates bridge Gd1 and Gd2 to their s.e. counterparts. The Gd2 coordination sphere is essentially similar to that of Gd1, being bound to the aforementioned μ_3-hydroxides, two phenolic oxygens (Gd2–O6, 2.408(6) Å and Gd2–O2, 2.404(5) Å), two oxygens atoms of the same μ_3-carbonate (Gd2–O16, 2.462(6) Å and Gd2–O18, 2.460(6) Å), a ligated water molecule (Gd2–O19, 2.411(7) Å) and a ligated dmf molecule (Gd2–O11, 2.305(7) Å).

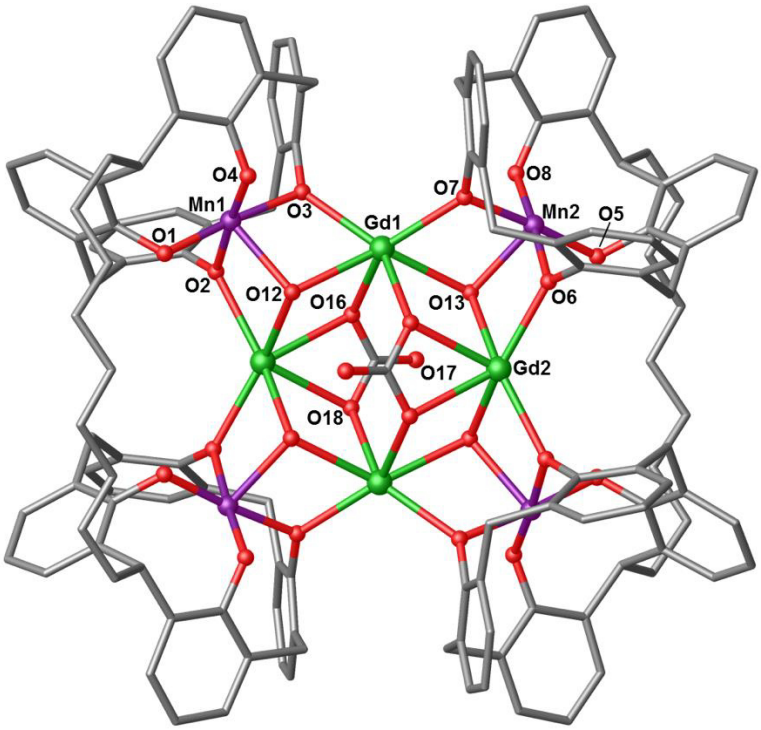

Figure 98. Partial single *X*-ray structure showing the $[Mn^{III}_4Gd^{III}_4(\mathbf{34}_{C9})(\mu_3\text{-}CO_3)_2(\mu_3\text{-}OH)_4(H_2O)_6(dmf)_6](dmf)_6(MeOH)_4$ cluster, **37**, and selected labels according to discussion (Colour code: Mn – purple; Gd – green; O – red; C – grey). ^{t}Bu groups, hydrogen atoms, ligated solvent molecules and solvent of crystallisation omitted for clarity.

Compound **37** is closely related to **4** (Chapter 1, Section 1.5.2, Figure 34) due to the presence of a square of Ln^{III} cations within a square of $[Mn^{III}(TBC[4])]^-$ units (or alternatively a Mn^{III} tetra-capped Ln^{III} square). The main difference between **37** and **4** is the presence of bridging carbonate rather than nitrate anions respectively. In the case of **4**, overall charge balance is provided by OH^- counterions that are located proximal to the polymetallic core; this is not encountered in the case of **37** which, due to the incorporation of atmospheric CO_2 and formation of μ_3-carbonates, is neutral overall.

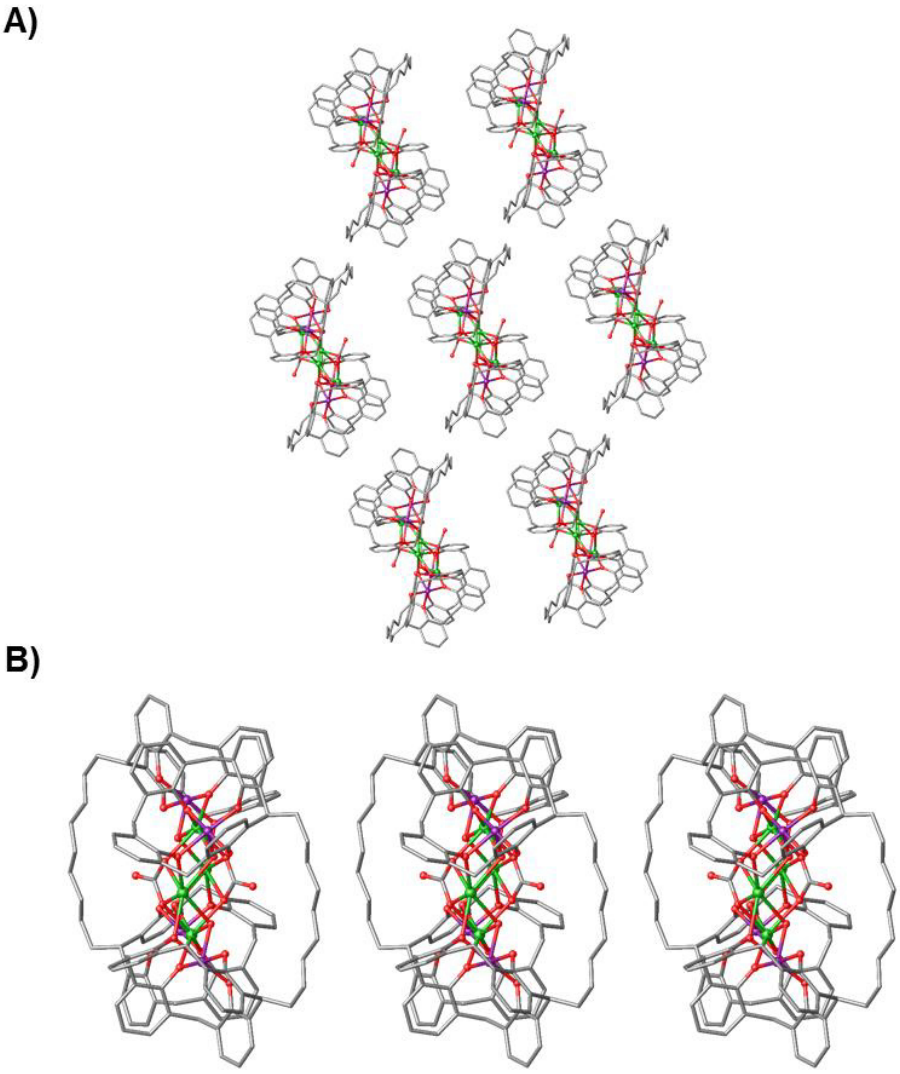

Figure 99. Views of the extended structure of **37**. A) The *ab* and B) *ac* plane showing the packing mode of the cluster and the orientation of the alkyl chains (Colour code: Mn – purple; Gd – green; O – red; C – grey). ^{t}Bu groups, hydrogen atoms, ligated solvent molecules and solvent of crystallisation omitted for clarity.

Furthermore, the Mn^{III} capped square of Ln^{III} ions is a motif that, although with a higher degree of distortion, has been discussed in the case of compounds **17** and **20** (Chapter 2, Section 2.2.2, Figure 50 and Section 2.3.3, Figure 59), confirming the tendency of TM^{III} / Ln^{III} mixtures to form such assemblies.

Structure expansion shows that molecules of **37** pack in such a way that each individual cluster is well isolated from its neighbour, with no significant intermolecular interactions being observed. The metal-metal intercluster distances were found to be very long, with an average distance of ~15 Å (Figure 99).

4.2.4. $[Mn^{III}_2Mn^{II}_2(\mathbf{34}_{C10})(\mu_3\text{-}OH)_2(dmf)_6](dmf)_{1.5}(MeOH)_{0.5}(H_2O)_{1.5}$, 38.

The last cluster of this series was synthesised by reaction of $\mathbf{H_8 34}_{C10}$ with Mn(II) chloride tetrahydrate. Single crystals of formula $[Mn^{III}_2Mn^{II}_2(\mathbf{34}_{C10})(\mu_3\text{-}OH)_2(dmf)_6](dmf)_{1.5}(MeOH)_{0.5}(H_2O)_{1.5}$ (**38**, Figure 100) were obtained upon slow evaporation of the mother liquor. The crystals were found to be in a triclinic cell and structure solution was performed in the space group *P*-1.

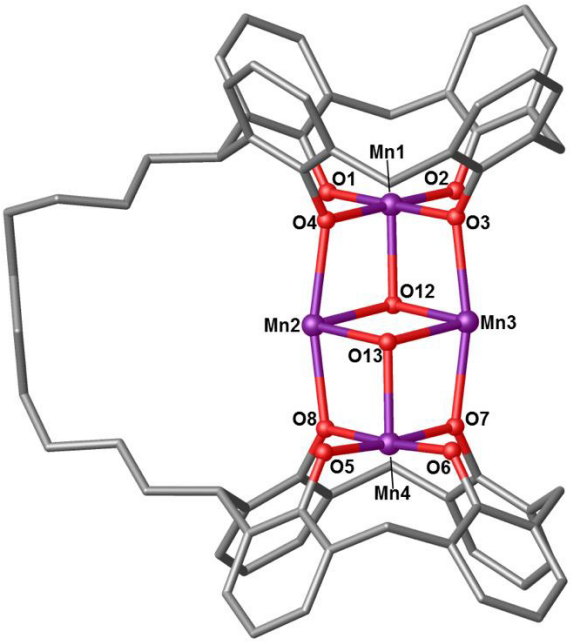

Figure 100. Partial single crystal *X*-ray structure showing the $[Mn^{III}_2Mn^{II}_2(\mathbf{34}_{C10})(\mu_3\text{-}OH)_2(dmf)_6](dmf)_{1.5}(MeOH)_{0.5}(H_2O)_{1.5}$ cluster, **38**, and selected labels according to discussion (Colour code: Mn – purple; O – red; C – grey). ^{t}Bu groups, hydrogen atoms, ligated solvent molecules and solvent of crystallisation omitted for clarity.

The ASU comprises the entire assembly as well as solvent of crystallisation. Cluster **38** is structurally analogous to **1** as well as clusters **35** and **36** discussed above, the only difference being the presence and / or the length of the alkyl chain tethering the two TBC[4] moieties. Therefore it is composed of a $Mn^{III}_2Mn^{II}_2$-butterfly core in which the wing-tip Mn^{III} ions are within the TBC[4] polyphenolic pockets, whilst the Mn^{II} ions occupy the body positions of the butterfly. Mn1 and Mn4 are the cations bound to the lower-rim phenolic oxygens (Mn1–O range 1.903(3) – 1.955(3) Å and Mn4–O range 1.903(3) – 1.958(3) Å), both with distorted octahedral geometry and with Jahn-Teller axes defined by the O9-Mn1-O12 and O11-Mn4-O13 vectors and angles of 167(2)º and 170.35(11)º respectively. Their coordination spheres are completed by ligated dmf molecules residing within the TBC[4] cavities (Mn1–O9, 2.372(7) Å and Mn4–O11, 2.282(3) Å) and μ_3-hydroxides (Mn1–O12, 2.117(3) Å and Mn4–O13, 2.144(3) Å), the latter of which bridge to Mn2 and Mn3 (Mn2–O12, 2.168(3) Å; Mn2–O13, 2.165(3) Å; Mn3–O12, 2.154(3) Å; Mn3–O13, 2.167(3) Å). Mn2 and Mn3 are in the second oxidation state and have distorted octahedral geometry. Their coordination spheres are completed by bonding to phenolates belonging to two different TBC[4] subunits (Mn2–O4, 2.244(2) Å; Mn2–O8, 2.204(2) Å; Mn3–O3, 2.232(3) Å; Mn3–O7, 2.234(3) Å) and ligated dmf molecules (Mn2–O14, 2.157(3) Å; Mn2–O15, 2.149(3) Å, Mn3–O21, 2.103(5) Å; Mn3–O22, 2.135(4) Å).

The capping behaviour in **38** is analogous to that found in **1**, **35** and **36**, with the presence of two common $[Mn^{III}(TBC[4])]^-$ moieties. Structure expansion shows that molecules of **38** pack in interdigitated layers (Figure 101) with the decyl alkyl chains oriented towards each other due to the symmetry of the crystal. The shortest metal-metal intercluster distance was found to be 9.197 Å, occurring between two symmetrical Mn3 cations.

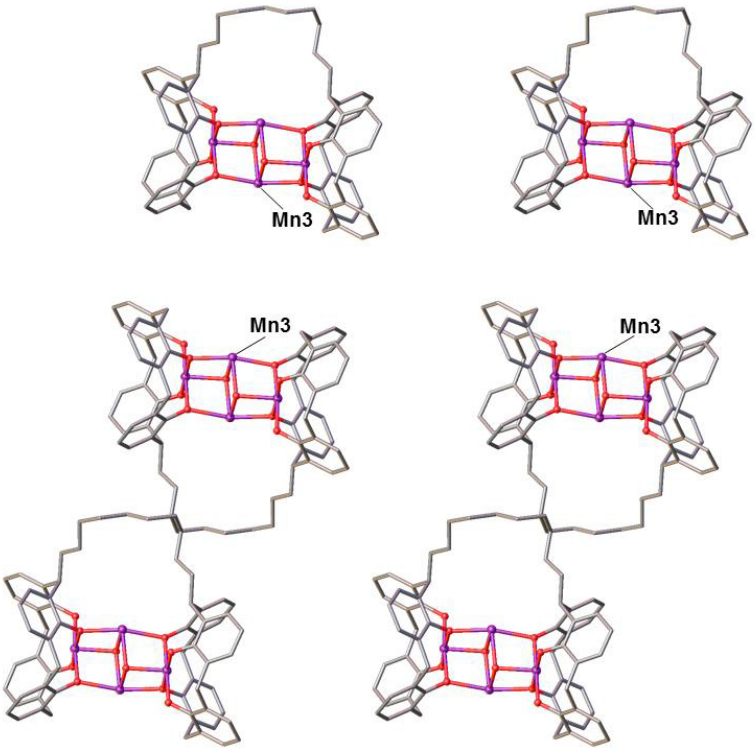

Figure 101. View of the *bc* plane in the extended structure of **38** showing the interdigitated packing of cluster and with closest ions labelled according to discussion (Colour code: Mn – purple; O – red; C – grey). ^{t}Bu groups, hydrogen atoms and ligated solvent molecules omitted for clarity.

4.3. Summary.

The results presented here clearly show that reactions of alkyl chain-tethered biscalix[4]arenes with TM^{II} and mixtures of TM^{II} and Ln^{III} metal ions afford clusters with topologies that are well known for TBC[4]. In particular, compounds **35**, **36** and **38** have a metallic core topology identical to **1**, whilst **37** is analogous to **4**. Given the structural similarities, as well as the comparable packing modes and intercluster distances, no magnetic studies were performed on these compounds; it is expected these would behave in the same way as **1** and **4**.

Although alkyl chain-tethered biscalix[4]arenes with chain lengths shorter than octyl are yet to afford polymetallic clusters, the colour changes observed are indicative of the formation of mixed valence Mn species for example; a typical colour change from pale pink to purple was observed in all cases. This may therefore be a challenge of crystallisation and structurally characterisation for these species, which will be the subject of future work in

this particular area. The results presented here have, however, established the minimum chain length required in the tethered bis-calix[4]arenes in order for one to form topologies similar to either **1** or **4** (Table 3). This suggestion is further corroborated by an empirical measurement of the Mn^{III}-Mn^{III} distances within the cluster for compounds **35**, **36** and **38**, and by comparison of these with the analogous distance found upon inspection of compound **1**. It is in fact possible to observe an increase in the Mn^{III}-Mn^{III} distances and a decrease in the **Φ** angle (measured considering the Mn^{III}-Mn^{II}-Mn^{III} ions, Figure 102) moving from **38** to **35** (**38** – 5.670 Å, 29.83º; **36** – 5.719 Å, 29.46º and **35** – 5.780 Å, 28.86º) with the latter being comparable to that measured for **1** (5.774 Å, 28.85º). This trend suggests that for alkyl chains shorter than eight carbon atoms, the Mn^{III}-Mn^{III} distance would be longer than that of **1** and that **Φ** would be smaller, which would inevitably create a large number of distortions. In contrast, with longer alkyl chains, the polymetallic core is allowed to "relax" due to the flexibility of the tether. At the same time, it is possible that shorter alkyl chains give rise to different species with disparate topologies and metal ion composition, and for which isolation may require alternative approaches to those employed here.

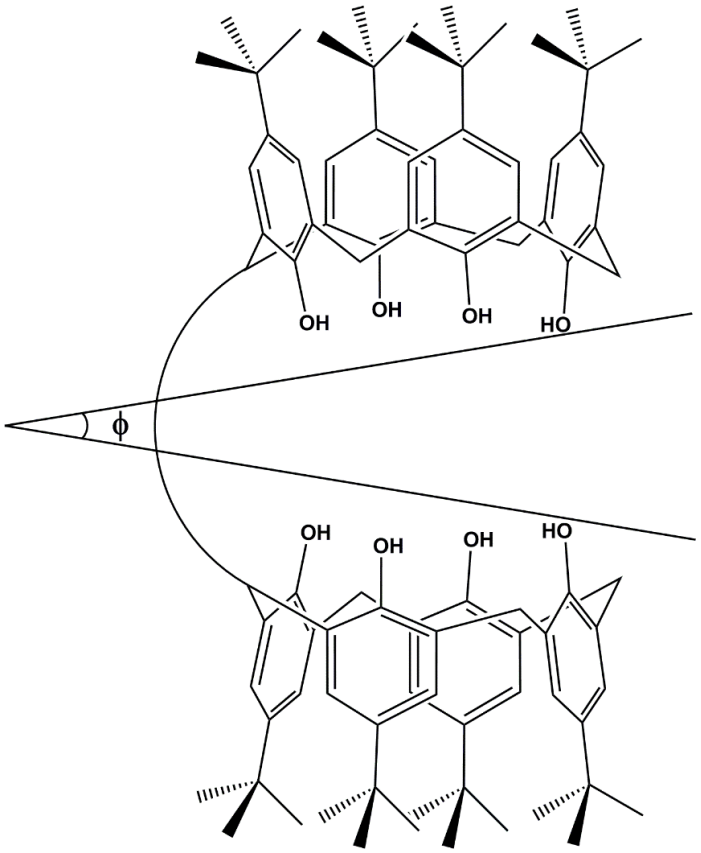

Figure 102. Schematic of **H$_8$34**$_{C3\text{-}C10}$ showing the variable angle **Φ** depending on the length of the tether.

	Mn^{II}/Mn^{III}	Cu^{II}	Fe^{III}	$Mn^{II/III}/Ln^{III}$	Cu^{II}/Ln^{III}	Fe^{III}/Ln^{III}	Ln^{III}	Cluster no.
H8340C3	✗	✗	✗	✗	✗	✗	✗	–
H8340C4	✗	✗	✗	✗	✗	✗	✗	–
H8340C5	✗	✗	✗	✗	✗	✗	✗	–
H8340C6	✗	✗	✗	✗	✗	✗	✗	–
H8340C7	✗	✗	✗	✗	✗	✗	✗	–
H8340C8	✓	✗	✗	✗	✗	✗	✗	**35**
H8340C9	✓	✗	✗	✓	✗	✗	✗	**36, 37**
H8340C10	✓	✗	✗	✗	✗	✗	✗	**38**

Table 3. Summary of the attempted reactions of alkyl chain-tethered biscalix[4]arenes **H8340C3-C10** with TM and Ln metal ions and relative compound number.

4.4. Experimental.

General procedure for the synthesis of bis-tetramethoxycalix[4]arenes 33C3-C10: *n*-BuLi (2.5 M in hexane, 1.5 eq.) was added to a stirred solution of tetramethoxycalix[4]arene (1 eq.) in dry THF (40 mL) under an N_2 atmosphere, causing a rapid colour change from pale yellow to blood red. After ten minutes of stirring the chosen dibromoalkane (1.15 eq.), as a solution in 20 mL of dry THF, was added dropwise over 40 minutes, with concomitant change in colour from blood red to yellow. Following addition, the reaction mixture was stirred for a further 12 hours before being quenched by addition of H_2O. Volatiles were removed and the resulting solid was dried under vacuum. The crude material was then dissolved in CH_2Cl_2 (300 ml) and washed with brine (3 × 100 ml). The organic layer was separated, dried over $MgSO_4$, and the solvent was removed under reduced pressure to afford a gummy yellow solid that was dried under vacuum. The resulting yellow solid was recrystallised from hot $CHCl_3$/MeOH to afford a white powder of the pure target **33C3-C10**. In all cases ^1H NMR spectra of the products are very difficult to interpret due to fluxionality casued by the lower-rim methoxy groups. Although this is the case it was possible to gauge reaction completion for these synthetic intermediates by the disappearance of characteristic

OH groups for the TBC[4] lower-rim. Compounds **33$_{C3-C10}$** were therefore used in the demethylation step below to afford the target lower-rim hydroxy TBC[4]s **H$_8$34$_{C3-C10}$**.

Synthesis of 2,2'-(Propane-1,3-diyl)bis(5,11,17,23-tetra-*p*-tert-butyl-25,26,27,28-tetramethoxycalix[4]arene), 33$_{C3}$: Reagents used in the general synthesis were 2.50 g (3.55 mmol) tetramethoxycalix[4]arene **13** in 40 mL dry THF, 2.1 mL (5.32 mmol) *n*-BuLi (2.5 M in hexane) and 358 mg (1.77 mmol) 1,3-dibromopropane in 20 mL of dry THF. Yield: 1.44 g (56 %).

Synthesis of 2,2'-(Butane-1,4-diyl)bis(5,11,17,23-tetra-*p*-tert-butyl-25,26,27,28-tetramethoxycalix[4]arene), 33$_{C4}$: Reagents used in the general synthesis were 2.50 g (3.55 mmol) tetramethoxycalix[4]arene **13** in 40 mL dry THF, 2.1 mL (5.32 mmol) *n*-BuLi (2.5 M in hexane) and 383 mg (1.77 mmol) 1,4-dibromobutane in 20 mL of dry THF. Yield: 1.30 g (50 %).

Synthesis of 2,2'-(Pentane-1,5-diyl)bis(5,11,17,23-tetra-*p*-tert-butyl-25,26,27,28-tetramethoxycalix[4]arene), 33$_{C5}$: Reagents used in the general synthesis were 10 g (14.18 mmol) tetramethoxycalix[4]arene **13** in 80 mL dry THF, 8.51 mL (21.3 mmol) *n*-BuLi (2.5 M in hexane) and 1.86 g (8.16 mmol) 1,5-dibromobutane in 30 mL of dry THF. Yield: 7.08 g (33.8 %).

Synthesis of 2,2'-(Hexane-1,6-diyl)bis(5,11,17,23-tetra-*p*-tert-butyl-25,26,27,28-tetramethoxycalix[4]arene), 33$_{C6}$: Reagents used in the general synthesis were 2.83 g (4.02 mmol) tetramethoxycalix[4]arene **13** in 40 mL dry THF, 2.4 mL (6.36 mmol) *n*-BuLi (2.5 M in hexane) and 564 mg (2.31 mmol) 1,6-dibromohexane in 20 mL of dry THF. Yield: 1.40 g (24 %).

Synthesis of 2,2'-(Heptane-1,7-diyl)bis(5,11,17,23-tetra-*p*-tert-butyl-25,26,27,28-tetramethoxycalix[4]arene), 33$_{C7}$: Reagents used in the general synthesis were 3 g (4.26 mmol) tetramethoxycalix[4]arene **13** in 40 mL dry THF, 2.55 mL (6.38 mmol) *n*-BuLi (2.5 M in hexane) and 650 mg (2.52 mmol) 1,7-dibromoheptane (97%) in 20 mL of dry THF. Yield: 2.14 g (33 %).

Synthesis of 2,2'-(Octane-1,8-diyl)bis(5,11,17,23-tetra-*p*-tert-butyl-25,26,27,28-tetramethoxycalix[4]arene), 33$_{C8}$: Reagents used in the general synthesis were 3g (4.26 mmol) tetramethoyxcalix[4]arene **13** in 40 mL dry THF, 2.55 mL (6.38 mmol) *n*-BuLi (2.5 M in hexane) and 670 mg (2.45 mmol) 1,8-dibromooctane in 20 mL dry THF. Yield: 2.83 g (44 %).

Synthesis of 2,2'-(Nonane-1,9-diyl)bis(5,11,17,23-tetra-*p*-tert-butyl-25,26,27,28-tetramethoxycalix[4]arene), 33$_{C9}$: Reagents used in the general synthesis were 3 g (4.26 mmol) tetramethoxycalix[4]arene **13** in 40 mL dry THF, 2.55 mL (6.38 mmol) *n*-BuLi (2.5 M in hexane) and 720 mg (2.53 mmol) 1,9-dibromononane (97%) in 20 mL dry THF. Yield: 2.08 g (32 %).

Synthesis of 2,2'-(Decane-1,10-diyl)bis(5,11,17,23-tetra-*p*-tert-butyl-25,26,27,28-tetramethoxycalix[4]arene), 33$_{C10}$: Reagents used in the general synthesis were 3 g (4.26 mmol) tetramethoxycalix[4]arene **13** in 40 mL dry THF, 2.55 mL (6.38 mmol) *n*-BuLi (2.5 M in hexane) and 760 mg (2.52 mmol) 1,10-dibromodecane (97%) in 20 mL dry THF. Yield: 2.29 g (35 %).

General procedure for the synthesis of bis-tetrahydroxycalix[4]arenes H$_8$34$_{C3-C10}$: Cyclohexyl iodide (90 eq.) was added to a dmf (30 ml) solution of the chosen bis-MeO-TBC[4] and the resulting mixture was heated at reflux for 48h with a concomitant change in colour from pale yellow to dark orange. The solution was poured into H_2O (250 ml), causing the precipitation of an orange solid. The orange precipitate was collected, was washed several times with water, and stirred in MeOH for 15 minutes to afford a white solid. The white solid was filtered, washed several times with MeOH, collected under reduced pressure and dried under vacuum. **Alternative workup procedure for bis-tetramethoxycalix[4]arenes:** Occasionally the workup procedure above leads to very low yields (particularly for longer alkyl chains). On occasions that a solid did not crash out of solution upon addition of water the product was extracted with $CHCl_3$, washing the water phase until the orange colour disappeared. The organic layer was collected, dried over $MgSO_4$ and filtered. The solvent was removed under reduced pressure and the resulting crude solid was recrystallised from hot $CHCl_3$/MeOH. In all cases the target bis-TBC[4]s were checked for purity by TLC ($CHCl_3$/Hex 1:1) and purified by column chromatography ($CHCl_3$/Hex 1:1 → EtOAc) to remove TBC[4] impurities.

Synthesis of 2,2'-(Propane-1,3-diyl)bis(5,11,17,23-tetra-*p*-tert-butyl-tetrahydroxy-calix[4]arene), H8$\mathbf{34}_{C3}$: Reagents used in the general synthesis were 0.880 g (0.61 mmol) of **33**$_{C3}$, 11.6 g (54.9 mmol) of cyclohexyl iodide in 30 mL of dmf. Purification by chromatography column ($CHCl_3$/Hex 1:1 → EtOAc) afforded 556 mg of pure product (Yield: 68 %). ^{1}H NMR ($CDCl_3$): 10.27 (s, 8H, -OH), 7.00 (m, 16H, ArH) 4.49 (t, 2H, $^3J_{HH}$ = 7.5 Hz, Ar-CH-CH_2-), 4.25 (m, 6H, Ar-CH_2-Ar), 3.50 (m, 6H, Ar-CH_2-Ar), 2.26 (m, 4H, Ar-CH-CH_2), 1.38 (m, 2H, CH_2-CH_2-CH_2), 1.23 (s, 36H, C(CH_3)$_3$), 1.20 (s, 36 H, C(CH_3)$_3$). ^{13}C NMR ($CDCl_3$): 146.85, 146.64, 144.38, 144.25, 131.20, 127.82, 127.70, 127.51, 127.21, 125.95, 125.91, 125.22, 121.77, 104.99, 34.17, 34.03, 32.76, 32.62, 31.43; MS calculated for $C_{91}H_{116}O_8$ (1336.87); found 1354.91 $(M+NH_4)^+$. **Crystal data for H8$\mathbf{34}_{C3}$**: $C_{99}H_{128}N_4O_8$, M = 1502.05, Colourless Block, 0.35 x 0.30 x 0.18 mm^3, monoclinic, space group $P2_1/c$ (No. 14), a = 19.3316(19), b = 25.164(2), c = 19.117(2) Å, β = 105.346(6)°, V = 8968.1(16) Å^3, Z = 4, Bruker X8 Apex II CCD Diffractometer, MoKα radiation (λ = 0.71073 Å), T = 100(2)K, $2\theta_{max}$ = 46.6°, 58266 reflections collected, 12880 unique (R_{int} = 0.1318). Final *GooF* = 1.211, R_1 = 0.0979, wR_2 = 0.2272, R indices based on 5751 reflections with I >2sigma(I) (refinement on F^2).

Synthesis of 2,2'-(Butane-1,4-diyl)bis(5,11,17,23-tetra-*p*-tert-butyl-tetrahydroxy-calix[4]arene), H8$\mathbf{34}_{C4}$: Reagents used in the general synthesis were 2.42 g (1.65 mmol) of **33**$_{C4}$, 31.3 g (0.150 mol) of cyclohexyl iodide in 40 mL of dmf. Purification by chromatography column ($CHCl_3$/Hex 1:1 → EtOAc) afforded 1.462 g of pure product (Yield: 65 %). ^{1}H NMR ($CDCl_3$): 10.30 (s, 8H, ArOH), 7.10-7.00 (m, 16H, ArH), 4.49 (t, 2H, $^3J_{HH}$ = 7.7 Hz, Ar-CH-CH_2-), 4.26 (m, 6H, Ar-CH_2-Ar), 3.51 (d, 6H, $^2J_{HH}$ = 13.94 Hz, Ar-CH_2-Ar), 2.19 (m, 4H, Ar-CH-CH_2), 1.41 (m, 4H, CH_2-CH_2-CH_2), 1.23 (s, 36H, C(CH_3)$_3$), 1.20 (s, 36 H, C(CH_3)$_3$). ^{13}C NMR ($CDCl_3$): 146.83, 146.69, 144.38, 144.28, 131.10, 127.80, 127.70, 127.55, 127.24, 125.94, 125.14, 121.77, 34.18, 34.03, 32.78, 32.64, 32.47, 31.43, 28.43; MS calculated for $C_{92}H_{118}O_8$ 1350.88, found 1369.92 $(M+NH_4)^+$.

Synthesis of 2,2'-(Pentane-1,5-diyl)bis(5,11,17,23-tetra-*p*-tert-butyl-tetrahydroxy-calix[4]arene), H8$\mathbf{34}_{C5}$: Reagents used in the general synthesis were 7.08 g (4.79 mmol) of **33**$_{C5}$, 45.3 g (0.216 mol) of cyclohexyl iodide in 150 mL of dmf. NMR and TLC ($CHCl_3$/Hex 1:1) showed that the compound was pure enough and did not need any further purification (Yield: 65 %, 4.86 g). ^{1}H NMR ($CDCl_3$): 10.30 (s, 8H, ArOH), 7.12-6.97 (m, 16H, ArH), 4.49 (t, 2H, $^3J_{HH}$ = 7.7 Hz, Ar-CH-CH_2-), 4.27 (m, 6H, Ar-CH_2-Ar), 3.50 (d, 6H, $^2J_{HH}$ = 14.31

Hz, Ar-C$\underline{H}_2$-Ar), 2.18 (m, 4H, Ar-CH-C$\underline{H}_2$), 1.32 (m, 6H, CH_2-C$\underline{H}_2$-CH_2), 1.24 (s, 36H, C(C$\underline{H}_3$)$_3$), 1.21 (s, 36H, C(C$\underline{H}_3$)$_3$). ^{13}C NMR ($CDCl_3$): 146.86, 146.75, 144.31, 144.27, 131.13, 127.85, 127.56, 127.20, 125.98, 125.93, 125.12, 121.84, 34.18, 34.04, 31.45. MS calcd. for $C_{93}H_{120}O_8$ (1365.98); found: 1383.93 $(M+NH_4)^+$.

Synthesis of 2,2'-(Hexane-1,6-diyl)bis(5,11,17,23-tetra-*p*-tert-butyl-tetrahydroxy-calix[4]arene), H834C6: Reagents used in the general synthesis were 1.40 g (0.95 mmol) of **33C6**, 18 g (85.5 mmol) of cyclohexyl iodide in 30 mL of dmf. Purification by chromatography column ($CHCl_3$/Hex 1:1 → EtOAc) afforded 333 mg of pure product (Yield: 25 %). ^{1}H NMR ($CDCl_3$): 10.30 (s, 8H, -OH), 7.13-6.98 (m, 16H, ArH), 4.48 (t, 2H, $^3J_{HH}$ = 7.82 Hz, Ar-C$\underline{H}$-CH_2-), 4.30-4.23 (m, 6H Ar-C$\underline{H}_2$-Ar), 3.50 (d, 6H, $^2J_{HH}$ = 13.7 Hz, Ar-C$\underline{H}_2$-Ar), 2.16 (m, 4H, Ar-CH-C$\underline{H}_2$), 1.33 (m, 8H, CH_2-C$\underline{H}_2$-CH_2) 1.23 (s, 36H, C(C$\underline{H}_3$)$_3$), 1.21 (s, 36H, C(C$\underline{H}_3$)$_3$). ^{13}C NMR ($CDCl_3$): 146.8, 144.3, 131.2, 127.7, 126.0, 34.2, 34.0, 32.8, 31.4, 29.0, 27.5. MS calcd. for $C_{94}H_{122}O_8$ (1379.90); found: 1397.9 $(M+NH_4)^+$.

Synthesis of 2,2'-(Heptane-1,7-diyl)bis(5,11,17,23-tetra-*p*-tert-butyl-tetrahydroxy-calix[4]arene), H834C7: Reagents used in the general synthesis were 2.04 g (1.35 mmol) of **33C7**, 25.6 g (121.9 mmol) of cyclohexyl iodide in 30 mL of dmf. Purification by chromatography column ($CHCl_3$/Hex 1:1 → EtOAc) afforded 1.123 g of pure product (Yield: 60 %). ^{1}H NMR ($CDCl_3$): 10.30 (s, 8H, -OH), 7.13-6.98 (m, 16H, ArH), 4.48 (t, 2H, $^3J_{HH}$ = 7.7 Hz, Ar-C$\underline{H}$-CH_2-), 4.30-4.23 (m, 6H Ar-C$\underline{H}_2$-Ar), 3.50 (d, 6H, $^2J_{HH}$ = 13.94 Hz, Ar-CH-C$\underline{H}_2$), 2.16 (m, 4H, Ar-CH-C$\underline{H}_2$), 1.33 (m, 10H, CH_2-C$\underline{H}_2$-CH_2) 1.23 (s, 36H, C(C$\underline{H}_3$)$_3$), 1.21 (s, 36H, C(C$\underline{H}_3$)$_3$). ^{13}C NMR ($CDCl_3$):146.8, 144.3, 131.2, 127.8, 125.97, 125.11, 121.11, 121.9, 34.2, 34.03, 32.8, 31.4, 29.5. MS calcd. for $C_{95}H_{124}O_8$ (1393.1); found: 1411.9 $(M+NH_4)^+$.

Synthesis of 2,2'-(Octane-1,8-diyl)bis(5,11,17,23-tetra-*p*-tert-butyl-tetraxydroxy-calix[4]arene), H834C8: Reagents used in the general synthesis were 2.83 g (1.86 mmol) of **33C8**, 35 g (167.4 mmol) of cyclohexyl iodide in 30 mL of dmf. NMR and TLC ($CHCl_3$/Hex 1:1) showed that the compound was pure enough and did not need any further purification. ^{1}H NMR ($CDCl_3$): 10.29 (s, 8H, -OH), 7.12-6.98 (m, 16H, ArH), 4.48 (t, 2H, $^3J_{HH}$ = 8 Hz, Ar-C$\underline{H}$-CH_2-), 4.30-4.22 (m, 6H, Ar-C$\underline{H}_2$-Ar), 3.49 (d, 6H, $^2J_{HH}$ = 13.94 Hz, Ar-C$\underline{H}_2$-Ar), 2.17 (m, 4H, Ar-CH-C$\underline{H}_2$), 1.32 (m, 12H, CH_2-C$\underline{H}_2$-CH_2), 1.23 (s, 36H, C(C$\underline{H}_3$)$_3$), 1.21 (s,

36H, C(C<u>H</u>$_3$)$_3$). ^{13}C NMR ($CDCl_3$):146.8, 144.3, 131.3, 127.7, 125.94, 36.5, 34.2, 34.02, 32.8, 31.4, 30.9, 29.5, 29.4. MS calcd. for $C_{96}H_{126}O_8$ (1407.01); found: 1425.9 $(M+NH_4)^+$.

Synthesis of 2,2'-(Nonane-1,9-diyl)bis(5,11,17,23-tetra-*p*-tert-butyl-tetrahydroxy-calix[4]arene), H$_8$34$_{C9}$: Reagents used in the general synthesis were 1.935 g (1.26 mmol) of **33$_{C9}$**, 23.8 g (113.5 mmol) of cyclohexyl iodide in 30 mL of dmf. Purification by chromatography column ($CHCl_3$/Hex 1:1 → EtOAc) afforded 0.55 g of pure product (Yield: 31 %). ^{1}H NMR ($CDCl_3$): 10.31 (s, 8H, -OH), 7.13-6.98 (m, 16H, ArH), 4.49 (t, 2H, $^3J_{HH}$ = 7.7 Hz, Ar-C<u>H</u>-CH$_2$-), 4.31-4.23 (m, 6H, Ar-C<u>H</u>$_2$-Ar), 3.51 (d, 6H, $^2J_{HH}$ = 13.9 Hz, Ar-CH-C<u>H</u>$_2$), 2.16 (s, 4H, Ar-CH-C<u>H</u>$_2$), 1.33 (m, 14H, CH$_2$-C<u>H</u>$_2$-CH$_2$), 1.23 (s, 36H, C(C<u>H</u>$_3$)$_3$), 1.21 (s, 36H, C(C<u>H</u>$_3$)$_3$). ^{13}C NMR ($CDCl_3$):146.8, 144.3, 131.2, 127.8, 127.55, 127.20, 125.96, 125.11, 121.9, 35.6, 34.2, 34.05, 32.8, 31.4, 30.98, 29.6, 29.5. MS calcd. for $C_{97}H_{128}O_8$ (1421.1); found: 1439.9 $(M+NH_4)^+$.

Synthesis of 2,2'-(Decane-1,10-diyl)bis(5,11,17,23-tetra-*p*-tert-butyl-tetrahydroxy-calix[4]arene), H$_8$34$_{C10}$: Reagents used in the general synthesis were 2.29 g (1.48 mmol) of **33$_{C10}$**, 28 g (133 mmol) of cyclohexyl iodide in 30 mL of dmf. Purification by chromatography column ($CHCl_3$/Hex 1:1 → EtOAc) afforded 0.455 g of pure product (Yield: 21 %). ^{1}H NMR ($CDCl_3$): 10.30 (s, 8H, -OH), 7.13-6.98 (m, 16H, ArH), 4.49 (t, 2H, $^3J_{HH}$ = 7.8 Hz, Ar-C<u>H</u>-CH$_2$-), 4.30-4.23 (m, 6H, Ar-C<u>H</u>$_2$-Ar), 3.50 (d, 6H, $^2J_{HH}$ = 13.94 Hz, Ar-C<u>H</u>$_2$-Ar), 2.16 (s, 4H, -C<u>H</u>$_2$-), 1.34 (m, 16H, CH$_2$-C<u>H</u>$_2$-CH$_2$), 1.23 (s, 36H, C(C<u>H</u>$_3$)$_3$), 1.21 (s, 36H, C(C<u>H</u>$_3$)$_3$). ^{13}C NMR ($CDCl_3$):146.8, 144.3, 131.2, 127.8, 125.95, 35.6, 34.2, 34.02, 31.4, 29.6, 29.5. MS calcd. for $C_{98}H_{130}O_8$ (1436.02); found: 1454.01 $(M+NH_4)^+$.

Synthesis of [Mn$^{III}_2$Mn$^{II}_2$(34$_{C8}$)(μ$_3$-OH)$_2$(dmf)$_{5.5}$(MeOH)$_{0.5}$] (H$_2$O)$_{1.5}$, 35.

$MnCl_2 \cdot 4H_2O$ (2 eq., 14.1 mg, 0.071 mmol) and **H$_8$34$_{C8}$** (1 eq., 50 mg, 0.0355 mmol) were dissolved in a 1:1 dmf / MeOH mixture (20 mL). After 10 minutes of stirring Et_3N (0.05 mL) was added and the resulting deep purple solution stirred for 2 hrs. The reaction mixture was filtered to leave a deep purple solution. Purple crystals suitable for diffraction studies were obtained upon slow evaporation of the mother liquor. **Crystal data for 35**: $C_{113}H_{165.5}N_{5.5}O_{18.5}Mn_4$, M = 2116.76, Purple Block, 0.02 x 0.02 x 0.09 mm^3, monoclinic, space group $P2_1/c$, a = 25.1565(8), b = 20.0930(6), c = 22.7572(7) Å, β = 97.681(2)°, V = 11399.9(6) Å^3, Z = 4, Bruker D8 equipped with a PHOTON 100 detector, synchrotron

radiation (λ = 0.77490 Å), T = 100(2)K, $2\theta_{max}$ = 41.5°, 65220 reflections collected, 8958 unique (R_{int} = 0.1114). Final *GooF* = 1.102, R_1 = 0.1210, wR_2 = 0.2991.

Synthesis of $[Mn^{III}_2Mn^{II}_2(34_{C9})(\mu_3\text{-}OH)_2(dmf)_5(MeOH)](MeOH)(dmf)(H_2O)_2$, 36.
$MnCl_2{\cdot}4H_2O$ (4 eq., 27.8 mg, 0.14 mmol) and $\mathbf{H_8 34_{C9}}$ (1 eq., 50 mg, 0.035 mmol) were dissolved in a 1:1 dmf / MeOH mixture (20 mL). After 10 minutes of stirring Et_3N (0.05 mL) was added and the resulting deep purple solution stirred for 2 hrs. The reaction mixture was filtered to leave a deep purple solution. Purple crystals suitable for diffraction studies were obtained upon slow evaporation of the mother liquor. **Crystal data for 36**: $C_{117}H_{176}N_6O_{20}Mn_4$, M = 2206.39, Purple Block, 0.3 x 0.3 x 0.4 mm^3, triclinic, space group P-1, a = 12.375(3), b = 18.727(4), c = 25.238(5) Å, α = 84.03(3), β = 88.68(3), γ = 89.00(3)°, V = 5815(2) Å^3, Z = 2, Bruker Apex-II diffractometer, Mo-Kα radiation (λ = 0.71073 Å), T = 100(2)K, $2\theta_{max}$ = 41.1°, 42921 reflections collected, 11547 unique (R_{int} = 0.1056). Final *GooF* = 1.077, R_1 = 0.0963, wR_2 = 0.2652.

Synthesis of $[Mn^{III}_4Gd^{III}_4(34_{C9})(\mu_3\text{-}CO_3)_2(\mu_3\text{-}OH)_4(H_2O)_6(dmf)_6](dmf)_6(MeOH)_4$, 37:
$MnCl_2{\cdot}4H_2O$ (2 eq., 13.9 mg, 0.071 mmol), $GdCl_3{\cdot}6H_2O$ (1 eq., 9.3 mg, 0.035 mmol) and $\mathbf{H_8 34_{C9}}$ (1 eq., 50 mg, 0.035 mmol) were dissolved in a 1:1 dmf / MeOH mixture (20 mL). After 10 minutes of stirring Et_3N (0.05 mL) was added and the resulting deep purple solution stirred for 2 hrs. The reaction mixture was filtered to leave a deep purple solution. Purple crystals suitable for diffraction studies were obtained upon slow evaporation of the mother liquor. **Crystal data for 37**: $C_{236}H_{356}N_{12}O_{48}Mn_4Gd_4$, M = 4978.07, Purple Block, 0.2 x 0.35 x 0.4 mm^3, triclinic, space group P-1, a = 14.9707(7), b = 21.9372(6), c = 22.0011(6) Å, α = 113.205(3), β = 93.322(3), γ = 107.520(3)°, V = 6203.1(4) Å^3, Z = 1, Bruker APEX-II diffractometer, Cu-Kα radiation (λ = 1.54178 Å), T = 153(2)K, $2\theta_{max}$ = 153.6°, 121039 reflections collected, 25512 unique (R_{int} = 0.1112). Final *GooF* = 1.039, R_1 = 0.0855, wR_2 = 0.2296.

Synthesis of $[Mn^{III}_2Mn^{II}_2(34_{C10})(\mu_3\text{-}OH)_2(dmf)_6](dmf)_{1.5}(MeOH)_{0.5}(H_2O)_{1.5}$, 38:
$MnCl_2{\cdot}4H2O$ (1 eq., 6.9 mg, 0.0348 mmol) and $\mathbf{H_8 34_{C10}}$ (1 eq., 50 mg, 0.0348 mmol) were dissolved in a 1:1 dmf / MeOH mixture (20 mL). After 10 minutes of stirring Et3N (0.05 mL) was added and the resulting deep purple solution stirred for 2 hrs. The reaction mixture was filtered to leave a deep purple solution. Purple crystals suitable for diffraction studies were obtained upon slow evaporation of the mother liquor. **Crystal data for 38**:

$C_{121}H_{181.5}N_{7.5}O_{19.5}Mn_4$, M = 2272.99, Purple Block, 0.1 x 0.15 x 0.04 mm^3, triclinic, space group P-1, a = 12.7808(5), b = 19.2134(8), c = 27.4523(12) Å, α = 74.294(2), β = 82.588(3), γ = 85.413(2)°, V = 6428.2(5) $Å^3$, Z = 2, Bruker D8 equipped with a PHOTON 100 detector, synchrotron radiation (λ = 0.77490 Å), T = 100(2)K, $2\theta_{max}$ = 62.4°, 98239 reflections collected, 31909 unique (R_{int} = 0.0399). Final *GooF* = 1.024, R_1 = 0.0914, wR_2 = 0.2740.

Chapter 5: Rigid spacer-tethered biscalix[4]arenes

The following chapter describes the synthesis of three geometric isomers of a biscalix[4]arene in which the two TBC[4] moieties are tethered by a rigid spacer. A brief description of these ligands will be presented, being strictly related to the synthetic procedure reported in Chapter 2 (Section 2.1) and Chapter 4 (Section 4.1). The coordination chemistry of these ligands will be discussed, underlining the structural features in comparison to the clusters presented in the previous chapters.

5.1. Synthesis of rigid spacer-tethered biscalix[4]arenes.

Considering the outcome of the exploratory coordination chemistry carried out when employing alkyl chain-tethered biscalix[4]arenes, coupled with proof that the introduction of substituents at the methylene bridge has minor effects on the topology of the resulting polymetallic clusters, it was worth investigating systems with a higher degree of rigidity. The use of more rigid tethers is a logical route of investigation so that one may control / direct cluster formation. In addition, it should provide the possibility of predicting the topological features of the polymetallic assemblies obtained when employing such ligands prior to synthesis. Furthermore, it may allow one to direct the formation of the clusters towards novel topologies.

With this in mind, *ortho*-, *meta*- and *para*-xylyl spacers were chosen as a starting point to synthesise rigid spaced *ortho*-, *meta*- and *para*-xylyl BisTBC[4]s respectively. Prior to the synthesis of the xylyl-BisTBC[4]s, DFT calculations were performed using B3LYP functional with added GD3 dispersion and 6-31G** basis set (Figure 103). Analysis of the calculated structures suggested that there is rotational freedom associated with the tether bonds attached to the methylene bridge. Furthermore, it can be seen that, in the case of the *ortho*- and *meta*-xylyl BisTBC[4]s, the two TBC[4] moieties are in a convergent fashion and are slightly offset, with an eclipsed arrangement. The lower-rim centroid-centroid distances, generated between sets of lower-rim hydroxyls, are 3.081 Å and 3.177 Å, respectively. In contrast, the conformation of *para*-xylyl BisTBC[4] is divergent, with the two TBC[4] subunits in a twisted arrangement and lower-rim centroid-centroid distance of 12.679 Å. It is therefore likely that the constraints imposed by the spacers in the *ortho*- and *meta*-xylyl BisTBC[4]s would allow the formation of any known cluster arrangement in which the

distance between the TBC[4] lower-rims was similar. Using this logic, the positioning of the TBC[4] moieties in *para*-xylyl BisTBC[4] would preclude the formation of any known TBC[4]-supported cluster given the divergence of the ligand.

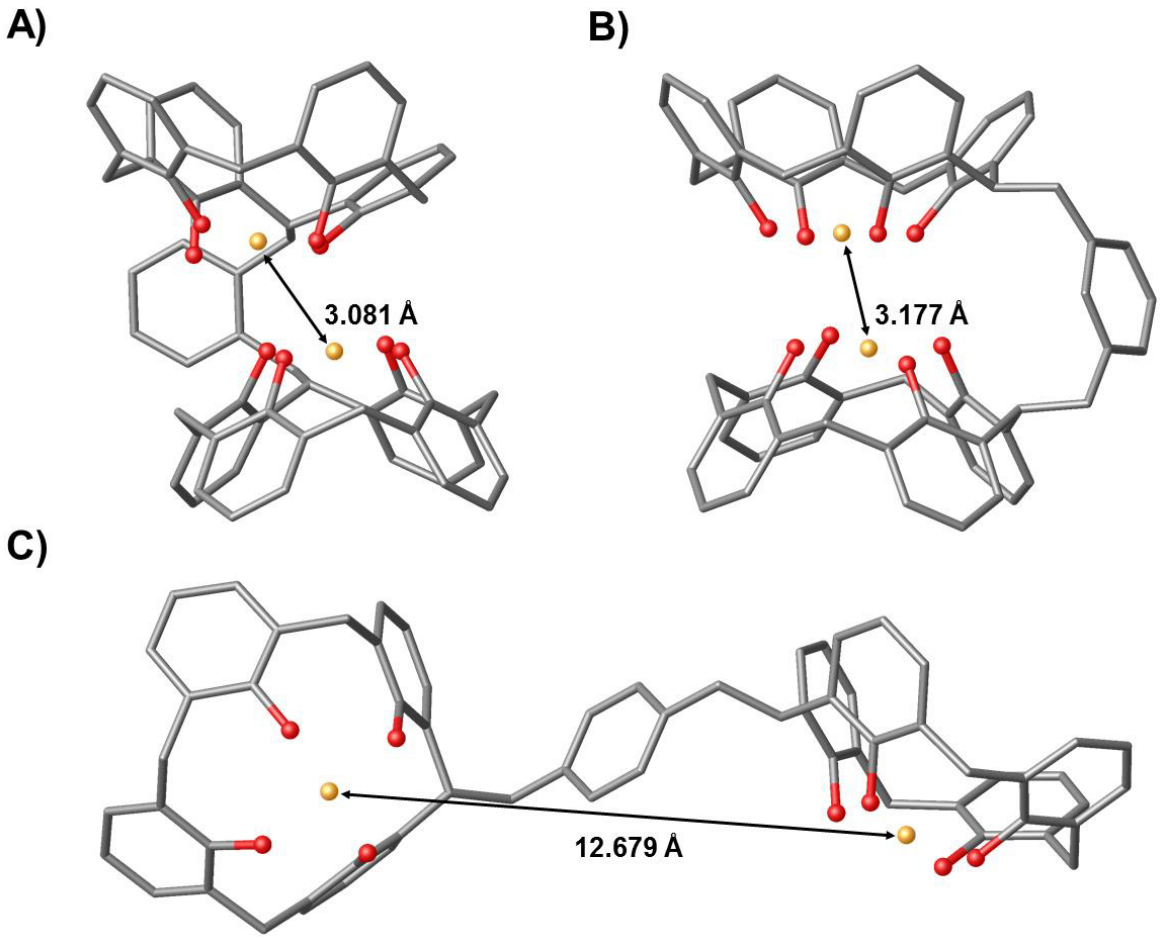

Figure 103. Calculated structures of A) convergent *ortho*-xylyl BisTBC[4], B) convergent *meta*-xylyl BisTBC[4] and C) divergent *para*-xylyl BisTBC[4] showing the distance between lower-rim centroids. Hydrogen atoms omitted for clarity (Colour code: C – grey, O – red, H – white, Centroid – yellow).

By inspection of the TBC[4]-supported metal clusters reported to date, it was possible to identify two clusters in which the lower-rims of two TBC[4] moieties are most proximal. The first is the case of compound **1** (Chapter 1, Section 1.5.2, Figure 31), even though this type of structure would be impossible to form when employing either *ortho*- or *meta*-xylyl BisTBC[4]s; this is due to the fact that the formation of a butterfly-like topology brings the TBC[4] lower-rims to a distance of circa 5.7 Å, but also forces them to be considerably offset with respect to one another. The second is the case of compound **5** (Chapter 1, Section 1.5.2,

Figure 35), in which the two TBC[4] lower-rims are significantly closer to one another (centroid-centroid distance of 4.1 Å) and are slightly tilted. This situation is much more similar to the calculated structures of *ortho*- and *meta*-xylyl BisTBC[4]s and, in particular, the latter seemed to be the best candidate to afford a polymetallic cluster similar to **5**, possessing fewer steric constraints relative to compound *ortho*-xylyl BisTBC[4].

Before proceeding to the synthesis of the aforementioned xylyl-tethered BisTBC[4]s, cluster formation was tested with a TBC[4] bearing a benzyl group at one methylene bridge; this was carried out given the structural similarity between Benzyl-H_4TBC[4] and the target ligands. This was undertaken in order to assess whether the presence of a bulky group (compared to the alkyl chains discussed in Chapter 4) would afford a cluster with a topology different to **1**, even without the constraints imposed by the xylyl tether. Benzyl-H_4TBC[4][72] was reacted with Mn(II) chloride under standard cluster synthesis conditions for **1** and single crystals suitable for *X*-ray diffraction studies were obtained upon vapour diffusion with MeCN. Structure solution revealed that the cluster comprises a $Mn^{III}_2Mn^{II}_2$ butterfly housed within two benzyl-TBC[4] moieties (**39**, Figure 104).

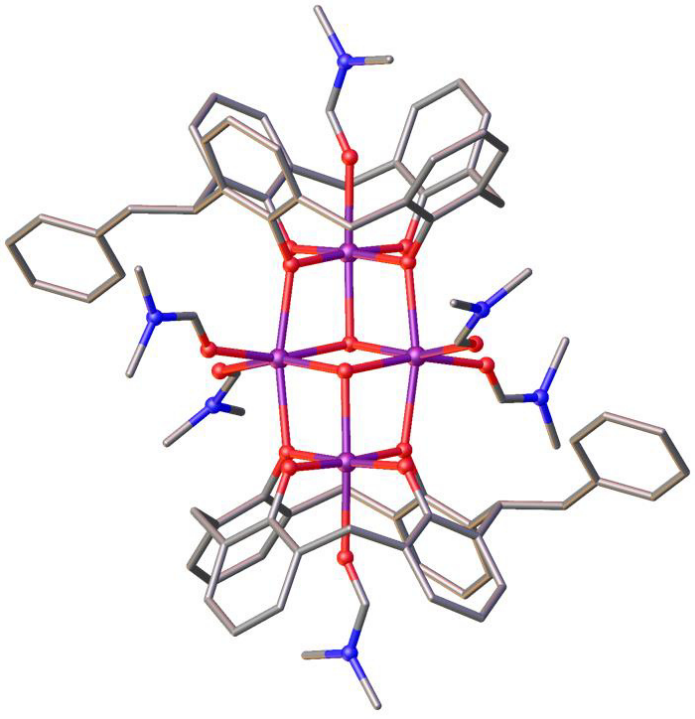

Figure 104. Partial single crystal *X*-ray structure of compound **39** showing the *trans*-positioning of the benzyl groups at the TBC[4] methylene bridge (Colour code: Mn – purple; O – red; C – grey). ^{t}Bu groups, hydrogen atoms and solvent of crystallisation omitted for clarity.

The cluster is therefore structurally analogous to **1** (and compounds **31, 32, 35, 36, 38**; Chapter 4, Sections 4.1 and 4.2), with the bridge benzyl group substituents positioned *trans* within the assembly; this is an expected arrangement when one considers the steric influence from the peripherally ligated solvent molecules.

As already established for the alkyl chain tethered BisTBC[4] discussed in Chapter 4, this is another case in which the bridging groups, although relatively bulky, have little or no effect on the formation of the archetypal $Mn^{III}_2Mn^{II}_2$ butterfly.

Having established that cluster formation was tolerant towards the introduction of benzyl groups at the methylene bridge, the synthesis of the *ortho*-, *meta*- and *para*-xylyl BisTBC[4]s was accomplished following the same synthetic route outlined in Chapter 4 (Section 4.1). Reaction of **13** with *n*-BuLi led to the formation of a methylene bridge lithiated species (**13-Li**) which is non-isolable and that, upon addition of the chosen α,α'-dibromoxylene (*ortho*-, *meta*- or *para*-), underwent substitution, affording the lower-rim methylated products **40**, **41** and **42** (Figure 105).

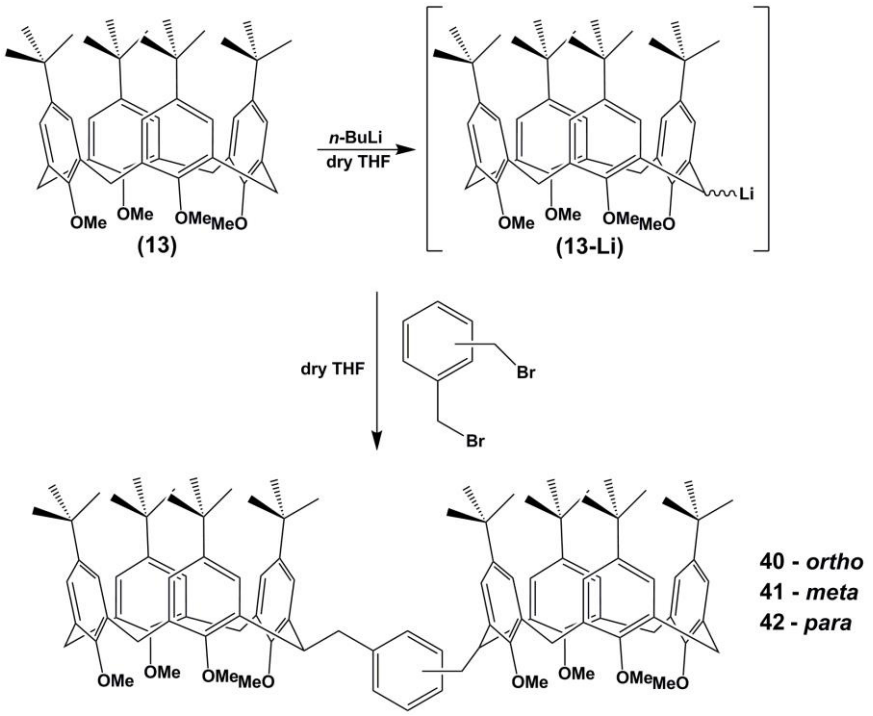

Figure 105. Synthesis of xylyl-tethered biscalix[4]arenes **40**, **41** and **42**.

As was the case for compounds **13** and **33**$_{C3\text{-}C10}$, the presence of conformational equilibria, promoted by the lower-rim methoxy groups, prevents any ^{1}H NMR characterisation as the spectra for these compounds have very broad signals. Demethylation reaction was performed by heating to reflux a solution of compound **40**, **41** and **42** for 48 hours, employing

iodocyclohexane as demethylating agent, affording compounds **H$_8$43**, **H$_8$44** and **H$_8$45** as a result (Figure 106).

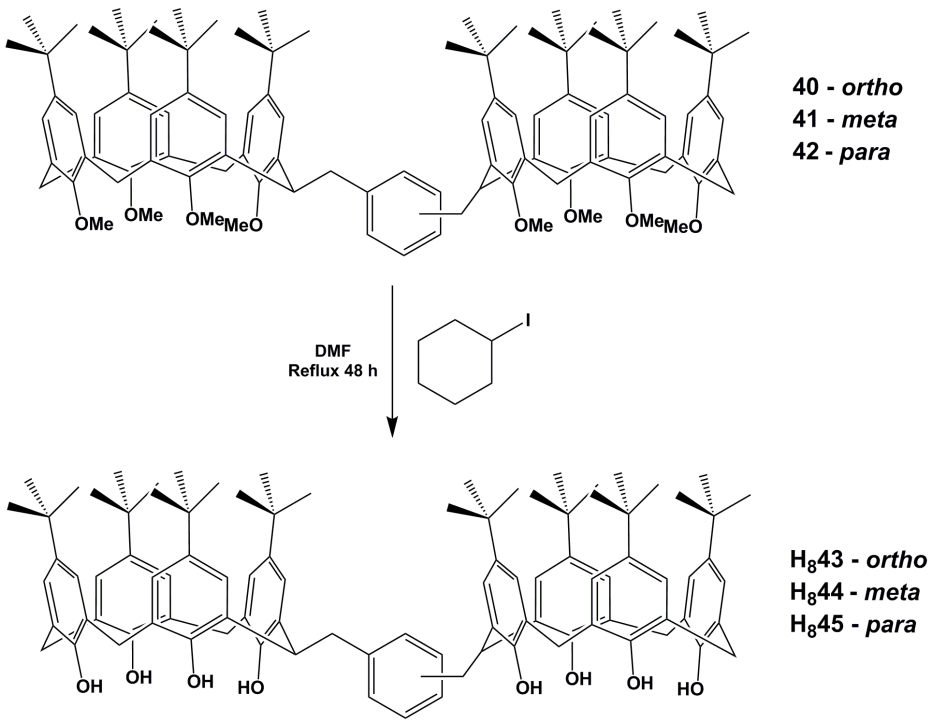

Figure 106. Demethylation reaction of **40**, **41** or **42** to afford compounds **H$_8$43**, **H$_8$44** or **H$_8$45**.

The products were checked for purity by standard TLC ($CHCl_3$ / Hex 1:1) as they can potentially contain impurities of **12** and, if it were the case, be purified by column chromatography ($CHCl_3$ / Hex 1:1 → EtOAc). ^{1}H NMR spectra confirmed the successful synthesis of compounds **H$_8$43**, **H$_8$44**, **H$_8$45** which, given their chemical composition relative to the alkyl chain-tethered biscalix[4]arenes **H$_8$34$_{C3\text{-}C10}$** discussed in Chapter 4, have similar spectra. Due to this, only the major differences will be highlighted. The presence of an aromatic ring spacing / tethering the two H_4TBC[4] moieties give rise to additional proton resonances in the aromatic region, and as a result the whole region appears as a multiplet integrating to twenty protons. The benzylic protons coupling with the methine proton on the H_4TBC[4] moiety appear as a singlet which, due to the shielding effect of the neighbouring aromatic ring, is located at 1.59 - 1.57 ppm, a considerable difference compared to the resonance given by the same protons in the alkyl chain-tethered biscalix[4]arenes (2.16 ppm). The three compounds were fully characterised by means of standard techniques, but only in one case was possible to isolate suitable *X*-ray diffraction quality single crystals, which was the case for the MeCN solvate of compound **H$_8$45** (Figure 107). The crystals

were found to be in a monoclinic space group and structure analysis was carried out in the space group C_2/c. The ASU comprises one half of a molecule of **H$_8$45**, with a MeCN molecule residing in the H$_4$TBC[4] cavity, stabilised by a CH-π interaction with one of the aromatic rings of the macrocycle. Symmetry expansion reveals the entire molecule as shown in Figure 105. Compared to the calculated structure discussed above, the crystal structure shows the two H$_4$TBC[4] cavities pointing in opposite directions, in a more favourable conformation. The distance between the two centroids generated around the phenolic OHs was found to be 11.947 Å, representing a small difference of 0.732 Å with respect to the calculated structure shown in Figure 103C.

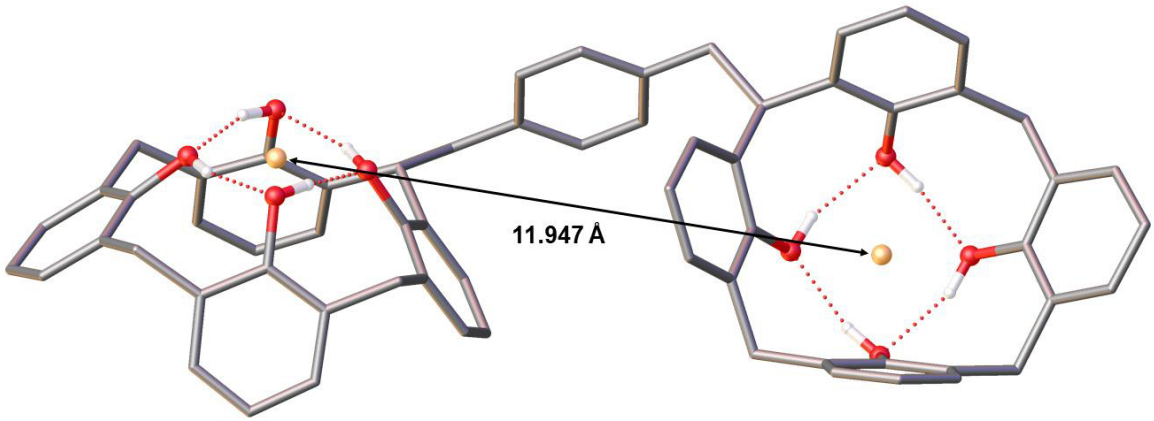

Figure 107. Partial single crystal *X*-ray of **H$_8$45**. ^{t}Bu groups, hydrogen atoms not involved in hydrogen bonds and crystallisation solvent molecules omitted for clarity (Colour code: C – grey, O – red, H – white, Centroid - yellow).

5.2. Rigid spacer-tethered biscalix[4]arene-supported metal clusters.

Exploratory cluster formation of the synthesised xylyl-tethered biscalix[4]arenes was performed under the standard conditions outlined in Chapter 2, Section 2.2. Two novel clusters were obtained as a result, one from a reaction of **H$_8$44** with Fe(III) and Ln(III) nitrates, and the other by reacting **H$_8$45** with a Mn(II) / Ln(III) chloride mixture.

5.2.1. [Fe$^{III}_2$Gd$^{III}_2$(44)(μ$_4$-O)(μ-OH)(dmf)$_7$(MeOH)(H$_2$O)$_2$](H$_7$44)(dmf)$_{0.5}$(H$_2$O)$_{1.5}$, 46.

Reaction of **H$_8$44** with Fe(III) nitrate nonahydrate and gadolinium(III) nitrate hexahydrate in a dmf / MeOH mixture with Et$_3$N as a base, afforded single crystals of formula

$[Fe^{III}_2Gd^{III}_2(\mathbf{44})(\mu_4\text{-}O)(\mu\text{-}OH)(dmf)_7(MeOH)(H_2O)_2](\mathbf{H_744})(dmf)_{0.5}(H_2O)_{1.5}$ (**46**, Figure 108) upon vapour diffusion of PET in the mother liquor. The crystals were found to be in a triclinic cell and structure solution was carried out in the space group *P*-1.

The ASU comprises of one molecule of **44** encapsulating the four metal cations which are arranged at the vertices of a distorted tetrahedron. There are bridging anions and terminal ligated solvent molecule within the cluster as well as co-crystallised solvent molecules and half of a di-anionic **44**, providing the correct charge balance for the positively charged cluster. Cluster **46** is structurally analogous to **5** (Chapter 1, Section 1.5.2) and, from comparison with the calculated structure discussed above, it is evident that **44** possesses the right structural features to facilitate the assembly of this cluster topology. Fe1 is bound in the tetraphenolic cavity formed by O1 – O4 (Fe1–O range 1.936(8) – 2.027(8) Å) and it is in the third oxidation state with a distorted octahedral geometry. Its coordination sphere is completed by a ligated dmf molecule (Fe1–O10, 2.278(19) Å) and a μ_4-oxide (Fe1–O17, 1.904(8) Å) that is bridging to the other three metal cations (Fe2–O17, 1.948(8) Å; Gd1–O17, 2.469(8) Å; Gd2–O17, 2.480(8) Å). The aforementioned ligated dmf molecule was modelled at half occupancy and this position is also occupied by a co-crystallised dmf molecule residing within the TBC[4] cavity.

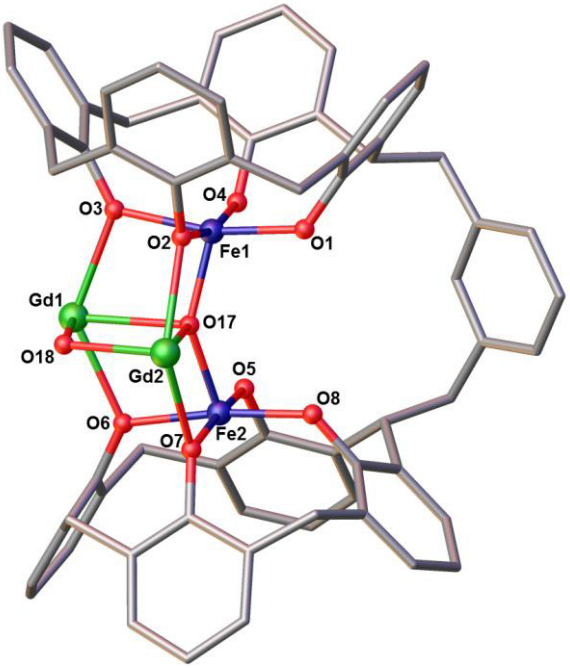

Figure 108. Partial single crystal *X*-ray structure of **46** showing $[Fe^{III}_2Gd^{III}_2(\mathbf{44})(\mu_4\text{-}O)(\mu\text{-}OH)(dmf)_7(MeOH)(H_2O)_2](\mathbf{H_744})(dmf)_{0.5}(H_2O)_{1.5}$ core and selected labels according to discussion (Colour code: Fe – dark blue; Ln – green; O – red; C – grey). ^{t}Bu groups, hydrogen atoms, ligated solvent molecules and solvent of crystallisation omitted for clarity.

Fe2 has a coordination environment analogous to Fe1, bound to O5 – O8 of the TBC[4] binding pocket (Fe2–O range 1.937(8) – 2.024(8) Å), a ligated dmf molecule located inside the TBC[4] cavity (Fe2–O9, 2.202(9) Å) and the aforementioned μ_4-oxide. Gd1 is octacoordinate, is in a square antiprismatic geometry and, in addition to the aforementioned μ_4-oxide, is bound to two phenolic oxygens belonging to the two TBC[4] moieties (Gd1–O3, 2.345(8) Å and Gd1–O6, 2.340(8) Å), two ligated dmf molecules (Gd1–O12, 2.416(17) Å and Gd1–O15, 2.357(19) Å), an aqua ligand (Gd1–O24, 2.494(9) Å) and a μ-hydroxide (Gd1–O18, 2.274(8) Å) that bridges to Gd2 (Gd2–O18, 2.287(8) Å). Gd2 shares a coordination sphere similar to Gd1, being bound to two phenolic oxygens (Gd2–O2, 2.327(8) Å and Gd2–O7, 2.321(8) Å), a ligated dmf molecule (Gd2–O19, 2.460(2) Å), a ligated methanol (Gd2–O21, 2.560(3) Å) and an aqua ligand (Gd2–O23, 2.485(8) Å).

In the case of **46**, the $[Fe^{III}(TBC[4])]^-$ moieties are capping the metallic core in an analogous manner to that observed in **5**, and in a similarly way to the $[Mn^{III}(TBC[4])]^-$ moiety in **1** and the many other TBC[4]- / BisTBC[4]-supported clusters discussed in the previous chapters (Figure 109).

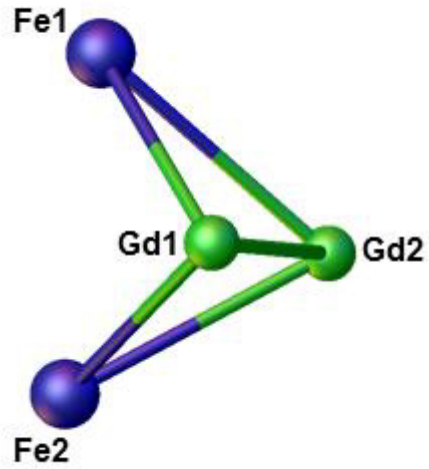

Figure 109. Capping behaviour in the structure of **46**. Capping by $[Fe^{III}(TBC[4])]^-$ moieties are shown as large spheres (Colour code: Fe – dark blue; Gd – green).

Structure expansion reveals that each molecule is close to its neighbour (Figure 110), with the shortest metal-metal intercluster distance occurring between Gd1 and Gd2 (Gd1…Gd2, 8.868 Å) along the *c* axis. Furthermore, the aromatic rings of neighbouring *m*-xylyl spacers are arranged in a *face-to-face* arrangement and are considerably offset with respect to one another; this is visible along the crystallographic *a* axis (Figure 110B). The aromatic

centroid-centroid distance measured is 4.710 Å, which is too long to consider weak π-π interactions,[130] although there is a significant CH-π interaction occurring between these centroids and the hydrogen atom (H74B) located on the benzylic CH_2 (H74B–centroid, 2.771 Å, Figure 110B).

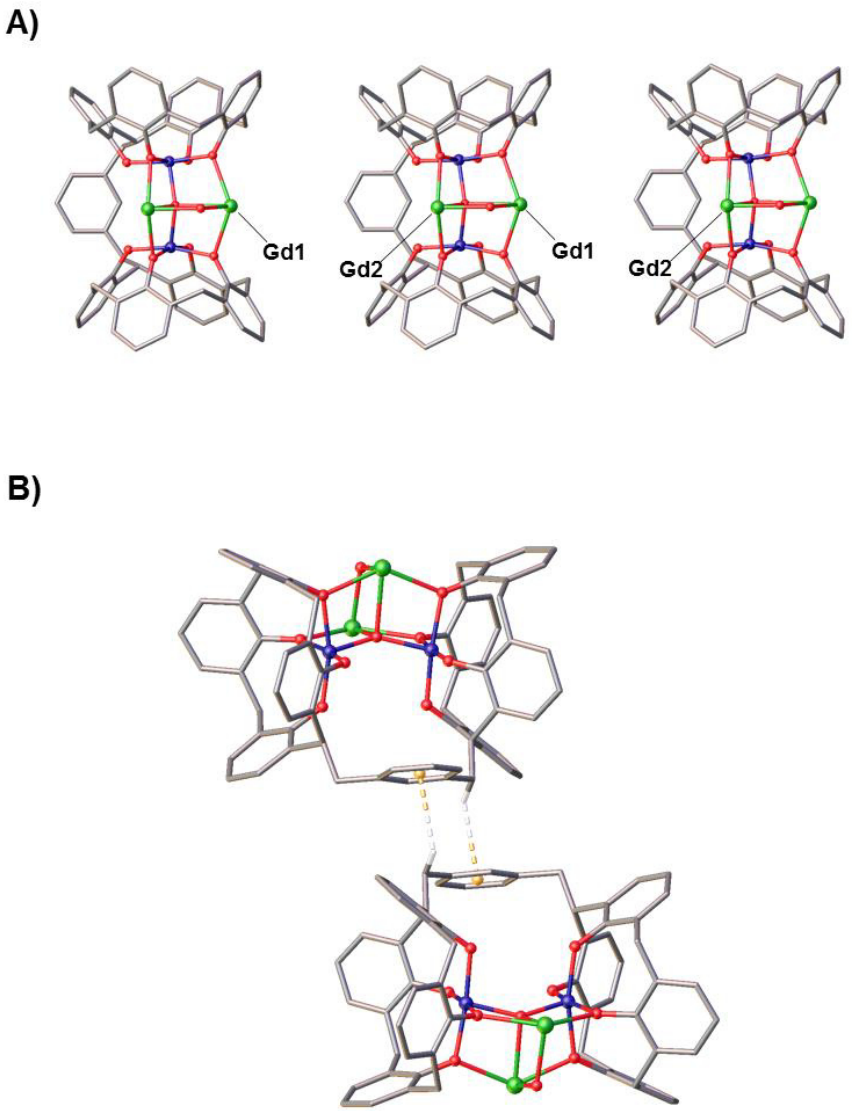

Figure 110. Views of the extended structure of **46**. A) The *ab* plane with the closest ions labelled according to discussion. B) The *bc* plane showing CH-π interactions as dashed lines (Colour code: Fe – dark blue; Ln – green; O – red; C – grey; H – white; Centroid – yellow). ^{t}Bu groups, hydrogen atoms, ligated solvent molecules and solvent of crystallisation omitted for clarity.

5.2.2. $[Mn^{III}_6Mn^{II}Ln^{III}_5(45)_3(\mu_3\text{-}OH)_8(dmf)_8(MeCN)_4(H_2O)_9](OH)_3(H_2O)_{1.5}(dmf)_{16}$, 47.

Analogous conditions were employed in order to synthesise single crystals of a novel series of Mn^{III} / Ln^{III} clusters. These were obtained by reaction of **$H_8$45** with manganese(II) and lanthanide(III) chlorides upon diffusion of MeCN vapours into the dmf / MeOH reaction mixture and were found to have general formula $[Mn^{III}_6Mn^{II}Ln^{III}_5(\mathbf{45})_3(\mu_3\text{-}OH)_8(dmf)_8(MeCN)_4(H_2O)_9](OH)_3(H_2O)_{1.5}(dmf)_{16}$, **47** (Ln = Gd, Tb or Dy, **47Dy** being shown in Figure 111). The crystals were found to be in a monoclinic cell and structure solution was carried out in the space group *C*2/*c*. The structure described is of the Dy derivative (**47Dy**), although the Gd and Tb analogues (**47Gd** and **47Tb** respectively) proved to be isostructural, after having determined the unit cell on single crystals of the compounds.

The ASU is complex and comprises half of the title formula. There are three half molecules of **45,** each accommodating a Mn^{III} cation in the polyphenolic pocket (Mn1–O range 1.881(10) – 2.005(10) Å; Mn2–O range 1.905(9) – 1.982(9) Å; Mn3–O range 1.910(9) – 1.986(11) Å). These Mn^{III} cations are arranged at the corners of a triangle and each has a ligated solvent molecule residing within the TBC[4] cavity (Mn1–N340(MeCN), 2.56(3) Å; Mn2–O30(dmf), 2.369(19) Å; Mn3–N360(MeCN), 2.16(4) Å). The Jahn-Teller axes for these cations are described by the O13–Mn1–N340, O14–Mn2 –O30 and O15–Mn3–N360 vectors, with respective angles of 164.2(11)º, 164.0(6)º and 163.4(16)º. Their coordination spheres are completed by μ_3-hydroxides positioned towards the centre of the aforementioned triangle (Mn1–O13, 2.073(12) Å; Mn2–O14, 2.135(11) Å and Mn3–O15, 2.084(10) Å). The O15 μ_3-hydroxide bridges to two Dy^{III} cations (Dy1 and Dy3), both of which are octacoordinate and in a square antiprismatic geometry (Dy1–O15, 2.406(10) Å and Dy3–O15, 2.378(9) Å). Dy1 is bound to two phenolic oxygens atoms belonging to TBC[4] moieties constituting separate molecules of **45** (Dy1–O3, 2.436(7) Å and Dy1–O10, 2.365(11) Å), three ligated solvent molecules (Dy1–O23(dmf), 2.393(14) Å, Dy1–O24(dmf), 2.396(13) Å and Dy1–O25(H_2O), 2.358(14) Å), and a μ_3-hydroxide (Dy1–O13, 2.374(11) Å). Dy3 has a similar coordination sphere, being bound to the phenolic oxygens O6 and O11 (Dy3–O6, 2.344(9) Å and Dy3–O11, 2.341(10) Å), three ligated solvent molecules (Dy3–O20(H_2O), 2.445(15) Å, Dy3–O21(dmf), 2.464(15) Å and Dy3–O22(H_2O), 2.331(13) Å) and a μ_3-hydroxide (Dy3–O14, 2.378(11) Å).

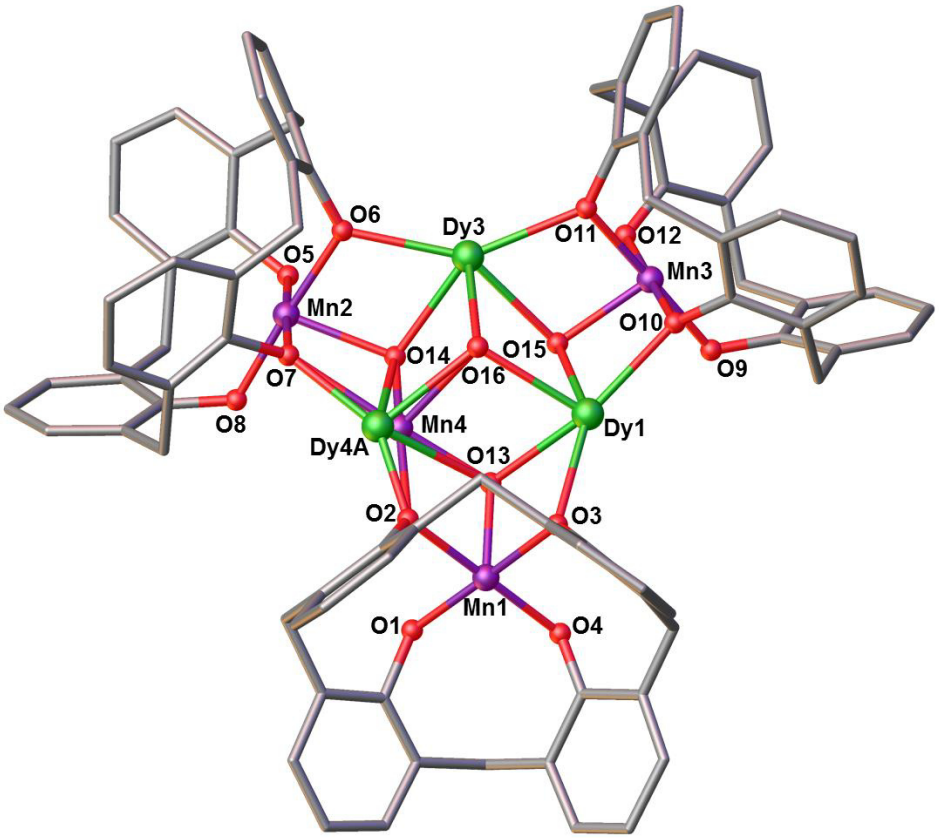

Figure 111. Part of the asymmetric unit of **47Dy** showing the triangular face and selected labels according to discussion (Colour code: Mn – purple; Dy – green; O – red; C – grey). ^{t}Bu groups, hydrogen atoms, ligated solvent molecules and solvent of crystallisation omitted for clarity.

The aforementioned O13 and O14 are also bridging to the last metal binding site which is occupied by disordered Mn^{II} / Dy^{III} ions, that were modelled at half-occupancy in each case (Mn4–O13, 2.003(13) Å; Dy4A–O13, 2.553(12) Å; Mn4–O14, 2.006(12) Å and Dy4A–O14, 2.511(11) Å). Mn4 is in a distorted octahedral geometry and is also bound to two lower-rim phenolic oxygens (Mn4–O2, 2.315(18) Å and Mn4–O7, 2.453(12) Å) and a ligated water molecule (Mn4–O19, 2.24(3) Å). Dy4A, unlike Dy1 and Dy3, is heptacoordinate with a capped trigonal prismatic geometry, and is bound to O2 (Dy4A–O2, 2.039(16) Å), O7 (Dy4A–O7, 2.116(11) Å) and two ligated solvent molecules (Dy4A–O17(dmf), 2.34(2) Å and Dy4A–O19A(H_2O), 2.30(3) Å). The coordination spheres of Dy1, Dy3 and disordered Mn4 / Dy4A are completed by a μ_3-hydroxide located at the centre of the aforementioned triangle (Dy1–O16, 2.399(10) Å; Dy3–O16, 2.387(10) Å; Mn4–O16, 2.241(13) Å, Dy4A–O16, 2.351(10) Å).

Symmetry expansion of the ASU affords the trigonal antiprismatic structure shown in Figure 112 in which the six vertices are defined by a $[Mn^{III}(TBC[4])]^-$ capping moiety, and that originates from the triply helical arrangement of the *p*-xylyl linkers. The cage carries an overall charge of 3+ with disordered counterions providing charge balance; these are located at positions consistent with hydrogen-bonding interactions with ligated water molecules and μ_3-hydroxides. There is diffuse electron density in and around the central cavity of the assembly due to the presence of badly disordered dmf of crystallisation; this could not be modelled appropriately given the severity of the disorder.

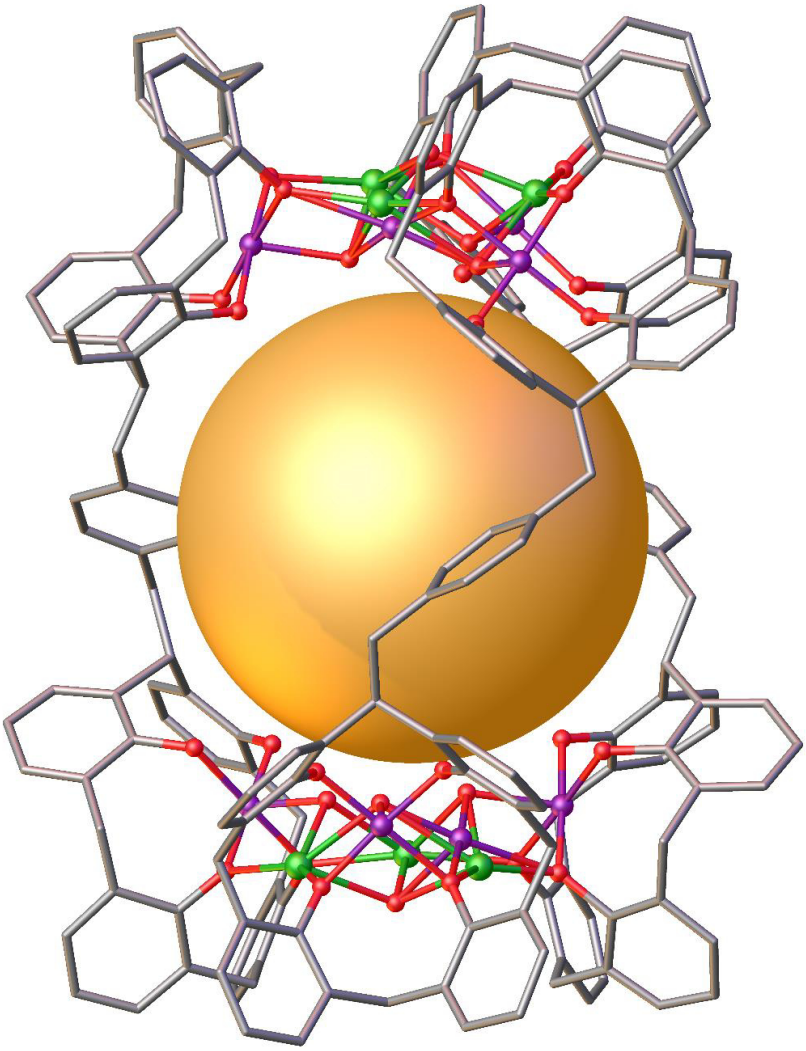

Figure 112. Symmetry-expanded structure of **47Dy** showing the trigonal antiprismatic cage with $[Mn^{III}(TBC[4])]^-$ capping moieties at each vertex. The sphere emphasises the central cavity possessed by **47Dy** (Colour code: Mn – purple; Dy – green; O – red; C – grey). ^{t}Bu groups, hydrogen atoms, ligated solvent molecules and solvent of crystallisation omitted for clarity.

Further symmetry expansion shows that neighbouring assemblies pack in a well-isolated fashion, with no significant interactions occurring between any moieties (Figure 113). The shortest metal-metal intercluster distance was found along the *b* axis, occurring between Mn2 and Dy4A (Mn2…Dy4A, 14.159 Å).

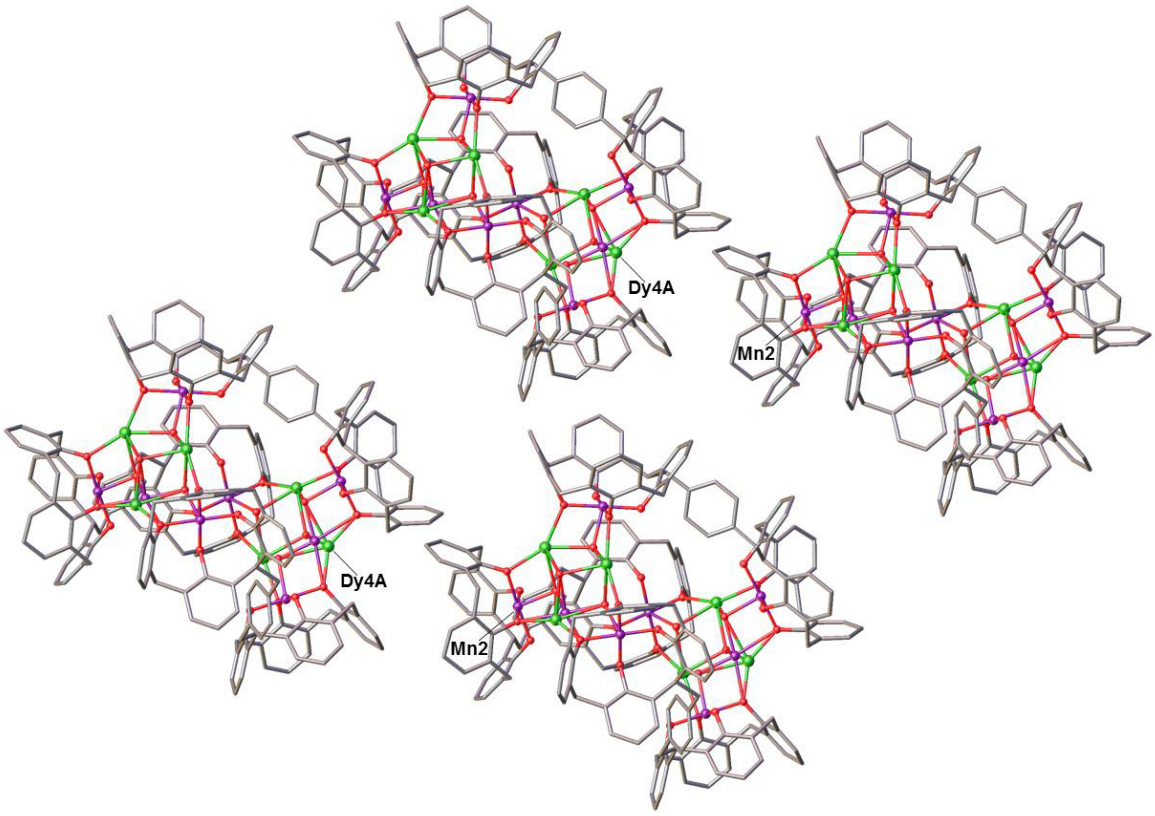

Figure 112. View of the *ac* plane in the extended structure of **47Dy** with the closest ions labelled according to discussion (Colour code: Mn – purple; Dy – green; O – red; C – grey). ^{t}Bu groups, hydrogen atoms, ligated solvent molecules, solvent of crystallisation and anions omitted for clarity.

The presence of disorder within the lattice, coupled with the large intrinsic anisotropy of the Mn^{III} / Ln^{III} ions, prevents accurate interpretation of the magnetic behaviour of **47**. Susceptibility data suggest weak ferromagnetic exchange occurring between the ions constituting the polymetallic core, which is consistent with previously discussed calixarene-based metal clusters, with weak ferromagnetic interaction between the Mn^{III}–Mn^{II} and Mn^{III}–Gd^{III} pairs, whereas the Gd^{III}–Gd^{III} and Mn^{II}–Gd^{III} interactions have been found to be weakly antiferromagnetic. The weak exchange is further validated by low-temperature high-field magnetisation data and ac susceptibility studies, which point towards a SMM behaviour for **47Dy** and **47Tb** but not for **47Gd**.

Given the presence of a cavity in **47**, it was worth investigating desolvation and gas sorption capabilities of this assembly. Since the Gd analogue (**47Gd**) was found to crystallise more rapidly, it was chosen for scale-up to perform this study. Prior to this study, **47Gd** was mildly heated under vacuum and its tolerance towards desolvation was confirmed by PXRD, showing structural integrity. Gas sorption studies were performed on samples of **47Gd** and from the isotherm for nitrogen adsorption it can be stated that **47Gd** has a behaviour indicative of either a non-porous solid or a solid with large pores. An analogous study with H_2 showed faster, relatively good gas uptake (2.7 $mmolg^{-1}$), suggesting an easier pore accessibility for smaller gases (Figure 114). This results suggests that systems such as these may be designed to include tuneable cavities for potentially selective gas uptake, or host-guest exchange that may alter the magnetic response of the host assembly.

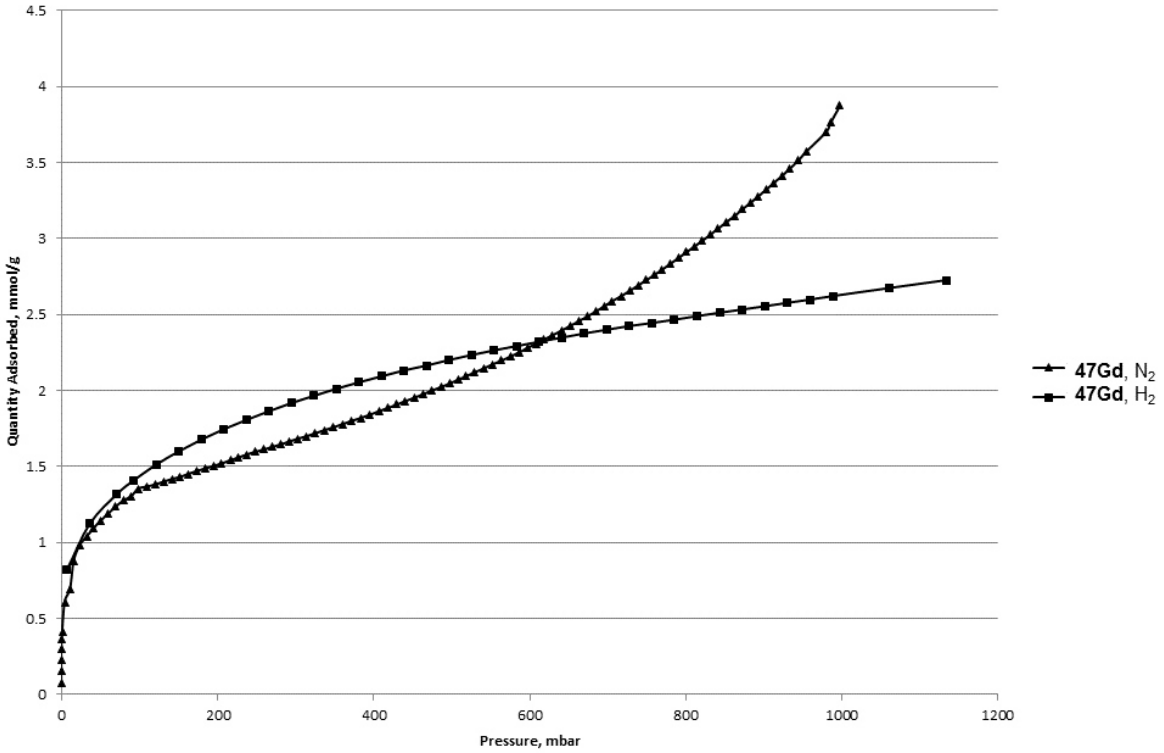

Figure 114. Nitrogen and hydrogen gas sorption isotherms for desolvated **47Gd**.

5.3. Summary.

The use of rigid tethers to connect two H_4TBC[4]s represents one of the most attractive and valuable synthetic routes in order to potentially gain control over cluster formation. Introduction of rigidity in the ligand used in the cluster synthesis can favour, in principle, the obtainment of specific and desired topologies, precluding the formation of others. Moreover, the ease with which tethers that vary in size and chemical properties can be introduced at the methylene bridge offers a vast range of synthetic possibilities for achieving this challenging goal.

The results obtained by employing rigid spacer-tethered biscalix[4]arenes in cluster formation (Table 4) present a plethora of possibilities for future study. In principle, it is possible to synthesise novel ligands characterised by a specific degree of rigidity through accurate selection of the spacer. Taking inspiration from **$H_8$45** and synthesising related ligands, it should be possible to obtain polymetallic clusters that possess the same topology, but that contain cavities of differing shape and size. This would present great opportunities to carry out a broad and interesting study of their related host-guest chemistries.

	Mn^{II}/Mn^{III}	Cu^{II}	Fe^{III}	$Mn^{II/III}/Ln^{III}$	Cu^{II}/Ln^{III}	Fe^{III}/Ln^{III}	Ln^{III}	Cluster no.
$H_8$43	✗	✗	✗	✗	✗	✗	✗	–
$H_8$44	✗	✗	✗	✗	✗	✓	✗	**46**
$H_8$45	✗	✗	✗	✓	✗	✗	✗	**47**

Table 4. Summary of the attempted reactions of rigid spacer-tethered biscalix[4]arenes **$H_8$43 – $H_8$45** with TM and Ln metal ions and relative compound number.

5.4. Experimental.

General procedure for the synthesis of rigid spacer-tethered bis-tetramethoxycalix[4] arenes 40 – 42:

n-BuLi (2.5 M in hexane, 1.5 eq.) was added to a stirred solution of tetramethoxycalix[4]arene (1 eq.) in dry THF (40 mL) under an N_2 atmosphere, causing a rapid colour change from pale yellow to blood red. After ten minutes of stirring the chosen α,α'-dibromoxylene (1.15 eq.), as a solution in 20 mL of dry THF, was added dropwise over 40 minutes, with concomitant change in colour from blood red to yellow. Following addition the reaction mixture was stirred for a further 12 hours before being quenched by addition of H_2O. Volatiles were removed and the resulting solid was dried under vacuum. The crude material was then dissolved in CH_2Cl_2 (300 ml) and washed with brine (3 × 100 ml). The organic layer was separated, dried over $MgSO_4$, and the solvent was removed under reduced pressure to afford a gummy yellow solid that was dried under vacuum. The resulting yellow solid was recrystallised from hot $CHCl_3$/MeOH to afford a white powder of the pure target bis-MeO-C[4]. In all cases ^{1}H NMR spectra of the products are very difficult to interpret due to fluxionality casued by the lower-rim methoxy groups. Although this is the case it was possible to gauge reaction completion for these synthetic intermediates by the disappearance of characteristic OH groups for the TBC[4] lower-rim. These compounds were therefore used in the deprotection step below to afford the target lower-rim hydroxy TBC[4]s **H$_8$43**, **H$_8$44** and **H$_8$45**.

Synthesis of 2,2'-(*o*-xylenyl)bis(5,11,17,23-tetra-*p*-tert-butyl-25,26,27,28-tetramethoxy -calix[4]arene), 40: Reagents used in the general synthesis were 6 g (8.51 mmol) tetramethoxycalix[4]arene **13** in 60 mL dry THF, 5.1 mL (12.77 mmol) *n*-BuLi (2.5 M in hexane) and 1.34 mg (5.08 mmol) α,α'-dibromo-*o*-xylene (96%) in 30 mL dry THF. Yield: 2.82 g (22%).

Synthesis of 2,2'-(*m*-xylenyl)bis(5,11,17,23-tetra-*p*-tert-butyl-25,26,27,28-tetramethoxy-calix[4]arene), 41: Reagents used in the general synthesis were 3 g (4.26 mmol) tetramethoxycalix[4]arene **13** in 40 mL dry THF, 2.55 mL (6.38 mmol) *n*-BuLi (2.5 M in hexane) and 670 mg (2.52 mmol) α,α'-dibromo-*m*-xylene (97%) in 20 mL dry THF. Yield: 2.33 g (36 %).

Synthesis of 2,2'-(*p*-xylenyl)bis(5,11,17,23-tetra-*p*-tert-butyl-25,26,27,28-tetramethoxy-calix[4]arene), 42: Reagents used in the general synthesis were 3 g (4.26 mmol) tetramethoxycalix[4]arene **13** in 40 mL dry THF, 2.55 mL (6.38 mmol) *n*-BuLi (2.5 M in hexane) and 670 mg (2.54 mmol) α,α'-dibromo-*p*-xylene (97%) in 20 mL dry THF. Yield: 2.25 g (35 %).

General procedure for the synthesis of bis-tetrahydroxycalix[4]arenes $H_8$43 – $H_8$45: Cyclohexyl iodide (90 eq.) was added to a dmf (30 mL) solution of the chosen rigid spacer-tethered BisTBC[4]OMe and the resulting mixture was heated at reflux for 48h with a concomitant change in colour from pale yellow to dark orange. The solution was poured into H_2O (250 mL), causing the precipitation of an orange solid. The orange precipitate was collected, was washed several times with water, and stirred in MeOH for 15 minutes to afford a white solid. The white solid was filtered, washed several times with MeOH, collected under reduced pressure and dried under vacuum.

Synthesis of 2,2'-(*o*-xylenyl)bis(5,11,17,23-tetra-*p*-tert-butyl-tetrahydroxycalix[4]arene), $H_8$43: Reagents used in the general synthesis were 2.8 g (1.85 mmol) of **40**, 17.5 g (83 mmol) of cyclohexyl iodide in 50 mL of dmf. Purification by chromatography column ($CHCl_3$/Hex 1:1 → EtOAc) afforded 1.104 g of pure product (Yield: 42.6%). ^{1}H NMR ($CDCl_3$): 10.31 (s, 8H, -OH), 7.34-6.81 (m, 20H, ArH + ArH core), 5.14 (t, 2H, $^3J_{HH}$ = 7.34 Hz, Ar-C<u>H</u>-CH2Ph-), 4.32-4.17 (m, 6H Ar-C<u>H</u>$_2$-Ar), 3.55-3.44 (m, 6H Ar-C<u>H</u>$_2$-Ar), 1.57 (s, 4H, Ar-CH-C<u>H</u>$_2$-Ph), 1.24 (s, 36H, -C(C<u>H</u>$_3$)$_3$), 1.24 (s, 36H, -C(C<u>H</u>$_3$)$_3$). ^{13}C NMR ($CDCl_3$):146.8, 144.2,139.5, 130.9, 127.8, 127.2, 125.94, 125.3, 122.07, 35.6, 34.2, 34.05, 32.8, 31.5. MS calcd. for $C_{96}H_{118}O_8$ (1399.04); found: 1417.9 $(M+NH_4)^+$.

Synthesis of 2,2'-(*m*-xylenyl)bis(5,11,17,23-tetra-*p*-tert-butyl-tetrahydroxycalix[4]arene), $H_8$44: Reagents used in the general synthesis were 2.28 g (1.51 mmol) of **41**, 28.5 g (135.5 mmol) of cyclohexyl iodide in 30 mL of dmf. Purification by chromatography column ($CHCl_3$/Hex 1:1 → EtOAc) afforded 1.52 g of pure product (Yield: 72 %). ^{1}H NMR ($CDCl_3$): 10.29 (s, 8H, -OH), 7.19-6.94 (m, 20H, ArH + ArH core), 4.87 (t, 2H, $^3J_{HH}$ = 8.07 Hz, Ar-C<u>H</u>-CH$_2$Ph-), 4.32-4.22 (m, 6H Ar-C<u>H</u>$_2$-Ar), 3.55-3.43 (m, 6H, Ph-C<u>H</u>$_2$-CH-Ar), 1.57 (s, 4H, Ar-CH-C<u>H</u>$_2$-Ph), 1.26 (s, 36H, -C(C<u>H</u>$_3$)$_3$), 1.25 (s, 36H, -C(C<u>H</u>$_3$)$_3$). ^{13}C NMR ($CDCl_3$):146.8, 144.2,139.5, 130.6, 127.7, 127.3, 125.97, 125.3, 122.2, 37.0, 34.2, 34.05, 32.8, 31.5. MS calcd. for $C_{96}H_{118}O_8$ (1399.04); found: 1417.9 $(M+NH_4)^+$.

Synthesis of 2,2'-(*p*-xylenyl)bis(5,11,17,23-tetra-*p*-tert-butyl-tetrahydroxycalix[4]arene), $H_8$45: Reagents used in the general synthesis were 2.23 g (1.47 mmol) of **42**, 27.8 g (132.5 mmol) of cyclohexyl iodide in 30 mL of dmf. Purification by chromatography column ($CHCl_3$/Hex 1:1 → EtOAc) afforded 0.6 g of pure product (Yield: 29 %). ^{1}H NMR ($CDCl_3$): 10.26 (s, 8H, -OH), 7.29-6.94 (m, 20H, ArH + ArH core), 4.87 (t, 2H, $^3J_{HH}$ = 7.6 Hz, Ar-C<u>H</u>-CH_2Ph-), 4.30-4.17 (m, 6H Ar-C<u>H_2</u>-Ar), 3.52-3.40 (m, 4H, Ph-C<u>H_2</u>-CH-Ar), 1.59 (s, 4H, Ar-CH-C<u>H_2</u>-Ph), 1.23 (s, 36H, -C(C<u>H_3</u>)$_3$), 1.21 (s, 36H, -C(C<u>H_3</u>)$_3$). ^{13}C NMR ($CDCl_3$):146.7, 144.2, 130.6, 128.8, 127.8, 127.2, 125.9, 125.2, 122.2, 37.9, 34.2, 34.02, 32.8, 31.4. MS calcd. for $C_{96}H_{118}O_8$ (1399.04); found: 1417.9 $(M+NH_4)^+$. **Crystal data for 45**: $C_{106}H_{130}N_5O_8$, M = 1602.24, Colourless Block, 0.45 x 0.03 x 0.01 mm^3, monoclinic, space group C2/c (No. 15), a = 12.3380(19), b = 24.1569(7), c = 24.156972) Å, β = 114.137(2)°, V = 9410.8(5) Å^3, Z = 4, Bruker D8 diffractometer with PHOTON 100 detector, synchrotron radiation, λ = 0.7749 Å, T = 100(15)K, $2\theta_{max}$ = 46.7°, 25922 reflections collected, 5273 unique (R_{int} = 0.0554). Final *GooF* = 1.211, R_1 = 0.0584, wR_2 = 0.1660, R indices based on 5273 reflections with I >2sigma(I) (refinement on F^2).

Synthesis of $[Fe^{III}_2Gd^{III}_2$(44)(μ$_4$-O)(μ-OH)(dmf)$_7$(MeOH)(H_2O)$_2$][$H_7$44](dmf)$_{0.5}$(H_2O)$_{1.5}$, 46.

m-xylyl-BisTBC[4] **$H_8$44** (50 mg, 0.0357 mmol), $Fe(NO_3)_3 \cdot 9H_2O$ (14.4 mg, 0.0357 mmol, 1 eq.), $Gd(NO_3)_3 \cdot 6H_2O$ (64.5 mg, 0.14 mmol, 4 eq.) were dissolved in a 1:1 dmf / MeOH mixture (20 mL). After 10 minutes of stirring Et_3N (0.05 mL) was added and the resulting deep purple solution stirred for 2 hrs. The reaction mixture was filtered to leave a dark brown solution. Dark brown crystals of **46** were grown upon vapour diffusion in PET.

Elemental Analysis (%) calculated for **46**, $C_{164.5}H_{229.5}Fe_2Gd_2N_{6.5}O_{27}$ (M = 3165.25.38): C, 62.6%; H, 7.33%; N, 2.88%. Found: C, 59.97%; H, 6.92%; N, 2.34%. **Yield** 18 mg (16 %).

Crystal data for 46: $C_{164.50}H_{229.50}Fe_2Gd_2N_{6.50}O_{27}$, M = 3156.25, Brown Block, 0.40 x 0.40 x 0.30 mm^3, triclinic, space group P-1 (No. 2), a = 12.438(18), b = 24.30(5), c = 31.27(7) Å, α = 77.96(10), β = 89.27(7), γ = 77.15(2)°, V = 9004(30) Å^3, Z = 2, Bruker X8 Apex II CCD Diffractometer, MoKα radiation (λ = 0.71073 Å), T = 100(2)K, $2\theta_{max}$ = 45.8°, 89845 reflections collected, 23767 unique (R_{int} = 0.0526). Final *GooF* = 1.080, R_1 = 0.0898, wR_2 = 0.2365, R indices based on 16406 reflections with I >2sigma(I) (refinement on F^2).

$[Mn^{III}_6Mn^{II}Ln^{III}_5(45)_3(\mu_3\text{-}OH)_8(dmf)_8(MeCN)_4(H_2O)_9](OH)_3(H_2O)_{1.5}(dmf)_{16}$, 47.

$Mn^{III}_6Mn^{II}Gd^{III}_5$, 47Gd: *p*-xylylBisTBC[4] **$H_8$45** (50 mg, 0.0357 mmol), $MnCl_2{\cdot}4H_2O$ (14.1 mg, 0.071 mmol, 2 eq), $GdCl_3{\cdot}6H_2O$ (9.4 mg, 0.0357 mmol, 1 eq.) were dissolved in a 1:1 dmf / MeOH mixture (20 mL). After 10 minutes of stirring Et_3N (0.05 mL) was added and the resulting deep purple solution stirred for 2 hrs. The reaction mixture was filtered to leave a deep purple solution. Elemental Analysis (%) calculated for **47Gd**, $C_{368}H_{542}Gd_5Mn_7N_{28}O_{69.50}$ (M = 7641.38): C, 57.84%; H, 7.15%; N, 5.13%. Found: C, 57.22%; H, 6.92%; N, 5.01%. **Yield** 38 mg (12.8 %).

$Mn^{III}_6Mn^{II}Dy^{III}_5$, 47Dy: *p*-xylylBisTBC[4] **$H_8$45** (50 mg, 0.0357 mmol), $MnCl_2{\cdot}4H_2O$ (14.1 mg, 0.071 mmol, 2 eq), $DyCl_3{\cdot}6H_2O$ (13.46 mg, 0.0357 mmol, 1 eq.) were dissolved in a 1:1 dmf / MeOH mixture (20 mL). After 10 minutes of stirring Et_3N (0.05 mL) was added and the resulting deep purple solution stirred for 2 hrs. The reaction mixture was filtered to leave a deep purple solution. Purple crystals of **47Dy** were grown upon vapour diffusion in MeCN. Elemental Analysis (%) calculated for **47Dy**, $C_{368}H_{542}Dy_5Mn_7N_{28}O_{69.50}$ (M = 7667.38): C, 57.65%; H, 7.13%; N, 5.11%. Found: C, 57.48%; H, 6.74%; N, 4.72%. **Yield** 25 mg (9.1 %). **Crystal data for 47Dy:** $C_{368}H_{542}Dy_5Mn_7N_{28}O_{69.50}$, M = 7667.38, Purple Block, 0.17 × 0.15 × 0.04 mm^3, monoclinic, space group $C2/c$ (No. 15), a = 36.4100(14), b = 23.3869(9), c = 47.4803(18) Å, β = 103.040(3)°, V = 39388(3) $Å^3$, Z = 4, Bruker X8 Apex II CCD Diffractometer, synchrotron radiation (λ = 0.88560 Å), T = 100(2)K, $2\theta_{max}$ = 53.9°, 152258 reflections collected, 22023 unique (R_{int} = 0.0665). Final *GooF* = 1.080, R_1 = 0.1134, wR_2 = 0.2970, R indices based on 16135 reflections with I >2sigma(I) (refinement on F^2).

$Mn^{III}_6Mn^{II}Tb^{III}_5$, 47Tb: *p*-xylylBisTBC[4] **$H_8$45** (50 mg, 0.0357 mmol), $MnCl_2{\cdot}4H_2O$ (14.1 mg, 0.071 mmol, 2 eq), $TbCl_3{\cdot}6H_2O$ (13.3 mg, 0.0357 mmol, 1 eq.) were dissolved in a 1:1 dmf / MeOH mixture (20 mL). After 10 minutes of stirring Et_3N (0.05 mL) was added and the resulting deep purple solution stirred for 2 hrs. The reaction mixture was filtered to leave a deep purple solution. Elemental Analysis (%) calculated for **47Tb**, $C_{368}H_{542}Tb_5Mn_7N_{28}O_{69.50}$ (M = 7648.76): C, 57.78%; H, 7.14%; N, 5.13%. Found: C, 57.15%; H, 6.83%; N, 4.98%. **Yield** 29 mg (10 %).

Chapter 6: Conclusions

The immense body of work carried out by many scientists over the past century unveiled many of the secrets surrounding the "resinous material" first synthesised by von Baeyer in 1872. Thanks to these efforts the modern day chemist has the possibility of synthesising a calixarene of any chosen ring size in relatively high yield under optimal reaction conditions and, in many cases, without any side product(s). Amongst others, Gutsche's contribution to calixarene chemistry was of primary importance. With a deeper understanding of the nature of the reaction occurring between phenols and formaldehyde derivatives, along with the creation of common as well as systematic nomenclature, he brought calixarenes to a prominent position in supramolecular chemistry. Gutsche's contributions provided other researchers the ability to undertake full studies concerning the wide-ranging structures and properties of calixarenes, all of which was accomplished by the use of many analytical techniques (NMR, IR, SCXRD, MS etc.), thus contributing to the growing interest in this class of macrocycle. These contributions were not only limited to the classical calixarenes, but also to a plethora of other macrocycles which, even though in many cases are only marginally related in structure, possess different and peculiar physical and chemical properties.

The family of calix[*n*]arenes now represents a valuable and versatile series of molecules that have potential applications in a vast number of fields. This is not only due to the inherent features of the macrocycles, *viz.* the presence of a cavity and phenolic oxygens atoms at the lower-rim, but also to the practically infinite number of synthetic modifications that can be performed around the macrocyclic framework. These represent a way for the chemist to opportunely tune calixarene scaffolds, introducing targeted structural features of interest and rendering them useful for applications such as sensors, complexing agents, enzyme mimics, optoelectronics etc., either in solution or in the solid state. The possibility of functionalisation of the calixarene methylene bridge, studied chiefly by Biali and co-workers, represents another attractive tool for one to decorate the calixarene scaffold with additional functionalities that are oriented perpendicular to the bowl of the macrocycle. Although these reactions are not usually as straightforward as those involving the upper- and lower-rims, they offer another viable route to obtain new derivatives, many of which featuring peculiar physical properties that are otherwise unachievable.

The Fantini group made an important contribution to functionalisation at the methylene bridge with the introduction of simple synthetic strategies to introduce a variety

of functional groups at the equatorial position. Furthermore, the synthesis of 2,2'-biscalix[4]arene, in which the two TBC[4] moieties are directly linked *via* the methylene bridge, was a novel addition to calixarene family, and is a ligand that was used widely in this doctoral study. The growing interest towards molecular assemblies that display magnetic behaviour that can be used for data storage, as well as the possibility of employing these magnetic properties to obtain sub-milliKelvin temperatures through exploitation of the magnetocaloric effect, pushed a number of researchers into the synthesis of polymetallic clusters comprising a ligand, being either a small molecule or a macrocycle, and a mixture of TM and Ln ions. Calix[4]arenes are excellent candidates for the synthesis of polymetallic clusters thanks to the presence of the lower-rim polyphenolic pocket (that is of the appropriate size for the complexation of a metal ion in an *exo* fashion) and their ability to bridge metal ions. In this respect, many tri- and tetranuclear clusters have been synthesised using sulphur-containing calix[4]arene derivatives belonging to the family of heteracalixarenes. Thia-, sulfinyl and sulfonycalix[4]arenes have afforded interesting metal clusters in which the metal cations are not exclusively bound to the lower-rim oxygen atoms, but also to the groups at the methylene bridge containing groups such as S, SO and SO_2. Interest in such clusters is not only limited to coordination chemistry and magnetic properties, but further expands to the synthesis of stable metal-organic polyhedra (MOP), formed thanks to the cooperativity between the aforementioned polymetallic units and topologically directing co-ligands.

The Dalgarno and Brechin groups have collaboratively studied the coordination chemistry of methylene-bridge calix[4]arenes, resulting in the characterisation of a library of new 3*d*, 4*f* and 3*d* / 4*f* TBC[4]-supported metal clusters. Although these clusters are disparate with respect to the nature, composition and topology of the polymetallic core, there are clear structural trends that have allowed for the establishment of empirical metal ion binding rules that, to some extent, can help 'predict' the composition and topology of an assembly prior to synthesis. TM^{II} / TM^{III} ions are bound in the TBC[4] lower-rim coordination site to produce $[TM(TBC[4])]^{-/2-}$ capping moieties, whereas Ln^{III} cations show similar behaviour, through the formation of $[Ln(TBC[4])]^{-}$ capping moieties; this only occurs in the absence of TM ions. In the cases of reactions involving 3*d* / 4*f* mixtures, the TM ions are preferentially bound by the TBC[4] but Ln ions are incorporated within the polymetallic core. The outcome of cluster forming reactions can vary depending on the conditions, stoichiometries, crystallisation method and solvent employed, but these structural trends are persistent throughout. Analysis of core topologies shows that for all

TBC[4]-supported metal clusters documented to date, the metal centres are linked by a variety of bridging groups, forming 3D assemblies with edges or faces capped by the aforementioned $[TM(TBC[4])]^{-/2-}$ / $[Ln(TBC[4])]^{-}$ moieties. Exploration of the coordination chemistry of BisTBC[4] has yielded several new polymetallic clusters in which the ligand behaves as expected when considering the aforementioned binding rules for TBC[4]. Upon complexation BisTBC[4] undergoes conformational inversion from *syn*- to *anti*-, with the two cavities pointing in the same direction as a result. In this way it is possible to identify two different binding sites or modes: Type I, corresponding to the tetraphenolic moiety in which the cations are residing, and Type II in which the metal ions reside in the binding sites generated by inversion of the ligand. All BisTBC[4]-supported metal clusters show a clear structural relation to their TBC[4]-supported analogues, with an obvious 'enhancement' in both nuclearity and capping behaviour, suggesting that the binding rules established for TBC[4] can indeed be extended to include BisTBC[4].

The versatility of BisTBC[4] as a ligand has been further explored by facilitating ion interchange upon variation of reaction stoichiometry, in a similar fashion to that performed with TBC[4]. This results in the synthesis of novel clusters with enhanced nuclearity, representing "expansion" of the related BisTBC[4] clusters synthesised under standard conditions. The library of BisTBC[4]-supported clusters has been further expanded by exploration of the coordination chemistry when BisTBC[4] is reacted with $TM^{II/III}$ / Ln^{III} ions in the presence of a selection of *N*,*O*–bi- and tridentate ligands (that are well known to form polymetallic clusters). The outcome of this study was the obtainment of a series of hybrid clusters in which the main coordination features of BisTBC[4] are retained, but with higher nuclearity thanks to additional cations being bound and incorporated through the competing co-ligands. In many cases these new clusters contain a greater number of metal ions and have topologies that are otherwise unobtainable when just BisTBC[4] is employed as a ligand. This is due to complementarity between BisTBC[4] and the co-ligands employed, which work in tandem to afford these larger 'expanded' assemblies. In other cases the competitive nature of such co-ligands is more prominent, resulting in the occupation of binding sites that would otherwise have resulted in known cluster topologies. Overall, the co-ligand approach is another tool available to the chemist in order to design, direct and, ultimately, control the composition and the topology of the metallic assembly.

Another viable route in order to control cluster topology and composition is to link TBC[4] moieties together with organic spacers of differing chemical makeup. The start of this exploration is presented in Chapter 4, with the synthesis of a series of alkyl chain-

tethered biscalix[4]arenes and their exploratory coordination chemistry. From these studies it is possible to state that the introduction of tethers at the methylene bridge has very little effect on the geometry of the resulting metal clusters, which retain a topology obtained using just TBC[4], as long as the alkyl chain is long enough to provide the flexibility necessary to form known assemblies. This result is further corroborated by the fact that no clusters were isolated for alkyl chain-tethered biscalix[4]arenes possessing an alkyl chain shorter than eight carbon atoms, suggesting that these ligands would introduce too large a strain on the the polymetallic core. At the same time, it is also plausible that shorter alkyl chain tethers give rise to species with different topologies and metal composition that may require an alternative synthetic strategy in order to isolate suitable crystals for diffraction purposes.

Given the above, analogous coordination chemistry was explored using systems with a higher degree of rigidity. The use of rigid tethers is, in fact, a logical synthetic strategy that allows one to control / direct cluster formation. The synthesis of three new xylyl-spaced BisTBC[4]s is presented in Chapter 5, along with DFT calculations showing the main features of these ligands and their potential behaviour when coordinating to metal ions. Examination of the calculated structures suggested that the TBC[4] units in two of the three ligands are oriented in a convergent fashion whereas they are divergent in the third. Only one cluster was obtained with *m*-xylylBisTBC[4], which is likely due to rigidity of the *meta* xylyl spacer that does not allow the formation of any butterfly-like topology; this result was expected when considering the outcome of the DFT calculations performed by Paterson and co-workers. The divergent nature of the *p*-xylylBisTBC[4] precludes the formation of any known topology, but led to the isolation of a spectacular triply helical 3*d* / 4*f* trigonal antiprism in which the six vertices of the MOP are occupied by $[Mn^{III}(TBC[4])]^-$ capping moieties. Given the presence of a cavity within the MOP, the system was tested for its gas sorption properties, showing it to be capable for the uptake of small quantities of N_2 and H_2; this result represents a proof of principle for the design and assembly of more elaborate MOPs through linker modification.

From the results discussed throughout this thesis it is clear that TBC[4]-supported cluster synthesis is a growing area of supramolecular coordination chemistry. The TBC[4]-supported metal clusters synthesised through our group's collaborative efforts with Brechin and co-workers has formed the foundation on which this work has been built. The composition, topology and properties of the polymetallic clusters formed clearly demonstrate that BisTBC[4] follows the binding rules established for TBC[4] due to direct linking at the methylene bridge. It is possible to tune and direct cluster formation through

stoichiometric control, the use of competitive and complementary co-ligands, or through the introduction of TBC[4] tethers that are either flexible or rigid in nature. This study is far from complete, as the results presented here have opened up many avenues for further investigation. These will form the basis of future work in this area, but importantly, stem from the ease with which TBC[4] and its derivatives can be further functionalised, in addition to the use of alternative co-ligands. All of the principles established so far can also be applied to the larger calixarenes which themselves have different coordination preferences. The ultimate goal of this combined body of work will be for the chemist to have the power to control and predictably assemble highly complex, multi-component systems that have tailored physical properties.

Appendix

Crystallographic tables for compounds 16Tb – 17Gd.

Compound number	**16Tb**	**17Gd**
Formula	$C_{215}H_{308}N_{14}O_{45}Cu_4Tb_5$	$C_{200}H_{274}N_{10}O_{41}Fe_5Gd_4$
*M*r	4857.50	4382.53
Crystal system	Monoclinic	Triclinic
Space group	$P2_1/n$	P-1
T / K	100(2)	100(2)
a / Å	19.0415(7)	16.926(2)
b / Å	55.063(2)	19.634(2)
c / Å	25.3349(9)	20.203(2)
α / °	90	114.498(2)
β / °	97.974(2)	98.345(2)
γ / °	90	99.663(2)
U / Å^3	26306.3(17)	5847.7(11)
Z	4	1
F(000)	9988	2258
D_c / g cm^{-3}	1.226	1.240
μ / mm^{-1}	2.130	1.857
$2\Theta_{max}$ / °	48.34	58
Data collected	475295	65628
Unique reflections	32357	23888
R_{int}	0.0986	0.0597
Obs data ($I > 2\sigma > (I)$)	25737	15711
Parameters	2219	1095
Restraints	123	165
R_1 (observed data)	0.0706	0.0766
ωR_2 (all data)	0.1635	0.2657
GooF	1.049	1.041
Max/min residuals [eÅ^3]	2.04 / -1.91	1.75 / -1.89

Crystallographic tables for compounds 18 – 19Gd.

Compound number	**18**	**19Gd**
Formula	$C_{216}H_{310}N_{12}O_{40}Mn_{10}$	$C_{206}H_{280}N_{10}O_{44}Mn_8Gd_2$
*M*r	4264.14	4354.40
Crystal system	Triclinic	Monoclinic
Space group	*P*-1	$P2_1/n$
T / K	100(2)	100(2)
a / Å	14.9101(5)	22.0960(7)
b / Å	17.9438(5)	19.1570(6)
c / Å	22.3792(7)	27.0764(9)
α / °	69.512(2)	90
β / °	75.796(2)	105.149(2)
γ / °	81.501(2)	90
U / Å^3	5424.6(3)	11063.0(6)
Z	1	2
F(000)	2260	4352
D_c / g cm^{-3}	1.305	1.307
μ / mm^{-1}	0.801	1.383
$2\Theta_{max}$ / °	48.252	59.772
Data collected	54412	136715
Unique reflections	13284	24604
R_{int}	0.0696	0.0542
Obs data ($I > 2\sigma > (I)$)	9258	18689
Parameters	1194	1208
Restraints	68	72
R_1 (observed data)	0.0762	0.0834
ωR_2 (all data)	0.2297	0.2740
GooF	1.045	1.077
Max/min residuals [eÅ^3]	1.23 / -1.74	1.64 / -1.98

Crystallographic tables for compounds 20Gd – 25Gd.

Compound number	**20Gd**	**25Gd**
Formula	$C_{209}H_{290}N_{10}O_{41}Mn_4Gd_4$	$C_{116}H_{151}N_7O_{16}Mn_2Gd$
*M*r	4447.44	2166.6
Crystal system	Monoclinic	Tetragonal
Space group	$P2_1/n$	$P4_12_12$
T / K	100(2)	100(2)
a / Å	17.7206(8)	23.2275(8)
b / Å	41.6212(17)	23.2275(8)
c / Å	33.0584(14)	44.2459(18)
α / °	90	90
β / °	102.014(2)	90
γ / °	90	90
U / Å^3	23848.3(18)	23871.4(19)
Z	4	8
F(000)	9388	9104
D_c / g cm^{-3}	1.270	1.206
μ / mm^{-1}	1.713	1.023
$2\Theta_{max}$ / °	54.448	48.852
Data collected	295606	151805
Unique reflections	40784	15095
R_{int}	0.0793	0.0531
Obs data ($I > 2\sigma > (I)$)	29236	12817
Parameters	2283	1057
Restraints	153	87
R_1 (observed data)	0.0842	0.0653
ωR_2 (all data)	0.2189	0.1718
GooF	1.203	1.033
Max/min residuals [eÅ^3]	3.27 / -2.54	1.01 / -0.96

Crystallographic tables for compounds 26 – 27.

Compound number	**26**	**27**
Formula	$C_{322}H_{418}N_{14}O_{48}Mn_{14}$	$C_{342}H_{509}N_{25}O_{68}Cu_{16}$
*M*r	6022.12	7075.73
Crystal system	Monoclinic	Triclinic
Space group	*C*2/*c*	*P*-1
T / K	100(2)	100(2)
a / Å	59.816(8)	21.4369(9)
b / Å	18.706(2)	21.9078(9)
c / Å	30.329(4)	22.0660(9)
α / °	90	105.596(3)
β / °	104.498(3)	111.468(2)
γ / °	90	95.527(3)
U / Å^3	32856(7)	9067(7)
Z	4	1
F(000)	11560	5814.0
D_c / g cm^{-3}	1.103	2.225
μ / mm^{-1}	0.590	8.353
$2\Theta_{max}$ / °	37.904	47.784
Data collected	33347	56658
Unique reflections	12916	21631
R_{int}	0.1430	0.0704
Obs data ($I > 2\sigma > (I)$)	6061	14908
Parameters	894	1644
Restraints	176	214
R_1 (observed data)	0.0990	0.0897
ωR_2 (all data)	0.2279	0.2790
GooF	0.927	1.029
Max/min residuals [eÅ^3]	0.68 / -0.81	2.00 / -1.31

Crystallographic tables for compounds 28Gd – 29.

Compound number	**28Gd**	**29**
Formula	$C_{163}H_{231}Cl_2N_7O_{26}Mn_4Gd_2$	$C_{108}H_{147}N_7O_{15}Mn_4$
*M*r	3309.85	2003.17
Crystal system	Triclinic	Monoclinic
Space group	*P*-1	$P2_1/m$
T / K	100(2)	100(2)
a / Å	21.3197(12)	13.8645(6)
b / Å	22.0763(12)	23.1636(9)
c / Å	27.1434(14)	17.4875(7)
α / °	75.597(3)	90
β / °	79.680(3)	107.315(2)
γ / °	61.784(3)	90
U / Å^3	10875.1(11)	5361.6(4)
Z	2	2
F(000)	3494.0	2128.0
D_c / g cm^{-3}	1.023	1.241
μ / mm^{-1}	1.131	0.657
$2\Theta_{max}$ / °	54.558	51.032
Data collected	114774	7904
Unique reflections	36242	7904
R_{int}	0.0610	0.0375
Obs data ($I > 2\sigma > (I)$)	24613	6691
Parameters	1632	593
Restraints	175	11
R_1 (observed data)	0.0680	0.0820
ωR_2 (all data)	0.1978	0.2279
GooF	1.043	1.038
Max/min residuals [eÅ^3]	2.65 / -1.90	1.24 / 1.06

Crystallographic tables for compounds 30 – H8341C3.

Compound number	**30**	**H8341C3**
Formula	$C_{236}H_{348}Cl_6N_{18}O_{56}Mn_{20}$	$C_{99}H_{128}N_4O_8$
*M*r	5644.97	1502.05
Crystal system	Monoclinic	Monoclinic
Space group	*C*2/*c*	$P2_1/c$
T / K	100(2)	100(2)
a / Å	18.3953(7)	19.3316(19)
b / Å	45.6912(18)	25.164(2)
c / Å	40.7908(16)	19.117(2)
α / °	90	90
β / °	99.212(2)	105.346(6)
γ / °	90	90
U / Å^3	33843(2)	8968
Z	4	4
F(000)	11664.0	3256.0
D_c / g cm^{-3}	1.104	1.112
μ / mm^{-1}	1.042	0.069
$2\Theta_{max}$ / °	58.238	46.64
Data collected	165158	58266
Unique reflections	34903	12880
R_{int}	0.0608	0.1318
Obs data ($I > 2\sigma > (I)$)	25904	4011
Parameters	1356	1002
Restraints	108	86
R_1 (observed data)	0.0834	0.0979
ωR_2 (all data)	0.2335	0.2709
GooF	1.075	1.211
Max/min residuals [eÅ^3]	2.36 / -1.45	0.43 / -0.50

Crystallographic tables for compounds 35 – 36.

Compound number	**35**	**36**
Formula	$C_{113}H_{165.5}N_{5.5}O_{18.5}Mn_4$	$C_{117}H_{176}N_6O_{20}Mn_4$
*M*r	2116.76	2206.39
Crystal system	Monoclinic	Triclinic
Space group	$P2_1/c$	P-1
T / K	100(2)	100(2)
a / Å	25.1565(8)	12.375(3)
b / Å	20.0930(6)	18.727(4)
c / Å	22.7572(7)	25.238(5)
α / °	90	84.03(3)
β / °	97.681(2)	88.68(3)
γ / °	90	89.00(3)
U / Å^3	11399(6)	5815(2)
Z	4	2
F(000)	4520.0	2360.0
D_c / g cm^{-3}	1.233	1.260
μ / mm^{-1}	0.624	0.492
$2\Theta_{max}$ / °	41.482	41.064
Data collected	65220	42921
Unique reflections	8958	11547
R_{int}	0.1114	0.1056
Obs data ($I > 2\sigma > (I)$)	6660	5861
Parameters	918	1197
Restraints	150	66
R_1 (observed data)	1.210	0.963
ωR_2 (all data)	0.3218	0.3351
GooF	1.102	1.077
Max/min residuals [eÅ^3]	1.21 / -0.86	1.10 / -0.99

Crystallographic tables for compounds 37 – 38.

Compound number	**37**	**38**
Formula	$C_{236}H_{356}N_{12}O_{48}Mn_4Gd_4$	$C_{121}H_{181.5}N_{7.5}O_{19.5}Mn_4$
*M*r	4978.07	2272.99
Crystal system	Triclinic	Triclinic
Space group	*P*-1	*P*-1
T / K	153(2)	100(2)
a / Å	14.9707(7)	12.7808(5)
b / Å	21.9372(6)	19.2134(8)
c / Å	22.0011(6)	27.4523(12)
α / °	113.205(3)	74.294(2)
β / °	93.322(3)	82.588(3)
γ / °	107.520(3)	85.413(2)
U / Å^3	6203.1(4)	6428(5)
Z	1	2
F(000)	2596.0	2432.0
D_c / g cm^{-3}	1.333	1.174
μ / mm^{-1}	8.972	0.563
$2\Theta_{max}$ / °	153.614	62.362
Data collected	121039	98239
Unique reflections	25512	31909
R_{int}	0.1112	0.0399
Obs data ($I > 2\sigma > (I)$)	16342	19927
Parameters	1293	1348
Restraints	148	97
R_1 (observed data)	0.0855	0.0914
ωR_2 (all data)	0.2659	0.3188
GooF	1.039	1.024
Max/min residuals [eÅ^3]	4.51 / -1.72	2.00 / -1.21

Crystallographic tables for compounds H845 – 46.

Compound number	**H8**45	**46**
Formula	$C_{106}H_{130}N_5O_8$	$C_{164.5}H_{229.5}N_{6.5}O_{27}Fe_2Gd_2$
*M*r	1602.24	3156.25
Crystal system	Monoclinic	Triclinic
Space group	*C*2/*c*	*P*-1
T / K	100(2)	100(2)
a / Å	34.5999(10)	12.438(12)
b / Å	12.3380(4)	24.30(5)
c / Å	24.1569(7)	31.27(7)
α / °	90	77.96(10)
β / °	114.137(2)	89.27(7)
γ / °	90	77.15(2)
U / Å^3	9410.8(5)	9004(30)
Z	4	2
F(000)	3461.8	3316.0
D_c / g cm^{-3}	1.1308	1.164
μ / mm^{-1}	0.084	0.947
$2\Theta_{max}$ / °	46.7	45.82
Data collected	25922	89845
Unique reflections	5273	23868
R_{int}	0.0554	0.0526
Obs data ($I > 2\sigma > (I)$)	4011	16406
Parameters	620	1491
Restraints	24	186
R_1 (observed data)	0.0584	0.0898
ωR_2 (all data)	0.1660	0.2801
GooF	1.081	1.080
Max/min residuals [eÅ^3]	0.53 / -0.44	1.92 / -1.74

Crystallographic table for compound 47Dy.

Compound number	**47Dy**
Formula	$C_{1368}H_{542}N_{28}O_{69.5}Mn_7Dy_5$
*M*r	7667.38
Crystal system	Monoclinic
Space group	*C*2/*c*
T / K	100(2)
a / Å	36.4100(14)
b / Å	23.3869(9)
c / Å	47.4803(18)
α / °	90
β / °	103.040(2)
γ / °	90
U / Å^3	39388(3)
Z	4
F(000)	16028.0
D_c / g cm^{-3}	1.293
μ / mm^{-1}	1.224
$2\Theta_{max}$ / °	53.92
Data collected	152258
Unique reflections	22023
R_{int}	0.0665
Obs data ($I > 2\sigma > (I)$)	16135
Parameters	1504
Restraints	276
R_1 (observed data)	0.1134
ωR_2 (all data)	0.3122
GooF	1.080
Max/min residuals [eÅ^3]	1.92 / -2.27

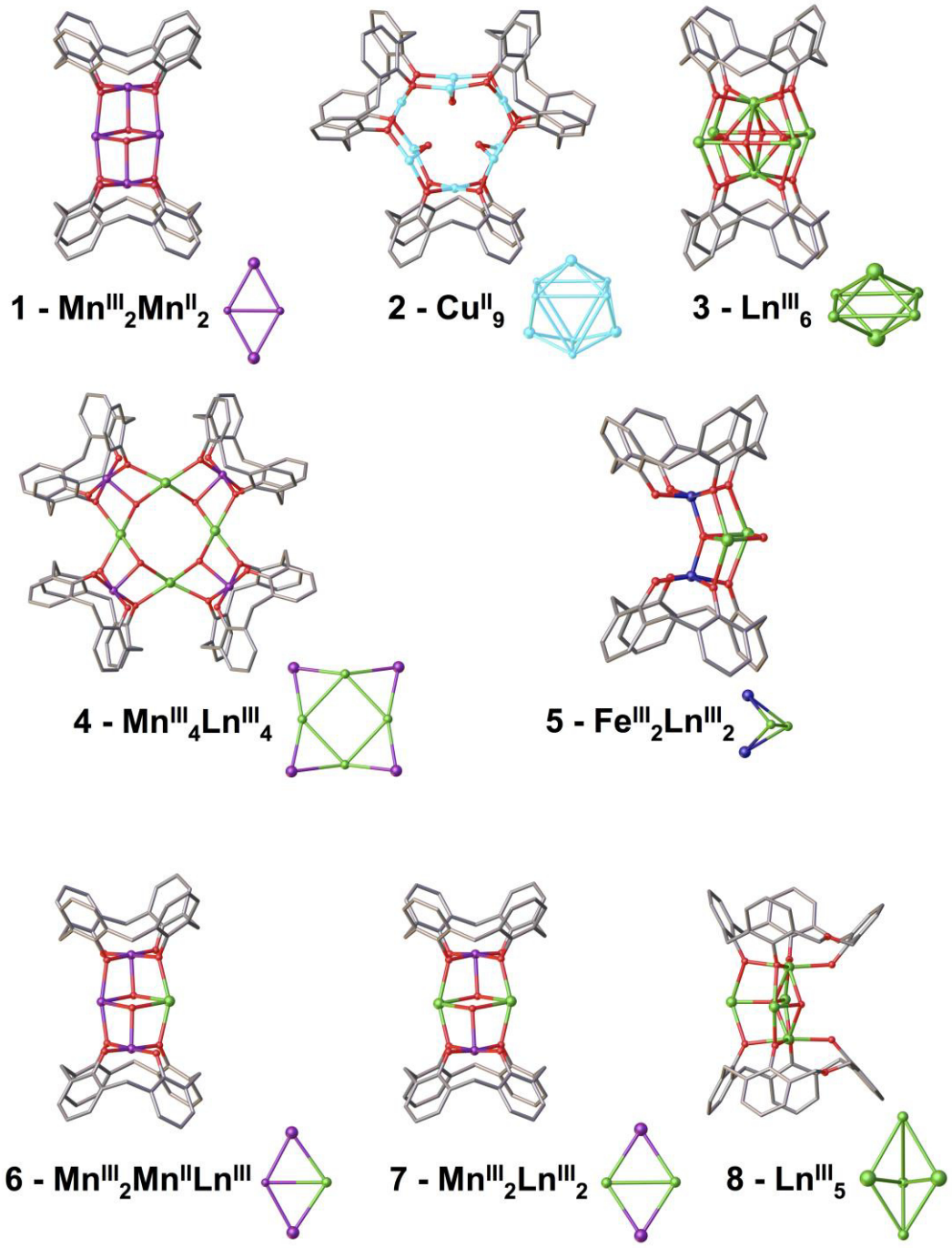

Figure S1. Partial single crystal *X*-ray structures and topologies of clusters **1** – **8**. Larger spheres are indicating core capping by either $[TM^{II}(TBC[4])]^{2-}$, $[TM^{III}(TBC[4])]^{-}$ or $[Ln^{III}(TBC[4])]^{-}$ moieties. H atoms, ^{t}Bu groups, ligated and co-crystallised solvent molecules omitted for clarity. Figures not to scale. Colour code: C – grey, O – red, Mn – purple, Cu – light blue, Fe – dark blue, Ln – green.

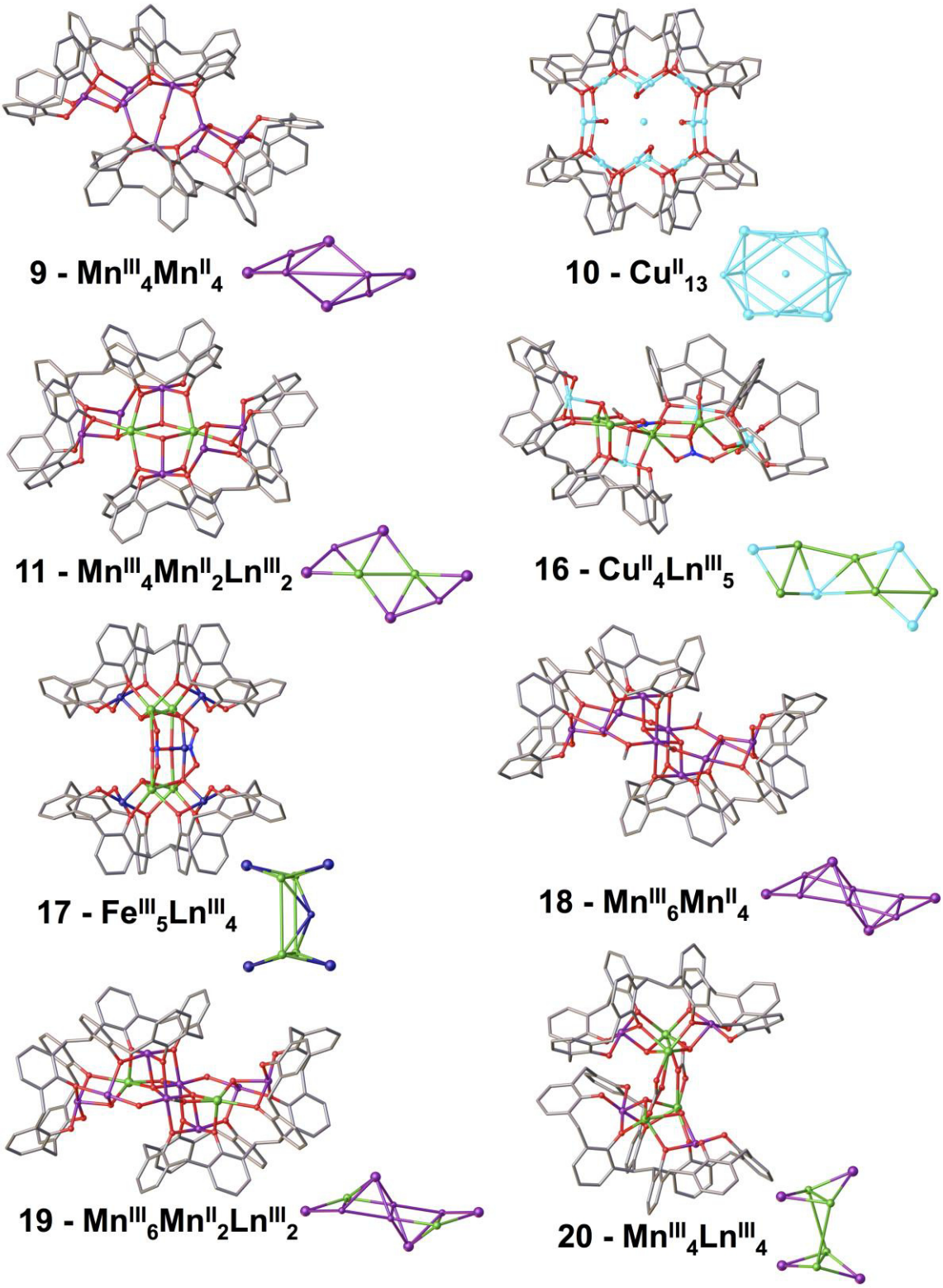

Figure S2. Partial single crystal *X*-ray structures and topologies of clusters **9** – **11** and **16** – **20**. Larger spheres are indicating core capping by either $[TM^{II}(TBC[4])]^{2-}$, $[TM^{III}(TBC[4])]^{-}$ or $[Ln^{III}(TBC[4])]^{-}$ moieties. H atoms, ^{t}Bu groups, ligated and co-crystallised solvent molecules omitted for clarity. Figures not to scale. Colour code: C – grey, O – red, Mn – purple, Cu – light blue, Fe – dark blue, Ln – green.

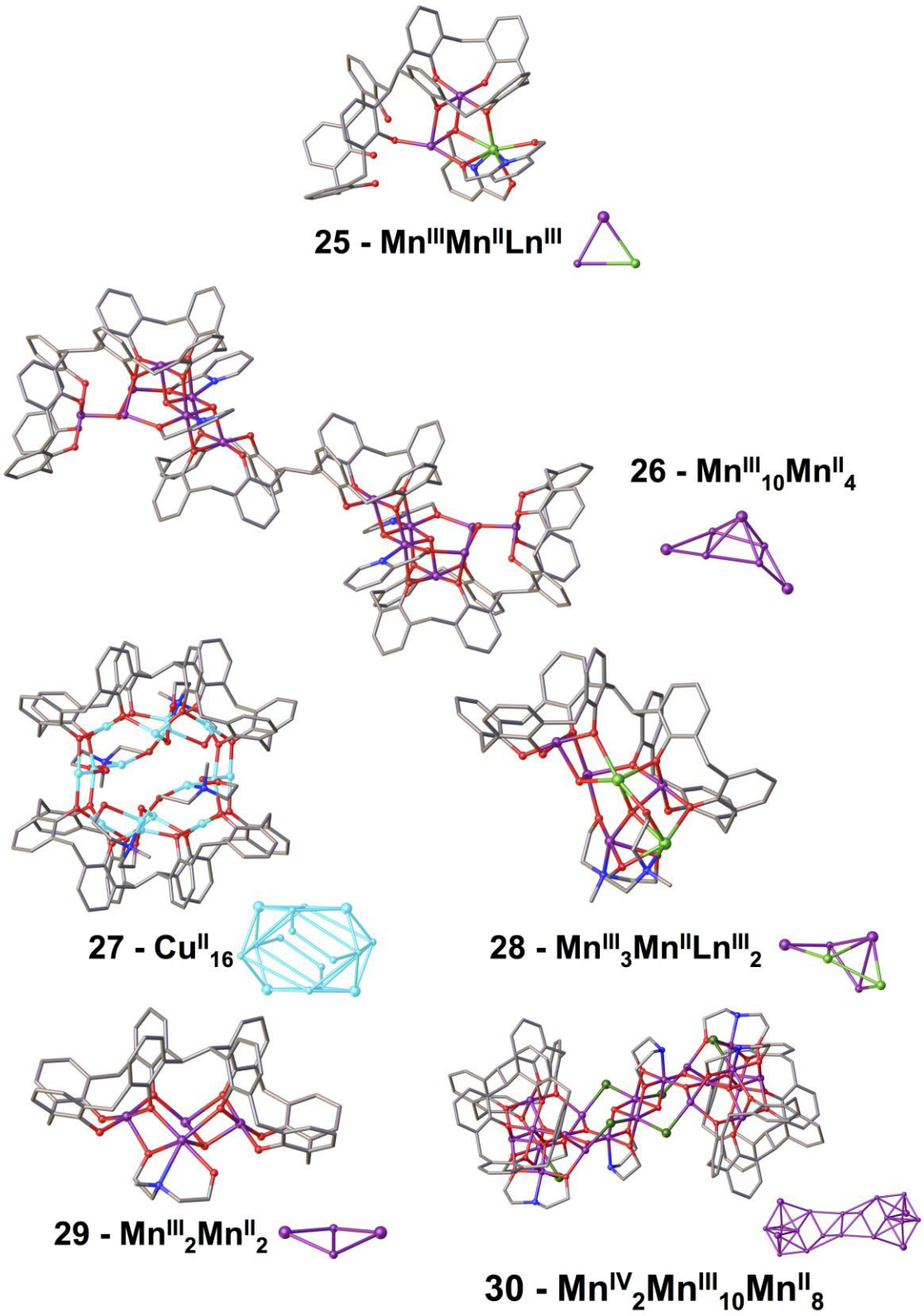

Figure S3. Partial single crystal *X*-ray structures and topologies of clusters **25** – **30**. Larger spheres are indicating core capping by either $[TM^{II}(TBC[4])]^{2-}$, $[TM^{III}(TBC[4])]^{-}$ or $[Ln^{III}(TBC[4])]^{-}$ moieties. H atoms, ^{t}Bu groups, ligated and co-crystallised solvent molecules omitted for clarity. Figures not to scale. Colour code: C – grey, O – red, N – blue; Mn – purple, Cu – light blue, Fe – dark blue, Ln – green.

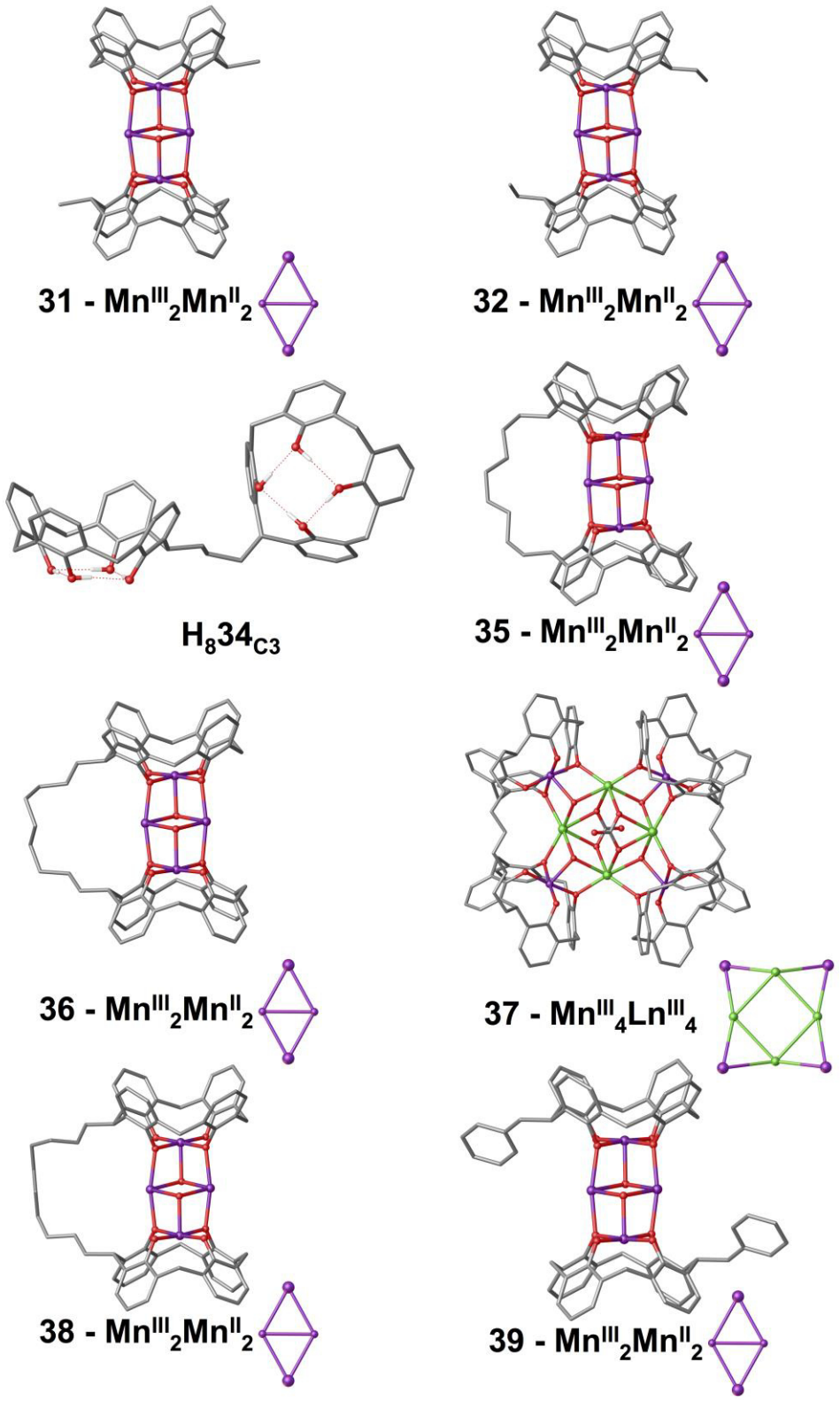

Figure S4. Partial single crystal *X*-ray structures and topologies of compounds **31** – **32** and **35** – **39**. Larger spheres are indicating core capping by either $[TM^{II}(TBC[4])]^{2-}$, $[TM^{III}(TBC[4])]^{-}$ or $[Ln^{III}(TBC[4])]^{-}$ moieties. H atoms not involved in hydrogen bonding, ^{t}Bu groups, ligated and co-crystallised solvent molecules omitted for clarity. Figures not to scale. Colour code: C – grey, O – red, Mn – purple, Fe – dark blue, Ln – green.

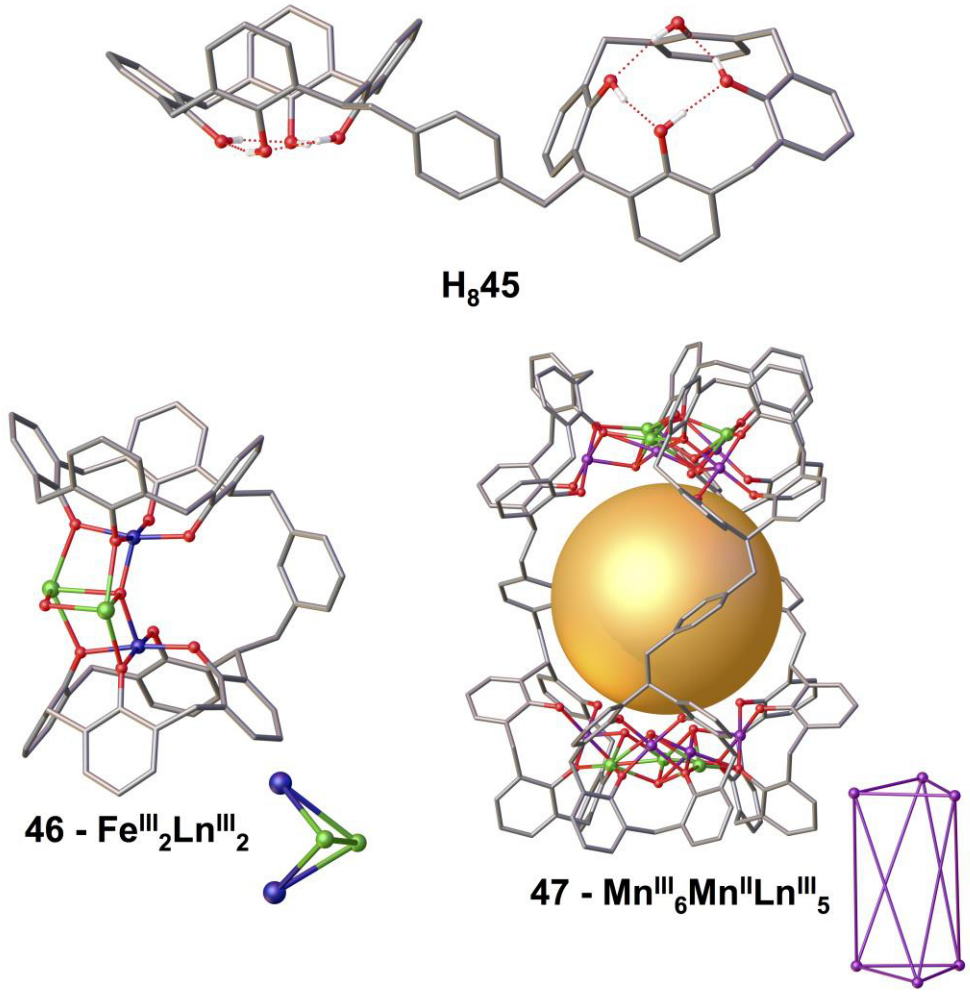

Figure S5. Partial single crystal *X*-ray structures and topologies of compounds **H8 45** – **47**. Larger spheres are indicating core capping by either $[TM^{II}(TBC[4])]^{2-}$, $[TM^{III}(TBC[4])]^{-}$ or $[Ln^{III}(TBC[4])]^{-}$ moieties. H atoms not involved in hydrogen bonding, ^{t}Bu groups, ligated and co-crystallised solvent molecules omitted for clarity. Figures not to scale. Colour code: C – grey, O – red, Mn – purple, Fe – dark blue, Ln – green.

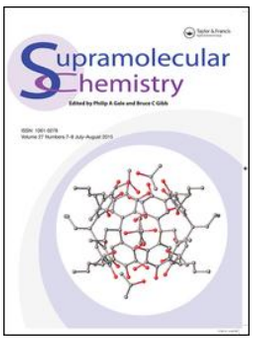

Supramolecular Chemistry

ISSN: 1061-0278 (Print) 1029-0478 (Online) Journal homepage: http://www.tandfonline.com/loi/gsch20

Investigations into cluster formation with alkyl-tethered bis-calix[4]arenes

Marco Coletta, Ross McLellan, Jean-Marie Cols, Kevin J. Gagnon, Simon J. Teat, Euan K. Brechin & Scott J. Dalgarno

To cite this article: Marco Coletta, Ross McLellan, Jean-Marie Cols, Kevin J. Gagnon, Simon J. Teat, Euan K. Brechin & Scott J. Dalgarno (2016): Investigations into cluster formation with alkyl-tethered bis-calix[4]arenes, Supramolecular Chemistry, DOI: 10.1080/10610278.2015.1136412

To link to this article: http://dx.doi.org/10.1080/10610278.2015.1136412

Published online: 29 Jan 2016.

SUPRAMOLECULAR CHEMISTRY, 2016
http://dx.doi.org/10.1080/10610278.2015.1136412

Taylor & Francis
Taylor & Francis Group

Investigations into cluster formation with alkyl-tethered bis-calix[4]arenes

Marco Coletta[a], Ross McLellan[a], Jean-Marie Cols[a], Kevin J. Gagnon[c], Simon J. Teat[c], Euan K. Brechin[b] and Scott J. Dalgarno[a]

[a]Institute of Chemical Sciences, Heriot-Watt University, Edinburgh, Scotland, UK; [b]EaStCHEM School of Chemistry, The University of Edinburgh, Edinburgh, Scotland, UK; [c]Lawerence Berkeley National Laboratory, Berkeley, CA, USA

ABSTRACT

Calix[4]arenes are versatile ligands capable of forming a wide range of cluster motifs when reacted with 3*d*, 4*f* or 3*d*/4*f* metal ions. Synthetic modification at the calix[4]arene methylene bridge offers a unique opportunity to explore cluster formation with these alternative building blocks. Here, we present the synthesis of a range of bis-calix[4]arenes that are tethered by alkyl chains, as well as exploratory structural studies into cluster-forming reactions. Single crystals were formed in four cases, and from the X-ray structures elucidated it is possible to conclude that sufficiently long alkyl tethers allow for the formation of established cluster topologies without disruption to the core coordination chemistry.

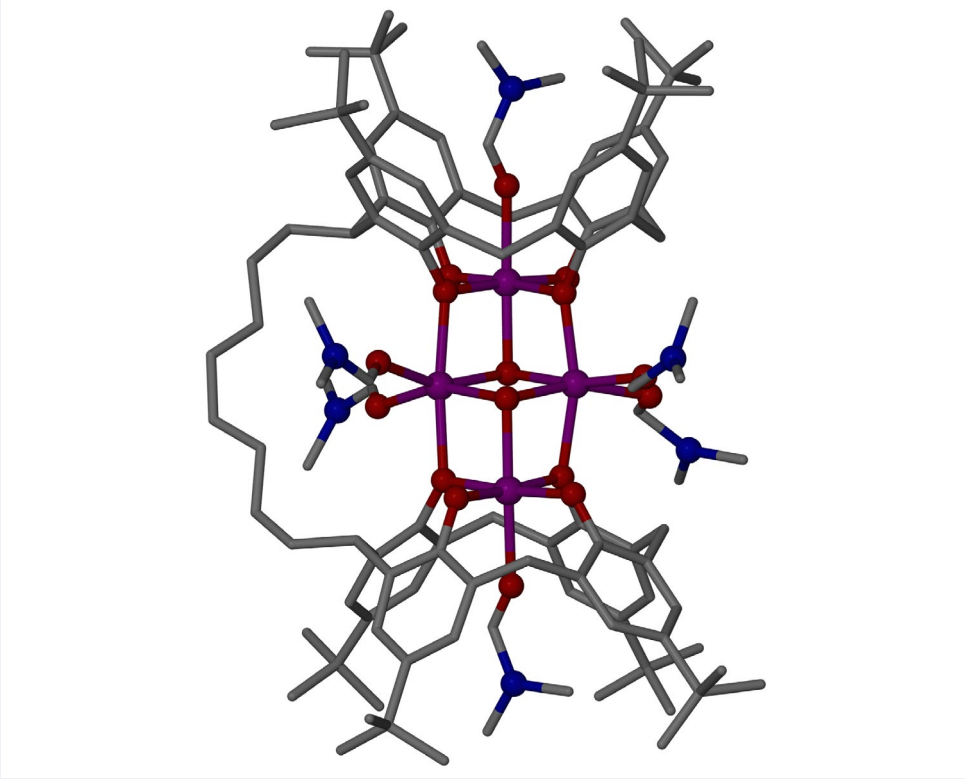

ARTICLE HISTORY
Received 21 October 2015
Accepted 4 December 2015

KEYWORDS
Calixarenes; coordination chemistry; clusters; transition metals; lanthanide metals

Introduction

Methylene-bridged calix[4]arenes (C[4]s, Figure 1(A) are cyclic polyphenols that have found widespread use in the synthesis of a variety of non-covalent or metal-directed structures (*1–6*). Their versatility in this regard relates to the fact that both the upper- and lower-rims can be modified with relative ease, thereby allowing the chemist to introduce a range

CONTACT Euan K. Brechin E.Brechin@ed.ac.uk; Scott J. Dalgarno S.J.Dalgarno@hw.ac.uk

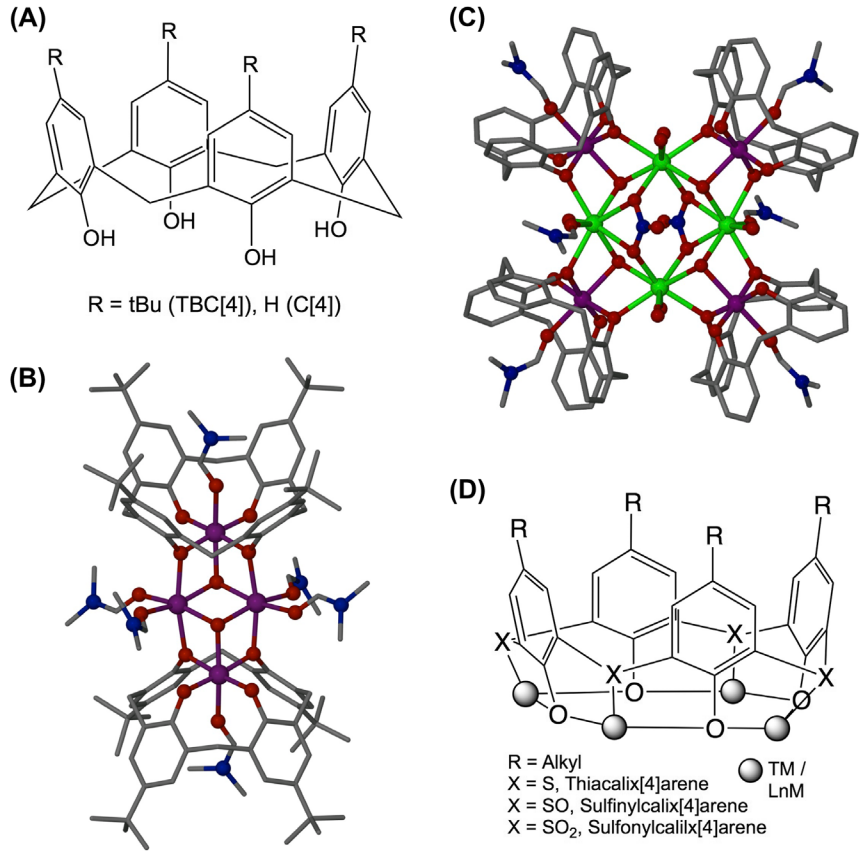

Figure 1. (Colour online). (A) Schematic of the general C[4] framework. (B) Structure of a $[Mn^{III}_2Mn^{II}_2(TBC[4])_2]$ Single-Molecule Magnet (SMM) (*9, 10*). (C) Structure of a $[Mn^{III}_4Ln^{III}_4(C[4])_4]$ cluster (*13, 14*). (D) Schematic of metal ion binding typically found for thia-, sulfinyl- and sulfonyl-bridged C[4]s (*21–31*).

of directing functionalities at either position (*7*). We, amongst others (*8–20*), recently 'mapped out' the transition metal, lanthanide metal and 3*d*–4*f* cluster-forming chemistry of methylene-bridged C[4]s. In doing so, we have reported a wide range of new polymetallic clusters that include (a) $[Mn^{III}_2Mn^{II}_2(TBC[4])_2]$ Single-Molecule Magnets (SMMs, Figure 1(B)) *(9, 10)*, (b) $[Mn^{III}_4Ln^{III}_4(C[4])_4]$ clusters (Figure 1(C)) that are magnetic refrigerants or SMMs depending on the lanthanide employed (*13, 14*) and (c) $[Cu^{II}_9(TBC[4])_3]$ clusters (*11*) that are versatile anion binding materials. More recently, we found that it is also possible to sequentially interchange Ln^{III} for Mn^{II} ions in the aforementioned $[Mn^{III}_2Mn^{II}_2(TBC[4])_2]$ SMMs to afford new $[Mn^{III}_2Mn^{II}Ln^{III}(TBC[4])_2]$ and $[Mn^{III}_2Ln^{III}_2(TBC[4])_2]$ species (*20*). Preferred metal ion binding is observed in a number of different scenarios, an example being the persistent incorporation of the $[Mn^{III}(TBC[4])]^-$ moiety within all 3*d* and 3*d*–4*f* clusters of manganese. These empirical metal ion 'binding rules' therefore offer a route to control the incorporation of a minimum number of specific paramagnetic ions in a resulting cluster through (a) choice of C[*n*] employed and (b) the metal ions used in cluster synthesis. It is noteworthy to mention that the thia-, sulfinyl- and sulfonyl-bridged C[4]s (*21–31*) have also been utilised in the construction of polymetallic clusters, and more recently in the programmed formation of nanometre scale metal-organic assemblies. Their utility stems from the fact that the S, SO or SO_2 bridging groups influence the resulting coordination chemistry (Figure 1(D)), binding four metal ions rather than one (as is the case for methylene-bridged analogues). Both systems therefore have different merits when considering the construction of polymetallic clusters, but standard C[4]s can also be modified at the methylene bridge. Synthetic alteration, in addition to the use of bridge-modified C[4]s for the construction of new/related clusters, is an area we are currently investigating and is the focus of this contribution.

Synthetic access to C[4]s that deviate from classical methylene bridge composition (i.e. those that contain ≥1 different bridge) has been known for some time (*32–37*). Elegant work by the Böhmer and Biali groups (amongst others) detailed the synthesis of such species through the use of stepwise and fragment condensation methods. Later efforts, chiefly by Biali, focused on functionalisation

at multiple C[4] bridge positions, but in this case utilising the pre-formed calixarene framework as a synthetic platform (*38–42*). Fantini has demonstrated the ability to undertake synthetic modification at one C[4] methylene bridge to (a) introduce a number of different substituents and (b) directly link C[4]s together at the bridge position (*43–46*). To us, expansion of this direct C[4]–C[4] link presented an opportunity to systematically influence (and thus potentially control) C[4]-supported cluster formation through the introduction of different organic spacers. Here, we report the synthesis of a series of alkyl-tethered bis-C[4]s and exploratory studies into cluster formation with these new ligands.

Results and discussion

Synthesis of alkyl-tethered bis-C[4]s

As reported, TBC[4] lower-rim protection (with resulting OMe groups) allows for mono-lithiation at one methylene bridge via reaction with ^{n}BuLi as shown in Figure 2(A). Reaction of mono-lithiated MeO-TBC[4] (**1**) with chosen dibromoalkanes afforded a series of bis-MeO-TBC[4]s with the calixarenes tethered by propyl, butyl and hexyl to decyl chains (*47, 48*). Subsequent lower-rim deprotection afforded the series of target bis-C[4]s in moderate yields, with all TBC[4] subunits adopting cone conformations due to typical stabilising H-bonding interactions. With an interest in examining the structures of compounds **9**–**15** in the absence of metal ions/prior to cluster formation, we attempted crystallisation from a range of solvents including toluene, ethyl acetate and acetonitrile. Single crystals suitable for X-ray diffraction studies were isolated in just one case, that being the acetonitrile solvate of TBC[4]-$(CH_2)_3$-TBC[4] (**9**). Crystals of **9**·4MeCN were found to be in a monoclinic space group and structure analysis was carried out in the space group $P2_1/c$. The asymmetric unit contains one molecule of **9** and four co-crystallised MeCN (Figure 2(B)), two of which reside in the TBC[4] cavities; in this arrangement they form CH···π interactions that are consistent with those found in the MeCN solvate of TBC[4] (*49*). From inspection, it is clear that the TBC[4] cavity is unperturbed by bridge modification and is thus open for occupation by metal ions as anticipated.

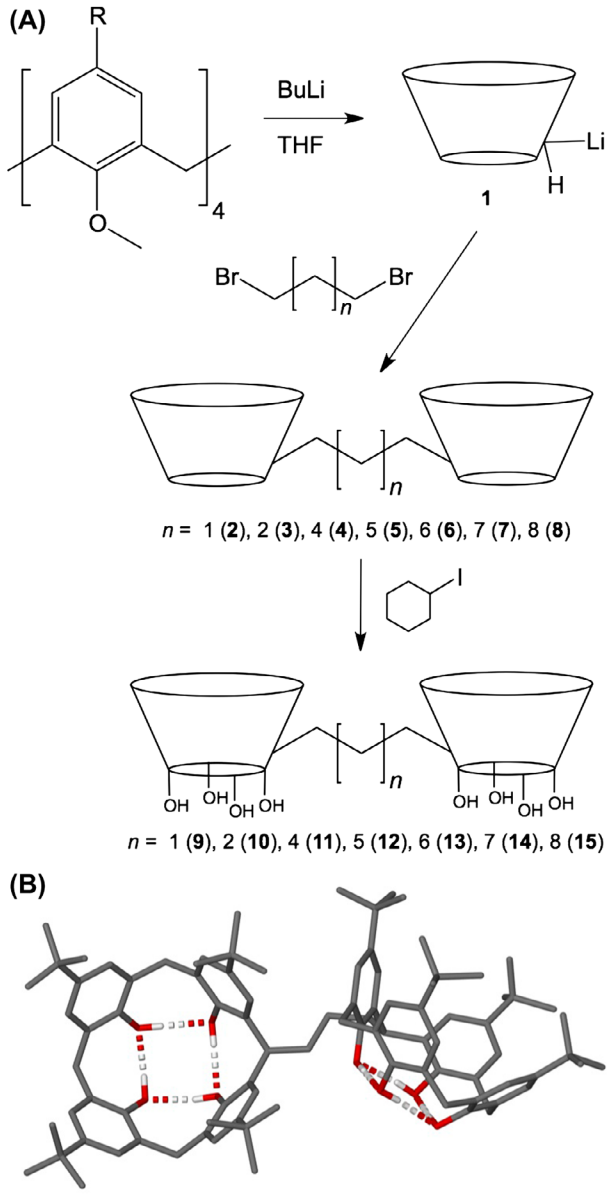

Figure 2. (Colour online). (A) Synthetic scheme for the series of bis-TBC[4]s tethered by propyl, butyl and hexyl–decyl chains (compounds **9**–**15,** respectively) (*47*). (B) Part of the single X-ray structure of **9** · 4MeCN showing the TBC[4] cavities stabilised by H-bonding interactions. H atoms (other than those involved in cavity stabilisation) are omitted for clarity.

Cluster synthesis and structural investigations

With compounds **9**–**15** isolated, we began investigations into cluster synthesis with these new ligands by targeting reaction conditions known to afford the $[Mn^{III}_2Mn^{II}_2(TBC[4])_2]$ (*9, 10*), $[Mn^{III}_4Ln^{III}_4(C[4])_4]$ (*13, 14*) and series of $[Mn^{III}_2Mn^{II}_2(TBC[4])_2]$/$[Mn^{III}_2Mn^{II}Ln^{III}(TBC[4])_2]$/$[Mn^{III}_2Ln^{III}_2(TBC[4])_2]$ species discussed in the introductory section (*20*). All reactions produced purple solutions but we were only able to grow single crystals suitable for diffraction studies in four cases. Structural analysis (below) revealed that three of these (**16**–**18**) were isostructural, with the main difference being the length of alkyl tether present between the TBC[4] subunits; these were formed with **13**–**15**, octyl-, nonyl- and decyl-tethered bis-TBC[4]s, respectively. In all three cases, the cluster core was analogous to the 'butterfly' topology found in $[Mn^{III}_2Mn^{II}_2(TBC[4])_2]$ (*9, 10*). The fourth case in which single crystals were isolated also involved compound **14**, and the

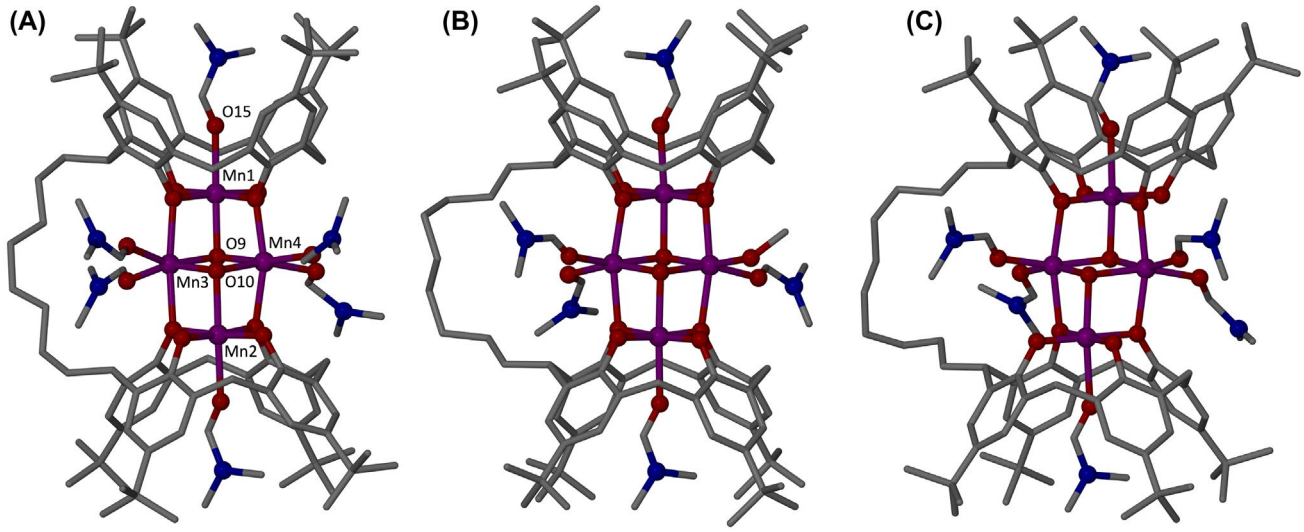

Figure 3. (Colour online). Partial single crystal X-ray structures of the new $Mn^{III}_2Mn^{II}_2$ clusters (**16**–**18**, A–C, respectively) formed with **13**–**15**. Selective labels in (A) relate to discussion of compound **16**. H atoms and solvent of crystallisation have been omitted for clarity. Figures not to scale.

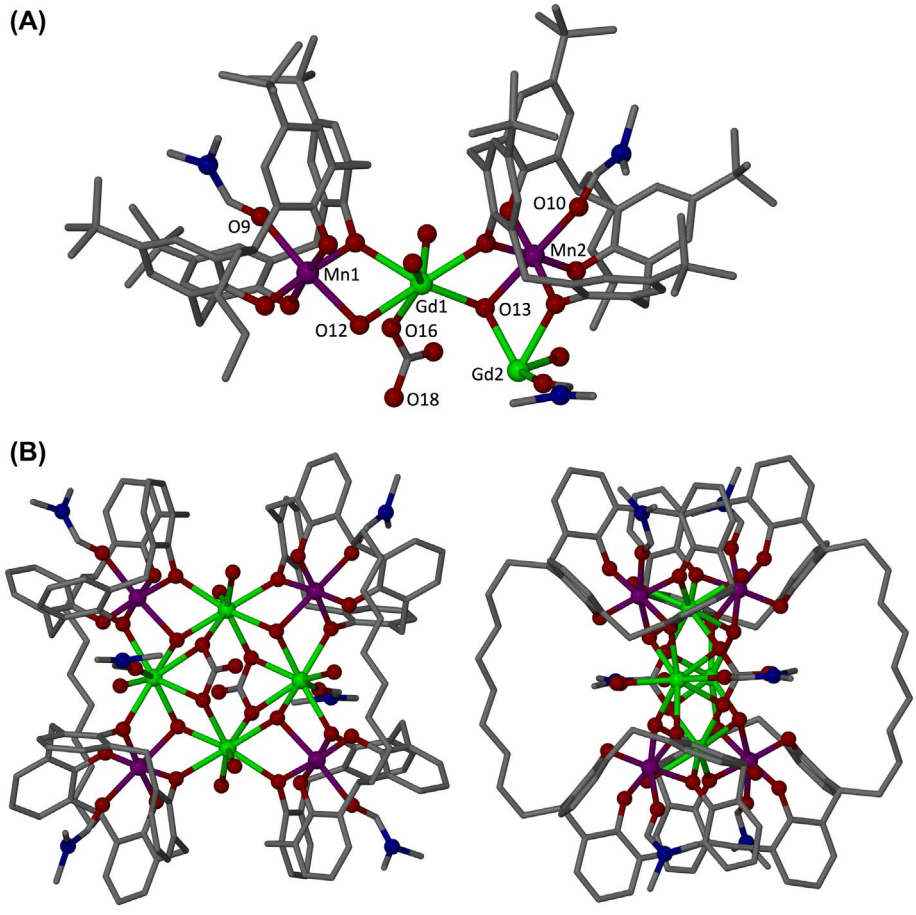

Figure 4. (Colour online). (A) Selectively labelled partial single crystal X-ray structure of the new $Mn^{III}_4Gd^{III}_4$ cluster (**19**) formed with **14**. H atoms and solvent of crystallisation have been omitted for clarity in (A) and (B). TBC[4] upper-rim ^{t}Bu groups are omitted in B such that the two views emphasise the nonyl tether between the TBC[4] subunits. Figures not to scale.

components were found to assemble into a new cluster (**19**) that is very closely related to $[Mn^{III}_4Ln^{III}_4(C[4])_4]$ (*13, 14*); the only significant difference in this new cluster is that there are changes to the anions incorporated within the core. In the interest of brevity, we have limited discussion here to the structures of **16** and **19**, with comparisons made between the former and **17–18**.

Reaction of **13** with manganese(II) dichloride tetrahydrate in a DMF/MeOH mixture, and in the presence of Et_3N as a base, afforded single crystals of $[Mn^{III}_2Mn^{II}_2$(**13–8**H)$(\mu_3\text{-}OH)_2(DMF)_{5.5}(MeOH)_{0.5}](H_2O)_{1.5}$ (**16**) upon slow evaporation of the mother liquor. The crystals were found to be in a monoclinic cell and structure solution was performed in the space group $P2_1/c$. The asymmetric unit (ASU) contains the entire cluster shown in Figure 3(A) in addition to co-crystallised solvent molecules. Comparison of Figures 1(B) and 3(A) shows the clear structural relation between these two clusters, with the major difference being the presence of an octyl tether between the TBC[4] subunits in **16**. Within the cluster, Mn1 is bound in the tetraphenolic TBC[4] pocket formed by oxygens O1–O4 (Mn1–O range of 1.919(9)–1.974(9) Å) and it is in the third oxidation state with Jahn–Teller distorted octahedral geometry. Its coordination sphere is completed by a ligated dmf residing in the TBC[4] cavity (Mn1–O15, 2.297(11) Å) and a μ_3-hydroxide (Mn1–O9, 2.141(9) Å), which is also bonded to Mn3 and Mn4 (2.184(9) and 2.183(9) Å, respectively), both in the second oxidation state and possessing distorted octahedral geometry. In addition, Mn3 coordination is completed by two dmf molecules (Mn3–O11 Mn3–O12 with respective distances of 2.138(10) and 2.124(11) Å), two μ-phenoxide oxygens (Mn3–O4 and Mn3–O8 with respective distances of 2.237(8) and 2.237(9) Å) and a μ_3-hydroxide (Mn3–O10, 2.155(9) Å), bridging Mn3 with Mn4 and Mn2, both of which have similar coordination environments to those described for Mn1 and Mn3; there are negligible differences in bond lengths observed. Analogous reactions with either **14** or **15** in place of **13** in the synthesis of **16** above afforded single crystals of $[Mn^{III}_2Mn^{II}_2$(**14–8**H)$(\mu_3\text{-}OH)_2(MeOH)(dmf)_5](MeOH)(dmf)(H_2O)$ (**17**) and $[Mn^{III}_2Mn^{II}_2$(**15–8**H)$(\mu_3\text{-}OH)_2(dmf)_6](dmf)_{1.5}(MeOH)_{0.5}(H_2O)_{1.5}$ (**18**), respectively, both of which are shown in Figure 3(B) and (C) for comparison. Although there are slight changes in the composition of peripheral ligated solvent, as well as solvent of crystallisation upon moving from **16** to **18**, the clusters and overall assemblies are near identical. It is therefore clear that the formation of the general 'butterfly' $Mn^{III}_2Mn^{II}_2$ cluster motif is favourable with alkyl tethers greater or equal to octyl in length.

Reaction of **14** with manganese (II) chloride tetrahydrate and gadolinium (III) chloride hexahydrate in a DMF/MeOH mixture, and in the presence of Et_3N as a base, afforded single crystals of $[Mn^{III}_4Gd^{III}_4$(**14–8**H)$(\mu_3\text{-}CO_3)_2(\mu_3\text{-}OH)_4(H_2O)_6(dmf)_6](dmf)_6(MeOH)_4$ (**19**) after slow evaporation of the mother liquor. The crystals were found to be in a triclinic cell and structure solution was performed in the space group P – 1. The ASU comprises one half of the assembly (Figure 4(A)), related to its symmetry equivalent through an inversion centre. The two Mn^{III} ions in the ASU are bound in the TBC[4] phenolic pockets with Mn1–O and Mn2–O distances in the ranges of 1.900(7)–1.988(6) and 1.913(6)–1.986(6) Å, respectively. Their Jahn–Teller distorted octahedral coordination spheres are completed by ligated dmf molecules residing in the TBC[4] cavities (Mn1–O9 and Mn2–O10 distances of 2.263(6) and 2.262(7) Å, respectively), and μ_3-hydroxides (Mn1–O12 and Mn2–O13 distances of 2.245(5) and 2.233(6) Å, respectively). The latter bridge to octacoordinate, square antiprismatic Gd^{III} ions within the cluster core, with respective Gd1–O12, Gd1–O13, Gd2–O12 and Gd2–O13 distances of 2.419(5), 2.427(6), 2.379(6) and 2.390(6) Å. Gd1 is also bound to two μ-phenoxides (Gd1–O3 and Gd1–O7 distances of 2.375(6) and 2.393(6) Å, respectively) belonging to TBC[4]s, two ligated water molecules (Gd1–O14 and Gd1–O15 distances of 2.410(7) and 2.428(6) Å, respectively) and two μ-carbonates (Gd1–O16 and Gd1–O18 distances of 2.397(6) and 2.394(6) Å, respectively). These carbonates are the bridging units between Gd1, Gd2 and their symmetry equivalents, with Gd2 coordination being essentially identical to that of Gd1; the only difference is the presence of a ligated dmf rather than a water molecule, occurring with a Gd2–O11 distance of 2.305(7) Å. Symmetry expansion of the ASU around the inversion centre affords the assembly shown in Figure 4(B). Comparison with Figure 1(C) shows that these square within square (or Mn^{III} tetra-capped Ln^{III} square) topologies are very closely related, the main difference being the incorporation of μ_3-carbonates in **19** rather than nitrates in our previously reported example (*13, 14*). Charge balance in the previously reported μ-nitrate cluster is provided by hydroxide counterions that are proximal to the cluster core; this is not seen in **19** due to the incorporation of $\mu_3\text{-}CO_3^{2-}$ anions (*50*). Further examination of Figure 4(B) shows that the bis-TBC[4]s are just of an appropriate tether length to allow for formation of this cluster type, suggesting that slightly shorter chains (e.g. hexyl/heptyl) would not be suitable for synthesis of this structural arrangement; significantly shorter chains such as propyl or butyl would clearly not be suitable.

Conclusions

We have expanded upon the synthetic chemistry associated with bis-TBC[4]s and report a range of new molecular building blocks possessing alkyl tethers of varied chain length. These molecules may find utility in the field of

supramolecular chemistry as a whole, but in this contribution we have begun to investigate their potential as platforms for cluster synthesis. Attempts to isolate single crystals of clusters with tether chain lengths shorter than octyl have yet to be successful, but this will be the focus of future work. Although this is the case, we have established information relating to the possible minimum chain length required in order to form some known cluster motifs, and by this rationale one can expect the formation of markedly different assemblies when shorter tethers are employed. Results from this continuing study will be communicated in due course.

Experimental

All reagents were purchased from Sigma–Aldrich and used as supplied without further purification.

General procedure for the synthesis of bis-tetramethoxycalix[4]arenes 2–8

n-BuLi (2.5 M in hexane, 1.5 eq.) was added to a stirred solution of tetramethoxycalix[4]arene (1 eq.) in dry THF (40 mL) under an N_2 atmosphere, causing a rapid colour change from pale yellow to blood red. After 10 minutes of stirring, the chosen dibromoalkane (1.15 eq.), as a solution in 20 mL of dry THF, was added dropwise over 40 min, with concomitant change in colour from blood red to yellow. Following addition, the reaction mixture was stirred for a further 12 h before being quenched by addition of H_2O. Volatiles were removed and the resulting solid was dried under vacuum. The crude material was then dissolved in CH_2Cl_2 (300 mL) and washed with brine (3 × 100 mL). The organic layer was separated, dried over $MgSO_4$, and the solvent was removed under reduced pressure to afford a gummy yellow solid that was dried under vacuum. The resulting yellow solid was recrystallised from hot $CHCl_3$/MeOH to afford a white powder of the pure target bis-MeO-C[4]. In all cases, ^{1}H NMR spectra of the products are very difficult to interpret due to fluxionality casued by the lower-rim methoxy groups. Although this is the case, it was possible to gauge reaction completion for these synthetic intermediates by the disappearance of characteristic OH groups for the C[4] lower-rim. Compounds **2–8** were therefore used in the deprotection step below to afford the target lower-rim hydroxy C[4]s **9–15**.

Synthesis of 2,2′-(Propane-1,3-diyl)bis(5,11,17,23-tetra-p-tert-butyl-25,26,27,28-tetra-methoxycalix[4]arene, 2

Reagents used in the general synthesis were 2.50 g (3.55 mmol) of tetramethoxycalix[4]arene in 40 mL of dry THF, 2.1 mL of (5.32 mmol) *n*-BuLi (2.5 M in hexane) and 358 mg of (1.77 mmol) 1,3-dibromopropane in 20 mL of dry THF. Yield: 1.44 g (56%).

Synthesis of 2,2′-(Butane-1,4-diyl)bis(5,11,17,23-tetra-p-tert-butyl-25,26,27,28-tetra-methoxycalix[4]arene, 3

Reagents used in the general synthesis were 2.50 g (3.55 mmol) of tetramethoxycalix[4]arene in 40 mL of dry THF, 2.1 mL of (5.32 mmol) *n*-BuLi (2.5 M in hexane) and 383 mg of (1.77 mmol) 1,4-dibromobutane in 20 mL of dry THF. Yield: 1.30 g (50%).

Synthesis of 2,2′-(Hexane-1,6-diyl)bis(5,11,17,23-tetra-p-tert-butyl-25,26,27,28-tetra-methoxycalix[4]arene, 4

Reagents used in the general synthesis were 2.83 g (4.02 mmol) of tetramethoxycalix[4]arene in 40 mL of dry THF, 2.4 mL (6.36 mmol) of *n*-BuLi (2.5 M in hexane) and 564 mg of (2.31 mmol) 1,6-dibromohexane in 20 mL of dry THF. Yield: 1.40 g (24%).

Synthesis of 2,2′-(Heptane-1,7-diyl)bis(5,11,17,23-tetra-p-tert-butyl-25,26,27,28-tetra-methoxycalix[4]arene, 5

Reagents used in the general synthesis were 3 g (4.26 mmol) of tetramethoxycalix[4]arene in 40 mL of dry THF, 2.55 mL (6.38 mmol) of *n*-BuLi (2.5 M in hexane) and 650 mg of (2.52 mmol) 1,7-dibromoheptane (97%) in 20 mL of dry THF. Yield: 2.14 g (33%).

Synthesis of 2,2′-(Octane-1,8-diyl)bis(5,11,17,23-tetra-p-tert-butyl-25,26,27,28-tetra-methoxycalix[4]arene, 6

Reagents used in the general synthesis were 3 g (4.26 mmol) of tetramethoyxcalix[4]arene in 40 mL of dry THF, 2.55 mL of (6.38 mmol) *n*-BuLi (2.5 M in hexane) and 670 mg of (2.45 mmol) 1,8-dibromooctane in 20 mL of dry THF. Yield: 2.83 g (44%).

Synthesis of 2,2′-(Nonane-1,9-diyl)bis(5,11,17,23-tetra-p-tert-butyl-25,26,27,28-tetra-methoxycalix[4]arene, 7

Reagents used in the general synthesis were 3 g (4.26 mmol) of tetramethoxycalix[4]arene in 40 mL of dry THF, 2.55 mL of (6.38 mmol) *n*-BuLi (2.5 M in hexane) and 720 mg of (2.53 mmol) 1,9-dibromononane (97%) in 20 mL of dry THF. Yield: 2.08 g (32%).

Synthesis of 2,2′-(Decane-1,10-diyl)bis(5,11,17,23-tetra-p-tert-butyl-25,26,27,28-tetramethoxycalix[4]arene, 8

Reagents used in the general synthesis were 3 g (4.26 mmol) of tetramethoxycalix[4]arene in 40 mL of dry THF, 2.55 mL of (6.38 mmol) *n*-BuLi (2.5 M in hexane) and 760 mg of (2.52 mmol) 1,10-dibromodecane (97%) in 20 mL of dry THF. Yield: 2.29 g (35%).

General procedure for the synthesis of bis-tetrahydroxycalix[4]arenes 9–15

Cyclohexyl iodide (90 eq.) was added to a DMF (30 mL) solution of the chosen bis-MeO-C[4] and the resulting mixture was heated at reflux for 48 h with a concomitant change in colour from pale yellow to dark orange. The solution was poured into H_2O (250 mL), causing the precipitation of an orange solid. The orange precipitate was collected, was washed several times with water and stirred in MeOH for 15 min to afford a white solid. The white solid was filtered, washed several times with MeOH, collected under reduced pressure and dried under vacuum. *Alternative workup procedure for bis-tetramethoxycalix[4]arenes:* Occasionally, the workup procedure above leads to very low yields (particularly for longer alkyl chains). On occasions that a solid did not precipitate from solution upon addition of water, the product was extracted with $CHCl_3$, washing the water phase until the orange colour disappeared. The organic layer was collected, dried over $MgSO_4$ and filtered. The solvent was removed under reduced pressure and the resulting crude solid was recrystallised from hot $CHCl_3$/MeOH. In all cases, the target bis-C[4]s were checked for purity by TLC ($CHCl_3$/Hex 1:1) and purified by column chromatography ($CHCl_3$/Hex 1:1 → EtOAc) to remove C[4] impurities.

Synthesis of 2,2′-(Propane-1,6-diyl)bis(5,11,17,23-tetra-p-tert-butyl-tetrahydroxy-calix[4]arene, 9

Reagents used in the general synthesis were 0.880 g (0.61 mmol) of **2**, 11.6 g (54.9 mmol) of cyclohexyl iodide in 30 mL of DMF. Purification by chromatography column ($CHCl_3$/Hex 1:1 → EtOAc) afforded 556 mg of pure product (Yield: 68%). ^{1}H NMR ($CDCl_3$): 10.27 (s, 8H, –OH), 7.00 (m, 16H, ArH) 4.40 (t, 2H, $^3J_{HH}$ = 7.9 Hz, Ar–CH–CH_2–), 4.17 (m, 6H, Ar–CH_2–Ar), 3.41 (m, 6H, Ar–CH_2–Ar), 2.18 (m, 4H, Ar–CH–CH_2), 1.31 (m, 2H, CH_2–CH_2–CH_2), 1.13 (m, 72H, $C(CH_3)_3$). ^{13}C NMR ($CDCl_3$): 146.85, 146.64, 144.38, 144.25, 131.20, 127.82, 127.70, 127.51, 127.21, 125.95, 125.91, 125.22, 121.77, 104.99, 34.17, 34.03, 32.76, 32.62, 31.43; MS calculated for $C_{91}H_{116}O_8$ (1336.87); found 1354.91 $(M + NH_4)^+$. *Crystal data for 9•4MeCN (CCDC 1008041):* $C_{99}H_{128}N_4O_8$, M = 1502.05, Colourless Block, 0.35 × 0.30 × 0.18 mm^3, monoclinic, space group $P2_1/c$ (No. 14), a = 19.3316(19), b = 25.164(2), c = 19.117(2) Å, b = 105.346(6)°, V = 8968.1(16) Å^3, Z = 4, Bruker X8 Apex II CCD Diffractometer, MoKa radiation (λ = 0.71073 Å), T = 100(2)K, $2\theta_{max}$ = 46.6°, 58266 reflections collected, 12880 unique (R_{int} = 0.1318). Final *GooF* = 1.211, *R*1 = 0.0979, *wR*2 = 0.2272, *R* indices based on 5751 reflections with $I > 2$sigma(I) (refinement on F^2).

Synthesis of 2,2′-(Butane-1,6-diyl)bis(5,11,17,23-tetra-p-tert-butyl-tetrahydroxy-calix[4]arene, 10

Reagents used in the general synthesis were 2.42 g (1.65 mmol) of **3**, 31.3 g (0.150 mol) of cyclohexyl iodide in 40 mL of DMF. Purification by chromatography column ($CHCl_3$/Hex 1:1 → EtOAc) afforded 1.462 g of pure product (Yield: 65%).

^{1}H NMR ($CDCl_3$): 10.27 (s, 8H, ArOH), 7.00–6.91 (M, 16H, ArH), 4.40 (t, 2H, $^3J_{HH}$ = 7.8 Hz, Ar–CH–CH_2–), 4.18 (m, 6H, Ar–CH_2–Ar), 3.42 (m, 6H, Ar–CH_2–Ar), 2.11 (m, 4H, Ar–CH–CH_2), 1.32 (m, 4H, CH_2–CH_2–CH_2), 1.13 (m, 72H, $C(CH_3)_3$). ^{13}C NMR ($CDCl_3$): 146.83, 146.69, 144.38, 144.28, 131.10, 127.80, 127.70, 127.55, 127.24, 125.94, 125.14, 121.77, 34.18, 34.03, 32.78, 32.64, 32.47, 31.43, 28.43; MS calculated for $C_{92}H_{118}O_8$ 1350.88, found 1369.92 $(M + NH_4)^+$.

Synthesis of 2,2′-(Hexane-1,6-diyl)bis(5,11,17,23-tetra-p-tert-butyl-tetrahydroxy-calix[4]arene, 11

Reagents used in the general synthesis were 1.40 g (0.95 mmol) of **4**, 18 g (85.5 mmol) of cyclohexyl iodide in 30 mL of DMF. Purification by chromatography column ($CHCl_3$/Hex 1:1 → EtOAc) afforded 333 mg of pure product (Yield: 25%). ^{1}H NMR ($CDCl_3$): 10.29 (s, 8H, –OH), 7.09–6.97 (m, 16H, ArH), 4.46 (t, 2H, $^3J_{HH}$ = 7.8 Hz, Ar–CH–CH_2–), 4.27–4.22 (m, 12H Ar–CH_2–Ar), 3.48 (d, 4H, $^2J_{HH}$ = 13.6 Hz, Ar–CH–CH_2), 2.16 (s, 8H, –CH_2–), 1.2 (s, 72H, $C(CH_3)_3$). ^{13}C NMR ($CDCl_3$): 146.8, 144.3, 131.2, 127.7, 126.0, 34.2, 34.0, 32.8, 31.4, 29.0, 27.5. MS calcd. for $C_{94}H_{122}O_8$ (1379.90); found: 1397.9 $(M + NH_4)^+$.

Synthesis of 2,2′-(Heptane-1,7-diyl)bis(5,11,17,23-tetra-p-tert-butyl-tetrahydroxy-calix[4]arene, 12

Reagents used in the general synthesis were 2.04 g (1.35 mmol) of **5**, 25.6 g (121.9 mmol) of cyclohexyl iodide in 30 mL of DMF. Purification by chromatography column ($CHCl_3$/Hex 1:1 → EtOAc) afforded 1.123 g of pure product (Yield: 60%). ^{1}H NMR ($CDCl_3$): 10.28 (s, 8H, –OH), 7.09–6.96 (m, 16H, ArH), 4.46 (t, 2H, $^3J_{HH}$ = 7.6 Hz, Ar–CH–CH_2–), 4.27–4.22 (m, 6H Ar–CH_2–Ar), 3.48 (d, 4H, $^2J_{HH}$ = 14.0 Hz, Ar–CH–CH_2), 2.16 (s, 10H, –CH_2–), 1.2 (s, 72H, $C(CH_3)_3$). ^{13}C NMR ($CDCl_3$):146.8, 144.3, 131.2, 127.8, 125.97, 125.11, 121.11,

121.9, 34.2, 34.03, 32.8, 31.4, 29.5. MS calcd. for $C_{95}H_{124}O_8$ (1393.1); found: 1411.9 $(M + NH_4)^+$.

Synthesis of 2,2′-(Octane-1,8-diyl)bis(5,11,17,23-tetra-p-tert-butyl-tetraxydroxy-calix[4]arene, 13

Reagents used in the general synthesis were 2.83 g (1.86 mmol) of **6**, 35 g (167.4 mmol) of cyclohexyl iodide in 30 mL of DMF. NMR and TLC ($CHCl_3$/Hex 1:1) showed that the compound was pure enough and did not need any further purification. ^{1}H NMR ($CDCl_3$): 10.28 (s, 8H, –OH), 7.09–6.97 (m, 16H, ArH), 4.42 (t, 2H, $^3J_{HH}$ = 8 Hz, Ar–CH–CH_2–), 4.28–4.23 (m, 6H Ar–CH_2–Ar), 3.48 (d, 4H, $^2J_{HH}$ = XX Hz, Ar–CH–CH_2), 2.16 (s, 12H, –CH_2–), 1.2 (s, 72H, C(CH_3)$_3$). ^{13}C NMR ($CDCl_3$):146.8, 144.3, 131.3, 127.7, 125.94, 36.5, 34.2, 34.02, 32.8, 31.4, 30.9, 29.5, 29.4. MS calcd. for $C_{96}H_{126}O_8$ (1407.01); found: 1425.9 $(M + NH_4)^+$.

Synthesis of 2,2′-(Nonane-1,9-diyl)bis(5,11,17,23-tetra-p-tert-butyl-tetrahydroxy-calix[4]arene, 14

Reagents used in the general synthesis were 1.935 g (1.26 mmol) of **7**, 23.8 g (113.5 mmol) of cyclohexyl iodide in 30 mL of DMF. Purification by chromatography column ($CHCl_3$/Hex 1:1 → EtOAc) afforded 0.55 g of pure product (Yield: 31%). ^{1}H NMR ($CDCl_3$): 10.29 (s, 8H, –OH), 7.1–6.98 (m, 16H, ArH), 4.47 (t, 2H, $^3J_{HH}$ = 7.7 Hz, Ar–CH–CH_2–), 4.27–4.22 (m, 6H Ar–CH_2–Ar), 3.49 (d, 4H, $^2J_{HH}$ = 14.05 Hz, Ar–CH–CH_2), 2.16 (s, 14H, –CH_2–), 1.2 (s, 72H, C(CH_3)$_3$). ^{13}C NMR ($CDCl_3$):146.8, 144.3, 131.2, 127.8, 127.55, 127.20, 125.96, 125.11, 121.9, 35.6, 34.2, 34.05, 32.8, 31.4, 30.98, 29.6, 29.5. MS calcd. for $C_{97}H_{128}O_8$ (1421.1); found: 1439.9 $(M + NH_4)^+$.

Synthesis of 2,2′-(Decane-1,10-diyl)bis(5,11,17,23-tetra-p-tert-butyl-tetrahydroxy-calix[4]arene, 15

Reagents used in the general synthesis were 2.29 g (1.48 mmol) of **8**, 28 g (133 mmol) of cyclohexyl iodide in 30 mL of DMF. Purification by chromatography column ($CHCl_3$/Hex 1:1 → EtOAc) afforded 0.455 g of pure product (Yield: 21%). ^{1}H NMR ($CDCl_3$): 10.28 (s, 8H, –OH), 7.1–6.97 (m, 16H, ArH), 4.47 (t, 2H, $^3J_{HH}$ = 7.8 Hz, Ar–CH–CH_2–), 4.27–4.22 (m, 6H Ar–CH_2–Ar), 3.48 (d, 4H, $^2J_{HH}$ = 13.6 Hz, Ar–CH–CH_2), 2.16 (s, 16H, –CH_2–), 1.2 (s, 72H, C(CH_3)$_3$). ^{13}C NMR ($CDCl_3$):146.8, 144.3, 131.2, 127.8, 125.95, 35.6, 34.2, 34.02, 31.4, 29.6, 29.5. MS calcd. for $C_{98}H_{130}O_8$ (1436.02); found: 1454.01 $(M + NH_4)^+$.

Synthesis of $[Mn^{III}_2Mn^{II}_2(13–8H)(\mu_3\text{-}OH)_2(DMF)_{5.5}(MeOH)_{0.5}](H_2O)_{1.5}$, 16

$MnCl_2{\cdot}4H_2O$ (2 eq., 14.1 mg, 0.071 mmol) and **13** (1 eq., 50 mg, 0.0355 mmol) were dissolved in a 1:1 DMF/MeOH mixture (20 mL). After 10 min of stirring, Et_3 N (0.05 mL) was added and the resulting deep purple solution stirred for 2 h. The reaction mixture was filtered to leave a deep purple solution. Purple crystals suitable for diffraction studies were obtained upon slow evaporation of the mother liquor. *Crystal data for 16 (CCDC 1432189):* $C_{113}H_{165.5}N_{5.5}O_{18.5}Mn_4$, M = 2116.76, Purple Block, 0.02 × 0.02 × 0.09 mm^3, monoclinic, space group $P2_1/c$, a = 25.1565(8), b = 20.0930(6), c = 22.7572(7) Å, β = 97.681(2)°, V = 11399.9(6) Å^3, Z = 4, Bruker D8 with PHOTON 100 detector, synchrotron radiation (λ = 0.77490 Å), T = 100(2)K, $2\theta_{max}$ = 41.5°, 65220 reflections collected, 8958 unique (R_{int} = 0.1114). Final *GooF* = 1.102, $R1$ = 0.1210, $wR2$ = 0.2991.

Synthesis of $[Mn^{III}_2Mn^{II}_2(14–8H)(\mu_3\text{-}OH)_2(MeOH)(dmf)_5](MeOH)(dmf)(H_2O)$, 17

$MnCl_2{\cdot}4H_2O$ (4 eq., 27.8 mg, 0.14 mmol) and **14** (1 eq., 50 mg, 0.035 mmol) were dissolved in a 1:1 DMF/MeOH mixture (20 mL). After 10 min of stirring, Et_3 N (0.05 mL) was added and the resulting deep purple solution stirred for 2 h. The reaction mixture was filtered to leave a deep purple solution. Purple crystals suitable for diffraction studies were obtained upon slow evaporation of the mother liquor. *Crystal data for 17 (CCDC 1432190):* $C_{117}H_{176}N_6O_{20}Mn_4$, M = 2206.39, Purple Block, 0.3 × 0.3 × 0.4 mm^3, triclinic, space group $P-1$, a = 12.375(3), b = 18.727(4), c = 25.238(5) Å, α = 84.03(3), β = 88.68(3), γ = 89.00(3)°, V = 5815(2) Å^3, Z = 2, Bruker Apex-II diffractometer, Mo-Kα radiation (λ = 0.71073 Å), T = 100(2)K, $2\theta_{max}$ = 41.1°, 42921 reflections collected, 11547 unique (R_{int} = 0.1056). Final *GooF* = 1.077, $R1$ = 0.0963, $wR2$ = 0.2652.

Synthesis of $[Mn^{III}_2Mn^{II}_2(15–8H)(\mu_3\text{-}OH)_2(dmf)_6](dmf)_{1.5}(MeOH)_{0.5}(H_2O)_{1.5}$, 18

$MnCl_2{\cdot}4H2O$ (1 eq., 6.9 mg, 0.0348 mmol) and **15** (1 eq., 50 mg, 0.0348 mmol) were dissolved in a 1:1 DMF/MeOH mixture (20 mL). After 10 min of stirring, Et3 N (0.05 mL) was added and the resulting deep purple solution stirred for 2 h. The reaction mixture was filtered to leave a deep purple solution. Purple crystals suitable for diffraction studies were obtained upon slow evaporation of the mother liquor. *Crystal data for 18 (CCDC 1432191):* $C_{121}H_{181.5}N_{7.5}O_{19.5}Mn_4$, M = 2272.99, Purple Block, 0.1 × 0.15 × 0.04 mm^3, triclinic, space group $P-1$, a = 12.7808(5), b = 19.2134(8), c = 27.4523(12) Å, α = 74.294(2), β = 82.588(3), γ = 85.413(2)°, V = 6428.2(5) Å^3, Z = 2, Bruker D8 with PHOTON 100 detector, synchrotron radiation (λ = 0.77490 Å), T = 100(2)K, $2\theta_{max}$ = 62.4°, 98239 reflections collected, 31909 unique (R_{int} = 0.0399). Final *GooF* = 1.024, $R1$ = 0.0914, $wR2$ = 0.2740.

Synthesis of $[Mn^{III}_4Gd^{III}_4(14–8H)(\mu_3\text{-}CO_3)_2(\mu_3\text{-}OH)_4(H_2O)_6(dmf)_6](dmf)_6(MeOH)_4$, 19

$MnCl_2{\cdot}4H_2O$ (2 eq., 13.9 mg, 0.071 mmol), $GdCl_3{\cdot}6H_2O$ (1 eq., 9.3 mg, 0.035 mmol) and **14** (1 eq., 50 mg, 0.035 mmol) were dissolved in a 1:1 DMF/MeOH mixture (20 mL). After 10 min of stirring, Et_3N (0.05 mL) was added and the resulting deep purple solution stirred for 2 h. The reaction mixture was filtered to leave a deep purple solution. Purple crystals suitable for diffraction studies were obtained upon slow evaporation of the mother liquor. *Crystal data for 19 (CCDC 1432192):* $C_{236}H_{356}N_{12}O_{48}Mn_4Gd_4$, $M = 4978.07$, Purple Block, $0.2 \times 0.35 \times 0.4$ mm^3, triclinic, space group $P-1$, $a = 14.9707(7)$, $b = 21.9372(6)$, $c = 22.0011(6)$ Å, $\alpha = 113.205(3)$, $\beta = 93.322(3)$, $\gamma = 107.520(3)°$, $V = 6203.1(4)$ Å^3, $Z = 1$, Bruker APEX-II diffractometer, Cu-Kα radiation ($\lambda = 1.54178$ Å), $T = 153(2)$K, $2\theta_{max} = 153.6°$, 121039 reflections collected, 25512 unique ($R_{int} = 0.1112$). Final *GooF* = 1.039, $R1 = 0.0855$, $wR2 = 0.2296$.

Acknowledgements

We thank the EPSRC for financial support of this work (EP/I03255X/1 & EP/I031421/1). Mass spectrometry data were acquired at the EPSRC UK National Mass Spectrometry Facility at Swansea University.

Disclosure statement

No potential conflict of interest was reported by the authors.

Funding

This work was supported by the EPSRC [EP/I03255X/1], [EP/I031421/1]; The Advanced Light Source is supported by the Director, Office of Science, Office of Basic Energy Sciences, of the US Department of Energy [contract number DE-AC02-05CH11231].

Supplemental material

Experimental data relating to this manuscript can be retrieved at: http://dx.doi.org/10.7488/ds/359

References

(1) MacGillivray, L.R.; Atwood, J.L. *Nature* **1997**, *389,* 469-472.
(2) Gerkensmeier, T.; Iwanek, W.; Agena, C.; Fröhlich, R.; Kotila, S.; Näther, C.; Mattay, J. *Eur. J. Org. Chem.* **1999**, *9*, 2257–2262.
(3) Atwood, J.L.; Barbour, L.J.; Hardie, M.J.; Raston, C.L. *Coord. Chem. Rev.* **2001**, *222*, 3–32.
(4) Barrett, E.S.; Dale, T.J.; Rebek, J., Jr. *J. Am. Chem. Soc.* **2007**, *129,* 3818–3819.
(5) Dalgarno, S.J.; Tucker, S.A.; Bassil, D.B.; Atwood, J.L. *Science* **2005**, *309,* 2037–2039.
(6) Ugono, O.; Holman, K.T. *Chem. Commun.* **2006**, *20*, 2144–2146.
(7) Gutsche, C.D. *Calixarenes 2001*; Dordrecht: Kluwer Academic, **2001**; pp. 1–25. Chapter 1 and references therein.
(8) Aronica, C.; Chastanet, G.; Zueva, E.; Borshch, S.A.; Clemente-Juan, J.M.; Luneau, D. *J. Am. Chem. Soc.* **2008**, *130,* 2365–2371.
(9) Karotsis, G.; Teat, S.J.; Wernsdorfer, W.; Piligkos, S.; Dalgarno, S.J.; Brechin, E.K. *Angew. Chem. Int. Ed.* **2009**, *48,* 8285–8288.
(10) Taylor, S.M.; Karotsis, G.; McIntosh, R.D.; Kennedy, S.; Teat, S.J.; Beavers, C.M.; Wernsdorfer, W.; Piligkos, S.; Dalgarno, S.J.; Brechin, E.K. *Chem. Eur. J.* **2011**, *17,* 7521–7530.
(11) Karotsis, G.; Kennedy, S.; Dalgarno, S.J.; Brechin, E.K. *Chem. Commun.* **2010**, *46,* 3884–3886.
(12) Taylor, S.M.; McIntosh, R.D.; Beavers, C.M.; Teat, S.J.; Piligkos, S.; Dalgarno, S.J.; Brechin, E.K. *Chem. Commun.* **2011**, *47,* 1440–1442.
(13) Karotsis, G.; Evangelisti, M.; Dalgarno, S.J.; Brechin, E.K. *Angew. Chem. Int. Ed.* **2009**, *48,* 9928–9931.
(14) Karotsis, G.; Kennedy, S.; Teat, S.J.; Beavers, C.M.; Fowler, D.A.; Morales, J.J.; Evangelisti, M.; Dalgarno, S.J.; Brechin, E.K. *J. Am. Chem. Soc.* **2010**, *132,* 12983–12990.
(15) Sanz, S.; Ferreira, K.; McIntosh, R.D.; Dalgarno, S.J.; Brechin, E.K. *Chem. Commun.* **2011**, *47,* 9042–9044.
(16) Sanz, S.; McIntosh, R.D.; Beavers, C.M.; Teat, S.J.; Evangelisti, M.; Brechin, E.K.; Dalgarno, S.J. *Chem. Commun.* **2012**, *48,* 1449–1451.
(17) Taylor, S.M.; McIntosh, R.D.; Piligkos, S.; Dalgarno, S.J.; Brechin, E.K. *Chem. Commun.* **2012**, *48,* 11190–11192.
(18) Su, K.; Jiang, F.; Qian, J.; Zhou, K.; Pang, J.; Basahel, S.; Mokhtar, M.; Al-Thabaiti, S.A.; Hong, M. *Inorg. Lett.* **2014**, *1,* 1–8.
(19) Taylor, S.M.; Frost, J.M.; McLellan, R.; McIntosh, R.D.; Brechin, E.K.; Dalgarno, S.J. *CrystEngComm* **2014**, *16,* 8098–8101.
(20) Palacios, M.A.; McLellan, R.; Taylor, S.M.; Beavers, C.M.; Teat, S.J.; Wernsdorfer, W.; Piligkos, S.; Dalgarno, S.J.; Brechin, E.K. *Chem. Eur. J.* **2015**, *21,* 11212–11218.
(21) Desroches, C.; Pilet, G.; Borshch, S.A.; Parola, S.; Luneau, D. *Inorg. Chem.* **2005**, *44,* 9112–9120.
(22) Desroches, C.; Pilet, G.; Szilágyi, P.A.; Molnár, G.; Borshch, S.A.; Bousseksou, A.; Parola, S.; Luneau, D. *Eur. J. Inorg. Chem.* **2006**, *2,* 357–365.
(23) Lamouchi, M.; Jeanneau, E.; Pillonnet, A.; Brioude, A.; Martini, M.; Stéphan, O.; Meganem, F.; Novitchi, G.; Luneau, D.; Desroches, C. *Dalton Trans.* **2012**, *41,* 2707–2713.
(24) Kajiwara, T.; Iki, N.; Yamashita, M. *Coord. Chem. Rev.* **2007**, *251,* 1734–1746.
(25) Bi, Y.; Wang, X.-T.; Liao, W.; Wang, X.; Wang, X.; Zhang, H.; Gao, S. *J. Am. Chem. Soc.* **2009**, *131,* 11650–11651.
(26) Liu, M.; Liao, W.; Hu, C.; Du, S.; Zhang, H. *Angew. Chem. Int. Ed.* **2012**, *51,* 1585–1588.
(27) Liu, M.; Liao, W. *CrystEngComm* **2012**, *14,* 5727–5729.
(28) Tian, H.; Du, S.; Bi, Y.; Liao, W. *Chem. Commun.* **2013**, *49,* 8211–8213.
(29) Xiong, K.; Jiang, F.; Gai, Y.; Yuan, D.; Chen, L.; Wu, M.; Su, K.; Hong, M. *Chem. Sci.* **2012**, *3,* 2321–2325.
(30) Su, K.; Jiang, F.; Qian, J.; Wu, M.; Gai, Y.; Pan, J.; Yuan, D.; Hong, M. *Inorg. Chem.* **2014**, *53,* 18–20.
(31) Su, K.; Jiang, F.; Qian, J.; Gai, Y.; Wu, M.; Bawaked, S.M.; Mokhtar, M.; AL-Thabaiti, S.A.; Hong, M. *Cryst. Growth Des.* **2014**, *14,* 3116–3123.

(32) Tabatabai, M.; Vogt, W.; Böhmer, V. *Tetrahedron Lett.* **1990**, *31,* 3295–3298.
(33) Sartori, G.; Maggi, R.; Bigi, F.; Arduini, A.; Pastorio, A.; Porta, C. *J. Chem. Soc., Perkin Trans. 1* **1994**, *13*, 1657–1658.
(34) Grüttner, G.; Böhmer, V.; Vogt, W.; Thondorf, I.; Biali, S.E.; Grynszpan, F. *Tetrahedron Lett.* **1994**, *35,* 6267–6270.
(35) Biali, S.E.; Böhmer, V.; Cohen, S.; Ferguson, G.; Grüttner, G.; Grynszpan, F.; Paulus, E.F.; Thondorf, I.; Vogt, W. *J. Am. Chem. Soc.* **1996**, *118,* 12938–12949.
(36) Biali, S.E.; Böhmer, V.; Columbus, I.; Ferguson, G.; Grüttner, G.; Grynszpan, F.; Paulus, E.F.; Thondorf, I. *J. Chem. Soc., Perkin Trans. 2* **1998**, *10*, 2261–2269.
(37) Böhmer, V. *Liebigs Ann./Recueil* **1997**, 2019–2030.
(38) Simaan, S.; Agbaria, K.; Biali, S.E. *J. Org. Chem.* **2002**, *67,* 6136–6142.
(39) Simaan, S.; Biali, S.E. *J. Org. Chem.* **2003**, *68,* 3634–3639.
(40) Simaan, S.; Biali, S.E. *J. Org. Chem.* **2003**, *68,* 7685–7692.
(41) Simaan, S.; Biali, S.E. *Org. Lett.* **2005**, *7,* 1817–1820.
(42) Columbus, I.; Biali, S.E. *J. Org. Chem.* **2008**, *73,* 2598–2606.
(43) Scully, P.A.; Hamilton, T.M.; Bennett, J.L. *Org. Lett.* **2001**, *3,* 2741–2744.
(44) Hertel, M.P.; Behrle, A.C.; Williams, S.A.; Schmidt, J.A.R.; Fantini, J.L. *Tetrahedron* **2009**, *65,* 8657–8667.
(45) Hardman, M.J.; Thomas, A.M.; Carroll, L.T.; Williams, L.C.; Parkin, S.; Fantini, J.L. *Tetrahedron* **2011**, *67,* 7027–7034.
(46) Carroll, L.T.; Aru Hill, P.; Ngo, C.Q.; Klatt, K.P.; Fantini, J.L. *Tetrahedron* **2013**, *69,* 5002–5007.
(47) The pentyl derivative was not synthesised due to commercial unavailability of 1,5-dibromopentane. Although this is the case the outcome is expected to be analogous to the other tethers employed.
(48) It should be noted that Fischer and Weber recently reported the synthesis of octa-methoxy derivatives 2 and 4, but by an alternative route incorporating an iodoalkane modified C[4] intermediate. See: Fischer, C.; Weber, E. *J. Incl. Phenom. Macrocycl. Chem.* **2014**, *79,* 151–160.
(49) Xu, W.; Puddephatt, R.J.; Manojlovic-Muir, L.; Muir, K.W.; Frampton, C.S. *J. Incl. Phenom. Mol.* **1994**, *19,* 277–290.
(50) *In-situ* carbonate formation is not unprecedented for this combination of reactants and has previously afforded unexpected cluster geometries. For example see: Xiong, K -C.; Jiang, F.-L.; Gai, Y.-L.; Yuan, D.-Q.; Han, D.; Ma, J.; Zhang, S.-Q.; Hong, M.-C. *Chem. Eur. J.*, **2012**, *18,* 5536–5540.

Chapter 25
Structural Trends in Calix[4]arene-Supported Cluster Chemistry

Marco Coletta, Euan K. Brechin, and Scott J. Dalgarno

25.1 Introduction

Polynuclear clusters of paramagnetic metal ions that display interesting magnetic phenomena, species also known as Molecular Magnets (MMs), continue to attract strong interest due to their potential application in fields such as information storage, spintronics, magnetic resonance imaging (MRI), magnetic refrigeration and thermotherapy [1]. Understanding or controlling the synthesis and construction of these (often highly) complex assemblies from multi-component mixtures is a challenging goal, and one that is frequently tackled through targeted/smart ligand design. As cone conformers, calix[4]arenes (denoted H_4C[4]s and C[4]s herein to represent the extremes of fully protonated or deprotonated forms respectively) are excellent synthetic platforms for both the complexation of metal ions and, due to the bridging capability of their lower-rim oxygen atoms, subsequent cluster formation. Cluster formation is of course the main thrust of this contribution, but before continuing to detailed discussion it should be noted that metal ions can be complexed by the lower-rim phenolic oxygens such that the ion resides either *endo* or *exo* to the calix[4]arene cavity [2]. In cases involving *endo* binding the metal ion interacts simultaneously with both the π systems of the macrocycle and the lower-rim oxygen atoms (Fig. 25.1a). In contrast, *exo* binding involves complexation of the metal ion to the lower-rim phenolic oxygens such that it resides just below the macrocycle plane (Fig. 25.1b). It is noteworthy that a limited number of

M. Coletta • S.J. Dalgarno (✉)
Institute of Chemical Sciences, Heriot-Watt University, Riccarton, Edinburgh EH14 4AS, UK
e-mail: s.j.dalgarno@hw.ac.uk

E.K. Brechin (✉)
EaStCHEM School of Chemistry, The University of Edinburgh, David Brewster Road, Edinburgh EH9 3FJ, UK
e-mail: ebrechin@ed.ac.uk

P. Neri et al. (eds.), *Calixarenes and Beyond*, DOI 10.1007/978-3-319-31867-7_25

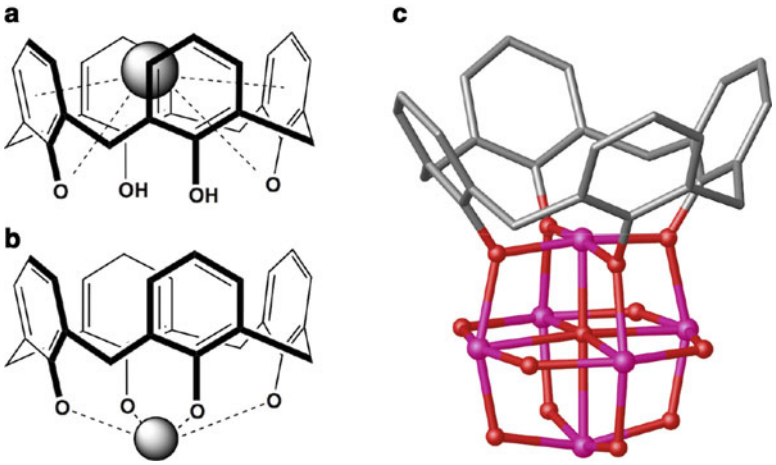

Fig. 25.1 (**a**) Schematic of *endo*-C[4] metal ion binding. (**b**) Schematic of *exo*-C[4] metal ion binding at the lower-rim oxygens. (**c**) C[4]-supported polyoxovanadate cluster showing the core and bridging atoms [3]. H atoms, C[4] ^{t}Bu groups and other atoms of bridging groups are omitted for clarity in C. Figures not to scale. Colour code: C – *grey*, O – *red*, V – *pink*

cations (e.g. alkaline and alkaline-earth metal ions) are sufficiently small to allow them to participate in *endo* complexation involving simultaneous cation-π interactions, rendering this type of interaction far less common in the literature. Moreover, *exo* complexation will always be preferred over *endo* if there are ligated solvent molecules present [2]. The remainder of this chapter deals almost exclusively with *exo* metal ion binding.

To our knowledge the first high-nuclearity C[4]-supported transition metal (TM) cluster was reported by Luneau and co-workers in 2008, this being a mixed valence polyoxovanadate species shown in Fig. 25.1c [3]. Recent times have witnessed an expansion in C[4]-supported cluster synthesis, but before that is reviewed in detail it is worth noting that significant attention has been devoted to analogous coordination chemistry with thia-, sulfinyl- and sulfonyl-bridged calix[4]arenes; these molecules possess S, SO and SO_2 bridging atoms/groups respectively [4]. This chemistry is discussed prior to that of methylene-bridged C[4]s.

25.1.1 Thia-, Sulfinyl- and Sulfonyl-Bridged Calix[4]arenes in Cluster Synthesis

While methylene-bridged C[4]s are able to bind one metal ion centrally at the lower-rim, the presence of heteroatoms or heteroatom-containing groups at the bridging positions (rather than CH_2) presents additional binding sites that markedly affect the complexation of metal ions, and thus the resulting cluster topologies.

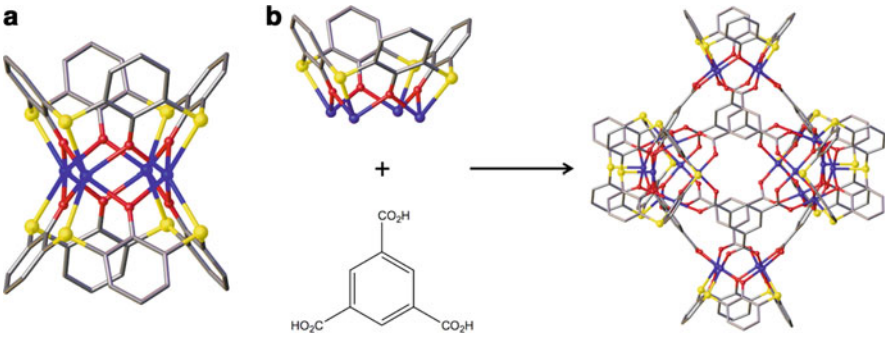

Fig. 25.2 (**a**) Structure of a tC[4]-supported tetranuclear TM ion cluster showing coordination to the bridge donor atoms as well as lower-rim oxygens [4]. (**b**) Directed assembly of a metal-organic octahedron through the use of a topologically directing linker and a [TM_4tC[4]] building block [16]. Figures not to scale. Colour code: C – *grey*, O – *red*, S – *yellow*, TM – *dark blue*

Given that the C-S bonds in thia-C[4] (H_4tC[4]) are longer than the corresponding C-C bonds in H_4C[4], each heteroatom generates an alternative binding site containing one soft sulphur and two proximal hard oxygen donors. Several H_4tC[4]-supported alkali metal clusters in the literature display cation binding akin to that of H_4C[4]s, examples of which include $[Na_6(tC[4])_2(dmf)_2]^{2-}$, $[K_2(H_3tC[4])_2(OEt_2)_2H_2O]$ and $[Rb_4(H_3tC[4])_4(H_2O)(dmf)_{10}]$ [5, 6]. Although this is the case, H_4tC[4] behaves very differently in comparison to H_4C[4] with respect to the coordination of first row transition metal (TM) ions such as Mn^{II}, Co^{II}, Cu^{II} and Zn^{II} [7–9]. The same is true for heavier TM as well as lanthanide metal (Ln) ions (e.g. Hg^{II} and Nd^{III} respectively) [10, 11], and this behaviour is also common to both sulfinyl- and sulfonyl-C[4]s. In the vast majority of cases these components form trinuclear or tetranuclear metal clusters, an example of the latter being shown in Fig. 25.2a. The coordination pattern is similar in all cases, with TM or Ln ions sandwiched between two partially or fully deprotonated tC[4]s. In this arrangement the four phenolic oxygens and four sulphur atoms are near co-planar, with complexation occurring in the alternative binding sites described above. The ubiquity of [TM_4tC[4]] moieties has recently led to them being used as structural building units in the assembly of large metal-organic polyhedra (MOPs) [12–21]. A number of groups have demonstrated the ability to assemble a range of stable (and in some cases porous) MOPs through linking [TM_4tC[4]] moieties with topologically directing ligands such as benzene tricarboxylic acid (Fig. 25.2b) [16, 17]. The ability to control MOP volume/shape and pore size is particularly attractive, as these stable assemblies have potential for application as gas storage materials or hosts for dye molecules [21] (amongst other species).

The fact that C[4] predictably binds one metal ion at the lower-rim gives rise to a different type of metal-organic building unit, one that we (amongst others) have used to assemble a range of new cluster species [3, 22–31]. In the absence of additional donor atoms at the bridge positions, a single TM or Ln ion can be bound

in the polyphenolic pocket and these oxygen atoms are well suited to bridge to additional metal ions (for example see bridging between vanadium centres in Fig. 25.1c). The remainder of Sect. 25.1 deals with (a) exploratory cluster synthesis with $H_4C[4]$s, (b) the effects of varying ambient reaction conditions, (c) the establishment of empirical metal ion binding rules for $H_4C[4]$s and (d) synthetic modification at the methylene bridge position. Sections 25.2 and 25.3 are concerned with the use of bis-$H_4C[4]$s tethered either directly at, or with a spacer via the methylene bridge, with a particular emphasis on extension of metal ion binding principles established here for $H_4C[4]$s.

25.1.2 *Methylene-Bridged Calix[4]arenes in Cluster Synthesis*

Attempts at C[4]-supported cluster synthesis with first row TM ions under ambient conditions gave rise to the formation of two new assembly types. The first of these was found to be a family of mixed valence $[Mn^{III}_2Mn^{II}_2(C[4])_2(\mu_3\text{-}OH)_2(dmf)_6]$ clusters (**1**, Fig. 25.3a), the metallic skeleton of which has a planar diamond- or butterfly-like topology (Fig. 25.4a) [22, 23]. The (Jahn-Teller distorted) Mn^{III} and (distorted octahedral) Mn^{II} ions occupy the wing-tip and body positions respectively and these are bridged via the C[4] lower-rim oxygens and μ_3-hydroxides. This cluster motif is not unusual in Mn cluster chemistry but, in this case, the oxidation states are reversed relative to those previously reported [24]. A notable feature of **1** is that the $[Mn^{III}(C[4])]^-$ moiety caps the cluster core, a feature observed in all clusters containing manganese ions.

The second general type of assembly isolated was a pair of enneanuclear Cu^{II} clusters. These were formed from different Cu^{II} salts and have formulae $[Cu^{II}_9(C[4])_3(\mu\text{-}OH)_3Cl_2(dmso)_6][Cu^{II}Cl_2]$ (**2**, Fig. 25.3b) and $[Cu^{II}_9(C[4])_3(\mu\text{-}OH)_3(NO_3)_2(dmso)_6](NO_3)$ (**3**); the only significant difference between these clusters is the nature of the anions present [25]. The common metallic skeleton has a tri-capped trigonal prismatic topology (Fig. 25.4b), the central core of which has three hydroxides bridging the Cu^{II} ions at the prism vertices. Chloride or nitrate anions occupy the triangular faces of the prism and additional counterions are present in the crystal lattice. Cluster core capping occurs on each of the rectangular faces of the prism with $[Cu^{II}(C[4])]^{2-}$ moieties, showing the versatility of C[4] in its ability to accommodate TM ions in either the second or third oxidation state. Other structurally analogous TM^{II}_9 clusters have followed (e.g. Co^{II}_9), all of which have similar cluster topologies but that possess variations in the anions present [26].

Similar screening of cluster formation with Ln ions resulted in the formation of a series of clusters with general formula $[Ln^{III}_6(C[4])_2(\mu\text{-}OH)_4(\mu_4\text{-}O)_2(HCO_2)_2(dmf)_8][Cu^{I}Cl_2]$ (**4**, Ln = Gd, Tb or Dy, Fig. 25.3c); [27] there is disorder in the bridging anions within these clusters but only one combination is described and shown for

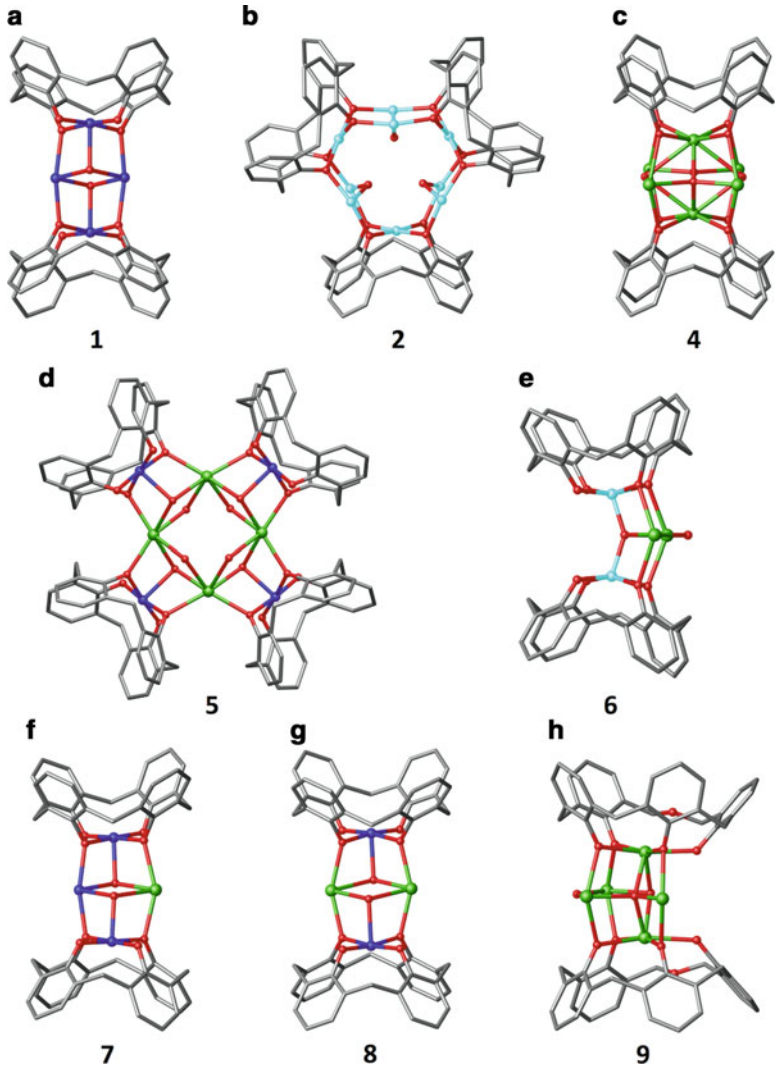

Fig. 25.3 Partial single crystal *X*-ray structures of clusters **1** (**a**) [22, 23], **2** (**b**) [25], **4** (**c**) [27], **5** (**d**) [29], **6** (**e**) [30], **7** (**f**) [31], **8**(**g**) [31], and **9** (**h**) [32]. H atoms, C[4] ^{t}Bu groups, ligated and co-crystallised solvent molecules omitted for clarity. Figures not to scale. Colour code: C – *grey*, O – *red*, TM – *dark/pale blue*, Ln – *green*

clarity. The core topology in **4** is markedly different to those discussed above for TM clusters, with the Ln ions arranged at the vertices of an octahedron (Fig. 25.4c). The cavity bound Ln ions sit slightly out of the plane defined by the C[4] lower-rim oxygens, and the four remaining ions define the central square of the octahedron. Capping behaviour is again observed, in this case as a $[Ln^{III}(C[4])]^{-}$ moiety, and this core topology can also be achieved through solvothermal synthesis [28].

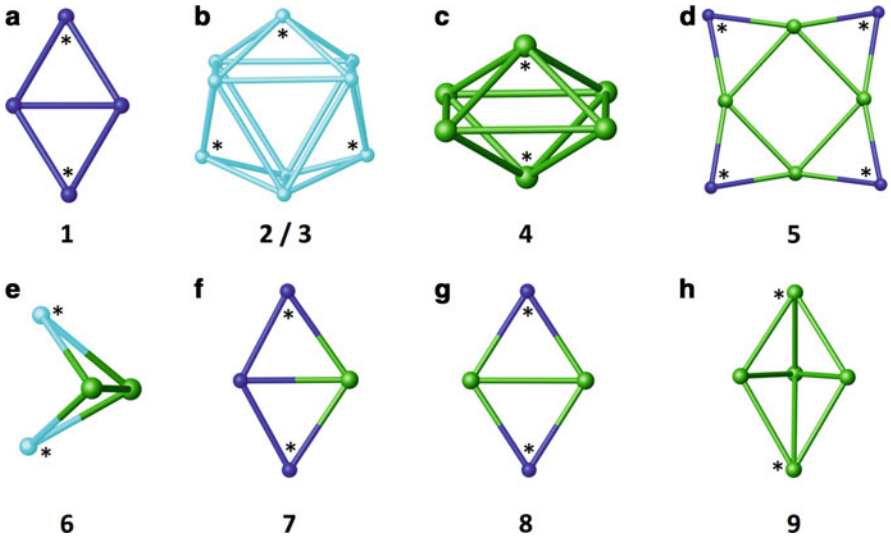

Fig. 25.4 Topologies of clusters **1**–**9** with asterisks indicating core capping by either $[TM^{II}C[4]]^{2-}$, $[TM^{III}C[4]]^{-}$ or $[Ln^{III}C[4]]^{-}$ moieties [22–31]. Figures not to scale. Colour code: TM – *dark/pale blue*, Ln – *green*

Given the versatility of $H_4C[4]$ towards cluster formation with TM or Ln ions we thought it reasonable to expect that, with tuning of the reaction conditions/stoichiometries, it would be possible to synthesise mixed 3*d*/4*f* assemblies. Addition of Ln^{III} ions to the reaction used to form **1** afforded the first series of C[4]-supported 3*d*/4*f* clusters that were found to be of general formula $[Mn^{III}{}_4Ln^{III}{}_4(C[4])_4(\mu_3\text{-}OH)_4(NO_3)_2(dmf)_6(H_2O)_6](OH)_2$ (**5**, Ln = Gd, Tb or Dy, Fig. 25.3d) [29]. These are best described as a square of Ln ions, each edge of which is capped by a $[Mn^{III}(C[4])]^{-}$ moiety (Fig. 25.4d). The library of 3*d*/4*f* clusters was expanded by synthesis of a series of C[4]-supported $Fe^{III}{}_2Ln^{III}{}_2$ clusters of general formula $[Fe^{III}{}_2Ln^{III}{}_2(C[4])_2(\mu_4\text{-}O)(\mu\text{-}OH)(dmf)_4(MeOH)_2(H_2O)_2]Cl$ (**6**, Ln = Gd, Tb or Dy, Fig. 25.3e) [30]. The metallic skeleton is a distorted tetrahedron in which all of the metal ions are connected via a $\mu_4\text{-}O^{2-}$ anion (Fig. 25.4e). The pentacoordinate Fe^{III} ions (distorted square pyramidal geometry) are bound by the C[4] lower-rim oxygens, capping the core in a manner akin to $[Mn^{III}(C[4])]^{-}$ in **1**.

By tuning the reaction conditions it was possible to interchange one or both of the body Mn^{II} ions in **1** for Ln^{III} ions. As a result we isolated clusters of general formulae $[Mn^{III}{}_2Mn^{II}Ln^{III}(C[4])_2(\mu_3\text{-}OH)_2(NO_3)(dmso)_6]$ (**7**, Ln = Gd, Tb or Dy, Fig. 25.3f) and $[Mn^{III}{}_2Ln^{III}{}_2(C[4])_2(\mu_3\text{-}OH)_2(dmso)_8]Cl_2$, (**8**, Ln = Gd, Tb or Dy, Fig. 25.3g), and through structural studies observed small structural changes due to difference in ion size [31]. The presence of the larger, more highly-coordinated Ln ion in **7** has the effect of distorting the formerly co-planar orientation of C[4]s in **1** (Fig. 25.4f). Co-planarity is restored upon the introduction of the second Ln ion

(**8**, Fig. 25.4g) and, from these exploratory studies, it is possible to make the following empirical rules for binding and structural assembly behaviour:

- TM(II)/TM(III) ions will be bound by C[4] to produce $[TM(C[4]))]^{-/2-}$ capping moieties
- Ln(III) ions will be bound by C[4] to produce $[Ln(C[4]))]^{-}$ capping moieties
- TM ions will be preferentially bound by C[4] in any 3*d*/4*f* mixture
- Clusters are always capped on faces and or edges by the aforementioned moieties

With respect to this section, one final cluster of interest is that formed by reaction of Ln ions with homooxacalix[4]arene (hoC[4]) and which has the formula $[Ln^{III}_5(hoC[4])_2(NO_3)_3(\mu\text{-MeO})(\mu_4\text{-O})(\mu_3\text{-OH})(dmf)_7(H_2O)]$ (**9**, Ln = Gd, Tb or Dy, Fig. 25.3h) [32]. Inspection of the structure shows that the introduction of one ethereal linker in the $H_4C[4]$ framework alters the size and shape of the lower-rim binding pocket, the result of which is expulsion of one metal ion from the C[4]-supported Ln^{III}_6 cluster motif (**4**, Fig. 25.3c). In this case $[Ln^{III}(hoC[4])]^{-}$ moieties cap a triangle to produce a distorted square pyramidal metallic skeleton (Fig. 25.4h). These subtle effects therefore represent another viable route to influencing cluster composition through understandable structure capping behaviour.

25.1.3 *Calix[4]arenes Functionalised at the Methylene Bridge*

While functionalisation of the calix[4]arene framework at both the upper- and lower-rims leads to a myriad of useful supramolecular building blocks, synthetic alteration at the methylene bridge also represents a viable synthetic route to obtain novel platforms that can be exploited in cluster formation; modification at the bridge leaves the lower-rim polyphenolic pocket free for metal ion binding [33]. In this regard Böhmer showed that it is possible to include new functionalities within the calixarene scaffold through convergent synthetic routes involving fragment condensation and subsequent cyclisation. Work by the Biali group explored direct functionalisation at the methylene bridge, producing an impressive number of new derivatives bearing different functionalities (including double bonds [34], alkyl chains and aryl groups [35]). Fantini and co-workers developed an alternative synthetic strategy to directly modify the methylene bridge, affording a series of C[4] derivatives with alkyl, benzyl, carboxylic acid and halide functionalities [36]. All of these developments are important in the context of C[4]-supported cluster formation as they present opportunities to introduce additional functionality that may, in turn, influence or direct both lower-rim coordination chemistry and cluster topology.

In addition to this, Fantini also recently developed a synthetic route to 2,2′-biscalix[4]arene (bis-H_4C[4]) [37], an important new building block in which the two macrocycles are directly linked via the methylene bridge. Single crystal *X*-ray diffraction data supported molecular modelling studies and demonstrated that the two H_4C[4] moieties are arranged *anti* with respect to one another, thus minimising interactions between bulky ^{t}Bu groups. Having established binding rules for H_4C[4]s, it was of interest to explore the coordination chemistry of bis-H_4C[4], with the expectation that it (a) would exhibit characteristic behaviour towards the complexation of TM and Ln ions and (b) allow one to increase and or control the nuclearity of the resulting polymetallic clusters.

25.2 Methylene-Bridge Linked Bis-calix[4]arene in Cluster Synthesis

Exploratory cluster formation experiments with bis-H_4C[4] began by mirroring conditions found to be successful in C[4]-supported cluster synthesis. Formation of bis-H_4C[4]-supported clusters would involve incorporation of two TM or Ln ions (one *per* C[4] pocket), coupled with inversion of one of the constituent C[4] rings from an *anti*- to *syn*- conformation [38]. Structural inversion was also expected to generate additional binding sites for TM/Ln ions as a result of four proximal lower-rim oxygens, two from each C[4] moiety. Bis-H_4C[4] behaved as one would expect, affording a series of clusters that are structurally related to their C[4]-supported analogues. Systematic increasing of cluster nuclearity, as well as double capping behaviour was also observed, all of which is discussed below.

25.2.1 Monometallic Systems

Reaction of bis-H_4C[4] with Mn^{II} chloride under analogous conditions used to form **1** afforded a new cluster of formula $[Mn^{III}_4Mn^{II}_4$(bis-C[4])$_2(\mu_3\text{-OH})_2(\mu\text{-OH})(\mu\text{-Cl})(H_2O)(MeOH)(dmf)_4]$ (**10**, Fig. 25.5a) [39]. Comparison of **1** and **10** shows that the mixed valence $Mn^{III}_4Mn^{II}_4$ metallic skeleton in the latter (Fig. 25.6a) is closely related to the $Mn^{III}_2Mn^{II}_2$ butterfly obtained with H_4C[4]. The metal ions in **10** are connected by phenolates, bridging hydroxide and chloride, with the ligand undergoing inversion as expected. In this *syn*-conformation the region between the two C[4]s has accommodated two additional Mn^{II} ions, and as a result the entire assembly is best described as two fused (and distorted) $Mn^{III}_2Mn^{II}_2$ butterflies. Finally, bis-H_4C[4] has formed a $[Mn^{III}_2$(bis-C[4])$]^{2-}$ capping moiety as anticipated, further highlighting the related structural features observed upon linking H_4C[4]s directly via the methylene bridge.

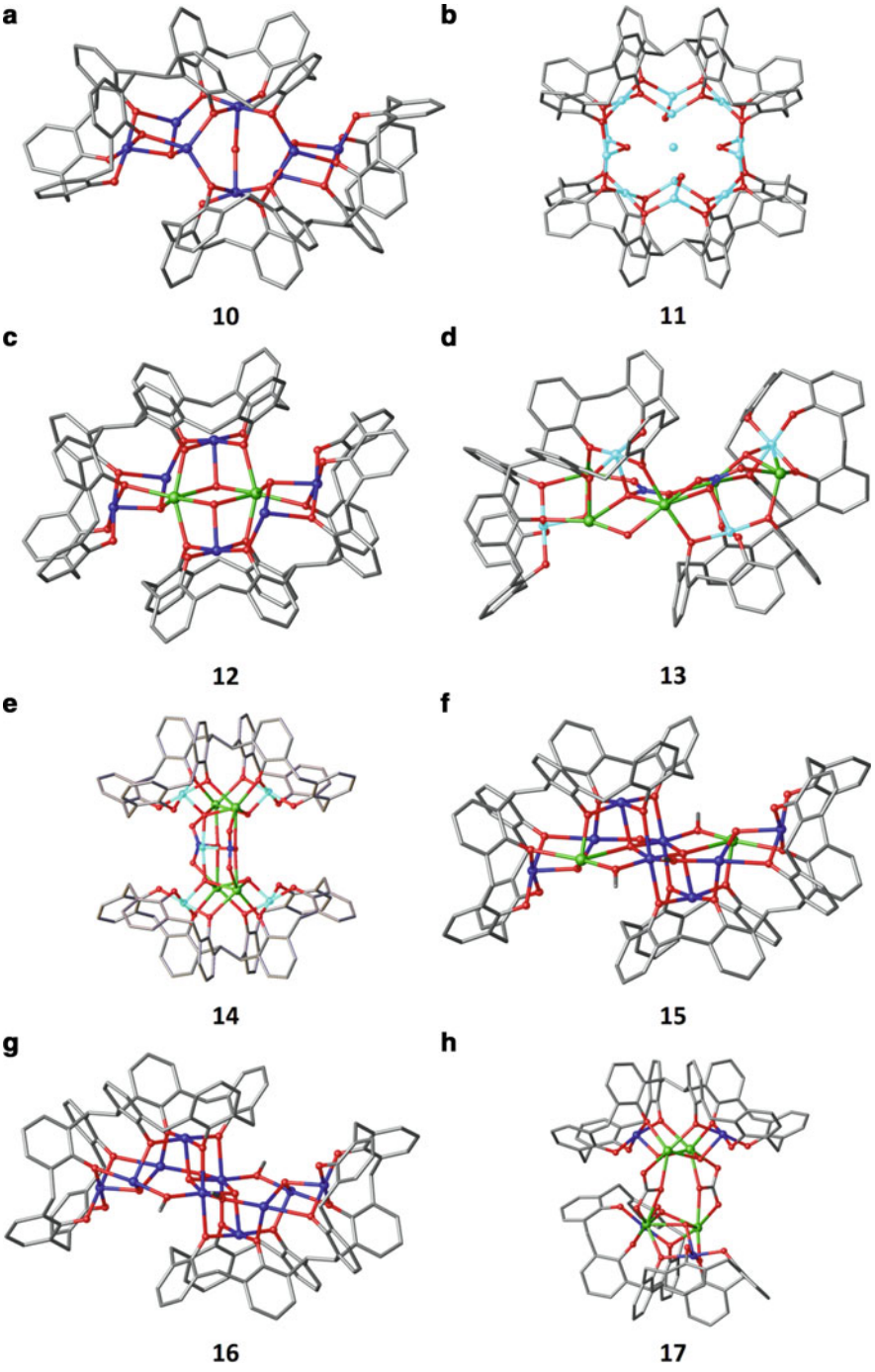

Fig. 25.5 Partial single crystal X-ray structures of clusters **10** (**a**) [39], **11** (**b**) [39], **12** (**c**) [39], **13** (**d**) [40], **14** (**e**) [40], **15** (**f**) [41], **16**(**g**) [41], and **17** (**h**) [41]. H atoms, C[4] ^{t}Bu groups, ligated and co-crystallised solvent molecules omitted for clarity. Figures not to scale. Colour code: C – *grey*, N – *navy blue*, O – *red*, TM – *dark/pale blue*, Ln – *green*

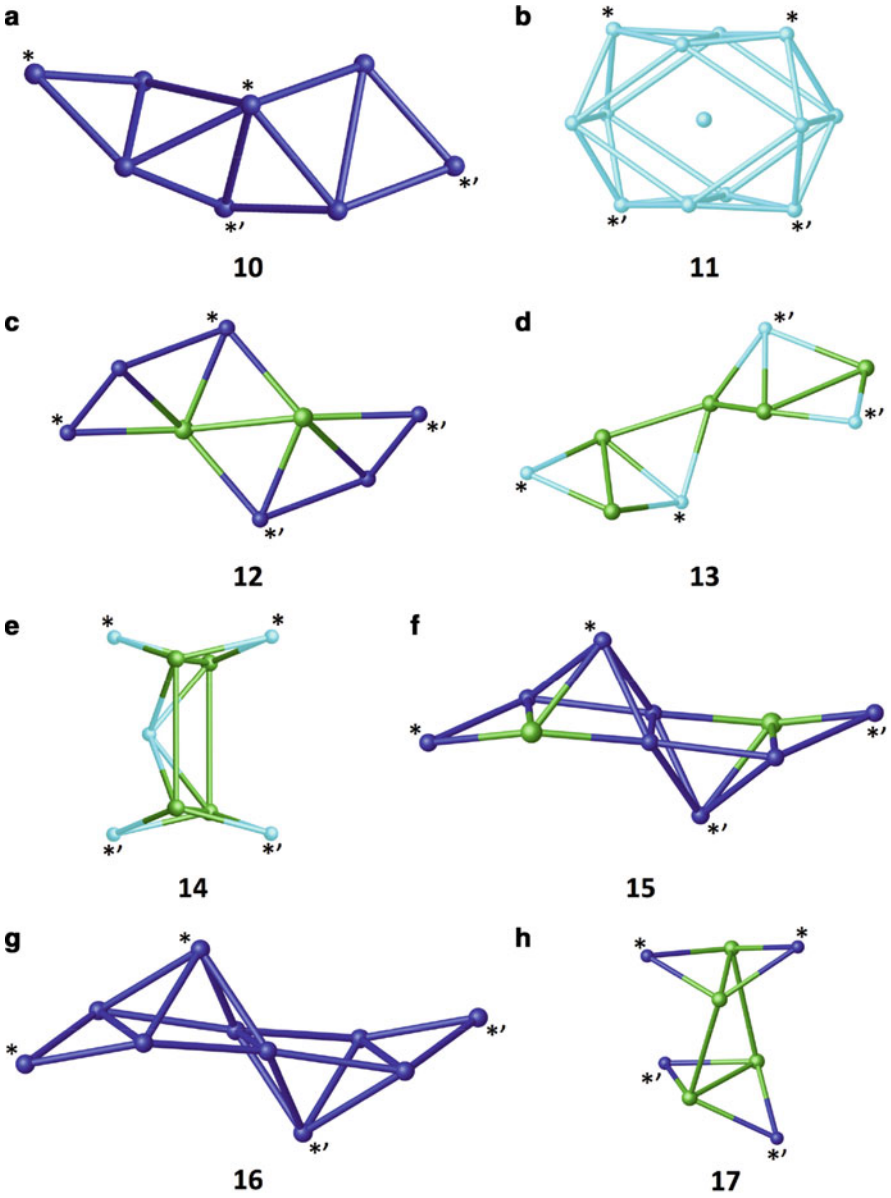

Fig. 25.6 Topologies of clusters **10**–**17** with asterisk/primed asterisk pairs indicating double core capping with either $[TM^{II}{}_2bisC[4]]^{4-}$ or $[TM^{III}{}_2bisC[4]]^{2-}$ moieties [39–41]. Figures not to scale. Colour code: TM – *dark/pale blue*, Ln – *green*

Reaction of bis-H_4C[4] with Cu^{II} nitrate under analogous conditions used to form **3** afforded a second structurally related cluster of formula $[Cu^{II}_{13}$(bis-C[4])$_2(NO_3)(\mu\text{-}OH)_8(dmf)_7](OH)$ (**11**, Fig. 25.5b) [39]. The metallic skeleton can be described as a tetracapped square prism (Fig. 25.6b), the central core of which has hydroxides bridging the Cu^{II} ions at the prism vertices, as well as the final Cu^{II} ion that resides in the centre of the assembly. This cluster shows striking similarity to the tri-capped trigonal prismatic Cu^{II}_9 species (**2** and **3**, Fig. 25.3b), with capping of the metallic core occurring with $[Cu^{II}_2$(bis-C[4])$]^{4-}$ moieties. This further validates binding rules observed for C[4], and the principle of their extension through H_4C[4] methylene bridge linking. Furthermore, it also demonstrates equivalent versatility towards accommodation of TMs in both the second and third oxidation states.

25.2.2 Bimetallic Systems

Screening cluster formation with bis-H_4C[4] and 3*d*/4*f* ions afforded several interesting results, all of which display structural trends observed for H_4C[4]. The first of the new clusters obtained was formed upon reaction of bis-H_4C[4] with Mn^{II} and Gd^{III} chlorides and has the formula $[Mn^{III}_4Mn^{II}_2Gd^{III}_2$(bis-C[4])$_2(Cl)_2(\mu_3\text{-}OH)_4(MeOH)_2(dmf)_8]$ (**12**, Fig. 25.5c). Compound **11** has clear similarities with **10** (Fig. 25.5a), the main difference being replacement of two Mn^{II} with two Gd^{III} ions [39]. The central butterfly in the metallic skeleton of **10** is retained to some extent, now being present as a central $Mn^{III}_2Gd^{III}_2$ analogue (Fig. 25.6c); this arises from the fusing of two distorted $Mn^{III}_2Mn^{II}Gd^{III}$ butterflies, with capping occurring through the expected $[Mn^{III}_2$(bis-C[4])$]^{2-}$ moieties.

Reaction of bis-H_4C[4] with Cu^{II} and Ln^{III} nitrates yielded a series of new clusters with general formula $[Cu^{II}_4Ln^{III}_5$(bis-C[4])$_2(\mu_3\text{-}OMe)(\mu\text{-}OMe)(\mu_3\text{-}OH)(\mu_4\text{-}NO_3)(\mu_5\text{-}NO_3)(MeOH)(dmf)_6(H_2O)_4](OH)_2$ (**13**, Ln = Gd, Tb or Dy, Fig. 25.5d) [40]. The metallic skeleton is best described as two $Cu^{II}_2Ln^{III}_2$-(bis-C[4]) butterflies tethered by a central Ln^{III} ion that is of square antiprismatic geometry (Fig. 25.6d). The core also contains a mixture of bridging anions, including μ_4- and μ_5-nitrates. As in the case of **11**, capping occurs through the expected $[Cu^{II}_2$(bis-C[4])$]^{4-}$ moieties.

A series of new Fe^{III}/Ln^{III} clusters was successfully isolated under analogous conditions used to synthesise **6** [40]. This new cluster type has a general formula of $[Fe^{III}_5Ln^{III}_4$(bis-C[4])$_2(\mu_4\text{-}O)_2(\mu_3\text{-}OH)_2(\mu_4\text{-}NO_3)_2(dmf)_8(H_2O)_6](OH)_3$ (**14**, Ln = Gd, Tb or Dy, Fig. 25.5e). The metallic skeleton is best described as a square of Ln ions doubly-capped on distal edges by $[Fe^{III}_2$(bis-C[4])$]^{4-}$ moieties (Fig. 25.6e). The fifth Fe^{III} ion caps one side of the square, with two μ_4-nitrates and a μ_4-oxygen bridging the central metal ions. The capped square of Ln^{III} cations is another common structural feature observed upon moving from H_4C[4] (cluster **5**, Fig. 25.3d) to bis-H_4C[4], and is also found in one other series of bis-C

[4]-supported 3*d*/4*f* clusters described below (and that are formed under stoichiometric control).

25.2.3 Stoichiometric Control Over Cluster Synthesis

Like $H_4C[4]$, bis-$H_4C[4]$ has proved to be a highly versatile ligand for the synthesis of 3*d* and 3*d*/4*f* polymetallic clusters; a polynuclear Ln cluster is yet to be formed, but should be achievable based on the chemistry of $H_4C[4]$. As variation in reaction stoichiometries facilitated ion interchange within the C[4]-supported butterfly-like cluster, we explored analogous chemistry with bis-$H_4C[4]$ and found that it was in fact possible to 'expand' clusters through variation in both reactant ratios and crystallisation conditions [41].

The first cluster isolated from this study was found to have a general formula of $[Mn^{III}_6Mn^{II}_2Ln^{III}_2(\text{bis-C[4]})_2(\mu_4\text{–O})_2(\mu_3\text{–OH})_2(\mu\text{–OCH}_3)_4(\text{MeOH})_4(\text{dmf})_8](NO_3)_2$ (**15**, Ln = Tb or Dy, Fig. 25.5f) and represents an 'expansion' of the $Mn^{III}_4Mn^{II}_2Ln^{III}_2$ core in cluster **12** [41]. The metallic skeleton in **15** is best described as three fused butterflies (Fig. 25.6f). Comparison of both structures shows the presence of two additional Mn^{III} ions in the body positions of the new central butterfly in **15**; μ-OMe anions are also incorporated and represent a significant difference between **12** and **15**. Cluster **15** is capped at either end by $[Mn^{III}_2(\text{bis-C[4]})]^{2-}$ moieties, as is the case in **12**.

Variation in the stoichiometries used to isolate **10** resulted in isolation of a cluster of formula $[Mn^{III}_6Mn^{II}_4(\text{bis-C[4]})_2(\mu_3\text{–OH})_4(\mu\text{–OCH}_3)_4(H_2O)_4(\text{dmf})_8]$ (**16**, Fig. 25.5g) that is structurally related to **15** [41]. The metallic skeleton in **16** (Fig. 25.6g) can be described as three fused butterflies, with the only major difference being that Mn^{II} ions have taken up the Ln^{III}-occupied positions in **15**, mirroring the coordination behaviour of bis-$H_4C[4]$ in cluster **12**. As in **15**, cluster **16** is capped at either end by $[Mn^{III}_2(\text{bis-C[4]})]^{2-}$ moieties.

The final cluster obtained from stoichiometric control resulted from variation in the reaction conditions used to form cluster **15**, and has a general formula of $[Mn^{III}_4Ln^{III}_4(\text{bis-C[4]})_2(\mu_3\text{-OH})_4(\mu\text{-CO}_3)_2(\text{dmf})_8(H_2O)_4]$ (**17**, Ln = Gd, Tb or Dy, Fig. 25.5h) [41]. The metallic skeleton is a distorted square of Ln^{III} ions that is doubly-capped on distal edges by $[Mn^{III}_2(\text{bis-C[4]})]^{4-}$ moieties (Fig. 25.6h), a structural feature observed in the $Fe^{III}_5Ln^{III}_4$ cluster described above (**14**, Fig. 25.5e). Each half of the assembly can be considered a distorted $Mn^{III}_2Ln^{III}_2$ butterfly-like cluster, with these being connected by μ-carbonates that arise from atmospheric CO_2 fixation, a relatively common phenomenon in Ln coordination cluster chemistry and one that we have also seen with C[4]-supported systems.

25.3 Methylene-Bridge Tethered Bis-calix[4]arenes in Cluster Synthesis

Tethering H_4C[4]s at the methlyene bridge with organic spacers varying in chemical nature, shape and size represents an exciting new way to control or direct the coordination chemistry of bis-H_4C[4]s, but most importantly, cluster composition and or nuclearity. Preliminary cluster forming studies with H_4C[4]s substituted at one methlyene bridge with small alkyl chains (methyl and ethyl) resulted in the isolation of $Mn^{III}_2Mn^{II}_2$ butterfly-like clusters analogous to those formed with H_4C[4] (**1**, Fig. 25.3a) [22] clearly demonstrating that lower-rim coordination chemistry is unperturbed by the presence of groups at the methylene bridge.

25.3.1 Flexibly Tethered Bis-calix[4]arenes

With the above in mind a series of bis-H_4C[4]s containing flexible alkyl tethers (propyl to decyl) were synthesised and their coordination chemistry explored [42]. Full characterisation of these new ligands was carried out as standard, but it was only possible to isolate single crystals that were suitable for *X*-ray diffraction studies in one case, this being the acetonitrile solvate of H_4C[4]-$(CH_2)_3$-H_4C[4] (Fig. 25.7a). The asymmetric unit (ASU) comprises one molecule of H_4C[4]-$(CH_2)_3$-H_4C[4] and four MeCN of crystallisation, two of which occupy H_4C[4] cavities, forming CH-π interactions with the aromatic rings.

Four new clusters resulted from preliminary cluster forming studies involving this series of molecules. Three of these were formed with bis-H4C[4]s tethered by octyl (H_4C[4]-$(CH_2)_8$-H_4C[4]), nonyl (H_4C[4]-$(CH_2)_9$-H_4C[4]) and decyl (H_4C[4]-$(CH_2)_{10}$-H_4C[4]) alkyl chains, and structural studies found these to be isostructural with formulae of $[Mn^{III}_2Mn^{II}_2$(C[4]-$(CH_2)_8$-C[4])$(\mu_3\text{-OH})_2(DMF)_6]$ (**18**, Fig. 25.7b), $[Mn^{III}_2Mn^{II}_2$(C[4]-$(CH_2)_9$-C[4])$(\mu_3\text{-OH})_2(MeOH)(dmf)_5]$ (**19**) and $[Mn^{III}_2Mn^{II}_2$(C[4]-$(CH_2)_{10}$-C[4])$(\mu_3\text{-OH})_2(dmf)_6]$ (**20**) [42]. In each case the butterfly-like $Mn^{II}_2Mn^{III}_2$ metallic skeleton is analogous to that of cluster **1** shown in Fig. 25.3a. The only difference in **18**–**20** is the length of the alkyl chain tethering the H_4C[4]s, thereby demonstrating that a sufficiently long tether will allow for formation of known structural motifs established in analogous C[4]-supported cluster chemistry.

The fourth cluster was obtained by reaction of H_4C[4]-$(CH_2)_{10}$-H_4C[4] with Mn^{II} and Ln^{III} chlorides under typical reaction conditions and has a formula of $[Mn^{III}_4Ln^{III}_4$(C[4]-$(CH_2)_{10}$-C[4])$_2(\mu_3\text{-}CO_3)_2(\mu_3\text{-OH})_4(dmf)_6(H_2O)_6]$ (**21**, Ln = Gd, Tb or Dy, Fig. 25.7c). This cluster bears a striking resemblance to the C[4]-supported $Mn^{III}_4Ln^{III}_4$ cluster, **5**, the metallic skeleton of which is a square of Ln^{III} ions capped on each edge by a $[Mn^{III}(C[4])]^-$ moiety. The only significant difference between **21** and **5** is that μ_3-nitrates in the latter are replaced by μ_3-carbonates. From inspection

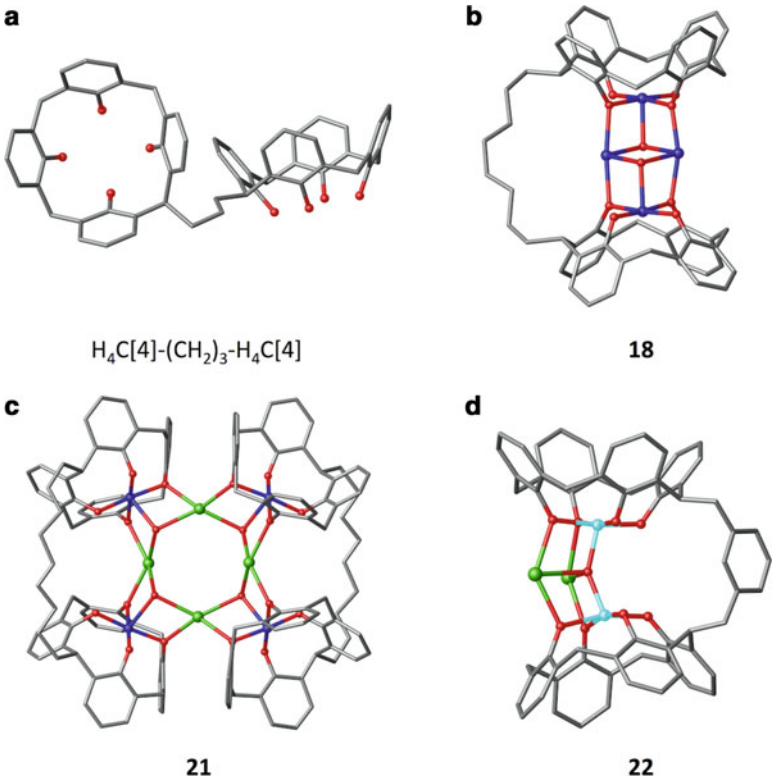

Fig. 25.7 Partial structures of $H_4C[4]$-$(CH_2)_3$-$H_4C[4]$ (**a**) and clusters **18** (**b**), **21** (**c**) and **22** (**d**) [42, 43]. Cluster core capping in **18**, **21** and **22** occurs, as is the case in C[4]-supported analogues, through $[TM^{II}_2bisC[4]]^{4-}$ or $[TM^{III}_2bisC[4]]^{2-}$ moieties. H atoms, C[4] ^{t}Bu groups, ligated solvent and solvent of crystallisation omitted for clarity. Figures not to scale. Colour code: C – *grey*, O – *red*, TM – *dark/pale blue*, Ln – *green*

it is again clear that sufficiently long alkyl tethers allow for formation of analogous C[4]-supported cluster types.

Although it has not yet been possible to isolate single crystals from reactions involving shorter tethers, it is reasonable to expect that these will preclude the formation of known cluster types/structural motifs, necessarily giving rise to new species that will be of interest due to disparate metal ion composition/coordination environments.

25.3.2 Rigidly Tethered Bis-calix[4]arenes

The use of more rigid tethers in the synthesis of bis-$H_4C[4]$s is potentially the most interesting route towards controlling or directing cluster formation; this can be

achieved by facile introduction of directionality through the tether. Initial efforts in this area have focused on the use of *ortho*-, *meta*- and *para*-xylyl tethers. Proof of concept DFT calculations were performed on these new ligands to rationalise if the constituent H4C[4]s would be favourably positioned in space to either allow for or direct the formation of existing and or new clusters from the known library of structures, all of which will take place through established core capping behaviour established for H_4C[4] and bis-H_4C[4] [43].

The H_4C[4] moieties in both the *ortho*- and *meta*- derivatives are necessarily convergent due to constraints imposed by the spacer and the presence of the methylene groups between the aromatic ring of the tether and the methylene bridges. Calculations showed these to adopt a lower-rim eclipsed arrangement with separation between phenolic pockets being at a distance of ~3 Å. Given these constraints, these ligands would only be suitable to form metal clusters from the structural library in which the lower-rim to lower-rim separation was close to this distance. For example, inspection of the library of known clusters showed that formation of an analogue to the $Mn^{III}_2Mn^{II}_2$(C[4])$_2$ (**1**) cluster would not be possible for both *ortho*- and *meta*-bis-H_4C[4], as lower-rim separation is measured to be ~5.7 Å. Analysis of all knonwn C[4]-supported clusters did, however, suggest that it would be possible to form a bis-C[4]-supported analogue of the $Fe^{III}_2Ln^{III}_2$(C[4])$_2$ cluster (**6**, Fig. 25.3e). In contrast, gas phase structure calculations for the *para*- derivative show that the H_4C[4] moieties are (as expected) divergent and positioned far from one another, with a lower-rim to lower-rim distance (centroid to centroid) of more than 12 Å. From inspection it is clear that, due structural constraints, formation of an analogue to any known C [4]-supported cluster is impossible.

Tolerance in cluster formation was tested prior to the synthesis of these ligands through the use of a methylene bridge benzyl substituted H_4C[4]. This was carried out in order to assess any effects of the bulky substituent on cluster formation with the series of xylyl-bis-H_4C[4]s. Given that it was possible to form $Mn^{III}_2Mn^{II}_2$ butterfly-like clusters with H_4C[4]s substituted at one methylene bridge with either methyl or ethyl groups, the same reaction conditions were used to test the benzyl analogue. This reaction was successful and a structure of the $Mn^{III}_2Mn^{II}_2$(benzyl-C [4])$_2$ cluster was obtained, clearly demonstrating that formation is tolerant to a wide range of groups at the methylene bridge. Subsequent synthesis of the aforementioned ligands was then undertaken and cluster formation explored; this resulted in the isolation and characterisation of two new xylyl-bis-C[4]-supported clusters.

Computational studies, coupled with inspection of the C[4]-supported cluster library, predicted that *ortho*- and *meta*-xylyl-bis-H_4C[4] would be well suited to support formation of a $Fe^{III}_2Ln^{III}_2$ cluster. Single crystals were isolated upon reaction of *meta*-xylyl-bis-H_4C[4] under conditions used to form cluster **6** (Fig. 25.3e), and structure analysis showed these to be of formula [$Fe^{III}_2Gd^{III}_2$ (*meta*-xylyl-bis-C[4])(μ_4-O)(μ-OH)(dmf)$_7$(MeOH)(H_2O)$_2$][*meta*-xylyl-bis-H_4C[4]-H] (**22**, Fig. 25.7d). The metallic skeleton is analogous to that found in **6**, and a mono-deprotonated *meta*-xylyl-bis-H_4C[4] is present as a counterion to the cationic

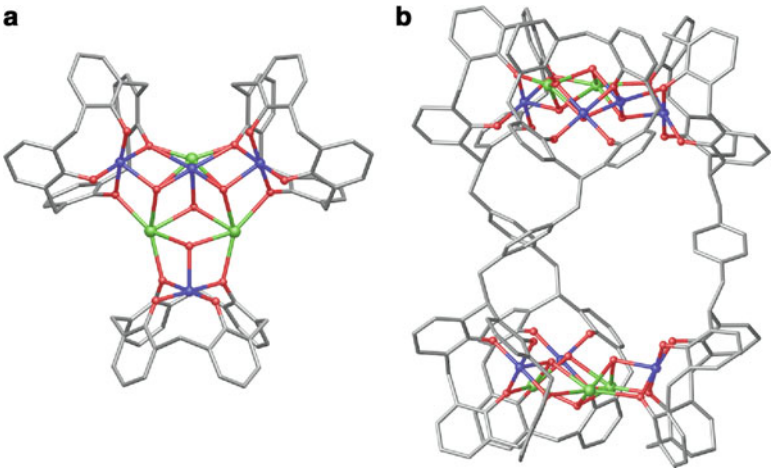

Fig. 25.8 Partial single crystal X-ray structure of **23** [43]. (**a**) Triangular cluster capped on each edge by a $[Mn^{III}C[4]]^-$ moiety within the ASU. (**b**) Symmetry expansion showing the metal-organic trigonal antiprism. Bridge linking *para*-xylyl units are omitted in A. H atoms, C[4] ^{t}Bu groups, ligated solvent, anions and solvent of crystallisation omitted for clarity in both A and B. Figures not to scale. Colour code: C – *grey*, O – *red*, Mn – *dark blue*, Ln – *green*

cluster. Although this does not represent a new structural motif, it does validate the approach of restricting cluster types through tether/ligand design.

As stated above, *para*-xylyl-bis-H_4C[4] is predicted to have a divergent structure in the gas phase. Reaction of this ligand with Mn^{II} and Ln^{III} chlorides under ambient reaction conditions resulted in formation of a cluster with general formula $[Mn^{III}{}_6Mn^{II}Dy_5$(*para*-xylyl-bis-C[4])$_3(\mu_3\text{-OH})_8(dmf)_8(MeCN)_4(H_2O)_9](OH)_3$ (**23**). The ASU consists of three half molecules of *para*-xylyl-bis-H_4C[4], all of which house a Mn^{III} ion at the constituent C[4] lower-rims as expected. The lower-rim oxygens of each C[4] moiety bridge to Ln^{III} and Mn^{II} ions (two of which are disordered) that define a central triangle, which is also held together by μ_3-hydroxides (Fig. 25.8a). As such the ASU is best described as a triangular cluster capped on each edge by a $[Mn^{III}(C[4])]^-$ moiety, again stressing that structural trends carry through upon modification of the general H_4C[4] scaffold; there are some similarities between cluster **23** and the enneanuclear Cu^{II} cluster, **2**, shown in Fig. 25.3b.

Symmetry expansion of the ASU results in formation of a metal-organic polyhedron (MOP) that has trigonal antiprismatic topology (Fig. 25.8b), and which is clearly influenced by the directing nature of *para*-xylyl-bis-H_4C[4]. Given the presence of a solvent/anion occupied space in the centre of the assembly, it was of interest to investigate if cluster **23** would be robust towards desolvation. Thermal studies found this to be the case and the assembly was capable of taking up gases (N_2 and H_2). Although the cavity in **23** is relatively small, these experiments represent a good proof of concept that bis-H_4C[4] ligand design is a viable route towards the controlled assembly of supramolecular architectures containing

magnetically interesting building units. Such assemblies would have great potential to act as hosts for smaller, magnetically interesting species and is an avenue of future investigation with these new molecules.

25.4 Conclusions

C[4]-supported cluster synthesis is a truly burgeoning area of supramolecular coordination chemistry. The ease with which the $H_4C[4]$ scaffold can be functionalised at the upper-rim generates potentially limitless opportunities for the synthetic chemist. Moreover, understanding of the empirical ion binding rules for $H_4C[4]$s towards 3*d*, 4*f* and 3*d*/4*f* ion mixtures allows one to predict, to a certain extent, the minimum number of metal ions to be incorporated into a cluster, as well as the structural capping behaviour of a C[4] derivative during design, and prior to synthesis. This represents a powerful tool in structural chemistry, especially when the formation of a cluster may be targeted for the incorporation of specific numbers of paramagnetic metal ions toward the construction of magnetically interesting entities. Functionalisation of the $H_4C[4]$ methylene bridge presents a new avenue to explore cluster formation, with the possibility to introduce a plethora of functional groups that do not impinge on lower-rim coordination chemistry.

Moving from $H_4C[4]$ to bis-$H_4C[4]$ via direct methylene bridge tethering gives an equally versatile molecular platform for cluster synthesis. Results obtained with this new molecule conform to the binding rules for $H_4C[4]$, thereby allowing one to enhance nuclearity of the resulting cluster. As was the case for $H_4C[4]$, stoichiometric control in reactions involving bis-$H_4C[4]$ also had the effect of altering the cluster core. Tethering $H_4C[4]$s with simple flexbile or rigid linkers has already resulted in fascinating new clusters/assemblies. Rigidly tethered bis-$H_4C[4]$s provide the chemist with yet another route to control structure, either by dictating formation of one cluster type, or directing assembly of a nanoscale MOP. All of these developments bode well for the future of C[*n*]-supported cluster chemistry, and all of these principles will likely be applicable to larger ring sizes.

References

1. For example see: Gatteschi, D.; Sessoli, R.; Villain, J. *Molecular Nanomagnets*, Oxford University Press, 2006.
2. Petrella, A. J.; Raston, C. L. *J. Organomet. Chem.* **2004**, *689*, 4125–4136.
3. Aronica, C.; Chastanet, C.; Zueva, E.; Borshch, S. A.; Clemente-Juan, J. M.; Luneau, D. *J. Am. Chem. Soc.* **2008**, *130*, 2365–2371.
4. Kajiwara, T.; Iki, N.; Yamashita, M. *Coord. Chem. Rev.* **2007**, *251*, 1734–1746.
5. Fischer, R.; Görls, H.; Walther, D. *Eur. J. Inorg. Chem.* **2004**, *6*, 1243–1252.

6. Bilyk, A.; Hall, K. A.; Harrowfield, J. M.; Hosseini, M. W.; Skelton, B. W.; White, A. H. *Inorg. Chem.* **2001**, *40*, 672–686.
7. Desroches, C.; Pilet, G.; Borshch, S. A.; Parola, S.; Luneau, D. *Inorg. Chem.* **2005**, *44*, 9112–9120.
8. Bilyk, A.; Hall, K. A.; Harrowfield, J. M.; Hosseini, M. W.; Mislin, G.; Skelton, B. W.; Taylor, C.; White, A. H. *Eur. J. Inorg. Chem.* **2000**, 823–826.
9. Mislin, G.; Graf, E.; Hosseini, M. W.; Bilyk, A.; Hall, A. K., Harrowfield, J. M.; Skelton, B. W.; White, A. H. *Chem. Commun.* **1999**, 373–374.
10. Akdas, H.; Graf, E.; Hosseini, M. W.; De Cian, A.; Bilyk, A.; Skelton, B. W.; Koutsantonis, G. A.; Murray, I.; Harrowfield, J. M.; White, A. H. *Chem. Commun.* **2002**,1042–1043.
11. Bilyk, A.; Hall, A. K., Harrowfield, J. M.; Hosseini, M. W.; Skelton, B. W.; White, A. H. *Aust. J. Chem.* **2000**, *53*, 895–898.
12. Bi, Y.; Wang, X.-T.; Liao, W.; Wang, X.; Wang, X.; Zhang, H.; Gao, S. *J. Am. Chem. Soc.* **2009**, *131*, 11650–11651.
13. Xiong, C.; Jiang, F.; Gai, Y.; Yuan, D.; Han, D.; Ma, J.; Zhang, S.; Hong, M. *Chem. Eur. J.* **2012**, *18*, 5536–5540.
14. Su, K.; Jiang, F.; Qian, J.; Pang, J.; Al-Thabaiti, S. A.; Bawaked, S. M.; Mokhtar, M.; Chen, Q.; Hong, M. *Cryst. Growth Des.* **2014**, *14*, 5865–5870.
15. Su, K.; Jiang, F.; Qian, J.; Pang, J.; Hu, F.; Bawaked, S. M.; Mokhtar, M.; Al-Thabaiti, S. A.; Hong, M.; *CrystEngComm*, **2015**, *17*, 1750–1753.
16. Liu, M.; Liao, W.; Hu, C.; Du, S.; Zhang, H. *Angew. Chem. Int. Ed.* **2012**, *51*, 1585–1588.
17. Dai, F.-R.; Wang, Z. *J. Am. Chem. Soc.* **2012**, *134*, 8002–8005.
18. Xiong, K.; Jiang, F.; Gai, Y.; Yuan, D.; Chen, L.; Wu, M.; Su, K.; Hong, M. *Chem. Sci.* **2012**, *3*, 2321–2325.
19. Bi, Y.; Du, S.; Liao, W. *Coord. Chem. Rev.* **2014**, *276*, 61–72.
20. Su, K.; Jiang, F.; Qian, J.; Chen, L.; Pang, J.; Bawaked, S. M.; Mokhtar, M.; Al-Thabaiti, S. A.; Hong, M. *Inorg. Chem.* **2015**, *54*, 3183–3188.
21. Dai, F.-R.; Becht, D. C.; Wang, Z. *Chem. Commun.* **2014**, *50*, 5385–5387.
22. Karotsis, G.; Teat, S. J.; Wernsdorfer, W.; Piligkos, S.; Dalgarno, S. J.; Brechin, E. K. *Angew. Chem. Int. Ed.* **2009**, *48*, 8258–8288.
23. Taylor, S. M.; Karotsis, G.; McIntosh, R. D.; Kennedy, S.; Teat, S. J; Beavers, C. M.; Wernsdorfer, W.; Piligkos, S.; Dalgarno,S. J.; Brechin, E. K. *Chem. Eur. J.* **2011**, *17*, 7521–7530.
24. Brechin, E. K., Yoo, J.; Nakano, M.; Huffman, J. C.; Hendrickson, D. N.; Christou, G. *Chem. Commun.* **1999**, 783–784
25. Karotsis, G.; Kennedy, S.; Dalgarno, S. J.; Brechin, E. K. *Chem. Commun.* **2010**, *46*, 3884–3886.
26. Su, K.; Jiang, F.; Qian, J.; Zhou, K.; Pang, J.; Basahel, S.; Mokhtar, M.; Al-Thabaiti, S. A. Hong, M. *Inorg. Lett.* **2014**, 1, 1–8.
27. Sanz, S.; McIntosh, R. D.; Beavers, C. M.; Teat, S. J.; Evangelisti, M.; Brechin, E. K., Dalgarno, S. J. *Chem. Commun.* **2012**, *48*, 1449–1451.
28. Bi, Y.; Xu, G.; Liao, W.; Du, S.; Deng, R.; Want, B. *Sci. China Chem.* **2012**, *55*, 967–972.
29. Karotsis, G.; Kennedy, S.; Teat, S. J.; Beavers, C. M.; Fowler, D. A.; Morales, J. J.; Evangelisti, M.; Dalgarno, S. J.; Brechin, E. K. *J. Am. Chem. Soc.* **2010**, *132*, 12983–12990.
30. Sanz, S.; Ferreira, K.; McIntosh, R. D.; Dalgarno, S. J.; Brechin, E. K. *Chem. Commun.* **2011**, *47*, 9042–9044.
31. Palacios, M. A.; McLellan, R.; Beavers, C. M.; Teat, S. J.; Weihe,H.; Piligkos, S.; Dalgarno,S. J.; Brechin, E. K. *Chem. Eur. J.* **2015**, *21*, 11212–11218.
32. Fairbairn, R. E.; McLellan, R.; McIntosh, R. D.; Taylor, S. M.; Brechin, E. K.; Dalgarno, S. J. *Chem. Commun.* **2012**, *48*, 8493–8495.
33. Scully; P. A.; Hamilton; T. M.; Bennett, J. L. *Org. Lett.* **2001**, *17*, 2741–2744.
34. Poms, D.; Itzhak, N.; Kuno, L.; Biali, Silvio E. *J. Org Chem.* **2014**, *79*, 538–545.
35. Kogan, K.; Biali, Silvio E. *J. Org Chem.* **2011**, *76*, 7240–7244.

36. Hertel M. P.; Behrle A. C.; Williams S. A.; Schmidt J. A.R.; Fantini J. L. *Tetrahedron*, **2009**, *65*, 8657–8667.
37. Carroll, L. T.; Hill, P. A.; Ngo, C. Q.; Klatt, K. P.; Fantini J. L. *Tetrahedron*, **2013**, *69*, 5002–5007.
38. Murphy, P.; Dalgarno, S. J.; Paterson, M. J. *J. Phys. Chem. A*, **2014**, *118*, 7986–8001.
39. McLellan, R.; Palacios, M. A.; Beavers, C. M.; Teat, S. J.; Piligkos, S.; Brechin, E. K.; Dalgarno, S. J. *Chem. Eur. J.* **2015**, *21*, 2804–2812.
40. Coletta, M.; McLellan, R.; Sanz, S.; Teat, S. J., Gagnon, K.; Brechin, E. K.; Dalgarno, S. J., **2015**, *submitted.*
41. Coletta, M.; McLellan, R.; Sanz, S.; Teat, S. J., Gagnon, K.; Brechin, E. K.; Dalgarno, S. J. **2015**, *submitted.*
42. Coletta, M.; McLellan, R.; Cols, J.-M.; Gagnon, K.; Teat, S. J., Brechin, E. K.; Dalgarno, S. J. **2016**, *28*, 557–566.
43. Coletta, M.; McLellan, R.; Murphy, P.; Leube, B.; Sanz, S.; Clowes, R.; Gagnon, K.; Teat, S. J.; Cooper, A. I.; Paterson, M. J.; Brechin, E. K.; Dalgarno, S. J. *Supramol. Chem.* **2016**, *22*, 8791–8795.

ChemPubSoc Europe

DOI: 10.1002/chem.201600762

CHEMISTRY
A European Journal
Communication

Directed Assembly

Bis-Calix[4]arenes: From Ligand Design to the Directed Assembly of a Metal–Organic Trigonal Antiprism

Marco Coletta,[a] Ross McLellan,[a] Paul Murphy,[a] Bernhard T. Leube,[a] Sergio Sanz,[b] Rob Clowes,[c] Kevin J. Gagnon,[d] Simon J. Teat,[d] Andrew I. Cooper,[c] Martin J. Paterson,[a] Euan K. Brechin,*[b] and Scott J. Dalgarno*[a]

Abstract: Calix[4]arenes (C[4]s) are versatile platforms for the construction of polymetallic clusters containing paramagnetic metal ions. Synthetic modification at the C[4] methylene bridge allows for the design of bis-C[4]s that, depending on the linker employed, can be used to either dictate which clusters can be formed or direct the assembly of a new metal–organic polyhedron (MOP). The assembly resulting from the latter approach displays thermal stability and uptake of N_2 or H_2 gas, confirming that this is a viable route to the synthesis of new, functional supramolecular architectures.

The assembly of synthetically challenging metallosupramolecular systems is a rapidly expanding area of chemistry that continues to attract strong interest. This activity stems partly from the chemist's desire to understand the self-assembly of complex multi-component architectures,[1] but also from the fact that the resulting assemblies can be discrete[1] or polymeric[2] in nature, possessing targeted physical properties[3] or finding utility in a wide variety of areas such as catalysis,[4] controlled guest uptake/release[5] and novel crystallisation media.[6] Strategies for directed assembly typically rely on the use of both coordination templates and ligand design,[7] the latter being the general focus of this contribution.

Calix[4]arenes (C[4]s) have featured prominently in supramolecular chemistry due to their conformational versatility, related topological directionality and ease of synthetic modification/functionalisation.[8] In the cone conformation these versatile hosts possess cavities that are accessible to a range of suitably sized neutral or charged guests. We (amongst others) recently exploited the lower-rim polyphenolic character of methylene-bridged C[4]s in mapping out their transition (TM), lanthanide (Ln) metal and 3d–4f cluster-forming chemistry.[9] In doing so, we have reported a wide range of new clusters that are typically polygonal in nature, and can themselves be considered as building blocks; examples would be the $[Mn^{III}_2Mn^{II}_2(C[4])_2]$ and $[Mn^{III}_4Ln^{III}_4(C[4])_4]$ cluster cores in Figure 1 A and B, respectively.[9b,c] Analysis of our library of cluster types and conditions employed has allowed us to establish empirical C[4] metal-ion binding rules that depend solely on the combination of metal ions present. An excellent example of this is the persistent incorporation of the $[TM(C[4])]^-$ moiety within all 3d–4f clusters, as can be seen by comparing Figure 1 A and B.[9b,c]

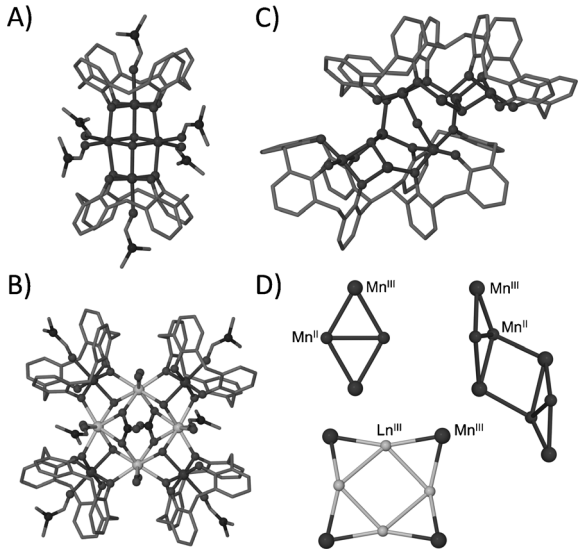

Figure 1. Structures of $[Mn^{III}_2Mn^{II}_2(C[4])_2]$[9b] (A), $[Mn^{III}_4Ln^{III}_4(C[4])_4]$[9c] (B) and $[Mn^{III}_4Mn^{II}_4(bis\text{-}C[4])_2]$[10] (C) clusters showing persistence of the $[Mn(C[4])]^-$ moiety. D) Cluster core topologies from A–C (rotated 90° for the Mn_8 cluster in C) to show structural capping behaviour of the $[Mn(C[4])]^-$ moiety and the relationship upon linking at the methylene bridge. H atoms and calix[4]arene *t*Bu groups omitted for clarity and not to scale.

We recently expanded our cluster-forming chemistry with C[4] to focus on bis-C[4], a building block comprising two

[a] *M. Coletta, Dr. R. McLellan, P. Murphy, B. T. Leube, Prof. M. J. Paterson, Dr. S. J. Dalgarno*
Institute of Chemical Sciences, Heriot–Watt University, Riccarton, Edinburgh, EH14 4AS (UK)
E-mail: S.J.Dalgarno@hw.ac.uk

[b] *Dr. S. Sanz, Prof. E. K. Brechin*
EaStCHEM School of Chemistry, The University of Edinburgh, David Brewster Road, Edinburgh, EH9 3FJ (UK)
E-mail: E.Brechin@ed.ac.uk

[c] *R. Clowes, Prof. A. I. Cooper*
Department of Chemistry, University of Liverpool, Crown Street, Liverpool, L69 7ZD (UK)

[d] *Dr. K. J. Gagnon, Dr. S. J. Teat*
Advanced Light Source, Lawrence Berkeley National Laboratory Berkeley, CA 947240 (USA)

Supporting information for this article can be found under http://dx.doi.org/10.1002/chem.201600762.

C[4]s linked directly through a methylene bridge. In doing so we found that when the constituent C[4] cavities are proximal the molecule behaves closely to how one would expect with respect to cluster formation.[10] To illustrate this, the analogous reaction used to form the $[Mn^{III}_2Mn^{II}_2(C[4])_2]$ cluster[9b] (Figure 1 A) affords a new $[Mn^{III}_4Mn^{II}_4(bis\text{-}C[4])_2]$ assembly (Figure 1 C), which is essentially 'double' the original cage (Figure 1 D). A number of structural parallels can therefore be drawn upon moving from C[4] to bis-C[4]. Based on the chemistry used to obtain bis-C[4], we anticipated that it should be possible to synthesise analogues containing linkers that possess varying degrees of rigidity, thereby giving rise to some level of control over the positioning of C[4] relative to one another. This would then potentially allow us to either a) preferentially direct the formation of specific cluster types, b) force the formation of new cluster types or, most importantly, c) direct the formation of new structures/assemblies.

Here we report the use of computational chemistry to arrive at structures of *ortho*-, *meta*- and *para*-xylyl bis-C[4], subsequent ligand synthesis and their use in cluster formation. In the first of the results obtained, we have directed the formation of a C[4]-supported $Fe^{III}_2Ln^{III}_2$ cluster with *meta*-xylyl bis-C[4], as well as a spectacular new trigonal antiprismatic metal–organic cage with the *para*- derivative. The latter is stable towards desolvation and its N_2 and H_2 gas sorption has been studied.

Calculated structures were obtained for the *ortho*-, *meta*- and *para*-xylyl bis-C[4] (**1**–**3** respectively) from DFT calculations using the B3LYP functional with added GD3 dispersion and 6-31G** basis set.[11–13] There is inherent rotational freedom associated with the tether bonds to the methylene bridge. Although this is the case, we undertook this work with a view to 1) investigating conformational possibilities in the free ligand prior to synthesis and 2) evaluating the likelihood of forming known C[4]-supported cluster types in the presence of target metal ions (based on the aforementioned empirical ion-binding rules and cluster library). From these calculations it can be seen that, when the C[4] moieties in both the *ortho*- and *meta*-tethered bis-C[4] are convergent (Figure 2 A, B), they are slightly offset with an eclipsed arrangement in which the lower-rim cavity···cavity distances are 3.081 Å and 3.177 Å, respectively (Figures S1 and S2 in the Supporting Information). In addition to this, calculations also showed a viable divergent conformation for **3**, in which the molecule adopts the twisted conformation shown in Figure 2 C (with lower-rim cavity···cavity distances of 12.679 Å, Figure S3 in the Supporting Information).

From inspection it is clear that, due to constraints imposed by the *ortho*- and *meta*-xylyl linkers, compounds **1** and **2** would only be suitable to form analogues to C[4]-supported clusters that possess similar distances between either $[TM^{II/III}(C[4])]^{2-/-}$ or $[Ln^{III}(C[4])]^{-}$ moieties; the potentially divergent nature of **3** precludes formation of any reported C[4]-supported cluster type, unless it were (for example) to form a polymeric structure of $[Mn^{III}_2Mn^{II}_2(C[4])_2]$ clusters. A survey of reported C[4]-supported clusters in which the C[4]s are most proximal returned two results.[14] The first of these is the $[Mn^{III}_2Mn^{II}_2(C[4])_2]$ cluster (Figure 1 A),[9b] but it is clearly not possible to form this arrangement with either **1** or **2** as a) the lower-rim centroid···centroid distance is ≈5.7 Å and b) the Mn^{II} ions/butterfly-like topology of the cluster forces the C[4] lower rims to be drastically offset. The second was an $[Fe^{III}_2Ln^{III}_2(C[4])_2]$ cluster with a significantly closer lower-rim centroid···centroid distance of ≈4.1 Å, and in which the C[4]s (binding the Fe^{III} ions) are tilted slightly to accommodate the incorporation of Ln^{III} ions (Figure S4 in the Supporting Information). This therefore suggested that, from **1** and **2**, the latter would be most likely to form a cluster, in particular a $[Fe^{III}_2Ln^{III}_2(\mathbf{2})]$ analogue to $[Fe^{III}_2Ln^{III}_2(C[4])_2]$; this is also likely when considering that **2** would have fewer steric constraints and/or greater flexibility than **1**.

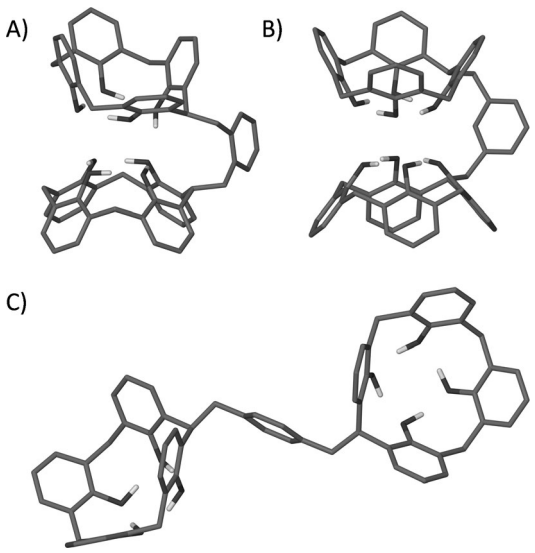

Figure 2. Calculated structures of **1**–**3**. A) Convergent *ortho*-xylyl bis-C[4] with H-bonding between the lower rims. B) Convergent *meta*-xylyl bis-C[4] with less strained conformation. C) Divergent *para*-xylyl bis-C[4] with twisted conformation. H atoms except those at the C[4] lower rims omitted for clarity.

Prior to synthesising the xylyl-tethered bis-C[4]s and exploring their coordination chemistry, we first tested cluster formation/tolerance with a C[4]-modified at one bridge with a benzyl group;[15] this molecule was previously reported and was selected a logical starting point given the direct structural relationship to **1**–**3** (compare Figure 2 and Figure 3 A), and that it would allow us to evaluate the effects (if any) of the methylene bridge substituent on cluster formation. The $[Mn^{III}_2Mn^{II}_2(C[4])_2]$ single-molecule magnet (SMM)[9b] was selected as the standard test system to see if this would form without the xylyl-tether constraints discussed above. Reaction between benzyl-C[4] and manganese(II) chloride hydrate in a DMF/MeOH mixture and in the presence of triethylamine afforded a dark purple solution from which single crystals grew upon vapour diffusion with acetonitrile. The crystals were in a triclinic cell and structural studies found them to be $[Mn^{III}_2Mn^{II}_2(benzyl\text{-}C[4])_2(OH)_2(DMF)_6]\cdot(MeOH)_{0.6}(MeCN)_{1.4}$, **4**, with structure solution being performed in the space group *P*-1. The asymmetric unit (ASU) comprises one half of the expected $Mn^{III}_2Mn^{II}_2$ butterfly-like cluster and symmetry generation

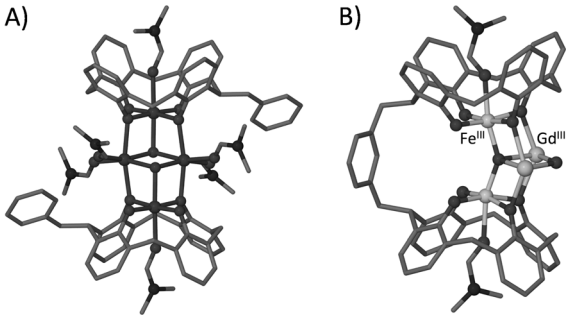

Figure 3. A) Structure of **4** showing *trans*-positioning of the benzyl groups at the C[4] methylene bridge. B) Structure of **5** showing *meta*-tethering at the methylene bridges and the cluster core. Calix[4]arene *t*Bu groups, ligated solvent molecules in **5**, H atoms, solvent of crystallisation and anion in **5** are omitted for clarity. Figure not to scale.

around the inversion centre (located between the μ_3-OH anions) produces the assembly in Figure 3 A. The bridge substituents are positioned *trans* within the cluster framework, but this is to be expected when considering steric influence from the peripheral ligated solvent molecules of the general $[Mn^{III}_2Mn^{II}_2(C[4])_2]$ assembly (Figure 1 A). As such, it can be concluded that bridging groups have little or no effect on the introduction of secondary metal ions (Mn^{II} in this case) that are bridged to through the C[4] lower rim.

Having established that cluster formation was tolerant towards benzyl substituents at the methylene bridge, we synthesised compounds **1**–**3** using a slightly modified procedure to that reported for benzyl-C[4] (see the Supporting Information); this general synthetic route involves the use of the relevant α,α'-dibromoxylene in place of benzyl bromide. Reaction conditions used to form $[Mn^{III}_2Mn^{II}_2(C[4])_2]$, $[Fe^{III}_2Ln^{III}_2(C[4])_2]$ and $[Mn^{III}_4Ln^{III}_4(C[4])_4]$ clusters were employed with **1**–**3** in place of C[4] and single crystals were obtained in two instances. The first involved reaction of **2** with iron(II) nitrate nonahydrate and gadolinium(III) nitrate hexahydrate in a DMF/MeOH mixture and in the presence of Et_3N as a base. Single crystals of **5** were obtained by vapour diffusion of petroleum ether into the mother liquor and structure analysis (*P*-1) showed these to be $[Fe^{III}_2Gd^{III}_2(\mathbf{2}\text{-}8\,H)(\mu_4\text{-}O)(\mu\text{-}OH)(DMF)_7(MeOH)(H_2O)_2][\mathbf{2}\text{-}H]\cdot(DMF)_{0.5}(H_2O)_{1.5}$. The ASU comprises an octa-anionic **2** 'encapsulating' four metal ions in a distorted tetrahedron (Figure 3 B), as well as bridging anions and terminal ligated solvent molecules in and around the cluster core. There are also co-crystallised solvent molecules and one half of a di-anionic **2** providing charge balance for the cationic cluster. From inspection of **5** and comparison with computational studies it is immediately obvious that compound **2** is indeed well-suited to formation of the $[Fe^{III}_2Ln^{III}_2(C[4])_2]$ cluster type. In this regard, and although this is a known topology, this result suggests that rigid spacers can be further used to fine-tune and/or control cluster synthesis through the design of topologically directing C[4]-based ligands.

The second situation from which single crystals resulted involved the reaction of **3** with manganese(II) chloride tetrahydrate and dysprosium(III) chloride hexahydrate in a DMF/MeOH mixture and in the presence of Et_3N as a base. Single crystals of **6** were obtained upon diffusion of acetonitrile vapour into the reaction mixture. Structural analysis of the Dy(III) analogue (*C*2/*c*) showed these to be of formula $[Mn^{III}_6Mn^{II}Dy_5(\mathbf{3}\text{-}8\,H)_3(\mu_3\text{-}OH)_8(DMF)_8(MeCN)_4(H_2O)_9]\cdot(OH)_3(H_2O)_{1.5}(DMF)_{16}$ (Figure 4). The ASU is complex and comprises one half of this formula. There are three half-molecules of **5**, all of which are tetra-anionic and house a Jahn–Teller distorted Mn^{III} ion (Mn1–Mn3); these are arranged at the corners of a triangle (Figure 4 A) with a total of twelve Mn-O(phenolate) distances in the range of 1.881(10)–2.005(10) Å. Each Mn^{III} ion has a ligated solvent positioned along the JT axis such that it occupies an associated C[4] cavity

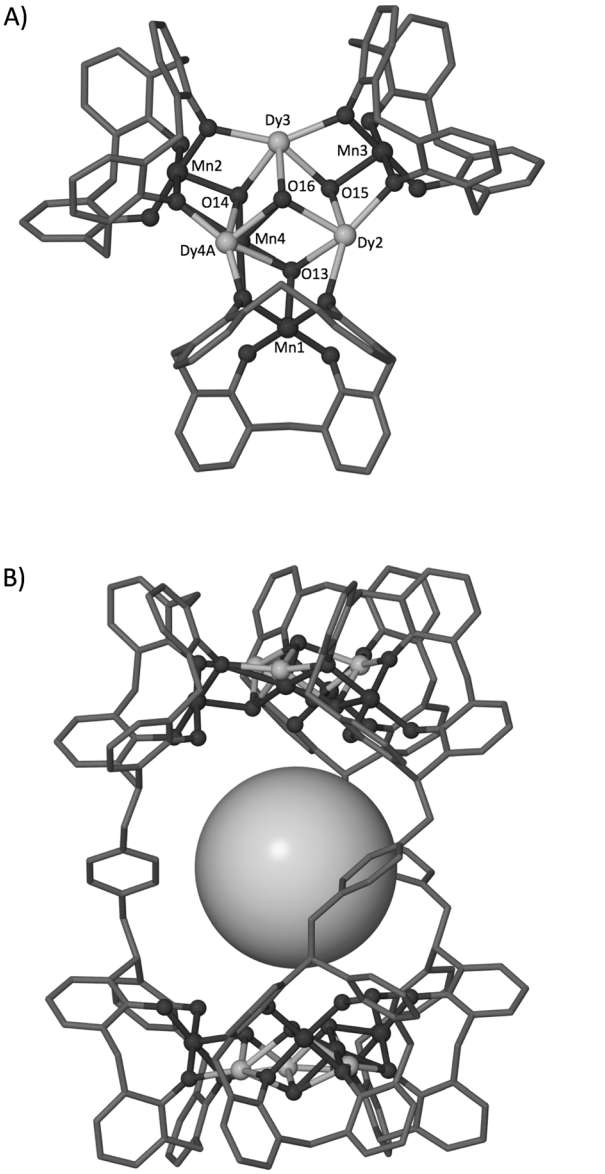

Figure 4. Structure of $[Mn^{III}_6Mn^{II}Dy_5(\mathbf{3}\text{-}8\,H)_3(\mu_3\text{-}OH)_8(DMF)_8(MeCN)_4(H_2O)_9]\cdot(OH)_3(H_2O)_{1.5}(DMF)_{16}$, **6**. A) Part of the asymmetric unit showing the triangular face and selected labels according to discussion. B) Symmetry-expanded structure showing the trigonal antiprismatic cage with $[Mn^{III}\text{-}C[4]]^-$ moieties at each vertex, with a sphere to emphasise the central cavity. Calix[4]arene *t*Bu groups, ligated solvent molecules, H atoms, solvent of crystallisation and anions omitted for clarity. Figure not to scale.

from **5** (Mn1-N340(MeCN), Mn2-O30(DMF) and Mn3-N360(MeCN) distances in the range of 2.16(4)–2.56(3) Å). The coordination spheres of Mn1–Mn3 are completed by μ_3-OH anions that are positioned towards the centre of the triangle (Mn1-O13, Mn2-O14 and Mn3-O15 distances in the range of 2.073(12)–2.135(11) Å). The O15 μ_3-OH bridges to two Dy^{III} ions (Dy1 and Dy3), both of which are octacoordinate and of square antiprismatic geometry. Dy1 has three terminal ligated solvent molecules with respective Dy1-O23(DMF), Dy1-O24(DMF) and Dy1-O25(H_2O) distances of 2.396(14), 2.396(13) and 2.358(14) Å. Dy3 also has three terminal ligated solvent molecules and these have respective Dy3-O20(H_2O), Dy3-O21(dmf) and Dy3-O22(H_2O) distances of 2.445(15), 2.464(15) and 2.331(13) Å. The O13 and O14 μ_3-OH anions bridge to Dy1 and Dy3 with O13-Dy1 and O14-Dy3 distances of 2.374(11) and 2.378(11) Å, respectively. These also bridge to the final metal-ion binding site that is occupied by disordered Mn^{II}/Dy^{III} ions, each present at 50% occupancy (respective O13-Mn4, O14-Mn, O13-Dy4A and O14-Dy4A distances of 2.003(13), 2.006(12), 2.553(12) and 2.511(11) Å). The Mn4 has distorted octahedral geometry and has a ligated water molecule with an Mn4-O19 distance of 2.24(3) Å. Dy4A is heptacoordinate, has capped trigonal prismatic geometry and has ligated water and DMF molecules with Dy4A-O19A(H_2O) and Dy4A-O17(DMF) distances of 2.23(3) and 2.34(2) Å, respectively. The central point of the triangle is occupied by a final μ_3-OH anion that bridges to all central metal ions in the triangle; this occurs with an O16-Mn4 distance of 2.241(13) Å and O16-Dy1, O16-Dy3 and O16-Dy4A distances in the range of 2.351(10)–2.399(10) Å. Symmetry expansion of the ASU affords the trigonal antiprismatic assembly shown in Figure 4B, in which the vertices are occupied by the expected $(Mn^{III}\text{-}C[4])^{-}$ moieties based on ligand composition. The antiprismatic nature of the assembly (Figure S5 in the Supporting Information) arises from the *p*-xylyl linkers that invoke a triply helical-like arrangement. The cage carries an overall charge of 3+ and disordered hydroxide counterions are located at positions consistent with hydrogen-bonding interactions to both ligated waters and bridging μ_3-OH anions.

Diffuse electron density located in and around the central cavity is indicative of very badly disordered DMF of crystallisation that could not be modeled. A search of the CSD for 3d–4f clusters with an O-bridged hemicubane core analogous to that in Figure 4A showed this to be relatively rare, returning only two general hits.[16,17] The first is a $Co^{III}_3Ln^{III}_3$ cluster core supported by *N*-butyldiethanolamines, acetates and bridging hydroxides,[16] differing from **6** in that one Co^{III} ion resides on the other side of the plane defined by the three central Ln^{III} ions; in **6** all three Mn^{III} ions are on the same side of the analogous plane. The second is a closely related series of phenolate, acetate and hydroxide-bridged $Ni^{II}_3Ln^{III}_3$ clusters, all of which possess three nickel ions residing on the same side of the plane as in **6**.[17] The orientation of C[4]s in **6** is reminiscent of our triangular C[4]-supported enneanuclear Cu^{II} clusters,[18] supporting the concept that ligand design may be combined with large clusters to access a wide range of new assemblies.

Crystallographic disorder and the anisotropy of the Ln^{III} and Mn^{III} ions precludes quantitative interpretation of the magnetic behaviour of **6**, **6(MnGd)** and **6(MnTb)**, though susceptibility data reveals weak [ferrimagnetic] intramolecular exchange interactions in all three cases, as expected from cages containing just 3d–4f and 4f–4f interactions (Figure S6 in the Supporting Information). This is consistent with previously reported, structurally related calixarene-based complexes such as $[Mn^{III}_2Mn^{II}_2(C[4])_2]$ and $[Mn^{III}_2Ln^{III}_2(C[4])_2]$ in which the Mn^{III}–Mn^{II} and Mn^{III}–Gd^{III} interactions have been found to be weakly ferromagnetic and the Gd^{III}–Gd^{III} and Mn^{II}–Gd^{III} interactions weakly antiferromagnetic.[9f] The presence of weak exchange is further corroborated by low-temperature, high-field magnetisation data, which tends toward saturation at S_{max} in all cases (Figure S7 in the Supporting Information). VTVB data, plotted against the reduced quantity $\mu_B B/kT$ (Figure S8 in the Supporting Information), show significant nesting of the VTVB data for **6** and **6(MnTb)**, with less nesting observed for **6(MnGd)**, a simple reflection of the larger anisotropy associated with the Ln ions in the former two cases. Ac susceptibility studies also reflect this, with the tails of frequency-dependent χ_M'' signals observed for both **6** and **6(MnTb)**, but not for **6(MnGd)**, indicative of the onset of slow magnetisation relaxation and SMM behaviour in the former two (Figure S9). Full details are given in the Supporting Information.

Given the cavity-containing nature of **6**, we investigated desolvation and gas sorption properties of the gadolinium analogue; **6**(MnGd) crystallises more rapidly than **6**(MnDy), so was selected for scale-up. Mild heating under vacuum was performed prior to gas sorption studies and structural integrity was confirmed by PXRD (Figure S10 in the Supporting Information). The Nitrogen Adsorption Isotherm resembles a Type 2 isotherm typically indicative of either a non-porous solid or solids with relatively large pores (Figure 5). The time taken for each data point to reach equilibration and a BET surface area of 125 m^2g^{-1} suggest partial porosity to N_2. The H_2 uptake measurement, in contrast, was much quicker and shows a good uptake of 2.7 $mmol\,g^{-1}$, further indicating the pore accessibility for smaller probe gases.

To conclude, we have used computational chemistry to explore the possible conformations of three xylyl-tethered bis-C[4]s prior to synthesis and application in cluster-forming

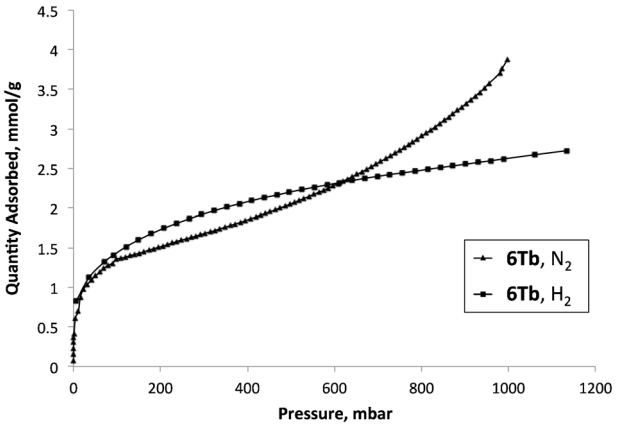

Figure 5. Nitrogen and hydrogen gas adsorption isotherms for desolvated **6**.

chemistry. The *meta*-xylyl bis-C[4] formed a known cluster type in line with inspection of our structural library, presenting this as a potential method of controlling metal-ion composition based on C[4] tethering. In a similar way, *para*-xylyl bis-C[4] is unable to form any of the known C[4]-supported cluster motifs due to ligand structure. Exploitation of this feature afforded a new trigonal antiprismatic metal–organic cage that displays thermal stability and uptake of both N_2 and H_2 gas. Future work will build on these results, focusing on the synthesis of a family of new nanoscale assemblies with targeted topologies through C[4]-tether design. These will be explored for utility as storage materials, host–guest sensors, platforms for postsynthetic modification and hosts for magnetically relevant guests.

Experimental Section

Benzyl-C[4] was synthesised according to literature procedure.[15] The synthesis of **1**–**6** is included in the Supporting Information in addition to details relating to crystallographic, magnetic and gas sorption studies. Open data for this manuscript are available through the following link: http://dx.doi.org/10.7488/ds/1346.

Acknowledgements

We thank the EPSRC for financial support of this work (EP/I03255X/1, EP/I031421/1 and EP/N004884/1). Mass spectrometry data was acquired at the EPSRC UK National Mass Spectrometry Facility at Swansea University. The Advanced Light Source is supported by the Director, Office of Science, Office of Basic Energy Sciences, of the US Department of Energy under contract no. DE-AC02-05CH11231.

Keywords: calixarenes · clusters · directed assembly · gas storage · metal-organic polyhedron

[1] For some examples concerned with the directed assembly of complex, discrete multi-component metal–organic architectures, see: a) J.-F. Ayme, J. E. Beves, D. A. Leigh, R. T. McBurney, K. Rissanen, D. Schultz, *Nat. Chem.* **2012**, *4*, 15; b) Q.-F. Sun, S. Sato, M. Fujita, *Angew. Chem. Int. Ed.* **2014**, *53*, 13510; *Angew. Chem.* **2014**, *126*, 13728; c) D. A. Leigh, R. G. Pritchard, A. J. Stephens, *Nat. Chem.* **2014**, *6*, 978; C. S. Wood, T. K. Ronson, A. M. Belenguer, J. J. Holstein, J. R. Nitschke, *Nat. Chem.* **2015**, *7*, 354.

[2] For examples, see: a) S. Matsuzaki, T. Aria, K. Ikemoto, Y. Inokuma, M. Fujita, *J. Am. Chem. Soc.* **2014**, *136*, 17899; b) Z. Zhang, L. Wojtas, M. J. Zaworotko, *Chem. Sci.* **2014**, *5*, 927; c) F. L. Thorp-Greenwood, A. N. Kulak, M. J. Hardie, *Nat. Chem.* **2015**, *7*, 526.

[3] For an example, see: X. Yan, T. R. Cook, P. Wang, F. Huang, P. J. Stang, *Nat. Chem.* **2015**, *7*, 342.

[4] For a recent review on supramolecular catalysis in metal-ligand hosts, see: C. J. Brown, F. D. Toste, R. G. Bergman, K. N. Raymond, *Chem. Rev.* **2015**, *115*, 3012.

[5] For an example, see: W. Cullen, S. Turega, C. A. Hunter, M. D. Ward, *Chem. Sci.* **2015**, *6*, 625.

[6] N. Zigon, M. Hoshino, S. Yoshioka, Y. Inokuma, M. Fujita, *Angew. Chem. Int. Ed.* **2015**, *54*, 9033; *Angew. Chem.* **2015**, *127*, 9161.

[7] For a relevant review, see: D. J. Tranchemontagne, Z. Ni, M. O'Keefe, O. M. Yaghi, *Angew. Chem. Int. Ed.* **2008**, *47*, 5136 and references therein.

[8] C. D. Gutsche in *Calixarenes*, Kluwer Academic Publishers, Dordrecht, **2001**, Chapter 1 and references therein.

[9] For an example, see: a) C. Aronica, G. Chastanet, E. Zueva, S. A. Borshch, J. M. Clemente-Juan, D. Luneau, *J. Am. Chem. Soc.* **2008**, *130*, 2365; b) G. Karotsis, S. J. Teat, W. Wernsdorfer, S. Piligkos, S. J. Dalgarno, E. K. Brechin, *Angew. Chem. Int. Ed.* **2009**, *48*, 8285; *Angew. Chem.* **2009**, *121*, 8435; c) G. Karotsis, M. Evangelisti, S. J. Dalgarno, E. K. Brechin, *Angew. Chem. Int. Ed.* **2009**, *48*, 9928; *Angew. Chem.* **2009**, *121*, 10112; d) S. Sanz, K. Ferreira, R. D. McIntosh, S. J. Dalgarno, E. K. Brechin, *Chem. Commun.* **2011**, *47*, 9042; e) S. Sanz, R. D. McIntosh, C. M. Beavers, S. J. Teat, M. Evangelisti, E. K. Brechin, S. J. Dalgarno, *Chem. Commun.* **2012**, *48*, 1449; f) M. A. Palacios, R. McLellan, S. M. Taylor, C. M. Beavers, S. J. Teat, W. Wernsdorfer, S. Piligkos, S. J. Dalgarno, E. K. Brechin, *Chem. Eur. J.* **2015**, *21*, 11212.

[10] R. McLellan, M. A. Palacios, C. M. Beavers, S. J. Teat, S. Piligkos, E. K. Brechin, S. J. Dalgarno, *Chem. Eur. J.* **2015**, *21*, 2804.

[11] A. D. Becke, *J. Chem. Phys.* **1993**, *98*, 5648.

[12] C. Lee, W. Yang, R. G. Parr, *Phys. Rev.* **1988**, *37*, 785.

[13] S. Grimme, J. Anthony, S. Ehrlich, H. Krieg, *J. Chem. Phys.* **2010**, *132*, 154104.

[14] There are smaller, C[4]-supported binuclear clusters in the literature but these are formed by air-sensitive rather than ambient conditions and so are not included. For an example, see: L. Clowes, C. Redshaw, D. L. Hughes, *Inorg. Chem.* **2011**, *50*, 7838.

[15] P. A. Scully, T. M. Hamilton, J. L. Bennett, *Org. Lett.* **2001**, *3*, 2741.

[16] J. A. Sheikh, S. Goswami, S. Konar, *Dalton Trans.* **2014**, *43*, 14577.

[17] J. Goura, R. Guillaume, E. Rivière, V. Chandrasekhar, *Inorg. Chem.* **2014**, *53*, 7815.

[18] G. Karotsis, S. Kennedy, S. J. Dalgarno, E. K. Brechin, *Chem. Commun.* **2010**, *46*, 3884.

Received: February 18, 2016
Published online on ■■ ▮▮, 0000

COMMUNICATION

Directed Assembly

M. Coletta, R. McLellan, P. Murphy, B. T. Leube, S. Sanz, R. Clowes, K. J. Gagnon, S. J. Teat, A. I. Cooper, M. J. Paterson, E. K. Brechin, S. J. Dalgarno**

■■ – ■■

Bis-Calix[4]arenes: From Ligand Design to the Directed Assembly of a Metal–Organic Trigonal Antiprism

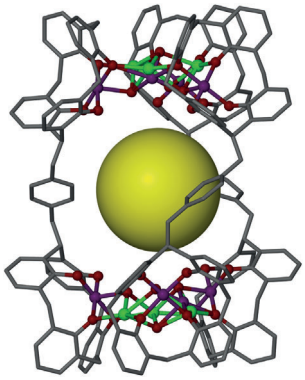

Synthetic modification at the calix[4]arene (C[4]) methylene bridge offers a unique opportunity to influence cluster-forming chemistry. The synthesis of xylyl-tethered bis-C[4]s and their use as directing species in cluster-forming reactions is presented. These new ligands have been used to direct the assembly of a previously known $Fe^{III}_2Ln^{III}_2$ cluster, as well as a spectacular new metal–organic trigonal antiprism, the latter of which also displays thermal stability and uptake of N_2 or H_2 gas.

ChemComm

COMMUNICATION

View Article Online
View Journal

Cite this: DOI: 10.1039/c6cc08059f

Received 6th October 2016,
Accepted 8th November 2016

DOI: 10.1039/c6cc08059f

www.rsc.org/chemcomm

Core expansion of bis-calix[4]arene-supported clusters†

Marco Coletta,[a] Ross McLellan,[a] Amy Waddington,[a] Sergio Sanz,[b] Kevin J. Gagnon,[c] Simon J. Teat,[c] Euan K. Brechin*[b] and Scott J. Dalgarno*[a]

Calix[4]arenes are excellent ligand supports for the synthesis of polymetallic clusters of transition and lanthanide metal ions, as well as 3d–4f ion mixtures. Bis-calix[4]arene, a recent addition to the calixarene family, forms structurally related cages that mirror the metal ion binding preferences of calix[4]arene. Here we show that stoichiometric control causes remarkable expansion in the cores of two known bis-calix[4]arene-supported clusters, with concomitant changes to the magnetic properties observed.

Polymetallic clusters that exhibit interesting magnetic properties have been synthesised from a wide range of ligands, exploiting equally diverse synthetic strategies such as ambient, solvothermal and microwave temperature regimes.[1] Rational ligand design, an approach based partly on targeted metal ion binding, continues to be one of the most valuable strategies employed as one can, for example, influence cluster composition and thus the prevailing magnetic properties.[2]

We (amongst others) have recently shown that methylene-bridged calix[4]arenes (*e.g.* *p*-^{t}Bu-calix[4]arene and *p*-H-calix[4]arene, termed collectively as C[4]s herein) are incredibly versatile ligands for the synthesis of polymetallic clusters, with a wide variety of structural motifs arising from reactions involving transition metal (TM),[3] lanthanide metal (Ln)[4] and 3d–4f ion combinations.[5] Through our experiments we have established a vast library of polymetallic clusters in which $[C[4]TM^{III}]^{-}$, $[C[4]TM^{II}]^{2-}$ or $[C[4]Ln^{III}]^{-}$ moieties act as capping vertices in polyhedra.[6] The generic C[4] polyphenolic pocket binds particular metal ions preferentially depending on those present in the reaction mixture, with the phenolates also bridging to other metal centres within the resulting cluster core; as a result of these studies we have established a reliable set of empirical metal ion binding rules for C[4]s. With respect to the current contribution it is pertinent to mention our first result in this area, that being the synthesis and characterisation of a family of $[Mn^{III}_2Mn^{II}_2(C[4])_2]$ single molecule magnets (SMMs), all of which possess a common butterfly-like $\{Mn^{III}_2Mn^{II}_2(OH)_2\}$ core (**1**, Fig. 1A).[3b,c] The oxidation state distribution in this general core is unusual in that it is reversed relative to the majority of those previously reported in the literature.[7] The body ions of **1** are in the 2+ oxidation state, whilst those housed in the C[4] lower-rim polyphenolic pockets at the wing-tip positions are 3+. Building on that result, we found that it was possible to systematically interchange the body Mn^{II} ions with either one or two Ln^{III} ions through variation in the metal salts, stoichiometry and reaction conditions employed (*e.g.* changes in solvent); this affords butterflies with $\{Mn^{III}_2Mn^{II}Ln^{III}(OH)_2\}$ and $\{Mn^{III}_2Ln^{II}_2(OH)_2\}$ cores respectively.[8] Similar reactions performed in the absence of $TM^{II/III}$ ions led to Ln^{III}_6TBC[4] octahedra,[4] while a series of $Mn^{III}_4Ln^{III}_4$TBC[4] clusters (**2**, Fig. 1B) were obtained in the presence of both TM and Ln ions. The latter are best described as four $[C[4]Mn^{III}]^{-}$ moieties capping the edges of a square of Ln^{III} ions (Ln = Gd, Tb, Dy).[5a]

Bis-*p*-^{t}Bu-calix[4]arene (Bis-TBC[4], L1, Fig. 1C) recently emerged as a new addition to the family of calixarenes.[9] With the aforementioned coordination chemistry in mind, direct C[4] linking *via* the methylene bridge suggested to us that this ligand may be an excellent tool for controlling cluster formation.[10] For example, we anticipated that L1 would be conformationally flexible and thus be capable of behaving as a double capping species given the likely formation of bis-$[C[4]Mn^{III}]^{-}$ moieties. Our initial investigations with L1 confirmed this hypothesis, and clusters isolated with this ligand to date have all mirrored the coordination chemistry of isolated C[4]. Two previously reported L1-supported clusters are relevant to this contribution, the first being of formula $[Mn^{III}_4Mn^{II}_4(L1\text{-}8H)_2(\mu_3\text{-}OH)_2(\mu\text{-}OH)(\mu\text{-}Cl)(H_2O)(MeOH)(dmf)_4]$ (**3**, Fig. 1D).[11] The polymetallic core in **3** can be thought of as two distorted and fused $\{Mn^{III}_2Mn^{II}_2\}$ butterfly cores, as can be seen by comparing Fig. 1A and D.

[a] *Institute of Chemical Sciences, Heriot-Watt University, Riccarton, Edinburgh, Scotland, EH14 4AS, UK. E-mail: S.J.Dalgarno@hw.ac.uk*
[b] *EaStCHEM School of Chemistry, The University of Edinburgh, David Brewster Road, Edinburgh, Scotland, EH9 3FJ, UK. E-mail: ebrechin@ed.ac.uk*
[c] *Station 11.3.1, Advanced Light Source, Lawrence Berkeley National Laboratory, 1 Cyclotron Road, Berkeley, CA94720, USA*

† Electronic supplementary information (ESI) available: Experimental and additional figures to support discussion. CCDC 1484325 and 1484326. For ESI and crystallographic data in CIF or other electronic format see DOI: 10.1039/c6cc08059f

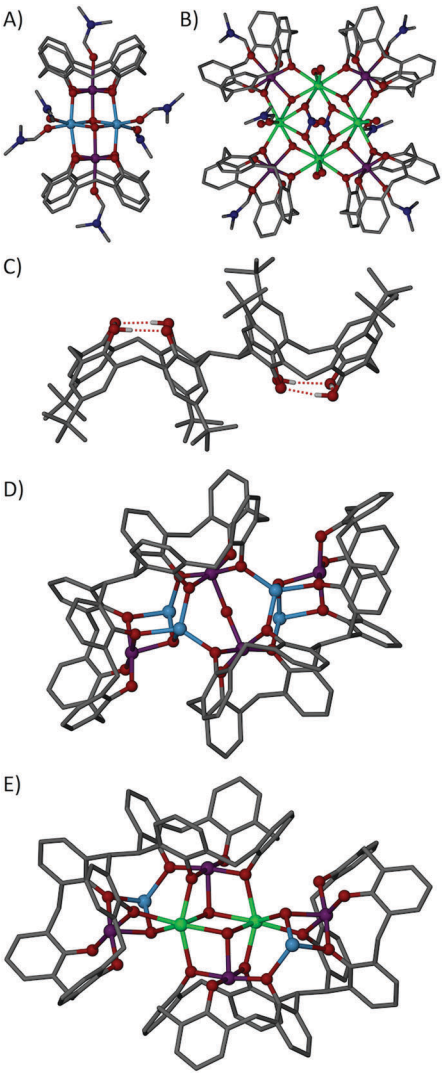

Fig. 1 Single crystal X-ray structures of (A) **1**, (B) **2**, (C) L1, (D) **3**, and (E) **4**.[3b,5a,11] Colour code C – grey, O – red, N – royal blue, Mn^{II} – pale blue, Mn^{III} – purple, Ln^{III} – green. Hydrogen atoms (except those involved in lower-rim H-bonding in (C)), ^{t}Bu groups of C[4] and L1 (except those shown in (C)), ligated solvent molecules in (D) and (E), and co-crystallised solvent/anions omitted for clarity. Not to scale.

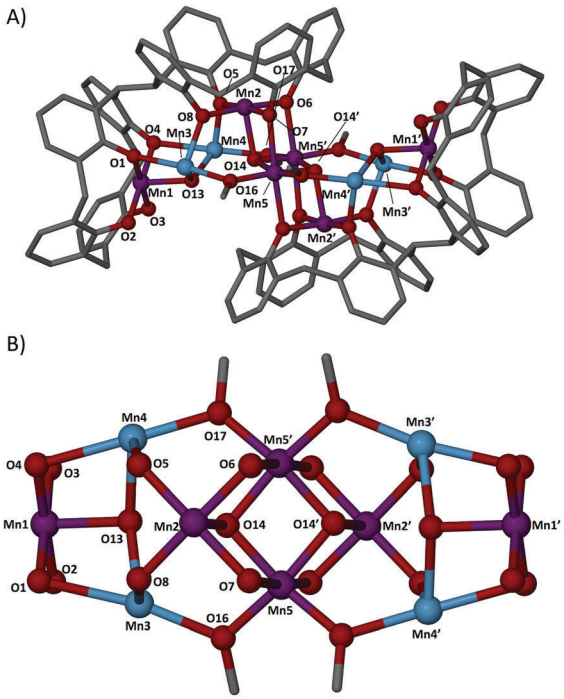

Fig. 2 (A) Single crystal X-ray structure of **5** with selected atoms labelled according to discussion. (B) Top-down view of (A) showing the cluster core and the presence of a central Mn^{III}_4 butterfly. Colour code C – grey, O – red, N – royal blue, Mn^{II} – pale blue, Mn^{III} – purple. H atoms, ^{t}Bu groups of L1, ligated solvent molecules and co-crystallised solvent/anions are omitted for clarity. Figures not to scale.

The main structural differences observed are that, upon linking *via* the methylene bridge, the Mn^{II} ions now occupy positions between the constituent C[4] lower-rims, and that all of the $Mn^{II/III}$ ions are linked by bridging phenolates and hydroxides; the additional pockets/binding positions for the Mn^{II} ions are generated by inversion of L1, as can be seen by comparing conformations in Fig. 1C and D. The second notable example is the $[Mn^{III}_4Mn^{II}_2Gd^{III}_2(L1\text{-}8H)_2(Cl)_2(\mu_3\text{-}OH)_4(MeOH)_2(dmf)_8]$ species (**4**) shown in Fig. 1E, which represents two distorted and fused $\{Mn^{III}_2Mn^{II}Ln^{III}\}$ butterfly cores. Four Mn^{III} ions occupy the C[4] pockets as expected, and two of the four Mn^{II} ions in **3** are interchanged with Ln^{III} ions, mirroring the coordination chemistry of isolated C[4].

Here we show that variation in reactant stoichiometry has a remarkable effect on cluster synthesis with L1, the result being the formation of two new Mn_xLn_y ($x = 10/y = 0$, $x = 8/y = 2$) clusters that are very closely related in structure to those shown in Fig. 1D and E; the polymetallic cores of these new assemblies can essentially be thought of as 'expanded' versions of **3** and **4**, with addition of two Mn^{III} ions in both cases. These were obtained by increasing the ratios of the reacting species, and in one case also by altering crystallisation conditions.

Reaction of L1 with manganese(II) chloride in a DMF/MeOH mixture (in the presence of Et_3N as a base) afforded single crystals found to be of formula $[Mn^{III}_6Mn^{II}_4(L1\text{-}8H)_2(\mu_3\text{-}O)_2(\mu_3\text{-}OH)_2(\mu\text{-}CH_3O)_4(H_2O)_4(dmf)_8(dmf)_4]$ (**5**, Fig. 2) upon slow evaporation of the mother liquor.‡ The crystals were found to be in a triclinic cell and structure solution was carried out in space group $P\bar{1}$.§ The asymmetric unit (ASU) comprises half of the cluster due to the presence of the inversion centre (located within the Mn5–O14–Mn5′–O14′ rhomboid, Fig. 2A), thus only half of the assembly is described in detail.

Inspection of the structure shows that Mn1 is bound in a C[4] lower-rim tetraphenolic pocket (oxygen atoms O1–O4, Mn–O distances in the range of 1.907(5)–1.935(4) Å) and is in the 3+ oxidation state as expected based on C[4] binding rules. The coordination sphere of Mn1 is completed by a ligated dmf molecule (Mn1–O9, 2.35(3) Å) that resides within a C[4] cavity, as well as a μ_3-hydroxide (Mn1–O13, 2.107(5) Å) which bridges to Mn3 and Mn4 (Mn3–O13, 2.192(5) Å and Mn4–O13, 2.187(5) Å, Fig. 2B); the Jahn–Teller axis of Mn1 is defined by the O9–Mn1–O13 vector. Both Mn3 and Mn4 are in a 2+ oxidation state and, as is the case for **3** (Fig. 1D), they reside in the pockets

between the constituent C[4] lower-rims of the L1 octa-anion. Mn3 is bonded to a dmf molecule (Mn3–O11, 2.163 Å), two μ-phenoxide oxygens (Mn3–O1, 2.436(4) Å and Mn3–O8, 2.109(4) Å), an aqua ligand (Mn3–O15, 2.241(5) Å) and a μ-methoxide (Mn3–O16, 2.154(5) Å). The coordination spheres of Mn4 (2+) and Mn1 (3+) are near identical to those of Mn3 (2+) and Mn2 (3+) respectively, with only negligible differences observed in the bond lengths in both cases (ESI†). Mn5 is in a 3+ oxidation state and has distorted octahedral geometry with its Jahn–Teller axis lying along the O7–Mn5–O6′ vector (Mn5–O7, 2.295 Å and Mn5–O6′, 2.331 Å). Two μ_3-oxides and two μ-methoxides complete the Mn5/Mn5′ coordination spheres with Mn5–O14, Mn5-O14′, Mn5–O16 and Mn5–O17 distances being 1.920(5), 1.921(5), 1.926(6) and 1.925(6) Å respectively. Structural comparison of **5** (Fig. 2) with **3** (Fig. 1D) shows that the $Mn^{III}_6Mn^{II}_4$ core in the former can best be described as an 'expanded' version of the previously reported $Mn^{III}_4Mn^{II}_4$ species.[11] As such, 'expansion' occurs with the incorporation of two additional methoxy-bridged Mn^{III} ions, forming the well-known butterfly-like motif in the centre of the cluster core.

Reaction of L1 with manganese(II) nitrate and gadolinium(III) nitrate in a DMF/MeOH mixture in the presence of Et_3N as a base, afforded single crystals of formula $[Mn^{III}_6Mn^{II}_2Gd^{III}_2(L_1\text{-}8H)_2(\mu_4\text{-}O)_2(\mu_3\text{-}OH)_2(\mu\text{-}OCH_3)_2(\mu\text{-}OH)_2(MeOH)_4(dmf)_8](NO_3)_2(H_2O)_2$ (**6**, Fig. 3) upon slow evaporation of the mother liquor. The crystals were found to be in a monoclinic cell and structure solution was carried out in the space group $P2_1/n$. The ASU comprises half of the cluster in which there is disorder relating to the position of the Mn^{II} and Gd^{III} ions; this has been modelled at half-occupancy and only one position is discussed below. Comparison of Fig. 2 and 3 reveals that **6** is closely related to **5**, the only major difference being the interchange of one Mn^{II} for a Gd^{III} ion.

Mn1 is bound in a C[4] lower-rim tetraphenolic pocket (oxygen atoms O1–O4, Mn–O distances in the range of 1.920(5)–1.969(5) Å), is in a 3+ oxidation state and has distorted octahedral geometry (Fig. 3A). The coordination sphere is completed by a ligated dmf (Mn1–O9, 2.229(5) Å) in the C[4] cavity and a μ_3-OH^- (Mn1–O13, 2.174(6) Å, Fig. 3B); the O9–Mn1–O13 vector defines the Jahn–Teller axis with considerable variation from linearity (164.8(1)°), a feature likely attributable to the aforementioned disorder. The Mn3 ion is in the 2+ oxidation state and is disordered at half-occupancy across the two binding sites present between the constituent C[4] lower-rims. Mn3 has distorted octahedral geometry and, in addition to being coordinated to two phenolic oxygens (Mn3–O1, 2.346(4) Å and Mn3–O8, 2.193(4) Å), the coordination sphere is completed by a ligated dmf (Mn3–O11, 1.998(6) Å), a ligated MeOH (Mn3–O15, 2.246(5) Å), the aforementioned μ_3-OH^- (Mn3–O13, 2.184(7) Å) and a μ-hydroxide (Mn3–O17, 2.170(4) Å, bridging to Mn4). Gd1 is in the 3+ oxidation state, is heptacoordinate and has distorted pentagonal bipyramidal geometry. The coordination sphere comprises two phenoxides (Gd1–O4, 2.493(4) Å and Gd1–O5, 2.201(4) Å), a μ_3-hydroxide (Gd1–O13, 2.299(7) Å), a ligated dmf (Gd1–O12, 2.473(7) Å), a ligated methanol (Gd1–O16, 2.361(6) Å), a μ-methoxide (Gd1–O18, 2.184(5) Å, bridging to Mn4) and a μ_4-oxide (Gd1–O14, 2.497(4) Å, bridging to Mn4, Mn4′ and Mn2). With the exception of coordination to O14, Mn2 (3+) has a near

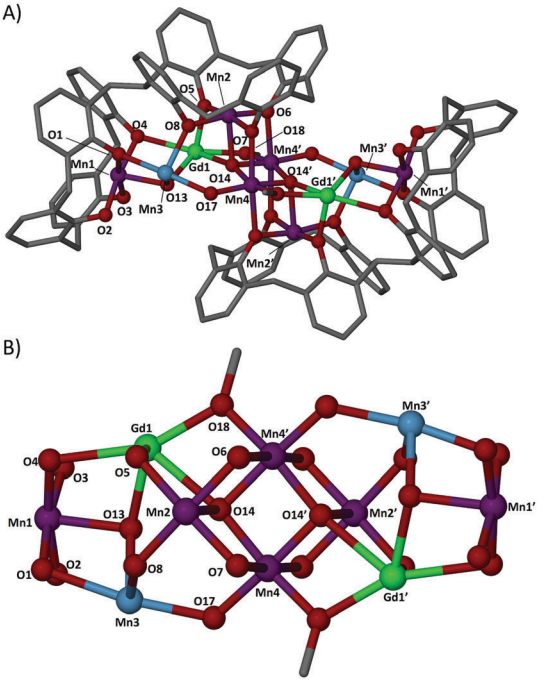

Fig. 3 (A) Single crystal X-ray structure of **6** with selected atoms labelled according to discussion. (B) Top-down view of (A) showing the cluster core and the presence of a central Mn^{III}_4 butterfly. Only one position is shown for the disorder concerning Mn3 and Gd1 (Mn3A, Gd1A and associated disordered ligands hidden from view). Colour code C – grey, O – red, N – royal blue, Mn^{II} – pale blue, Mn^{III} – purple, Ln^{III} – green. H atoms, ^{t}Bu groups of L1, ligated solvent molecules and co-crystallised solvent/anions are omitted for clarity. Figures not to scale.

identical coordination sphere to Mn1 (3+), with only negligible differences observed in the bond lengths (ESI†). Finally, Mn4 is in a 3+ oxidation state and has distorted octahedral geometry with a Jahn–Teller axis lying along the O7–Mn4–O6′ vector (Mn4–O7, 2.354(4) Å and Mn4–O6′, 2.256(4) Å). The aforementioned μ_4-oxides and μ-methoxides complete the Mn4/Mn4′ coordination spheres with respective Mn4–O14, Mn4–O14′, Mn4–O17 and Mn4–O18′ distances of 1.925(4), 1.901(5), 1.914(5) and 1.917(4) Å.

Comparison of Fig. 2B and 3B shows that the cluster cores in **5** and **6** are near isostructural, the only major difference being the effective interchange of Mn^{II} for Gd^{III} ions (or Ln^{III} ions in general) in one binding site between the constituent C[4] lower-rims in each L1. This is remarkable considering the large overall changes required to move from **3** and **4** to **5** and **6** respectively, but is further evidence that analogous metal ion binding rules for bis-C[4] will closely mirror those of C[4]. In addition to this, the expected capping behaviour is also observed as shown in the cluster comparison in Fig. S1 (ESI†). Examination of the extended structures of **5** and **6** reveals that the closest M···M distances are ~8.5 and ~14.2 Å respectively. The structure of **5** is interesting in that the assemblies pack closely so as to form chains along the *a* axis; this occurs as chains of intermolecular interactions. Inspection reveals a unique CH···O interaction between neighbouring aqua and dmf ligands, with a CH···O distance of 3.08 Å, as well as a unique CH···π interaction with a CH···aromatic centroid

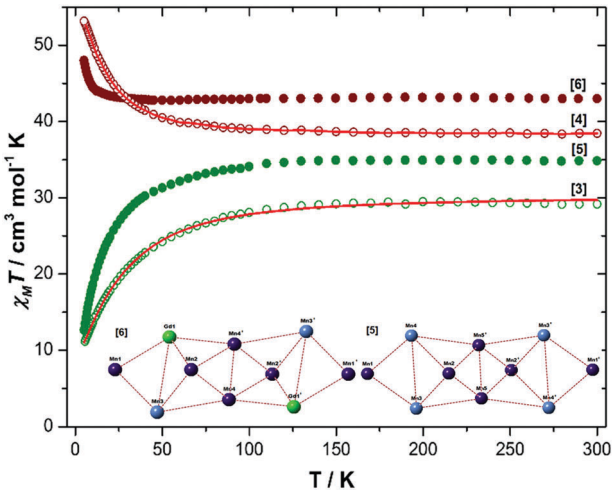

Fig. 4 Experimental $\chi_M T$ *versus* T data for **3–6** measured in the T = 5–300 K temperature range in an applied field of 0.1 T.

distance of 3.67 Å (Fig. S2, H atoms in staggered positions due to torsion shifts, ESI†). In contrast the clusters in **6** can be considered well isolated (Fig. S3, ESI†), as evidenced by the larger inter-cluster spacing.

The dc molar magnetic susceptibility, χ_M, of polycrystalline samples of **5** and **6** were measured in an applied magnetic field, B, of 0.1 T, over the 5–300 K temperature, T, range (Fig. 4, where $\chi = M/B$, and M is the magnetization). At room temperature, the $\chi_M T$ products of **5** and **6** have values of 34.9 and 43.02 cm^3 mol^{-1} K, respectively. These are in excellent agreement with those expected from the spin-only contributions to the magnetism of a $[Mn^{III}_6Mn^{II}_4]$ (35.5 cm^3 mol^{-1} K) and $[Mn^{III}_6Mn^{II}_2Gd^{III}_2]$ (42.5 cm^3 mol^{-1} K) moieties, with g = 2.00. On lowering the temperature the $\chi_M T$ value of **5** remains essentially unchanged to T = 100 K, where it begins to decrease more rapidly to a minimum value of 12.7 cm^3 mol^{-1} K at 5 K. Upon cooling, the $\chi_M T$ value of **6** remains practically constant to 50 K, from where there is a small increase until ~20 K, below which there is a more abrupt increase to a value of 48 cm^3 mol^{-1} K at 5 K. Due to the size and structural complexity of **5** and **6**, a quantitative fit of the susceptibility data is not possible. Qualitatively, the magnetic behaviour of **5** and **6** is similar to that of **3** $[Mn^{III}_4Mn^{II}_4]$ and **4** $[Mn^{III}_4Mn^{II}_2Gd^{III}_2]$, respectively, as can been seen from inspection of Fig. 4. In the latter species three independent isotropic exchange parameters were obtained for both **3** ($J_{Mn(II)\text{–}Mn(III)}$ = +0.92 cm^{-1}; $J_{Mn(II)\text{–}Mn(II)}$ = −4.48 cm^{-1} and $J_{Mn(III)\text{–}Mn(III)}$ = −1.52 cm^{-1}) and **4** ($J_{Mn(III)\text{–}Gd(III)}$ = −0.062 cm^{-1}; $J_{Mn(II)\text{–}Gd(III)}$ = +0.066 cm^{-1} and $J_{Gd(III)\text{–}Gd(III)}$ = −0.061 cm^{-1}), revealing the existence of both ferro- and antiferromagnetic exchange interactions. Given the structural similarity of **5** and **6** to these previously published complexes it would seem safe to assume that a similar pattern of exchange exists. Variable-temperature-and-variable-field (VTVB) magnetization data is consistent with this picture in which M rises slowly with increasing B, failing to reach saturation in both cases (Fig. S4, ESI†).

To conclude, we have shown that changes in reaction stoichiometry cause remarkable cluster core expansion in bis-calix[4]arene-supported cages. Both of the expansions shown here involve the analogous incorporation of two additional Mn^{III} ions, generating larger assemblies based on a generic butterfly-like $\{Mn^{III}_2Mn^{III}_2(OH)_2\}$ core. This metallic addition, does not have a major impact on the magnetism, with the magnetic behaviour of **5** and **6**, akin to the previously reported **3** and **4**. The results presented suggest that other bis-C[4]-supported clusters may exhibit similar expansion behaviour, thereby allowing one to tune the resulting magnetic properties through extension of the metal ion binding rules established for C[4]. This will be studied and reported in due course.

We thank the EPSRC for financial support of this work under grant reference EP/I03255X/1. The Advanced Light Source is supported by the Director, Office of Science, Office of Basic Energy Sciences, of the US Department of Energy under contract no DE-AC02-05CH11231. Data for this paper are available *via* the following link: http://hdl.handle.net/10283/1927.

Notes and references

‡ Compound L1 was synthesised according to literature procedure.[9] Single crystal X-ray data for **5** and **6** were collected on a Bruker D8 diffractometer operating a PHOTON 100 detector (shutterless scans) at 100(2) K and with synchrotron radiation (λ = 0.7749 Å).

§ Crystal data for **5** (CCDC 1484325): $C_{216}H_{310}Mn_{10}N_{12}O_{40}$, dark violet plate, 0.1 × 0.06 × 0.01 mm^3, triclinic, space group $P\bar{1}$ (No. 2), a = 14.9101(5), b = 17.9438(5), c = 22.3792(7) Å, α = 69.512(2), β = 75.796(2), γ = 81.501(2)°, V = 5424.6(6) Å^3, Z = 1, $2\theta_{max}$ = 48.252°, 54 412 reflections collected, 13 284 unique (R_{int} = 0.0696). Final GooF = 1.045, R^1 = 0.1116, wR^2 = 0.2297. Crystal data for **6** (CCDC 1484326): $C_{206}H_{280}Mn_8Gd_2N_{10}O_{44}$, M = 4354.40, dark violet block, 0.4 × 0.35 × 0.3 mm^3, monoclinic, space group $P2_1/n$ (No. 14), a = 22.090(7), b = 19.1570(6), c = 27.0764(9) Å, β = 105.149(2)°, V = 11063.0(7) Å^3, Z = 2, $2\theta_{max}$ = 59.772°, 136 715 reflections collected, 24 604 unique (R_{int} = 0.0542). Final GooF = 1.077, R^1 = 0.1061, wR^2 = 0.2740.

1 (*a*) M. Murrie, *Chem. Soc. Rev.*, 2010, **39**, 1986; (*b*) R. Bagai and G. Christou, *Chem. Soc. Rev.*, 2009, **38**, 1011; (*c*) L. N. Dawe, K. V. Shuvaev and L. K. Thompson, *Chem. Soc. Rev.*, 2009, **38**, 2334; (*d*) R. E. P. Winpenny, *Chem. Soc. Rev.*, 1998, **27**, 447.
2 (*a*) G. Aromí and E. K. Brechin, *Struct. Bonding*, 2006, **122**, 1; (*b*) J.-N. Rebilly and T. Mallah, *Struct. Bonding*, 2006, **122**, 103.
3 (*a*) C. Aronica, G. Chastanet, E. Zueva, S. A. Borshch, J. M. Clemente-Juan and D. Luneau, *J. Am. Chem. Soc.*, 2008, **130**, 2365; (*b*) G. Karotsis, S. J. Teat, W. Wernsdorfer, S. Piligkos, S. J. Dalgarno and E. K. Brechin, *Angew. Chem., Int. Ed.*, 2009, **48**, 8285; (*c*) S. M. Taylor, G. Karotsis, R. D. McIntosh, S. Kennedy, S. J. Teat, C. M. Beavers, W. Wernsdorfer, S. Piligkos, S. J. Dalgarno and E. K. Brechin, *Chem. – Eur. J.*, 2011, **17**, 7521; (*d*) G. Karotsis, S. Kennedy, S. J. Dalgarno and E. K. Brechin, *Chem. Commun.*, 2010, **46**, 3884.
4 S. Sanz, R. D. McIntosh, C. M. Beavers, S. J. Teat, M. Evangelisti, E. K. Brechin and S. J. Dalgarno, *Chem. Commun.*, 2012, **48**, 1449.
5 (*a*) G. Karotsis, S. Kennedy, S. J. Teat, C. M. Beavers, D. A. Fowler, J. J. Morales, M. Evangelisti, S. J. Dalgarno and E. K. Brechin, *J. Am. Chem. Soc.*, 2010, **132**, 12983; (*b*) S. Sanz, K. Ferreira, R. D. McIntosh, S. J. Dalgarno and E. K. Brechin, *Chem. Commun.*, 2011, **47**, 9042.
6 M. Coletta, E. K. Brechin and S. J. Dalgarno, in *Calixarenes and Beyond*, ed. P. Neri, J. L. Sessler and M.-X. Wang, Springer International Publishing, Switzerland, 1st edn, 2016, ch. 25, pp. 671–689.
7 E. K. Brechin, J. Yoo, M. Nakano, J. C. Huffman, D. N. Hendrickson and G. Christou, *Chem. Commun.*, 1999, 783.
8 M. A. Palacios, R. McLellan, C. M. Beavers, S. J. Teat, H. Weihe, S. Piligkos, S. J. Dalgarno and E. K. Brechin, *Chem. – Eur. J.*, 2015, **21**, 11212.
9 L. T. Carroll, P. Aru Hill, C. Q. Ngo, K. P. Klatt and J. L. Fantini, *Tetrahedron*, 2013, **69**, 5002.
10 P. Murphy, S. J. Dalgarno and M. J. Paterson, *J. Phys. Chem. A*, 2014, **118**, 7986.
11 R. McLellan, M. A. Palacios, C. M. Beavers, S. J. Teat, S. Piligkos, E. K. Brechin and S. J. Dalgarno, *Chem. – Eur. J.*, 2015, **21**, 2804.

